Open Research Online

The Open University's repository of research publications
and other research outputs

High Mass X-ray Binaries: The Donor Stars and their Compact Companions

Thesis

How to cite:

Baker, Amira Val (2008). High Mass X-ray Binaries: The Donor Stars and their Compact Companions. PhD thesis The Open University.

For guidance on citations see FAQs.

© 2008 The Author

Version: Version of Record

Copyright and Moral Rights for the articles on this site are retained by the individual authors and/or other copyright owners. For more information on Open Research Online's data policy on reuse of materials please consult the policies page.

oro.open.ac.uk

High Mass X-ray Binaries: The Donor Stars and their Compact Companions

Amira Val Baker

A Thesis submitted for the degree of Doctor of Philosophy

The Open University

Faculty of Science

Department of Physics and Astronomy

Contents

High Mass X-ray Binaries: The Donor Stars and their Compact Companions

Amira Val Baker

Abstract

This thesis presents new spectroscopic observations of the donor star in several High Mass X-ray Binary systems. The various types of X-ray Binary systems that exist are outlined and the methods and limitations of mass determination of the stellar components are discussed. The masses of the compact objects are determined for the systems SMC X-1 and LMC X-3. In both cases the heating of the donor star by the X-ray source is taken into account and its importance demonstrated.

In the case of SMC X-1, we determine the radial velocity semi-amplitude of Sk 160 to be 24.7 ± 1.9 km s^{-1}. Assuming Sk 160 fills its Roche-lobe we obtain upper limits for the mass of the neutron star as $M_x = 1.36 \pm 0.10$, and by assuming that the system is seen edge on we obtain lower limits for the masses of the neutron star as $M_x = 1.05 \pm 0.09$ M$_\odot$. However, based on the model predictions of Timmes et al. (1996), it is concluded that the mass lies in the upper end of the heating corrected mass determinations.

In the case of LMC X-3 the spectral type of the donor star is observed to change with phase due to irradiation by the X-ray source. We find the spectral type is likely to be B5V, and only appears as B3V when viewing the heated side of the donor. Combining our measurements with those previously published, and taking into account the effects of X-ray irradiation, results in a value for the donor star radial velocity semi-amplitude of $K_o = 256.7 \pm 4.9$ km s^{-1}. Assuming an inclination of $50° \leq i \leq 70°$ we find the mass of the black hole lies in the range 9.5 ± 1 M$_\odot \leq$ M$_x \leq 13.2 \pm 1$ M$_\odot$.

The idea of using these mass determination techniques as a tool for detecting potential black hole/Be star XRB systems is presented and the radial velocities for seven such systems are determined. Of these, one system, LS 4356 shows a radial velocity variation large enough (i.e. ~ 95 km s^{-1}) to indicate the presence of a black hole. If the compact companion is confirmed as a black hole, it will make LS 4356 the first known black hole/Be XRB. Finally the emission lines

observed in the spectra of two Be XRBs, X Per and A0535+26 are analysed and compared to the previous studies of Clark et al. (2001) and Grundstrom et al. (2007). The Hα emission line profiles are discussed in terms of their evolution with time and the changing state of the circumstellar disc, thereby confirming and adding to the long term data set. The emission line profiles of the other spectral lines, namely Hβ, Hγ, He I 5876, He I 6678 and He I 7065, are presented and compared with that of Hα.

Chapter 1

Introduction

This thesis looks into mass determinations of the compact components of High Mass X-ray Binaries (HMXB). This first chapter outlines the various types of X-ray Binary (XRB) systems that exist and discusses how the masses of the stellar components can be found along with the problems encountered in the different types of systems. The 2nd chapter outlines the data reduction techniques, the individual techniques used for the overall mass determination, and the methods used to overcome encountered problems. Chapters 3 and 4 introduce, present and discuss the results of the mass determinations of the two main systems of study in this thesis, SMC X-1 and LMC X-3. The results for each system have already been published as Val Baker et al. (2005) and (2007) respectively. Chapter 5 discusses the theory behind the existence of black hole/Be star XRBs and presents the idea of using mass determination techniques as a tool for identifying such systems. The results of the analysis of seven potential black hole/Be star XRBs is presented and discussed, along with the conclusions made. Chapter 6 discusses the more common neutron star/Be star XRB systems, with reference to their circumstellar discs. The evolution of the emission lines originating from the circumstellar disc of the two systems, X Per and A0535 is presented and compared to previous studies. Finally Chapter 7 will finish with a discussion on the potential for future work related to this thesis. The future work suggested in Section 7.1.2 is based on a proposal for time on the Very Large Telescope (VLT) which was written by A. J. Norton, but

with input from me. That proposal has now been awarded time, for observations to be done in 2008.

1.1 Overview of X-ray binaries

Interacting binary stars are binary systems in which mass transfer from one star, known as the donor star, to its companion star has occurred. Mass transfer is known to happen in one of two ways. Firstly the donor star may eject some of its mass in the form of a stellar wind, such that material is able to be gravitationally accreted by the companion, refer to Figure 1.1. Such a scenario usually happens when both stars are well within their Roche-lobes. Secondly, if the donor star expands or if the binary separation shrinks such that the donor star is filling its Roche-lobe, then the gravitational potential energy of the companion star is able to accrete matter from the donor star's outer layers, refer to Figure 1.2.

Figure 1.1: Artist impression of accretion via a stellar wind (©NASA, http://imagine.gsfc.nasa.gov).

If the companion star has a radius smaller than the circularization radius, like that of a white dwarf, a neutron star or a black hole, the accreting matter will be forced into a circular orbit which eventually spreads out to form a flat disc of gas around the companion star, known as an accretion disc. As the gas from the accretion disc shrinks deeper and deeper into the gravitational potential well of

Figure 1.2: Artist impression of accretion via Roche-lobe overflow (©Mark Garlick, http://www.space-art.co.uk).

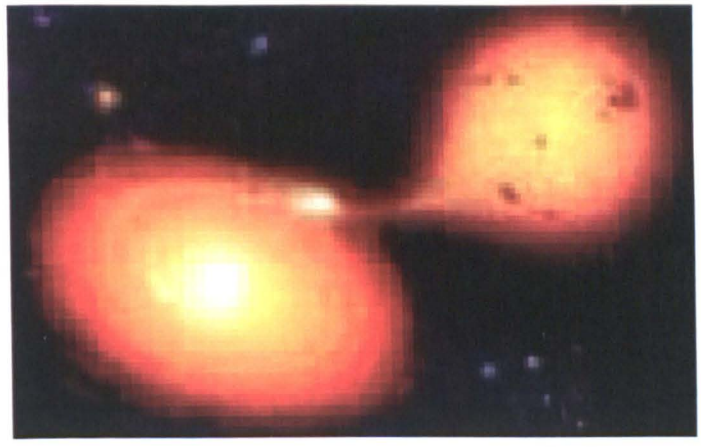

the companion star, the disc heats up through viscous dissipation as angular momentum is transported outwards and matter inwards. The energy released in this accretion process is given by:

$$E_{acc} = \frac{GMm}{R} \tag{1.1}$$

where G is the Gravitational constant, M is the mass of the accreting star, m is the mass accreted and R is the stellar radius. Thus the accretion luminosity is:

$$L_{acc} = \frac{GM}{R}\frac{\delta m}{\delta t} = \frac{GM\dot{M}}{R} \equiv \eta \dot{M} c^2 \tag{1.2}$$

where $\dot{M}$ is the mass accretion rate and η is the accretion efficiency parameter.

The accretion rate in close binary systems involving compact stars is typically of the order $10^{16} - 10^{19}$ $M_\odot$ yr^{-1}, resulting in accretion luminosities of the order 1.3×10^{33} erg s^{-1} and 1.3×10^{36} erg s^{-1} for white dwarfs and neutron stars respectively. In the case of black hole systems the dimensionless quantity η is introduced to account for the uncertainty in the size of the region into which matter falls. Assuming $0 \leq \eta \leq 1$ (i.e. compared to $\eta \sim 0.2$ for a neutron star and $\eta \sim 2 \times 10^{-4}$ for a white dwarf) we see that for a black hole L_{acc}

is of the order 10^{35-36} erg s^{-1}. The inner regions of the accretion disc are optically thin and emit thermal bremsstrahlung radiation, whereas the cooler outer regions of the disc are optically thick and emit blackbody radiation at a range of temperatures. The temperature of the disc is therefore given in terms of both the black body temperature and the thermal temperature:

$$T_b = \left(\frac{L_{acc}}{4\pi R^2 \sigma}\right)^{1/4} \tag{1.3}$$

$$T_{th} = \frac{GMm_p}{3kR} \tag{1.4}$$

where σ is the Stefan-Boltzman constant, m_p is the proton mass and k is the Boltzman constant. The temperature of the emitted radiation ($T_{rad} = hf/k$, where h is Planck's constant and f is the frequency), will therefore lie between these values i.e. $T_b \leq T_{rad} \leq T_{th}$.

In the case of compact companions such as neutron stars and black holes, as Equations 1.1 – 1.4 illustrate, the loss of gravitational potential energy is so great, that the material is heated up to tens of millions of kelvin causing the stellar matter to emit high energy radiation such as X-rays. Such systems, known as X-ray binaries (XRBs), constitute the brightest class of X-ray sources in the sky and are therefore perfect laboratories for studying these high density objects. (Frank et al. 2002).

Since the discovery of the first XRB, Sco X-1 (Giacconi et al. 1962), multi-wavelength observations of these systems, particularly in the X-ray and the optical, have led to a greater understanding of the nature of their emission and enabled us to determine many of their fundamental characteristics. For example photometric observations made in the optical can give us the orbital period of the system, and can also show us if the system is eclipsing. Likewise X-ray photometry can reveal the orbital period in the form of periodically recurring X-ray outbursts, absorption features, or X-ray eclipses. If the compact companion is an X-ray pulsar, then X-ray pulsations can reveal the spin period of the neutron star. In addition, Doppler shifted pulsations can also reveal the periodic change in speed of the neutron star in its orbit and hence allow the orbital period and projected size of the orbit to be measured. The spectral type of the donor

star can be determined from optical spectroscopy which in turn gives us the donor star's temperature and luminosity class. The variations observed in the spectral lines can give us the radial velocity variations from which we are able to infer the binary motion and in some cases the donor star's mass which we are then able to use to determine the mass of the compact companion and the geometry of the accretion flow.

The mass accretion rate greatly influences the geometry of the accretion flow and hence the X-ray luminosity, L_x, of the system such that the X-ray spectra either appear in the high/soft state or the low/hard state. With the former consisting of low-energy X-rays ($kT \leq 10$keV) with a high L_x and the latter consisting of high-energy X-rays ($kT \geq 10$keV) with a low L_x. An extreme of each state has also been observed, with black hole systems displaying at least 5 spectral states (i.e. quiescent; low/hard; intermediate; high/soft; very high), which are well explained by the Advection-Dominated Accretion Flow (ADAF) model (Esin et al. 1997).

1.2 Classification

X-ray binary systems can be split into different classes and sub-classes, where the first distinction is usually made in terms of the donor star's mass. The estimated mass is usually based on its spectral type which is obtained from an optical identification and/or the mass function. If neither is available the classification is inferred from the similarity of the X-ray properties to other identified systems. As a result XRBs are divided into low mass X-ray binaries (LMXBs) with donor star mass, $M_o \leq 2\mathrm{M}_\odot$, and high mass X-ray binaries (HMXBs) with donor star mass, $M_o \geq 5\mathrm{M}_\odot$, refer to Figure 1.3. It should be noted that over recent years a significant number of XRBs have been identified whose masses are intermediate between high mass and low mass. In such cases it is usually the nature of the mass transfer process that distinguishes a LMXB from a HMXB i.e. mass transfer is stellar wind dominated in HMXBs and by Roche-lobe overflow in LMXBs. As these modes of mass transfer produce quite different properties (i.e. mass transfer by Roche-lobe overflow generally gives higher $\dot{M}$ and therefore higher L_x), such a distinction is generally straight forward.

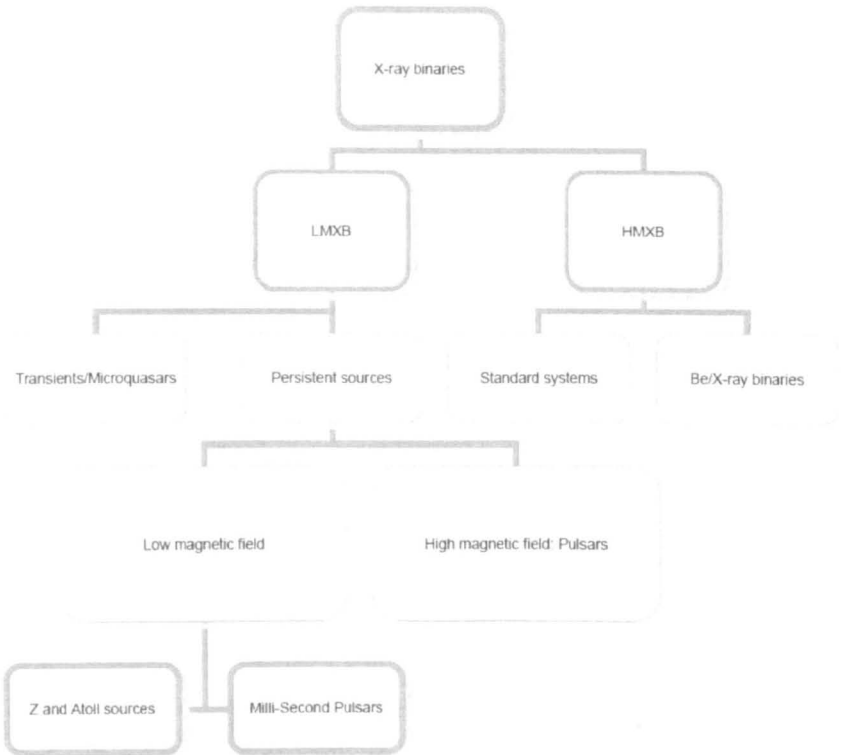

Figure 1.3: XRB Taxonomy

The following section describes the properties of HMXBs, and the various sub-types of these. In each case a typical system of the sub-class is described in order to illustrate the characteristics that are observed.

1.3 HMXBs

HMXBs make up a third of the brightest Galactic X-ray sources and were therefore among the very first X-ray sources to be discovered and optically identified. They are commonly found in the Galactic plane and the Magellanic clouds with a Galactic disc distribution characteristic of Pop I stars (i.e. with an age around $\sim 10^7$ yrs). The systems consist of a compact companion, mostly a magnetized neutron star or a black hole orbiting a massive donor star of spectral type O or B (typically of $M \geq 5M_{\odot}$). These early type stars have a substantial stellar wind, which is captured by the compact companion and powers the X-ray source.
The spectral and temporal characteristics of HMXBs differ from those of LMXBs in a number of ways. For example, due to the mode of mass transfer, the ratio of their X-ray to optical luminosities are much lower such that the optical light curves are dominated by the donor star and the optical spectra are stellar-like (Rappaport & Joss, 1983). The orbital periods of HMXBs range from 4.8 hrs – 187 days (White et al. 1995), and may be inferred from modulations in either the optical or X-ray light curve, where eclipses can sometimes be seen. Alternatively, or additionally, by measuring the periodic change in the Doppler shift of X-ray pulse profiles, i.e. timing delays, the orbital period can be measured and the radial velocity of the neutron star determined. Long term periodicies in the optical light curves of several HMXBs have been reported and it has been proposed that these changes are caused by the precession of a tilted accretion disc (Petterson, 1977).
The X-ray spectra of HMXBs are typically much harder than those of LMXBs with a characteristic temperature of $\geq$ 15keV, which can be modelled by power-laws with an exponential cut-off around 100keV. Unlike the LMXBs, quasi-periodic oscillations are not as commonly observed in the HMXB sources as the accretion rate in these systems is generally much lower than that of LMXBs (van der Klis, 2004). They often show X-ray periodic pulsations due to their highly magnetized rotating neutron star (typically of the order 10^{12}G), and as a

consequence do not exhibit type I X-ray bursts. The pulsations occur with periods ranging from $0.069 - 1455$ seconds, and are present in 25% of the HMXBs. With both the orbital and pulse periods easily observed, these systems can provide absolute orbital solutions and hence the masses of the two components. Numerous physical characteristic differences are also apparent within the class of HMXBs, splitting them into a further 2 distinguishable sub-classes, the 'standard' systems and the 'Be X-ray binaries' (van Paradijs, 1983). There are 130 HMXBs known so far, where 65% of them are Be X-ray binaries and only 35% of them are standard systems, (Lui et al. 2000). However some of these are only classified based on their transient character (i.e. typical of Be X-ray binaries) and/or their hard X-ray spectrum, whereas other doubtful cases have been excluded.

1.3.1 Standard systems

The standard HMXBs consist of an early type donor star, typically of luminosity class I-III, in orbit with either a black hole or a neutron star. They generally exhibit persistently bright emission in both the optical and the X-ray, which is indicative of their predominantly circular orbits and short orbital periods (typically $\leq$ 15 days). The mode of mass transfer is usually due to a strong stellar wind, which is typical of the O or early type B donor star. In such a situation the donor star loses matter in its radially out-flowing wind, which the compact companion is able to capture and hence form an accretion disc. However as the stellar wind is usually almost spherical the accretor is only able to capture a fraction of the wind such that the accretion rate is relatively low and the disc is thin compared to that of LMXBs where mass transfer is mainly by Roche-lobe overflow.[1]

In some cases the donor star can also lose mass by incipient Roche-lobe overflow, where reduced gravity can cause a focusing of the wind towards the compact companion (Friend & Castor, 1982). One such example is the system Cen X-3, which although it has a strong stellar wind, the observed luminosity ($L_x \sim 5 \times 10^{37}$ erg s^{-1}) suggests that the mode of mass transfer is predominantly via a disc fed by incipient Roche-lobe overflow (Nagase et al. 1992; van Paradijs, 1998).

[1] compared to the Be systems, the standard systems have relatively steady wind outflow.

This system is an eclipsing X-ray binary pusar which allows for direct mass determination of the stellar components. There are only 10 of these 'eclipsing X-ray binary pulsars' known so far, where the majority are HMXBs with only one, known as Her X-1, being a LMXB. Morever as the donor stars in these systems are much brighter than those in the LMXBs, accurate masses are more readily found.

Cen X-3 has also been found to exhibit γ-ray emission, which is expected to be due to the high energy processes that occur in HMXB systems (Bednarek, 2000). The γ-rays are thought to be produced by either interactions of relativistic particles (Bignami et al. 1977; Kirk et al. 1999) or by shock waves produced from the collision of a pulsar with the donor star's stellar wind (Harding & Gaisser, 1990).

The emission of γ-rays is also associated with the sub-class of microquasars. Such systems are known for their outbursts in the form of bi-polar radio jets consisting of material in the accretion disc which is accelerated to superluminal motion by the disc's strong magnetic field. It should be noted that microquasars exist in LMXBs as well as HMXBs and are not unique to a specific group (i.e. they exist in the standard systems as well as the Be systems). For example, Cyg X-1 is both a standard HMXB and a microquasar. It was discovered in 1964 by Bowyer (Bowyer et al. 1965), and has been studied extensively since then. The system consists of a black hole in orbit with a bright ($m_V = 8.9$) OB supergiant donor star, and is actually the prototype for black hole XRBs. It is the brightest of the persistent HMXBs and is mostly observed in the low/hard state but has recently been observed in both the intermediate state and the high/soft state (Zdziarski et al. 2002; Gleissner et al. 2004). Being both a HMXB and a microquasar, it is not suprising that this system also exhibits γ-ray emission (Bednarek & Giovannelli, 2007).

1.3.2 Be stars

The Be X-ray binaries were first recognised by Maraschi et al. (1976) and are the most numerous class of HMXBs, with approximately 80 systems known. They are binary systems where the donor star is a rapidly rotating B-emission main-sequence star known as a Be star. The Be star is usually un-evolved and in most

cases the compact companion is a neutron star exhibiting pulsations (Rappaport & Van den Heuvel, 1982).[2] Their characteristic emission lines are predominantly the Balmer series, and are believed to originate from circumstellar material. These circumstellar discs are believed to have been formed through the ejection of matter from their photospheres, possibly due to internal disturbances caused by the rapidly rotating (generally close to break-up velocity) Be star, (Struve, 1931).

Be donor stars are usually deep within their Roche-lobes. This is indicated by the generally elliptical long orbital periods ($\geq$ 15 days), and by the absence of X-ray eclipses and of ellipsoidal light variations. The luminosities and spectral types indicate the masses of the donor star to be in the range of about $8-20M_{\odot}$, typical of spectral type OB. In fact, contrary to isolated Be stars, there are no known Be X-ray binaries with spectral type later than B3. The reason for this is because the wide orbits predicted by evolutionary models (van den Heuvel, 1983; Verbunt & van den Heuvel, 1995) are vulnerable to disruption during the supernova explosion (Van Bever & Vanbeveren, 1997), which is more significant in the less massive stars (i.e. of spectral type later than B3).

The mode of mass transfer in these systems is usually by a variant of stellar wind accretion and equatorial mass shedding due to the fast rotation of the Be star. In this situation the compact star orbits the Be star on an elliptical orbit and usually only at periastron passage is the compact star able to accrete material from the Be stars wind thus exhibiting periodic type I X-ray outbursts (typically $L_x \sim 10^{36} - 10^{37}$ erg s^{-1}), refer to Figure 1.4. Outbursts of type II can also happen and are thought to be due to the build up of matter on the circumstellar disc, which is then dumped on to the compact star forming an accretion disc.[3] These type II X-ray outbursts are much brighter (typically $L_x > 10^{37}$ erg s^{-1}) and generally show no correlation with the orbital phase (Okazaki & Negueruela, 2001).

As a result of these accretion processes and the time variability of disc loss and reformation, the X-ray emission from the Be X-ray systems tends to be extremely variable ranging from complete absence to large transient outbursts (Underhill & Doazan, 1982; Hubert & Floquet, 1998). Such Be systems are

[2]Note: To date there are no known Be X-ray binary systems containing a black hole candidate, refer to Chapter 5.

[3]Note: These type I and type II outbursts are different then those in the case of LMXBs.

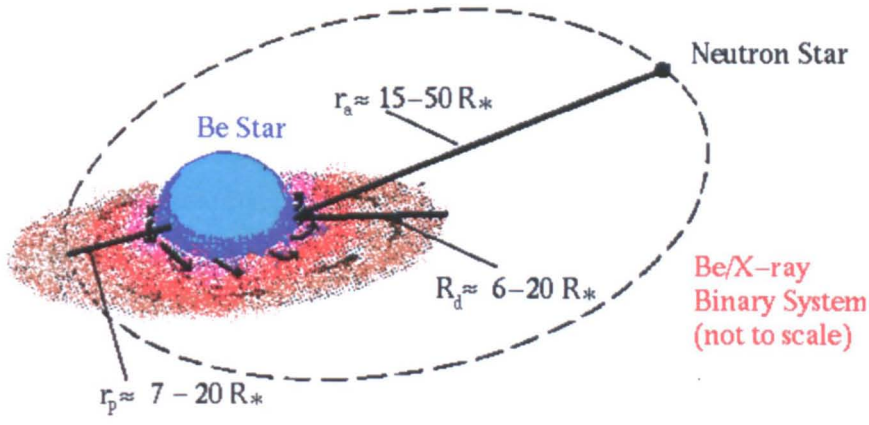

Figure 1.4: Example diagram of a Be X-ray binary system, showing how mass is accreted by the neutron star at periastron passage, (http://xmm.u-strasbg.fr/staff/ignacio/be.html).

known as transient sources and have relatively hard spectra. However, some known as X Per-like systems (i.e. like the system X Persei which is the prototype for such systems) are persistent sources with low luminosities (i.e. $L_x \sim 10^{34}$ erg s^{-1}), (Reig & Roche, 1999). The X-ray emission observed in these persistent sources is of low variability, exhibiting only rare non-periodic weak X-ray outbursts. The orbital periods are not so well known, but the lack of eclipses and pulse timing measurements indicate periods of several hundred days.

The Be systems in general are very complicated and have presented many difficult physical problems. Negueruela (1998) has suggested that the X-ray properties of these systems can be explained by the size of their orbit i.e. close orbits are bright transients which show no quiescent emission; wide orbits are persistent sources and display no large outbursts; and intermediate orbits present a mixture of both behaviours. There are many different models to try and explain the overall phenomena of Be stars, but the most applicable model at present is the viscous decretion disc model proposed by Lee et al. (1991). In this model the mass flow is outward from the Be star, in contrast with that in an accretion disc, and angular momentum is transferred from the central star to the inner edge of the disc, increasing the angular velocity to Keplerian. The mechanisim responsible for this transfer of angular momentum is still to be determined, but has been suggested to be associated with non-radial pulsations (Okazaki &

Negueruela, 2001).

The viscous disc model succesfully accounts for most properties of Be stars, and when applied to the Be X-ray binaries it naturally predicts the truncation of the circumstellar disc. Truncation occurs at certain radii where resonance occurs between the orbital period of the neutron star and the Keplerian orbital period of material at the outer edge of the disc. For instance, if the material in the outer disc orbits the Be star twice for each orbit of the neutron star, this would be a 2:1 resonance. Evidence for truncation of the circumstellar disc was found by Haigh et al. (2004), who showed that the observed infra-red excess of the system A0535+26 is quantised with relative fluxes that match theoretical predictions. Such truncation is believed to be the result of resonant torque exerted by the neutron star, which removes angular momentum from the circumstellar disc. Negueruela and Okazaki (2001) found that the distance at which the circumstellar disc is truncated depends mainly on the orbital parameters and the disc viscosity, where the criterion for disc truncation at a given resonance radius is given by:

$$T_{vis} + T_{res} < 0 \tag{1.5}$$

where T_{vis} is the viscosity torque and T_{res} is the resonance torque.

The truncation of accretion discs in circular binaries with low mass ratio, $q(= M_x/M_o)$ (i.e. $0.05 \leq q \leq 0.2$) is known to occur at the 3:1 resonance radius (Osaki, 1996; Okazaki & Negueruela, 2001; Clark et al. 2001). As all Be X-ray binaries have such low q, it is expected that for Be systems with low eccentricity (i.e. $e \leq 0.2$), the disc will also be truncated at the 3:1 resonance radius. At this resonance radius the gap between the disc's outer radius and the critical lobe radius of the Be star is so wide that under normal conditions the neutron star cannot accrete enough gas at periastron passage to show periodic type I X-ray outbursts. Therefore such systems will only display occasional giant type II X-ray outbursts i.e. due to accumulation of matter in the outer parts of the circumstellar disc and the overcoming of truncation by the effects of global one-armed oscillations or disc warping (Negueruela et al. 2001). However in systems with high orbital eccentricity (i.e. $e \geq 0.6$), the disc truncation occurs at a much higher resonance radius which is very close to or slightly beyond the

critical lobe radius at periastron[4]. In such a system the disc truncation cannot be efficient, therefore allowing the neutron star to capture gas from the disc at every periastron passage and display regular type I X-ray outbursts.
It has been shown that these two models can explain very well the X-ray behaviour of the Be X-ray binaries, with one such example being the extensively studied, bright pulsating transient source 4U0115+63. This system was found by the *Uhuru* satellite survey (Giacconi et al. 1972), and consists of the strongly reddened Be star (V $\sim$ 15.5) (Johns et al. 1978; Hutchings & Crampton, 1981) V635 Cas, in a 24.3 day orbit (Rappaport et al. 1978) with the 3.6 second pulsar (Cominsky et al. 1978). Long term monitoring of the donor star in this system has shown that it undergoes cyclic changes with a period of 5yrs (Negueruela et al. 2001). Such variability is attributed to the losing and reforming of the circumstellar disc, where each cycle involves a low state when the disc is weak or absent and a high state when the disc is truncated, distorted and exhibits warped retrograde precession. During the high state the system exhibits type II X-ray outbursts in pairs where the first outburst occurs before the disc is strongly perturbed and the second outburst occurs after and leads to the eventual dispersal of the disc (Reig et al. 2007).

1.4 Masses of XRBs

One of the key parameters necessary to investigate X-ray binary systems is the masses of both the donor star and the compact companion. From the masses we are then able to infer the nature of the stars and further our understanding of the emission properties and mass transfer processes of the system. For example if the compact companion is found to have a mass $\geq 3M_{\odot}$, which is the theoretical maximum mass of a neutron star, then it is assumed to be a black hole. There are a number of other ways of distinguishing a black hole from a neutron star, such as observing the typical features exhibited by black hole systems (i.e. very soft spectra; fast variability; high energy power-law spectrum), but as such features can also exist in neutron stars they cannot be taken on their own as proof of a black hole, (Tanaka & Lewin, 1997). Therefore mass determination is believed

[4]This is not the case if the Shakura-Sunyaev viscosity parameter, α_{ss} is very low i.e. if $\alpha_{ss} << 1$) (Okazaki & Negueruela, 2001).

to be the most reliable method of identification if specific features, such as type I X-ray bursts seen in LMXBs or X-ray pulsations (i.e. specific to neutron stars), have not been observed. By constraining the mass and confirming the system as a black hole we are then able to study these black hole XRBs in greater detail. At present there are only 18 confirmed black hole candidates with masses $\geq$ $3M_{\odot}$, with only 4 of them being HMXBs and the rest being LMXBs (McClintock & Remmillard, 2004), and of these none have tightly constrained masses, see Figure 1.5). However if the compact companion is $< 3M_{\odot}$ and is found to be a neutron star then this is equally exciting, especially if the system is an eclipsing X-ray binary pulsar, as such systems offer a means of directly measuring the neutron star's mass. These measurements are very important as if the masses of neutron stars can be measured to high accuracy then we can constrain the equation of state (EoS) for nuclear matter and test theories that describe it. At present the EoS is not well constrained by nuclear theory (e.g. Lattimer & Prakash, 2000). These masses are also important to the study of XRBs in general and their formation and evolution. For example the neutron stars in binary radio pulsars have tightly constrained masses consistent with the Chandrasekhar limit of $1.4M_{\odot}$, (i.e. $\sim 1.35 \pm 0.04$ $M_{\odot}$, Thorsett & Chakrabarty, 1999) and those of milli-second radio pulsars with white dwarf companions are known to have higher masses (i.e. ~ 2.1 $M_{\odot}$, Nice et al. 2005). However the neutron star masses in eclipsing X-ray pulsars are not well constrained observationally (refer to Figure 1.5), and as they follow a different evolutionary path to that of radio pulsars they may therefore display a systematically different range of neutron star masses. Obviously before we can answer such questions, the neutron star masses need to be determined to within great certainty. At present only 10 such systems are currently known (refer to Table 1.1) and the neutron star masses in each case are not determined to high accuracy, refer to Figure 1.5.

1.4.1 Calculating the compact companion mass

The masses of the stellar components in a binary system may be determined as follows. The mass ratio q is defined as:

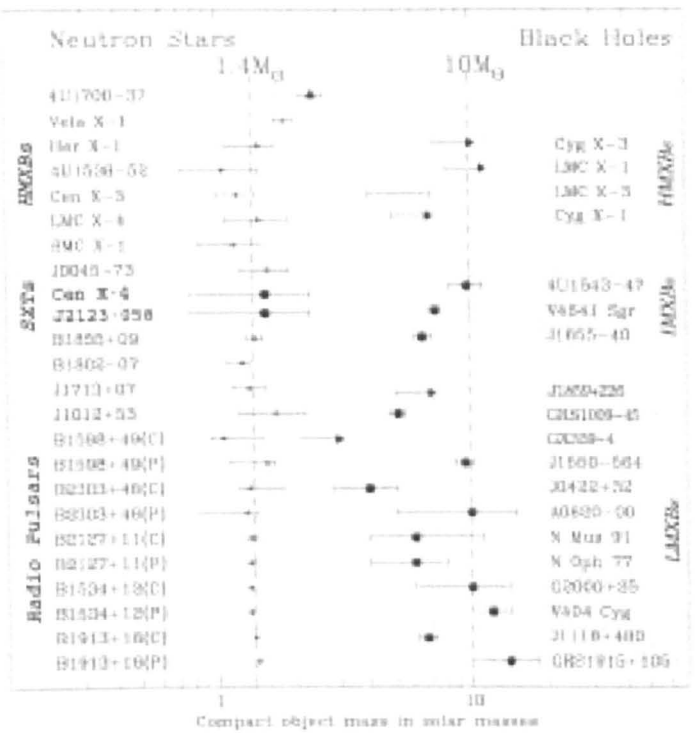

Figure 1.5: The mass distribution of neutron star's and black hole's, (Charles & Coe, 2003).

Table 1.1: Eclipsing X-ray Binary Pulsars

System	Type	P_{spin} (seconds)	P_{orb} (days)	Reference
Her X-1	LMXB	1.24	1.7	Deeter et al. 1981; Nagase, 1989
SMC X-1	HMXB	0.71	3.89	Primini et al. 1977
LMC X-4	HMXB	13.5	1.408	Kelley et al, 1983a; Nagase, 1989
Vela X-1	HMXB	283	8.965	Deeter et al. 1989; van der Klis et al. 1984
Cen X-3	HMXB	4.84	2.09	Primini et al. 1977; Kelley et al. 1983b
QV Nor	HMXB	529	3.73	Cominsky & Moraes, 1991
OAO 1657-415	HMXB	38.2	10.44	Nagase, 1989; Chakrabarty et al. 1993
EXO 1722-363	HMXB	413	9.7403	Tawara et al. 1989; Thompson et al. 2007
IGR J18027-2016	HMXB	139.612	4.6	Augello et al. 2003
XTE J1855-026	HMXB	361	6.067	Corbet & Mukai, 2002

$$q = \frac{M_x}{M_o} = \frac{K_o}{K_x} \tag{1.6}$$

where M_x is the mass of the compact companion, M_o is the mass of the donor star, K_x is the semi-amplitude of the compact companion's radial velocity curve, which can be found from pulse timing delays and K_o is the semi-amplitude of the donor star's radial velocity curve, which can be found from optical spectroscopy. In terms of the orbital parameters the masses of both components can be defined as:

$$M_o = \frac{K_x^3 P \left(1 - e^2\right)^{3/2} (1+q)^2}{2\pi G \sin^3 i} \tag{1.7}$$

and similarly,

$$M_x = \frac{K_o^3 P \left(1 - e^2\right)^{3/2} \left(1 + \frac{1}{q}\right)^2}{2\pi G \sin^3 i} \tag{1.8}$$

where e is the eccentricity, which in most close binaries can be approximated to zero, i is the inclination of the orbital plane to the line of sight, and P is the period of the orbit. A value for i can be found from the following geometrical approximation:

$$\sin i \sim \frac{\left(1 - \beta^2 \left(\frac{R_L}{a}\right)^2\right)^{\frac{1}{2}}}{\cos \theta_e} \tag{1.9}$$

where a is the separation of the centres of mass of the two stars, θ_e is the eclipse half angle and β is the ratio of the radius of the donor star to that of its Roche-lobe, R_L. R_L has been found (Plavec 1968; Avni 1976) to be reasonably well fitted by the expression[5] :

$$\frac{R_L}{a} \sim A + B \log q + C \log^2 q \tag{1.10}$$

[5]Note, this is only in the case of circular orbits as if the eccentricity, e, is not zero then the Roche-lobe radius will vary around the orbit.

where A, B, and C are parameters that depend on Ω, the ratio of the rotational period of the donor star to that of the orbital period. These in turn have been determined by Rappaport & Joss, (1983) to be:

$$A \sim 0.398 - 0.026\Omega^2 + 0.004\Omega^3 \tag{1.11}$$

$$B \sim -0.264 + 0.052\Omega^2 - 0.015\Omega^3 \tag{1.12}$$

$$C \sim -0.023 - 0.005\Omega^2 \tag{1.13}$$

From these equations we can see that the mass of both stars in the binary system can be determined, provided the system is eclipsing and that the other orbital parameters are known to high accuracy.

1.4.2 Problems with mass determination

As mentioned in Section 1.3.1 eclipsing X-ray binary pulsars provide us with a perfect situation in which all the necessary parameters to measure the masses of the stellar components are observable. However for the rest of the XRBs the situation is not so perfect. For example in the case of the black hole XRBs and some transient or weakly magnetized neutron star systems, there are no pulsations in which to probe the motion of the compact companion and hence determine its radial velocity semi-amplitude K_x. Therefore the mass of the donor star has to be deduced from its spectral type, which can then be used with the mass function equations to find M_x i.e.

$$f(M_x) \equiv \frac{PK_o^3}{2\pi G} = \frac{M_x sin^3 i}{\left(1 + \frac{1}{q}\right)^2} \tag{1.14}$$

$$f(M_o) \equiv \frac{PK_x^3}{2\pi G} = \frac{M_o sin^3 i}{(1+q)^2} \tag{1.15}$$

However this can lead to huge uncertainties if the spectral type is not known to high accuracy. This is relatively straight forward in the case of the intrinsically luminous HMXBs and the quiescent X-ray novae, however for the weakly magnetized persistent LMXBs a spectral analysis is extremely difficult. If the spectral type and hence mass of the donor star cannot be found then an absolute lower limit to the masses is set as $M_o \geq f(M_o)$ and $M_x \geq f(M_x)$, which corresponds to a zero mass compact companion viewed at the maximum inclination angle of $i = 90^o$. This extreme case (i.e. setting $i = 90^o$ to obtain lower mass limits) is quite often the case in the non-eclipsing systems as a value for i has to be estimated. Grazing eclipses are observed in some systems and estimates can be found from light curve modeling, which can provide more constrained limits on i. For example in high q systems (i.e. $q > 5$), typical of LMXBs, the ellipsoidal modulation is largely insensitive to q and can therefore provide excellent constraints on i, (Shahbaz et al. 2003).

In addition to the basic problem of obtaining the parameters necessary to determine accurate masses of the stellar components, there are also other characteristics of the system that will have an effect on the observed spectra and will therefore need to be taken into consideration. The most significant effect on the observed parameters is that of X-ray heating of the donor star by the X-ray source, which is what we will focus on in this thesis.

1.4.3 X-ray heating

In a binary system the stellar components orbit the centre of mass of the system and in addition the stellar components themselves have a centre of mass. Radial velocity measurements of the donor star should reflect its motion about the centre of mass of the system. However, If the donor star is affected by X-ray heating from the compact companion then the observed radial velocities may not represent the true motion about the centre of mass. To see why this is the case, consider the following. When we measure a radial velocity from a photospheric absorption line, we are in effect averaging the line across the whole face of the star that is facing us. Those parts of the star that are closer to the centre of mass of the binary will give a slightly smaller Doppler shift to the lines than those parts of the star that are further from the centre of mass of

the binary. In the case of an unheated donor star, the lines are of equal depth at all places on the face of the star that we see. So at any instant of time, the average radial velocity measured from the lines represents the speed of motion of the centre of the face of the donor star which is facing us. This 'centre of light then coincides with the centre of mass of the donor star. However, in the case of a heated donor star, the lines from the heated side of the star may have a different depth to the lines from the unheated face, such that the 'centre of light' does not coincide with the centre of mass of the donor star.

Due to the heating and temperature dependence of the spectral lines, the shift in line centre may vary significantly with the intensity of irradiation, and can therefore have one of two different effects on the observed radial velocity curve of the donor star. If the X-ray spectrum is soft, the X-rays will not be able to penetrate into the continuum forming layers and instead are absorbed at the surface of the donor star, so infilling the absorption lines. As a result, the effective 'centre of light' of the donor star integrated over the entire stellar disc is shifted away from the centre of mass of the system, such that the observed velocity amplitude is greater than the true Keplerian radial velocity amplitude, refer to Figure 1.6. Conversely, if the X-ray spectrum is hard the X-rays are either absorbed deep in the atmosphere of the donor star or directly reflected, causing the absorption lines from the heated atmosphere of the star to be stronger than they would otherwise be. As a result the effective 'centre of light' of the donor star integrated over the entire stellar disc is shifted towards the centre of mass of the system, and this reduces the observed velocity amplitude to be less than the true Keplerian radial velocity amplitude, refer to Figure 1.7.

X-ray heating is an effect that is typically much more significant in LMXB systems in which the optical component is of relatively low mass and surface temperature. However it is also of importance in HMXBs and can be particularly significant if the compact companion is a black hole.

1.5 Summary

We have shown that a range of different types of objects exist amongst the XRBs, displaying many different kinds of behaviour. As noted earlier, in the rest of this thesis we focus on determining compact companion masses in some

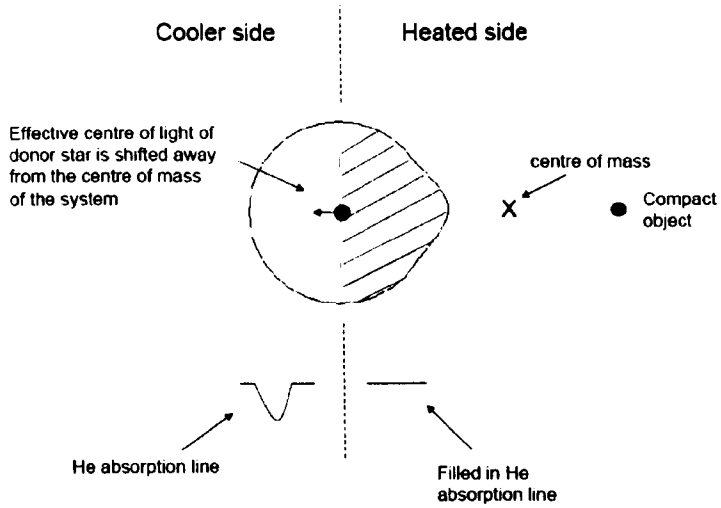

Figure 1.6: The effects of soft X-ray heating

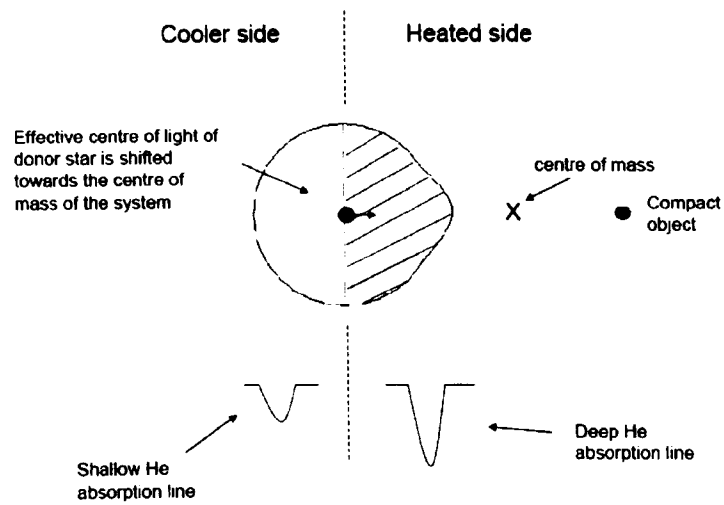

Figure 1.7: The effects of hard X-ray heating

individual systems and on understanding their behaviour. These investigations are carried out using optical spectroscopy and in the next chapter we explain the techniques necessary for analysing such data.

Chapter 2

Data reduction and analysis techniques

2.1 CCD reduction

The research carried out in this thesis utilizes optical spectroscopic observations, obtained from several ground based observatories. In all cases a charge-couple device array (CCD) is used to receive the information in the form of a two-dimensional image. However to obtain any useful scientific information from these two-dimensional images whether the datasets are photometric or spectroscopic, we must first translate the data into one-dimensional data so that we can then remove the 'additive' effects due to the instrumental response.

2.1.1 Bias removal

To avoid negative values in the readout process a pedestal level of several hundred ADUs (Analogue Digital Units) is added to the detector output signal. Then once the measured analogue voltage has been converted into a digitized sum of counts we can remove this bias level. However in removing this bias level we need to take into account both the temporal and spatial variations.

The temporal variations can be accounted for by using the data in the outer columns of the CCD image, known as the overscan region. The data in this region is averaged over all columns and fitted as a function of line-number. In most cases this fit is a simple constant, but if variations are significant then a low-order polynomial or spline function is fitted to avoid introducing unwanted noise into the image. In each case the fit is then subtracted from all columns in the frames including calibration frames. The spatial variations can be accounted for by taking a set of images with zero integration time, known as 'zero' or 'bias frames. These images will then give us information about the level of counts that have been superimposed on each image as well as the column to column variation in the structure of the bias level. Many of these 'zero frames are taken, which are then bias subtracted as above and averaged to obtain a mean zero frame. Finally the mean zero frame is subtracted from all the other frames.

2.1.2 Dark current subtraction

In some cases a signal may be generated in the CCD pixels due to the thermal motion of electrons. The signal is generated when no light is present and is therefore known as 'dark current'. As this thermal noise in the detector is proportional to the exposure time, for it to be removed a series of exposures with the shutter closed need to be taken with the same exposure time as the images to be corrected. These 'dark frames' are then subtracted from the other frames. In most cases the dark current is insignificant as the CCDs are cooled to liquid-nitrogen temperatures. In the work carried out in this thesis, none of the datasets have needed to be corrected for dark current.

2.1.3 Flat-fielding

The pixels of a CCD detector will have a varying sensitivity to a constant flux of light. This is due to irregularities introduced in the manufacturing process and causes each individual CCD to have a unique response. In addition to this effect, uneven illumination can occur due to either dust on the CCD equipment or from shadowing of the optics known as vignetting. In order to correct for these effects, we need to expose the CCD to a uniformly illuminated light source

such as an illuminated screen in the dome or the twilight sky. These images are known as flatfields and should be taken with the same instrumental setup as the 'real' data frames, and should also be taken throughout the night to account for any time dependence. The flatfield frames are then averaged to obtain a mean flatfield frame which is then scaled to a mean of unity with small deviations from unity reflecting the response variation on the pixels. This scaled mean flatfield frame is then divided into all the 'object' frames.

2.2 Spectroscopy

Spectroscopic observations give us information about how the light intensity from an object is distributed as a function of wavelength. Such data can then be used to infer the dynamics and more detailed characteristics of the object. In most cases the spectrograph uses a grating as the dispersing element, which separates the beam into one or more orders according to the grating equation:

$$d\,(\sin i + \sin\theta) = m\lambda \tag{2.1}$$

where λ is the wavelength, m is the order number, θ is the angle of diffraction, i is the angle of incidence and d is the distance between adjacent grooves. Therefore a coarse grating will produce many orders and a fine grating will produce only one or two orders. The type of grating used and number of orders obtained will also effect the angular dispersion of the spectrum i.e.

$$\frac{\delta\theta}{\delta\lambda} = \frac{1}{\cos\theta}\frac{m}{d} \tag{2.2}$$

So by working in higher spectral orders, a higher angular dispersion can be obtained.

The spectral resolving power of the spectrograph (i.e. its ability to separate two wavelengths) is also dependent on the number of spectral orders:

$$\frac{\lambda}{\Delta\lambda} = \frac{m}{d}W_g = Nm \tag{2.3}$$

where N is the total number of rulings on the grating and W_g is the width of the grating.

2.2.1 Long-slit spectral extraction

The spectrograph uses a slit to limit the amount of light entering, therefore acting as a point source and reducing the amount of overlap between spectral features. The resolving power of a spectrograph is not only limited by the grating characteristics but also also by the resolving power of the optics and the projected slit width. To increase the resolving power and allow the spectral features to be distinguished more easily the slit width is decreased.

In most cases a fine grating is used allowing either one or two orders, where each order is dealt with separately. The resultant target frame is then reduced, as outlined above, so that we are able to extract the one-dimensional spectra. To extract the spectra we first have to find and define the extraction window of our spectra, which can be done manually by collapsing the spectrum into the spatial direction and measuring the width of the spatial profile, refer to Figure 2.1.

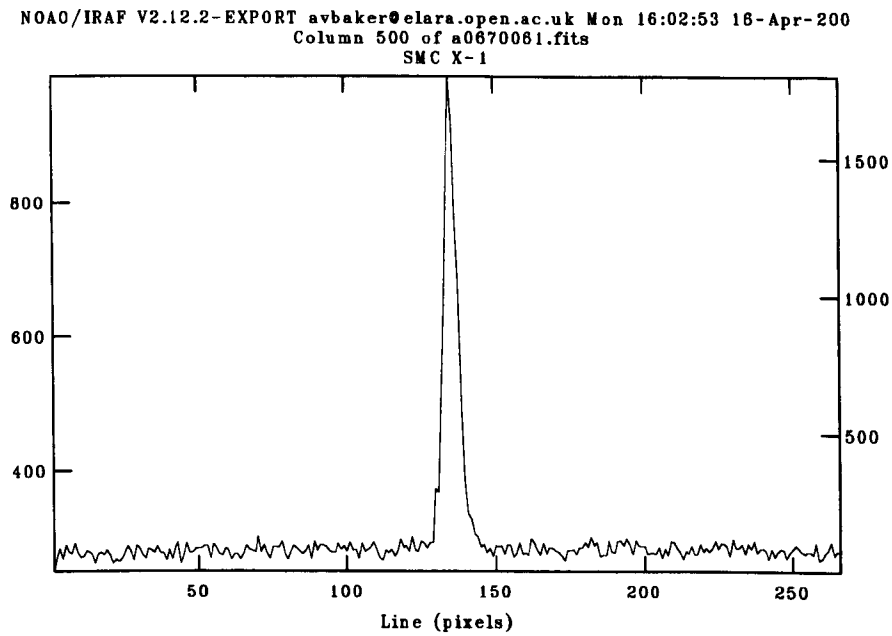

Figure 2.1: An example of a cross-section of the dispersion profile of SMC X-1.

We then need to trace the centre of the spatial profile as a function of the dispersion axis, as in most cases the dispersion direction will not be parallel to the CCD x- or y-axis. This shift of the centre of the spatial profile is due to either the camera optics, the gratings and/or the differential atmospheric refraction. However we can correct for such effects by fitting a polynomial function to the dispersion direction. Each pixel is weighted according to its relative position within the order (i.e. pixels towards the outer edge of the order will have a lower signal-to-noise ratio). The spectrum is then finally extracted by summing the weighted pixel contribution over the spatial profile (centred spatially based upon the value that the trace is at that point) to yield a value for each element in the dispersion direction. The contributions from the sky background, which are based on polynomials fitted to the selected sky regions in the spatial direction, are then subtracted from these values. The algorithm used for this extraction process, known as the 'optimal extraction' algorithm, was first developed by Keith Horne (1986) and makes use of known noise characteristics of the CCD to do a mathematically optimal extraction. It is also capable of eliminating cosmic rays and bad pixels from the spectrum by detecting the distortion they produce in the spatial profile.

2.2.2 Echelle spectral extraction

As mentioned in Section 2.2 and with reference to Equations 2.1 – 2.3, higher spectral resolution can be achieved with the use of a coarsely-ruled, high-angle (i.e. blaze angle) grating. An echelle spectrograph is based on such a setup, thus allowing higher orders and hence broader wavelength coverage to be observed at high resolution. However by introducing more orders, the amount of overlapping between orders increases i.e. the free spectral range ($\Delta\lambda_{fsr} = \lambda/m$), decreases with higher orders. To overcome this problem a second low-order cross dispersing element is used. This second grating disperses the light in a direction perpendicular to that of the first grating, separating and stacking the spectral images of the different orders above one another. The resulting image on the CCD camera is a series of roughly parallel high-dispersion spectra. The reduction and extraction of echelle data is therefore much more complicated than that of ordinary spectroscopic data. Firstly a few central columns or rows

(depending on which is perpendicular to the orders) are selected and combined, such that the reduction software can assign each peak an order number (e.g. Figure 2.2).

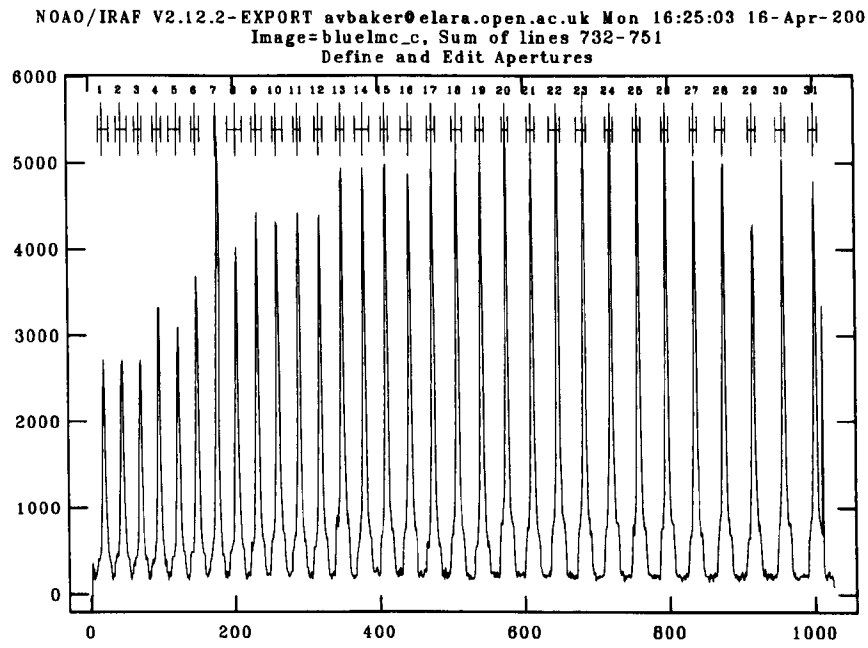

Figure 2.2: An example of a cross-section of the dispersion profile of LMC X-3.

Each order is then traced and extracted as outlined in sect 2.2.1. The contributions from the sky background are taken from the inter-order regions, and are largely the result of scattered light from the echelle, rather than from the sky. The data used in this study were obtained using either standard single slit or echelle spectroscopy.

2.2.3 Wavelength calibration

To fit a wavelength scale to the spectrum a correspondence between pixel number and wavelength needs to be defined. This is done by taking observations of calibration arc spectra i.e. observations of a neon or thorium-argon lamp. We are then able to identify a large number of arc lines and hence determine a correspondence between wavelength and pixel position by fitting a low order polynomial to the arc spectrum. However due to instrumental flexure as

the telescope moves across the sky the pixel to wavelength correspondence will change. To account for this time dependence, observations of the calibration arc spectra are obtained repeatedly through the night. The wavelength scale of each object spectrum is then interpolated from the wavelength scale of two neighbouring spectra. In the case of echelle data, several spectral lines in each order need to be defined to obtain an accurate calibration.

2.2.4 Normalization

Once our spectra have been wavelength calibrated we are ready to start identifying the absorption and/or emission lines, and begin the analysis of the data. However, at this point the spectra still show the intensity response of the wavelength. In order to remove this effect, so that we may see the relative intensity of the spectral lines, we need to normalize the continuum to a mean level of unity. This is done by fitting a smooth curve to the continuum and then dividing the spectrum by this smooth curve.

2.3 Measuring the radial velocity

The radial velocity of an object is its velocity in the direction of the line of sight, and therefore in a binary system its value will change as the star travels through its orbit. This changing radial velocity is reflected in the light from the stellar components, which is Doppler shifted towards and away from the line of sight according to the following equation:

$$\frac{\Delta\lambda}{\lambda} = \frac{v}{c} \tag{2.4}$$

By measuring this Doppler shift in the spectral lines of the stellar spectra we are therefore able to calculate its radial velocity as a function of time. From which the semi-amplitude and hence masses of the stellar components can be determined.

2.3.1 Gaussian fits

The easiest way to determine the Doppler shift in a spectral line and hence the radial velocity, is by simply fitting a Gaussian function to the data and comparing the line centre with that of the rest wavelength i.e. Figure 2.3.

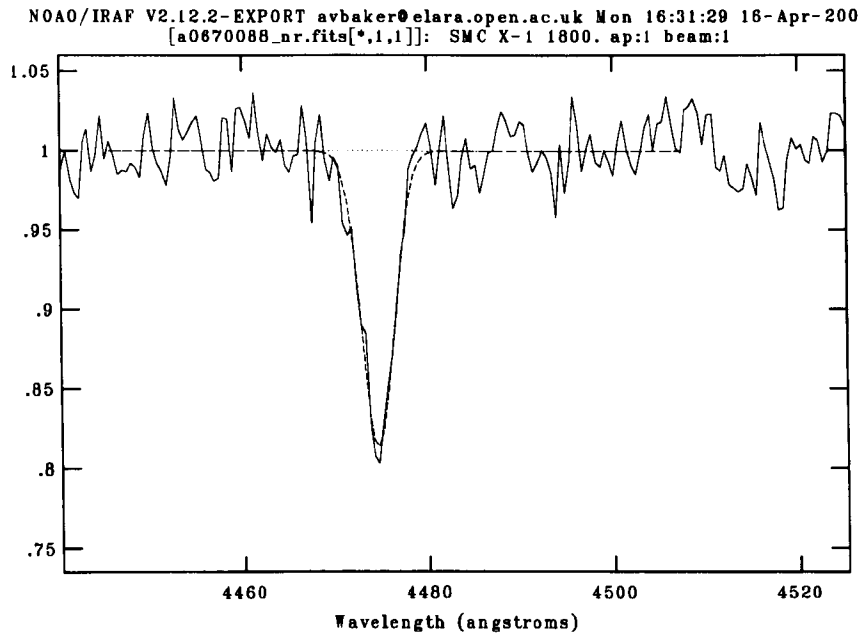

Figure 2.3: An example of a Gaussian fit to the line profile of He 4471, from SMC X-1

A Gaussian function is of the form:

$$f(x) = ae^{-(x-b)^2/2c^2} \tag{2.5}$$

where a, b and c are all free parameters which define the overall shape of the distribution. The parameter a defines the height of the Gaussian peak, b defines the position of the centre of the peak and c is related to the full-width-half-maximum (FWHM) by:

$$FWHM = 2\left(\sqrt{2\ln(2)}\right)c \tag{2.6}$$

Defining the correct continuum level in the normalization procedure, is therefore very important, as any error will result in a Gaussian profile not representative of the true data and hence inaccurate spectral line measurements.

2.3.2 Cross-correlation

To achieve more accurate results we can use the technique of cross-correlation. The purpose of cross-correlation here is to determine the relative shift in wavelength (and hence velocity) between the spectrum of the target and the spectrum of the radial velocity standard star. Traditionally such a cross-correlation would be done by multiplying the two spectra together, on a point by point basis at a whole range of wavelength shifts, and then summing the point-by-point products at each shift in order to find out the shift for which the cross-correlation is maximised. This process is referred to as a convolution between the two spectra, and can be speeded up and simplified by doing the cross correlation in the spatial frequency domain, rather than using the spectra themselves. To do this, the fast Fourier transforms (FFTs) of each spectrum are calculated. The FFTs are then simply multiplied together, and we then determine the inverse Fourier transform of the result. This is the cross-correlation function. Symbolically, if 'A' is the spectrum of the target and 'B' is the spectrum of the radial velocity standard star, then:

$$A \otimes B = \text{Cross Correlation Function} \tag{2.7}$$

where the $\otimes$ symbol denotes a convolution operation.

and,

$$FT\,(A) \times FT\,(B) = FT\,(\text{Cross Correlation Function}) \tag{2.8}$$

The resulting CCF therefore shows the degree of correlation for increasing and decreasing lags between the target and comparison spectra i.e. Figure 2.5.

As the radial velocity of the standard star is known, the peak value in the CCF occurs at a velocity difference where there is a high correlation between the spectra. Such a procedure is generally carried out with specific analytical software. The comparison spectrum is that of a standard star with a known radial velocity, whose spectral type is the same as or similar to that of the target star.

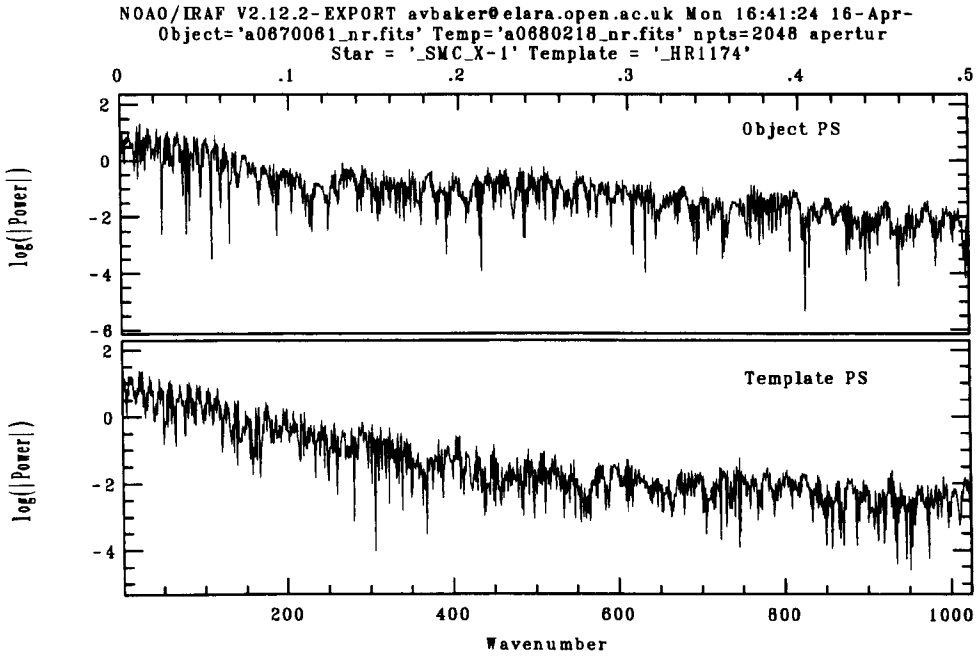

Figure 2.4: An example of the Fourier transform of SMC X-1 and a template spectrum.

2.3.3 Barycentric and heliocentric corrections

In calculating radial velocities which are plotted against time, the observed time of each determined radial velocity, first needs to be corrected to a heliocentric/barycentric time. The observed time is assumed to be made at the centre of the Earth frame of reference. Therefore for reference to the solar system barycentre/heliocentre a time shift needs to be applied.

As well as the observed time, the observed radial velocity also needs to be corrected to a heliocentric radial velocity. This is done by correcting for the Doppler shift due to the motion of the observer in the direction of the observation. The

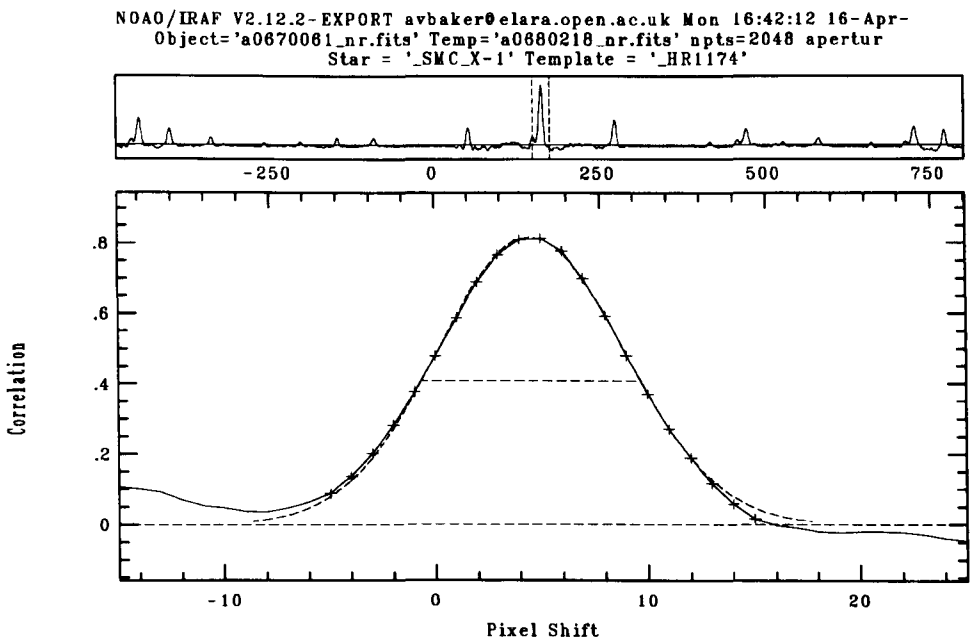

Figure 2.5: An example of the cross correlation function for SMC X-1 with a template spectrum.

components of the observer's motion are those due to the Earth's rotation (diurnal velocity), the motion of the Earth centre about the Earth-Moon barycentre (lunar velocity), the motion of the Earth-Moon barycentre about the centre of the Sun (annual velocity) and the motion of the Sun relative to some specified standard of rest (solar velocity).

2.4 LIGHT2

LIGHT2 is a sophisticated light curve synthesis program developed by Hill (1988), which we used in the course of analysing the data from SMC X-1 presented in Chapter 3 and the data from LMC X-3 presented in Chapter 4. The initial program, known as LIGHT, was written in 1979 (Hill, 1979) and was restricted to contact or under-contact systems. This new and improved version is identical to LIGHT except for its operation and the fact that with the incorporation of Rucinski's (1969) code it now allows for over-contact systems. The program is based on Roche geometry, which is specified by the polar values of the

radii and by the mass ratio q, and uses Gauss-Legendre quadrature to approximate the theoretical light curve. For effective temperatures, $T_{eff} < 8000°$K the atmospheres of Carbon & Gingerich (1969) are adopted and for $T_{eff} > 8000°$K those of Kurucz et al. (1974) are adopted. The effects of limb darkening are also taken into account, where the values from Carbon & Gingerich (1969) are used. Mutual heating of the binary components, known as the 'Reflection effect' can in some cases manifest itself in the light curves and therefore also needs to be accounted for. In LIGHT2 such effects are computed according to the methods outlined by Hill & Hutchings (1970; 1973), and Hutchings (1968).
They assume that the additional contribution to the source function at any point P of the irradiated atmosphere due to the irradiating atmosphere is additive and is computed according to Sobieski (1965):

$$F(\mu_0, \tau) = S[\mu_0^2 + 2/3\mu_0 - (\mu_0^2 - 1/3)\, e^{-\tau/\mu_0}] \tag{2.9}$$

where S is the total bolometric flux incident at point P, τ is the optical depth and $\cos^{-1}\mu_0$ is the mean angle of incidence of this flux relative to the surface normal.

The incidence flux, S at any point P of the irradiated star is found by following the equation of Kopal (1959), where the integration is performed over the visible surface of the irradiating star:

$$S = \int I\left(\theta'\right) \frac{\cos\xi \cos\theta'}{\rho'^2} \delta\sigma \tag{2.10}$$

where $I\left(\theta'\right)$ is the emergent bolometric intensity at any point on the irradiating star as seen from point P, θ' is the corresponding emergent angle, $\delta\sigma$ is the surface element on the irradiating star, ξ is the angle between the surface normal of the irradiated star and the horizontal plane between the two stars at point P, where ρ' is this distance between the two stars at point P.

The effects of such irradiation, as outlined in Section 1.4.3, can also significantly affect the spectroscopic analysis of the radial velocities and these too need to be corrected for. LIGHT2 generates such non-Keplerian velocity corrections by

averaging a velocity based on contributions from elements of the giant star's (i.e the donor star) projected stellar disc, where each element is weighted according to the flux at that point i.e.

$$< V >= \frac{\sum I \cdot V_{rot}}{\sum F} \tag{2.11}$$

where V_{rot} is the projected rotational velocity, I is the intensity and F is the flux at any point P of the irradiated star.

It is this mode in which LIGHT2 was used in this thesis.

Chapter 3

The mass of the neutron star in SMC X-1

This chapter presents new optical spectroscopy of the eclipsing X-ray binary pulsar SMC X-1. From the He I absorption lines, taking heating corrections into account, the radial velocity semi-amplitude of the donor star, Sk 160 and hence the masses of the stellar components are determined. It is also shown that the He II 4686 Å emission line is coming from the vicinity of the neutron star, but with a radial velocity amplitude somewhat less than that of the neutron star itself.

3.1 Overview of SMC X-1

SMC X-1 is an intermediate mass eclipsing X-ray binary pulsar located in the Small Magellanic Cloud (SMC). It was originally detected by Price et al. (1971), when X-rays from 'an extended region or set of sources' in the SMC were discovered in a rocket observation. Later observations, with the *Uhuru* satellite, identified a discrete source in the 'wing' of the SMC and named it SMC X-1 (Leong et al. 1971). The binary nature of SMC X-1 was then established when further analysis of these and additional *Uhuru* observations by Schreier et al.

(1972), revealed the presence of X-ray eclipses. The optical counterpart was identified as the B0 supergiant, Sk 160, by Webster et al. (1972), and was later confirmed by Liller (1972), who observed an optical intensity variation with the same period as that of the X-ray eclipses. By observing the times of ingress and egress of these X-ray eclipses, an eclipse half angle, of $\theta_e = 28.2° \pm 0.9°$, was measured corresponding to an eclipse duration of 0.610 ± 0.019 days (Primini et al. 1976). X-ray pulsations from SMC X-1 were discovered in rocket and *Apollo-Soyuz* observations by Lucke et al. (1976). Pulse timing studies by Primini et al. (1977) allowed the radial velocity semi-amplitude of the X-ray component to be measured as 301.5 km s^{-1}. They also showed that the orbit is highly circularized, with very low eccentricity $e \leq 0.0016$, an orbital period of $P = 3.892$ days and a pulse period of $P_{pulse} = 0.72$ seconds. Later pulse timing studies, by Levine et al. (1993), gave a value of $(a_x \sin i) = 53.4876 \pm 0.0004$ light seconds for the projected semi-major axis and a corresponding limit on the eccentricity of $e < 0.00004$.

The X-ray spectrum is hard and can be described as a power-law with an exponential cut off, exhibiting broad emission lines and a soft excess. This soft component can be modelled as black-body or thermal bremmsstrahlung emission (Marshell et al. 1983; Woo et al. 1995; Wojdowski et al. 1998; Nagase, 2002). The X-ray emission has been shown to exhibit both high and low intensity states (Bonnet-Bidaud & van der Klis, 1981), with aperiodic variations on timescales from tens of milli-seconds to months (Wojdowski et al. 1998). As well as these aperiodic variations a long quasi-stable super-orbital period of 50 – 60 days has been observed, which is believed to be the result of obscuration of the neutron star by a precessing accretion disc, similar to that in Her X-1, (Wojdowski et al. 1998). The presence of an accretion disc was first suggested in 1977 by van Paradijs & Zuiderwijk (1977), who claimed that ellipsoidal light variations and X-ray heating effects were insufficient to account for the observed light curve. The mode of mass transfer in SMC X-1 is believed to have significant contributions from Roche-lobe overflow (Khruzhina & Cherepashchuk, 1983; van Paradijs & Kuiper, 1984), as the stellar winds observed in Sk 160 are not strong enough to power the accretion from the secondary onto the primary (Hammerschlag-Hensberge et al. 1984).

Previous attempts to derive the orbital parameters of SMC X-1 have been made by Primini et al. (1976), Hutchings et al. (1977), Reynolds et al. (1993) and

most recently by van der Meer et al (2005; 2007). The first two studies were based on image-tube photographic spectroscopy, the latter of whom found a mass for the neutron star of $M_x = 1.02 \pm 0.20 M_\odot$. The later study by Reynolds et al. (1993) used Anglo-Australian Telescope (AAT) observations and found $K_o = 23.0 \pm 1.9$ km s^{-1}. They were the first to account for heating of the donor star by the X-ray flux from the neutron star. This heating has the effect of significantly altering the observed radial velocity amplitude and so distorting the inferred neutron star mass. When Reynolds et al. (1993) applied heating corrections they found a revised amplitude of $K_o = 27.5 \pm 1.9$ km s^{-1} and hence a mass for the neutron star of $M_x = 1.6 \pm 0.1 M_\odot$. However van Kerkwijk et al. (1995) pointed out the uncertainties introduced in this approach by not allowing for the presence of an accretion disc, whose shadow on the face of the donor star may reduce the effect of X-ray heating. van Kerkwijk et al. (1995) therefore suggested that any corrections for heating effects may be an over estimation, and so chose to ignore any heating correction entirely, instead simply assuming a larger uncertainty on the measured radial velocity amplitude. This led them to suggest a mass for the neutron star of $M_x = 1.17^{+0.36}_{-0.32} M_\odot$. The most recent analysis by van der Meer et al. (2005; 2007) also found a low value for the neutron star mass of, $M_x = 1.05 \pm 0.09 M_\odot$ and $M_x = 1.06 \pm 0.1 M_\odot$ respectively. They too did not account for any heating correction in their analysis, but in the latter study they obtained radial velocities from high resolution spectra of individual lines and only took into account values found from spectral lines that did not appear to suffer distortions. It should also be noted that each of the previous mass determinations implicitly assumed the donor star to fill its Roche-lobe in order to solve for the system parameters, so the masses are in effect upper limits in each case.

3.2 Observations

Observations of Sk 160 were obtained by Dr Hannah Quaintrell using the 1.9 metre telescope at the Sutherland Observatory, South Africa. The grating spectrograph was used with a reciprocal dispersion of 0.5 Å/pixel, spanning the wavelength range 4300 - 5100 Å. Over the course of three weeks, from the 30th August - 18th September 2000 (1 week on, 1 week off, 1 week on) we obtained

56 usable spectra on 9 nights, mostly during the first week of observations (see Table 3.1). We note that these observations just preceded the coordinated *Hubble Space Telescope (HST)/ Chandra* campaign on SMC X-1 reported by Vrtilek et al. (2001), and occurred during a low state of the $\sim$ 55 day super-orbital cycle, as indicated by the *Rossi X-ray Timing Explorer (RXTE) All Sky Monitor (ASM)* lightcurve.

We also observed the radial velocity standard star HD6655, an F8V star with an accurately known radial velocity of +15.5 km s^{-1}, on each night. In addition, on the last night, we observed a template star of similar spectral type to Sk 160, for cross-correlation with our target spectra. This was HR 1174, a B3V star, which was also used as the cross-correlation template by Reynolds et al. (1993).

3.3 Data reduction

All spectra were reduced using standard IRAF routines and extracted using optimal extraction procedures as outlined in Section 2.1 and 2.2. A median, continuum normalized spectrum of Sk 160 is shown in Figure 3.1, indicating some prominent He I and Hydrogen Balmer lines, as well as the regions of the spectrum used for cross-correlation. Note the apparent double peak in the He II 4686 Å emission line is the result of sampling this line mostly at the quadrature phases of the system. The median spectrum therefore shows two peaks separated by $\sim$ 8 Å corresponding to a $\sim$ 500kms^{-1} velocity difference.

In order to check the stability of the observations from night to night, we cross-correlated the individual spectra of the radial velocity standard star HD 6655 against a single spectrum of this object from the middle of the run. These were all consistent with zero shift from night to night.

Having confirmed the stability of the system, each individual spectrum of Sk 160 was cross-correlated against the median spectrum of the template star, HR 1174. Only regions between 4370 - 4500 Å, 4700 - 4735 Å and 4900 - 5060 Å were used, spanning several He I absorption lines. These regions were selected to exclude the Balmer lines which were found to show large, random changes from one spectrum to the next, and no clear trend in their radial velocities. It is well known that Balmer lines in high mass stars may be contaminated by emission

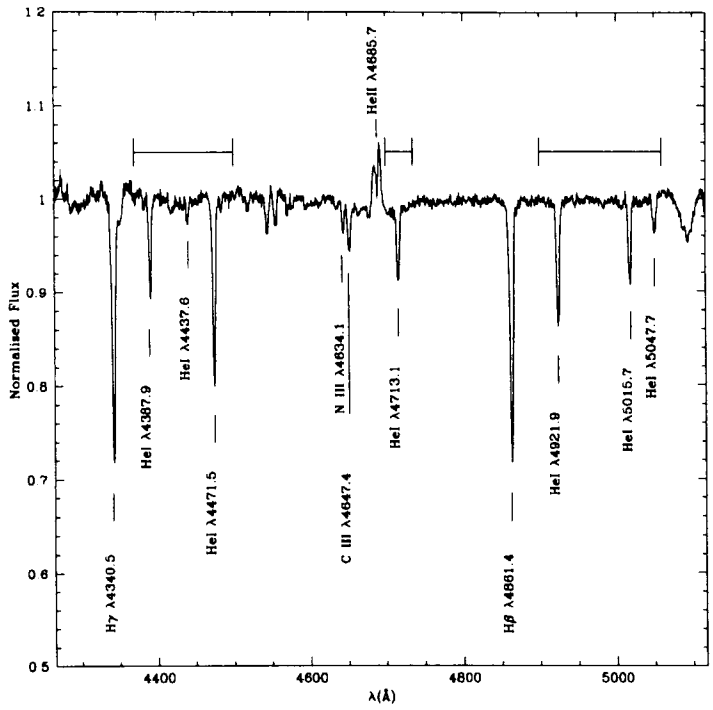

Figure 3.1: The median, continuum normalized spectrum of Sk 160. The horizontal bars indicate the regions of the spectrum containing He I absorption lines used for cross-correlation and determination of radial velocities.

from the stars wind and so may not accurately reflect the orbital radial velocity in a binary system. The extent of the emission contamination depends on the strength of the stellar wind and is reduced for higher level Balmer transitions. Final heliocentric radial velocities corresponding to each spectrum of Sk 160 were calculated from the cross-correlation results by applying the heliocentric velocity corrections and then offsetting the result by the radial velocity of HR 1174, measured by fitting Gaussians to the He I lines in its spectrum as +16.7 km s^{-1}. These final radial velocities are listed in Table 3.1 along with their 1 σ uncertainties, and plotted in Figure 3.2.

Orbital phases corresponding to each spectrum were calculated using the ephemeris from Wodjdowski et al. (1998), which gives the centre time of the Nth eclipse as:

$$t_N/MJED = 42836.18278(20) + 3.89229090(43)N - (6.953(28) \times 10^{-8})N^2 \tag{3.1}$$

Numbers in brackets indicate the uncertainties in the last decimal places in each case. The orbital period at the time of our observations, $\sim$ 2300 periods after the reference time of this ephemeris, is $P = 3.891971(1)$ days. In Table 3.2, and included in Figure 3.2, are the radial velocity measurements of Reynolds et al. (1993), with phases calculated according to the revised ephemeris above.[1]

3.4 Data analysis

3.4.1 Fitting the raw radial velocity curve

The data shown in Figure 3.2 were fitted with a simple sinusoid allowing just the mean level (γ) and semi-amplitude (K_o) as free parameters. The best fit was found by minimizing the reduced chi-squared value, which gave $\chi^2_r = 0.99$, indicating that the data are well fit by this function and that the uncertainties are of an appropriate magnitude. This resulted in the semi-amplitude of the

[1]Note that Reynolds et al. (1993) originally referred their phase zero to maximum radial velocity, rather than to the eclipse as is done here.

Table 3.1: The raw and heating-corrected He I absorption line heliocentric radial velocity (RV) data for Sk 160 resulting from the August/September 2000 observations at SAAO. Also shown are the heliocentric radial velocities measured from the He II 4686Å emission line.

MJD	Phase	He I RV_{raw} (km s^{-1})	1σ uncertainty (km s^{-1})	He I RV_{corr} (km s^{-1})	He II RV_o (km s^{-1})
51786.976	0.715	130	13	126	429
51786.999	0.721	134	11	129	410
51787.022	0.727	139	13	134	423
51787.069	0.739	141	14	136	413
51787.091	0.745	145	11	139	436
51788.808	0.186	207	9	209	-41
51788.847	0.196	195	10	198	-55
51788.870	0.202	196	12	199	-36
51788.892	0.208	196	11	199	-57
51788.932	0.218	189	14	193	-92
51788.955	0.224	187	17	190	-70
51788.977	0.230	181	12	185	-93
51789.000	0.235	174	14	178	-119
51789.022	0.241	168	13	172	-91
51789.045	0.247	164	13	169	-100
51789.068	0.253	166	14	172	-141
51789.108	0.263	184	12	189	-136
51789.130	0.269	169	13	174	-106
51790.845	0.709	162	12	157	436
51790.867	0.715	167	13	162	408
51790.889	0.721	157	14	152	422
51790.911	0.726	162	13	157	418
51791.094	0.773	156	12	152	365
51791.116	0.779	156	14	153	413
51791.138	0.785	150	14	146	414
51791.845	0.966	163	12	164	301

MJD	Phase	He I RV_{raw} (km s^{-1})	1σ uncertainty (km s^{-1})	He I RV_{corr} (km s^{-1})	He II RV_o (km s^{-1})
51791.896	0.979	191	19	191	190
51791.925	0.987	193	16	193	274
51791.979	0.001	184	14	184	247
51792.002	0.007	178	10	178	222
51792.024	0.012	182	10	182	227
51792.046	0.018	184	10	184	256
51792.091	0.030	188	10	188	221
51799.819	0.015	206	16	206	260
51801.817	0.528	189	14	190	
51802.774	0.774	161	13	157	
51802.792	0.779	178	15	174	
51802.811	0.784	165	21	161	351
51802.829	0.789	160	20	157	370
51802.847	0.793	195	16	192	
51802.865	0.798	157	16	154	426
51802.884	0.803	158	18	155	427
51803.083	0.854	167	15	166	
51804.836	0.304	183	20	187	
51804.854	0.309	193	26	196	-116
51804.910	0.323	192	12	195	-81
51804.928	0.328	186	15	188	
51804.947	0.333	164	15	167	
51804.966	0.338	191	11	194	
51804.994	0.345	186	10	188	
51805.013	0.350	188	13	190	
51805.031	0.354	196	11	197	
51805.049	0.359	196	14	197	
51805.068	0.364	193	9	194	
51805.086	0.369	203	11	205	
51805.841	0.562	173	14	174	335

Table 3.2: Reynolds et al. (1993) radial velocity data for Sk 160, with phases and heating corrections matching those adopted for our observations.

MJD	Phase	RV_{raw} (km s^{-1})	RV_{corr} (km s^{-1})
47811.391	0.250	206	211
47811.424	0.259	193	198
47811.441	0.263	195	200
47811.457	0.267	193	198
47811.546	0.290	197	202
47812.390	0.507	171	171
47812.450	0.522	164	164
47813.383	0.762	149	145
47813.391	0.764	153	149
47813.427	0.773	154	150
47813.462	0.782	149	145
47813.496	0.791	151	148
47814.379	0.018	166	166
47814.388	0.020	170	170
47814.470	0.041	194	194
47814.480	0.044	176	176
47814.557	0.064	174	174
47814.571	0.067	187	187

radial velocity curve as $K_o = 18.0 \pm 1.8\text{kms}^{-1}$ and the systemic velocity as $\gamma = 174.1 \pm 1.5\text{kms}^{-1}$. The 1σ uncertainties in each of the fitted parameters are calculated in a standard way as the change in a given parameter which individually results in a change of $+1$ in the χ^2_r value, away from the best-fit value. These values are listed in Table 3.3.

However, if we look at Figure 3.2 in detail we can see that there appears to be a trend in the data around phase 0.2 – 0.3 where the radial velocity becomes progressively smaller over the course of one night. This trend consists of the 13 data points from MJD 51788.808 – MJD 51789.130. To exclude the effects of this anomalous data a simple sinusoid was re-fitted to the remaining data points, refer to Figure 3.3. As before the best fit was found by minimizing the reduced chi-squared value, which gave $\chi^2_r = 0.99$ and resulted in the semi-amplitude of the radial velocity curve as $K_o = 21.0 \pm 1.9\text{kms}^{-1}$ and the systemic velocity as $\gamma = 175.9 \pm 1.4\text{kms}^{-1}$. These values are listed in the upper part of Table 3.4.

3.4.2 System parameters from the raw He I radial velocity curve

The masses of the stellar components were calculated according to the method outlined in Section 1.4.1, using the Monte-Carlo method for uncertainty determination. This involved calculating 10^6 solutions with input values drawn from a Gaussian distribution within the respective 1σ uncertainties of each parameter. The final values were then calculated as the mean result of these 10^6 solutions, with the 1σ uncertainties given by the root-mean-square deviation in each case.

The input parameters used for the calculation are as follows: $P = 3.891971(1)$ days, based on the ephemeris of Wojdowski et al. (1998); $\theta_e = 28.2 \pm 0.9°$ (Primini et al. 1976); $e < 0.00004$ (Levine et al. 1993); $\Omega = 1.0$; $K_o = 18.0 \pm 1.8\text{kms}^{-1}$, found from the uncorrected radial velocity curve; and

$$K_x = \frac{2\pi}{P} \frac{a_x \sin i}{(1-e^2)^{1/2}} = 299.607 \pm 0.002\text{kms}^{-1} \tag{3.2}$$

when taking $a_x \sin i = 53.4876 \pm 0.0004$ lt seconds, (Levine et al. 1993).

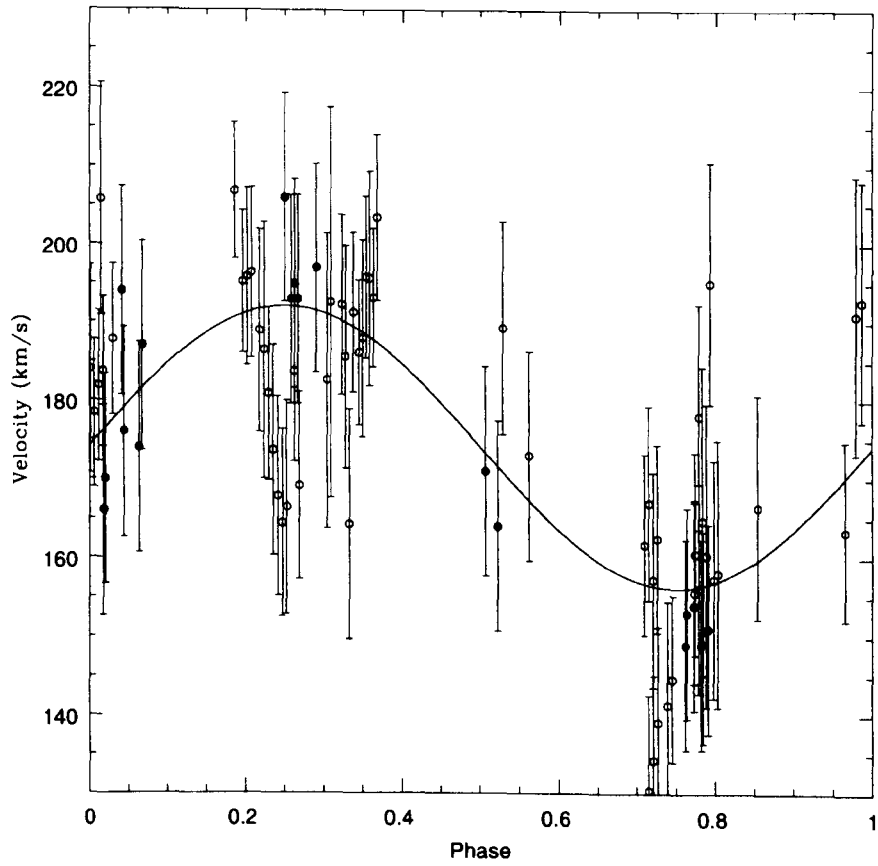

Figure 3.2: The uncorrected He I absorption line radial velocity curve for Sk 160. Our data are shown as open circles and those of Reynolds et al. (1993) are shown as filled circles. The best fit to the combined data set is indicated by the solid line. Note, the error bars indicate the scaled (by ~ 0.95) errors necessary to minimize the reduced chi-squared to unity.

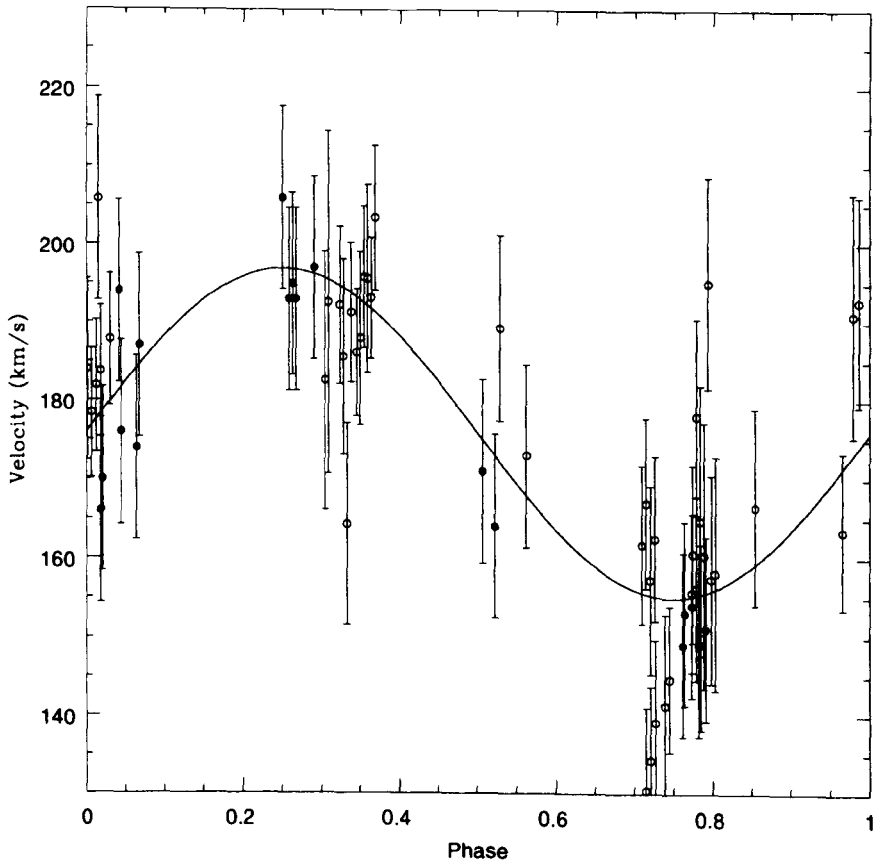

Figure 3.3: The uncorrected He I absorption line radial velocity curve for Sk 160, with the anomalous data excluded. Our data are shown as open circles and those of Reynolds et al. (1993) are shown as filled circles. The best fit to the combined data set is indicated by the solid line. Note, the error bars indicate the scaled (by ~ 0.84) errors necessary to minimize the reduced chi-squared to unity.

The values for β and i in Equation 1.9 cannot be obtained independently from observations. We can assume that β will not vary much as the system has a circular orbit, but in the absence of an exact value for R_L we cannot determine β uniquely. Since mass transfer in SMC X-1 has significant contributions from Roche-lobe overflow, but Sk 160 is unlikely to be overfilling its Roche-lobe, we can however set an upper limit of $\beta \leq 1.0$, which in turn sets a lower limit on i. Conversely if we set an upper limit on the inclination angle of $i = 90°$ and assume the donor star is under-filling its Roche-lobe, we obtain a lower limit for β. Given these two limits on each of β and i, upper and lower limits on the mass of both the neutron star and the donor star may be calculated. The results are shown in the upper part of Table 3.3, where solutions lying between the two extremes, corresponding to intermediate values of i and β, are of course also valid.

It should be noted that these mass determinations were originally carried out and published before the significance of the anomalous data had been realised. The mass determinations have now been carried out using the new value for K_o, found by excluding the 13 anomalous data points. These results are shown in the upper part of Table 3.4.

3.4.3 X-ray heating corrections

As was outlined in Section 1.4.3, X-ray heating of the donor star by the X-ray source can lead to erroneous radial velocity determinations. Therefore, in order to determine accurate masses from radial velocity curves, these non-Keplerian deviations must be accounted for.

To correct for the heating effects we followed the example of Reynolds et al. (1993) and ran models using LIGHT2 (Hill 1988), refer to section 2.4. SMC X-1 is known to be a hard X-ray source and therefore the observed radial velocity amplitudes will be less than the true Keplerian radial velocity amplitude, refer to Section 1.4.3. So, in the case of SMC X-1, the heating corrections must be subtracted. We note that SMC X-1 does have a soft component, therefore in applying heating corrections assuming the effects of hard X-rays may result in a larger heating correction than necessary. However as the emission is predominently in the hard energy range any effects from the soft component can be

assumed negligible.

Due to the limitations of the code we were unable to accurately represent the dimensions of the neutron star in the model. Instead, we selected the radius and polar temperature of the object representing the neutron star such that it produced a blackbody luminosity equivalent to the observed X-ray luminosity, which is essentially all that matters to calculate the heating correction. We used a value for the luminosity of $L_x = 2.4 \times 10^{38}$ erg s^{-1} from Paul et al (2002). This agrees well with the value of $L_x = 2.0 \times 10^{38}$ erg s^{-1}, that we determined using the *RXTE All Sky Monitor* flux for the epoch of observation, assuming a simplified X-ray spectral shape and a value for the distance to the SMC of $D = 60.6$ kpc (Hilditch et al. 2005).

The initial input values used for i and q, were those obtained from the Monte Carlo program using the raw value for the donor star's radial velocity amplitude. Having calculated the radial velocity correction at the phase corresponding to each of the spectra, the individual radial velocity measurements were adjusted accordingly, and a new solution for the radial velocity amplitude was found. This amplitude was fed into the Monte Carlo program to determine new values for the inclination angle and mass ratio, and the results then fed back into LIGHT2 to recalculate the radial velocity corrections. We found that the code was required to run through three iterations before the size of the corrections became comparable to those of the previous iteration. The heating corrected velocities are shown in Table 3.1 and 3.2 for ours and Reynolds respectively. The change in the radial velocity amplitude due to the X-ray heating was found to be an increase of 3.8 km s^{-1}. The results are shown in the lower part of Table 3.3 and the final corrected radial velocity curve is shown in Figure 3.4.

The heating corrections were also determined for the radial velocity curve obtained by excluding the anomalous data from phase 0.2 – 0.3. The heating corrections to the individual remaining data points are identical (except for a few which are within ± 1 km s^{-1}) to those found when the anomalous data were included. However, the fit to the resulting heating corrected radial velocity curve gives an increase of 3.7 km s^{-1} in the radial velocity amplitude, when compared with the raw radial velocity curve excluding the anomalous data. The results of this process are shown in the lower parts of Table 3.4 and the final corrected radial velocity curve is shown in Figure 3.5.

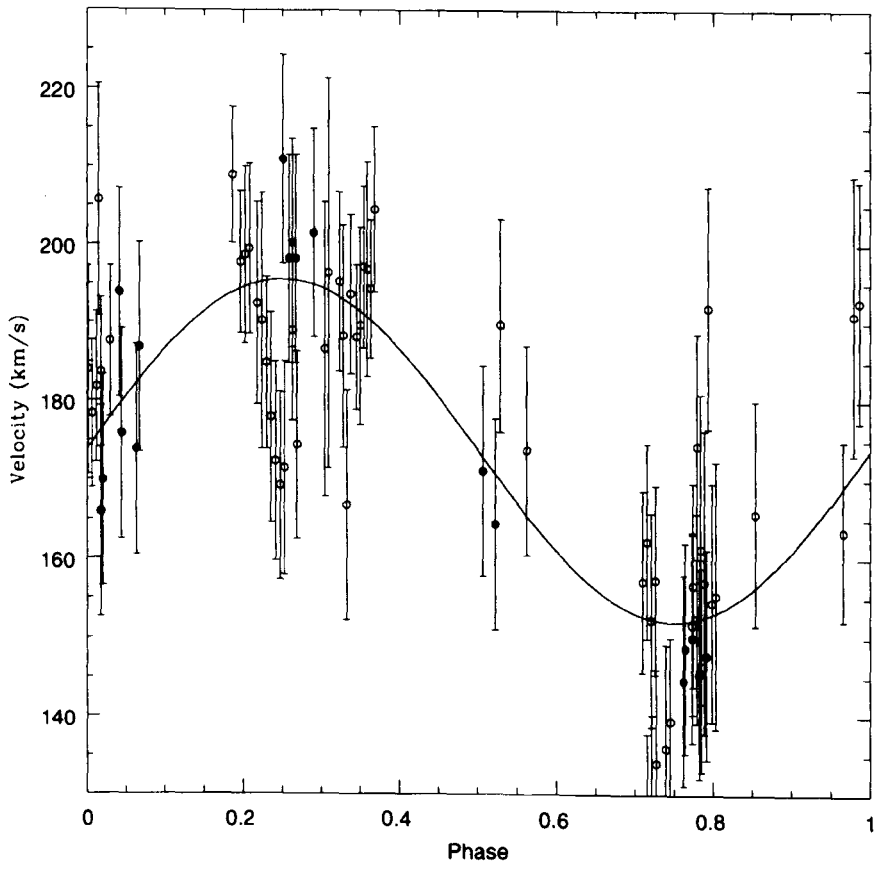

Figure 3.4: The heating-corrected He I absorption line radial velocity curve for Sk 160. Our data are shown as open circles and those of Reynolds et al. (1993) are shown as filled circles. The best fit to the combined data set is indicated by the solid line. Note, the error bars indicate the scaled (by ~ 0.95) errors necessary to minimize the reduced chi-squared to unity.

Table 3.3: System parameters for Sk 160 / SMC X-1. The upper part of the table shows the resulting parameters from the raw radial velocity curve and the lower part shows the resulting parameters from the corrected radial velocity curve. In each case the two columns for the various inferred paremeters are the limiting values assuming $i = 90°$ and $\beta = 1$.

Parameter	Fit to raw radial velocity curve	
γ (km s^{-1})	174.1 ± 1.5	
K_o (km s^{-1})	18.0 ± 1.8	
q	0.060 ± 0.006	
	Roche-lobe filling	edge-on
	(upper mass limits)	(lower mass limits)
β	1.00	0.77 ± 0.02
i (degrees)	64.0 ± 1.3	90.0
M_x ($M_\odot$)	1.01 ± 0.10	0.73 ± 0.08
M_o ($M_\odot$)	16.8 ± 0.5	12.1 ± 0.2

Parameter	Fit to corrected radial velocity curve	
γ (km s^{-1})	173.8 ± 1.5	
K_o (km s^{-1})	21.8 ± 1.8	
q	0.073 ± 0.006	
	Roche-lobe filling	edge-on
	(upper mass limits)	(lower mass limits)
β	1.00	0.79 ± 0.02
i (degrees)	65.3 ± 1.3	90.0
M_x ($M_\odot$)	1.21 ± 0.10	0.91 ± 0.08
M_o ($M_\odot$)	16.6 ± 0.4	12.5 ± 0.1

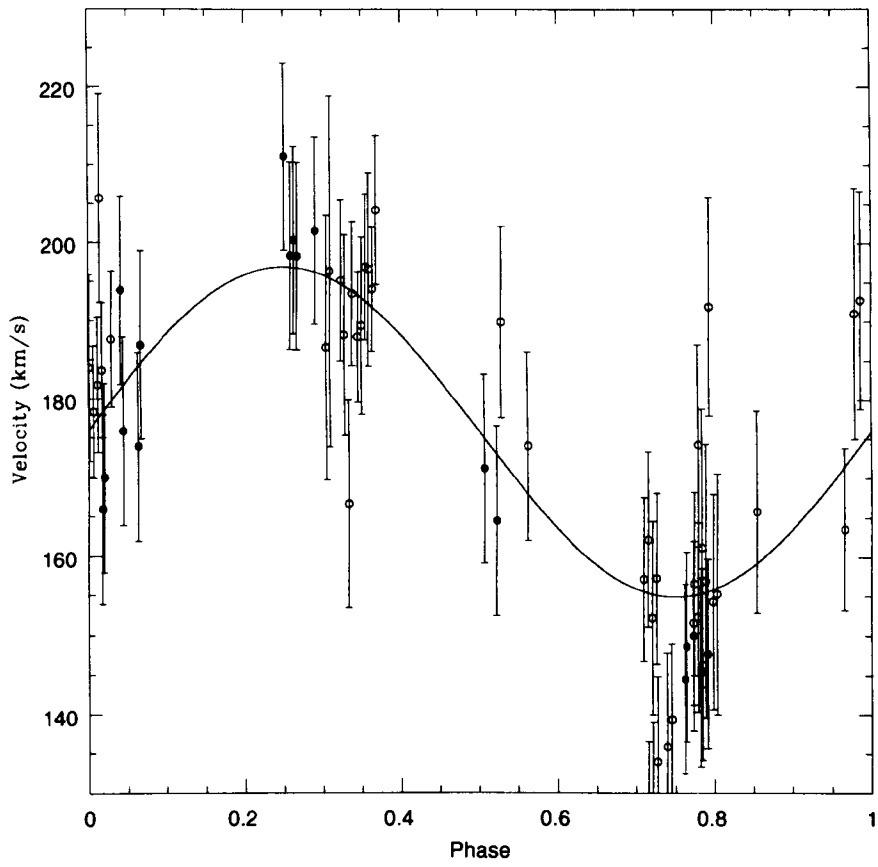

Figure 3.5: The heating-corrected He I absorption line radial velocity curve for Sk 160, with the anomalous data excluded. Our data are shown as open circles and those of Reynolds et al. (1993) are shown as filled circles. The best fit to the combined data set is indicated by the solid line.Note, the error bars indicate the scaled (by ~ 0.86) errors necessary to minimize the reduced chi-squared to unity.

Table 3.4: System parameters for Sk 160 / SMC X-1, with the anomalous data excluded. The upper part of the table shows the resulting parameters from the raw radial velocity curve and the lower part shows the resulting parameters from the corrected radial velocity curve. In each case the two columns for the various inferred paremeters are the limiting values assuming $i = 90°$ and $\beta = 1$.

Parameter	Fit to raw radial velocity curve	
γ (km s^{-1})	175.9 ± 1.4	
K_o (km s^{-1})	21.0 ± 1.9	
q	0.070 ± 0.006	
	Roche-lobe filling	edge-on
	(upper mass limits)	(lower mass limits)
β	1.00	0.77 ± 0.02
i (degrees)	65.1 ± 1.3	90.0
M_x ($M_\odot$)	1.17 ± 0.10	0.87 ± 0.09
M_o ($M_\odot$)	16.6 ± 0.4	12.4 ± 0.2

Parameter	Fit to corrected radial velocity curve	
γ (km s^{-1})	175.4 ± 1.5	
K_o (km s^{-1})	24.7 ± 1.9	
q	0.082 ± 0.006	
	Roche-lobe filling	edge-on
	(upper mass limits)	(lower mass limits)
β	1.00	0.79 ± 0.02
i (degrees)	66.4 ± 1.3	90.0
M_x ($M_\odot$)	1.36 ± 0.10	1.05 ± 0.09
M_o ($M_\odot$)	16.5 ± 0.4	12.8 ± 0.2

3.4.4 He II 4686 Å emission line

Hutchings et al. (1977) noted that the He II 4686 Å emission line seen from Sk 160 moves approximately in antiphase with respect to the He I lines, and follows the radial velocity of the neutron star, albeit with a lower amplitude, i.e. ~ 250 km s^{-1} as opposed to ~ 300 km s^{-1}. In order to investigate this, Gaussian fits to the He II emission lines were performed in each spectrum. The resulting heliocentric velocities were then plotted against phase in Figure 3.6, refer to Table 3.1 for the data values. In the more noisy spectra, it was not possible to measure the He II 4686 Å emission line, so there are less data points here than in Figures 3.2 – 3.5. Overplotted on these data is the best-fit sinusoid which has a semi-amplitude of 265 ± 8 km s^{-1}, a systemic velocity of 167 ± 7 km s^{-1}, and a phase shift of 0.46 ± 0.01 with respect to the ephemeris of Wojdowski et al. (1998). What is seen in Figure 3.6 is very similar to the behaviour noted by Hutchings et al. (1977), in that the He II emission appears to be coming from the vicinity of the neutron star but with a lower amplitude than that of the neutron star itself. The slight phase shift from the motion of the neutron star is also similar to that seen in the He II emission line radial velocity of Cyg X-1 (Giles & Bolton, 1986a; 1986b). As noted by Hutchings et al. (1977), this might indicate an origin for the emission that lies between the neutron star and the surface of Sk 160. We suggest that a possible site for this emission may be a hot-spot where a stream of material accreting via Roche-lobe overflow impacts the outer edge of the neutron star's accretion disc.

In excluding the anomalous data from phase 0.2 – 0.3, we find a best-fit sinusoid with essentially the same values (i.e. $K_o = 268 \pm 5$ km s^{-1}, $\gamma = 173 \pm 4$ km s^{-1}, and a phase shifft of 0.46).

3.5 Discussion

With regard to our initial results found by using all 56 data points, we find the heating corrected systemic velocity of $\gamma = 173.8 \pm 1.5$ km s^{-1} is in excellent agreement with the value obtained from the heating corrected radial velocity curve of Reynolds et al. (1993), namely 173.0 ± 1.5 km s^{-1}. However, our raw and heating corrected values found for K_o and the corresponding upper limits

Figure 3.6: The radial velocity curve of the He II 4686Å emission line. The solid line indicates a sinusoid with systematic velocity of 167 km s^{-1}, an amplitude of 265 km s^{-1} and a phase shift of 0.46 with respect to Wojdowski et al. (1998) ephemeris.

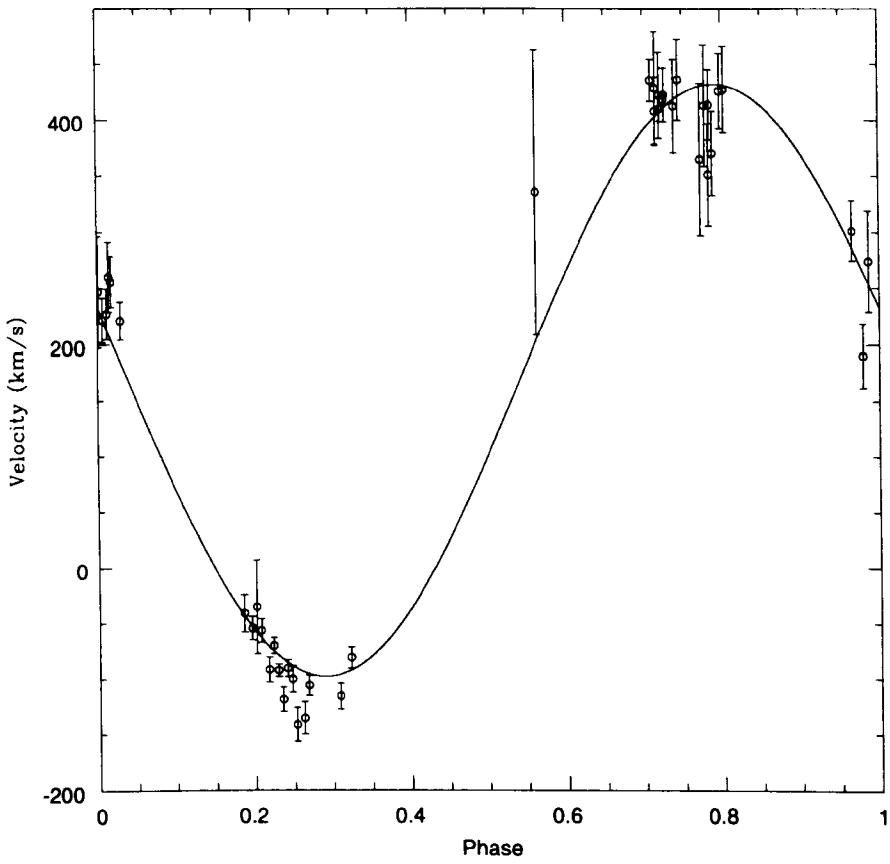

to the neutron star mass (i.e. those corresponding to $\beta = 1$) are each lower than those found by Reynolds et al (1993). The discrepancy could be due to the limited phase coverage of their data set and the fact that the value they assume for L_x, when determining the non-Keplerian corrections, is significantly higher than the value we used. In comparison, our raw value for K_o and the corresponding upper limit on the neutron star mass are both in good agreement with those found by van der Meer et al (2005; 2007), namely $K_o = 20.3 \pm 0.9$ km s^{-1}; 20.2 ± 1.1 km s^{-1} and $M_x = 1.05 \pm 0.09 M_\odot$; $1.06 \pm 0.1 M_\odot$, respectively. In both of these previous studies, however, the authors assume that the donor star is Roche-lobe filling. Whilst this is completely plausible, it only gives an upper limit for the mass of the neutron star, as noted above.

However, by taking into account the anomalous data and subsequently excluding them from the analysis we find higher values for γ, K_o and M_x. The resulting systemic velocity of $\gamma = 175.4 \pm 1.4$ km s^{-1} is still in reasonable agreement with that of Reynolds et al. (1993), and both the raw and heating corrected values for K_o and the corresponding upper limits to the neutron star mass are still lower than Reynolds et al (1993), but now more comparable. Likewise our raw value for K_o and the corresponding upper limit on the neutron star mass are now both higher than those found by van der Meer et al (2005; 2007), but still comparable. The origin of the anamalous data remains to be verified, but is likely due to tidally induced non-radial oscillations.

Such oscillations are believed to be the result of tidal action exerted by one binary component on the other (Willems, 2002), where the frequency of the oscillations are harmonically related to the orbital frequency (Willems & Aerts, 2002; Handler, 2002). Previous occurences have been reported in the eclipsing X-ray binary pulsar Vela X-1, where van Kerkwijk et al. (1995) suggested that the variable gravitational force exerted by the neutron star excites short-lived oscillations on the surface of the donor star, hence effecting the measured radial velocity. Later studies by Quaintrell et al. (2003) showed the harmonic relation between the oscillations and the orbital period, thus confirming the cause as being tidally induced oscillations. In the case of the anomalous data observed in our study of SMC X-1, we note that the sort of radial velocity excursion seen here are similar to those seen during individual nights worth of data from Vela X-1. We therefore suggest that it is likely that the anomalous data are tidally induced non-radial oscillations and therefore conclude that the more believable

results are those found by excluding the anomalous data.

The other cause of uncertainty in the mass estimates, is of course the heating correction. From Reynolds et al's (1993) study of the line profile variations of Sk 160, we know that the effects of X-ray heating on the inner hemisphere of the donor star are present but not dramatic. We investigated the effect of allowing the heating efficiency within LIGHT2 to vary, and found that the magnitude of the radial velocity corrections did not change appreciably even when the efficiency varied from 50% to 100%. Consequently we adopted a heating efficiency of 50% in our analysis, and it is results using this value that are presented.

There remains the question of whether an accretion disc will cast a shadow on the donor star so reducing the effect of X-ray heating, as raised by van Kerkwijk et al. (1995). In a study of Her X-1, Reynolds et al. (1997) corrected for non-Keplerian deviations using both a disc-less model (LIGHT2) and a disc model. In that case the quantitative agreement between the two models was found to be good. As Her X-1 clearly has a disc, and also has a donor star that is significantly smaller than that in SMC X-1, we can assume that the absence of a disc in the LIGHT2 code has negligible effect on the heating corrections in our case.

Model calculations of type II supernovae suggest that these events produce a bimodal distribution of initial neutron star masses, with averages within those peaks of 1.28 and $1.73M_{\odot}$, whereas type Ib supernovae produce neutron stars with masses around $1.32M_{\odot}$ (Timmes et al. 1996). Neutron stars produced in type Ia supernoave are expected to have masses close to the Chandrasekhar limit, $1.38M_{\odot}$ (for a Carbon-Oxygen white dwarf). Based on our heating-corrected mass determination of $1.05 \pm 0.09 - 1.36 \pm 0.10M_{\odot}$, depending on the Roche-lobe filling factor, the neutron star in SMC X-1 is consistent with both the first peak in the type II supernovae bimodal neutron star mass distribution and the type Ib distribution. We note that mass determinations which do not account for X-ray heating in SMC X-1 give a small neutron star mass that is inconsistent with all of the predictions stated above. Note also that these theoretical models do not take into account any mass that subsequently accretes in a binary system, so the theoretical values for the neutron star masses in accreting binaries are even higher. Therefore based on these model predictions it is concluded that the mass of the neutron star in SMC X-1 lies in the upper end of the heating corrected mass determinations i.e. $\sim 1.36 \pm 0.10M_{\odot}$. This

suggests that the neutron star is either at or close to filling its Roche-lobe. Finally, we note the implications of our interpretation for the origin of the He II 4696Å emission line. If this arises in a stream-disc impact hot spot, it confirms that some of the accretion occurs via Roche-lobe overflow, as previously surmised. It also suggests a potential test of the idea. The accretion disc in SMC X-1 is supposed to precess with a period of $\sim$ 55 days (e.g. Wojdowski et al. 1998). In this case, the stream-disc impact site should change its location on this period, moving closer to and further away from the neutron star as the eccentric disc precesses. Both the equivalent width and the radial velocity amplitude of the He II emission line should therefore vary throughout the precession cycle. Unfortunately, our data do not extend over enough of the super-orbital cycle, nor are they of high enough signal-to-noise to test this, but such an investigation would be worth carrying out in the future.

Chapter 4

The mass of the black hole in LMC X-3

This Chapter presents new high resolution, optical spectroscopy of the high mass X-ray binary LMC X-3. From observing the donor star at different phases we observe the change in spectral type due to irradiation by the X-ray source. Possible spectral types at the two extremes of irradiation are discussed along with the resulting mass determinations of the stellar components.

4.1 Overview of LMC X-3

LMC X-3 is a non-eclipsing persistent HMXB in the Large Magellanic Cloud (Cowley et al. 1983; White & Marshall, 1984). It was originally detected as an individual point-like X-ray source by Leong et al. (1971), and was later reported to be the brightest (i.e. $L_x > 10^{38}$ erg s^{-1}) and most variable of the Large Magellanic Cloud sources during the *Ariel 5* survey (Griffith & Seward, 1977; Johnston et al. 1979). The optical counterpart was identified as a faint OB star by Warren & Penfold in 1975. This identification was further strengthened by improved-accuracy determinations of the position of LMC X-3 (Delvaille et al. 1976; Johnston et al. 1978; Long et al. 1981), and the spectral

type was subsequently re-classified as a B3V (Cowley et al. 1983; Treves et al. 1988; 1990). However this spectral type remains uncertain, due to the effects of irradiation by the X-ray source, which in turn leads to uncertainties in the mass determinations of the compact companion.

Low-amplitude ellipsoidal modulations (Khruzina & Cherepashchuk, 1984; Kuiper et al. 1988) as well as spectroscopic observations (Cowley et al. 1983) revealed the nature of the X-ray source to be a strong black hole candidate. These spectroscopic observations also revealed the orbital period as $P = 1.70479 \pm 0.00004$ days (Cowley et al. 1983; van der Klis et al. 1983; 1985), with a slightly eccentric orbit (i.e. $e \sim 0.13 \pm 0.05$), and a systemic velocity of $\gamma = 310$ km s^{-1} (Cowley et al. 1983). This value was found to be in good agreement with the predicted systemic velocity of 343 km s^{-1}, found for the actual location of LMC X-3 derived from the work of Feast et al. (1961).

Optical photometry shows the system to vary in magnitude (i.e. $V \sim 16.7 - 17.5$), with a period of $\sim$ 198 (or possibly 99) days (Warren & Penfold, 1975; van der Klis et al. 1983; 1985; van Paradijs et al. 1987; Cowley et al. 1991). The X-ray flux is also known to vary with this same long-term period, and it has therefore been suggested that this variation may arise from a precessing accretion disc or from variations in the mass accretion rate (White & Marshall, 1984; Cowley et al. 1991; 1994). LMC X-3 has also been shown to exhibit strong spectral variability on timescales of days to weeks, which is consistent with transitions from the soft state to the canonical hard state (Wilms et al. 2001; Boyd et al. 2000; Wu et al. 2001). The spectral shape can be described by a phenomenological disc black body model (kT $\sim$ 1 keV) with a soft power-law ($\Gamma \geq 3$) component (Wilms et al. 2001; Page et al. 2003). Wilms et al. (2001) suggests that the long term variability and state changes observed in LMC X-3 are due to an accretion disc wind-driven limit cycle (e.g. Shields et al. 1986).

The mode of mass transfer in LMC X-3 has been a long unsolved problem. Recent authors have assumed mass transfer to occur via Roche-lobe overflow, as stellar wind accretion is insufficient to account for the high luminosities and low hydrogen column densities (N_H) observed (e.g. Soria et al. 2001). This has been confirmed by Wu et al. (2001) and Page et al. (2003), who found that the measured line of sight absorption ($N_H < 10^{21}$ and $< 8 \times 10^{20}$ cm^{-2}, respectively) was too small to support a model in which a strong stellar wind fuelled the observed high/soft state.

Previous attempts to derive the orbital parameters of LMC X-3 have been made by Cowley et al. (1983), and more recently by Soria et al. (2001). Cowley et al. (1983) used spectroscopic observations obtained with a silicon intensified target (SIT) vidicon at the Cerro Tololo Inter-American observatory (CTIO). From the hydrogen and He I absorption lines they found a value for the semi-amplitude of the radial velocity curve to be, $K_o = 235 \pm 11$ km s^{-1}. Assuming a spectral type of B3V, they set the donor star mass as, $4 \leq M_o \leq 8\mathrm{M}_\odot$ (Popper, 1980). Due to the absence of eclipses they set an upper limit on the inclination angle of $i \leq 70°$, and by measuring the projected rotaional velocity $V_{rot} \sin i$, and assuming a maximum possible value for V_{rot} they set a lower limit of $i \geq 50°$. Although they found their data was better fit by an eccentric orbit, it is expected that short period binaries will quickly circularise so an eccentricity of zero was assumed. Their resulting value for the mass of the compact companion was $7 \leq M_x \leq 14\mathrm{M}_\odot$, thereby confirming LMC X-3 as the second strong black hole candidate, (i.e. after Cyg X-1 which was discovered in 1964 by Bowyer et al. (1965)). Soria et al. (2001) based their studies on the data of Cowley et al. (1983), but assumed a different spectral type and hence mass for the donor star. From optical photometric observations with the *XMM-Newton* optical monitor, taken during an X-ray low/hard state, they were able to determine the intrinsic colours of the donor star. Using stellar models (Buser & Kurucz, 1978; Cramer, 1984) and applying bolometric corrections (Lejeune, 1998), they found the observed colour indicies indicated bolometric luminosities and temperatures corresponding to an evolved star of mass, $4.7 \leq M_o \leq 5.3\mathrm{M}_\odot$ i.e. of spectral type B5IV. Assuming Roche-lobe overflow Soria et al. (2001) set the donor star mass as $M_o \sim 4.7\mathrm{M}_\odot$. Then taking $50° \leq i \leq 70°$ and $K_o = 235$ km s^{-1} (Cowley et al. 1983), they found $M_x > 7.3 \pm 0.6\mathrm{M}_\odot$. However they note that Cowley's observations were carried out during a high/soft state, such that the absorption lines were most likely suppressed or weakened and the observed semi-amplitude of the radial velocity curve exaggerated. They estimate a heating correction of $\Delta K_o \sim 30 \pm 5$ km s^{-1} and hence a mass of $M_x > 5.8 \pm 0.6\mathrm{M}_\odot$.

4.2 Observations

The observations presented here were obtained with UVES instrument on the very large telescope (VLT) at the European southern observatory (ESO). They are the first spectroscopic observations of LMC X-3 resported since those obtained by Cowley et al. (1983). Five spectra were taken over a period of three months between December 2004 and March 2005, refer to Table 4.1. They were taken in both the blue and red part of the spectrum with central wavelengths of 4370Å and 8600Å respectively. An echelle grating spectrograph was used which gave a resolution of 0.02Å per pixel. Note, only the blue part of the spectra ($\sim$ 3780Å - 4980Å) were used in this study. The red data were unusable because the spectral region covered was dominated by telluric lines from the Earths atmosphere. The target star itself was relatively faint in this spectral region and it proved impossible to extract the source spectrum from the dominating background lines. However, since there were several hydrogen and helium lines in the blue spectra to use for both spectral classification purposes and for the radial velocity study, this was not a problem. So no further time was wasted trying to extract useable information form the red spectra.

4.3 Data reduction

All spectra were reduced using standard IRAF routines and extracted using optimal extraction procedures as outlined in Section 2.1 and 2.2. The extracted spectra were then continuum fitted using DIPSO, as shown in Figures 4.1 and 4.2. Gaussian fits to the He I 4026 and He I 4713 absorption lines were performed on each of the five spectra. These particular He lines were chosen, as opposed to the other observed absorption lines, as they consistently appeared the strongest. Final heliocentric radial velocities corresponding to each spectrum of LMC X-3 were calculated by applying the heliocentric velocity corrections to the mean velocities found from Gaussian fits to the He I 4026 and He I 4713 line. These final radial velocities are listed in Table 4.1 along with their calculated r.m.s uncertainties.

Orbital phases corresponding to each spectrum were calculated using the ephemeris

from van der Klis et al. (1985), which gives the time of the Nth superior conjunction of the X-ray source as:

$$t_N/HJD = 2445278.005(\pm 0.011) + 1.70479(\pm 0.00004)N \qquad (4.1)$$

A barycentric correction was applied to the HJD, before the phases were calculated. Note, in Table 4.2, and included in Figures 4.13 - 4.15, are the radial velocity measurements of Cowley et al. (1983), with phases calculated according to the revised ephemeris above.

Table 4.1: The raw and heating-corrected heliocentric radial velocity data for the donor star in LMC X-3 found from Gaussian fits to the He I 4026 and He I 4713 absorption lines.

MJD	Phase	RV_{raw} (km s^{-1})	1σ uncertainty (km s^{-1})	RV_{corr} (km s^{-1})	
				$i = 50$	$i = 70$
53358.062	0.858	114	34	112	113
53374.219	0.336	506	2	516	521
53378.135	0.633	113	20	103	98
53448.024	0.628	116	8	107	102
53449.034	0.223	517	9	523	524

4.4 Spectral classification

There are no X-ray pulsations with which to probe the motion of the compact companion and hence determine its radial velocity semi-amplitude K_x. Therefore the mass of the donor star has to be deduced from its spectral type, which as discussed in Section 1.4.2 can lead to huge uncertainties if the spectral type is not known accurately. The donor star in LMC X-3 is currently classified as a B3V star (Cowley et al. 1983), but has also recently been classified as a B5IV (Soria et al. 2001). They note however, that their inferred bolometric luminosities were comparable to a B3V but the inferred temperature was too low.

Figure 4.1: The continuum normalized optical spectrum of LMC X-3 at phase 0.22, shown with B2IV and B3V standard star spectra for comparison.

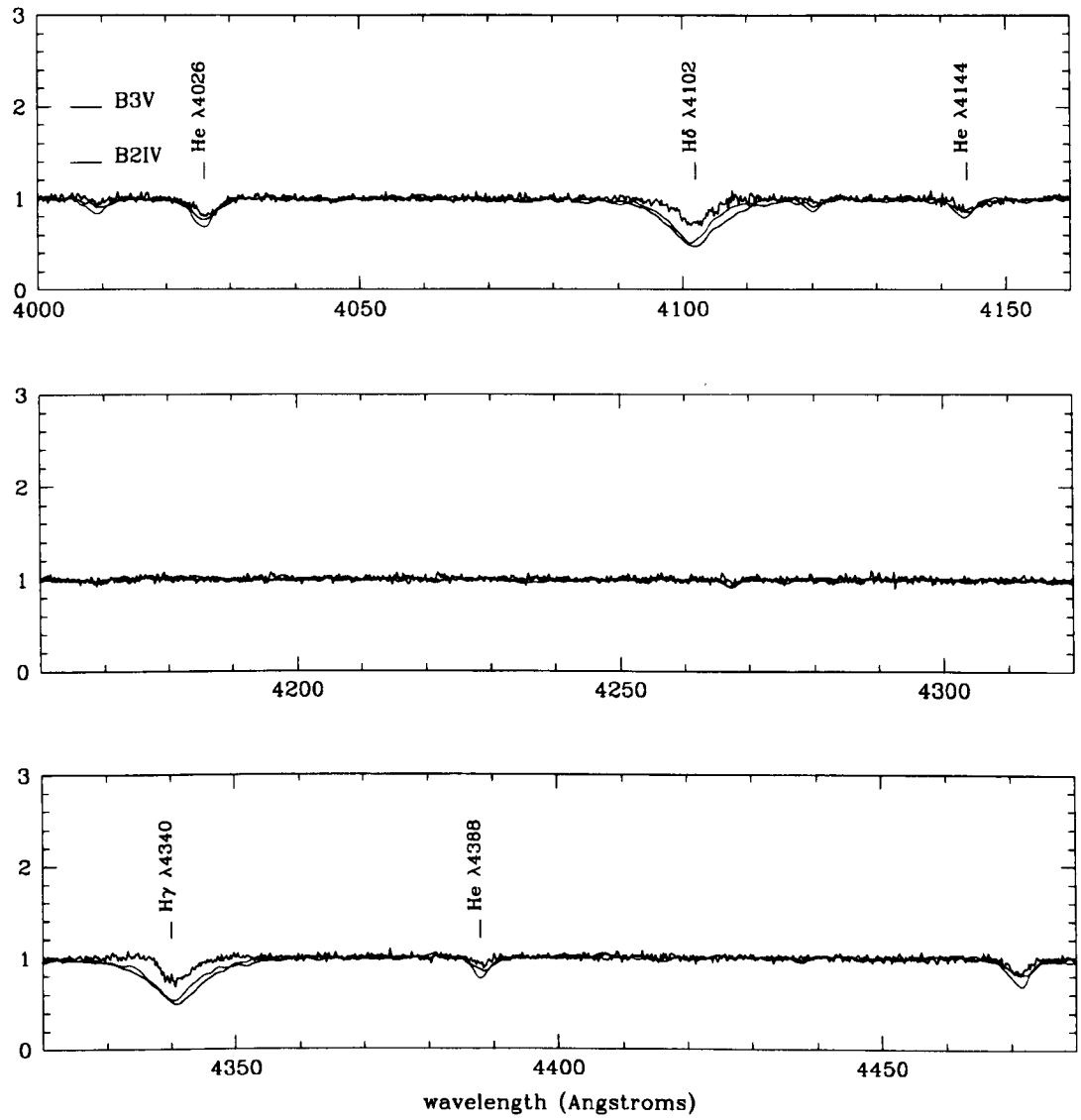

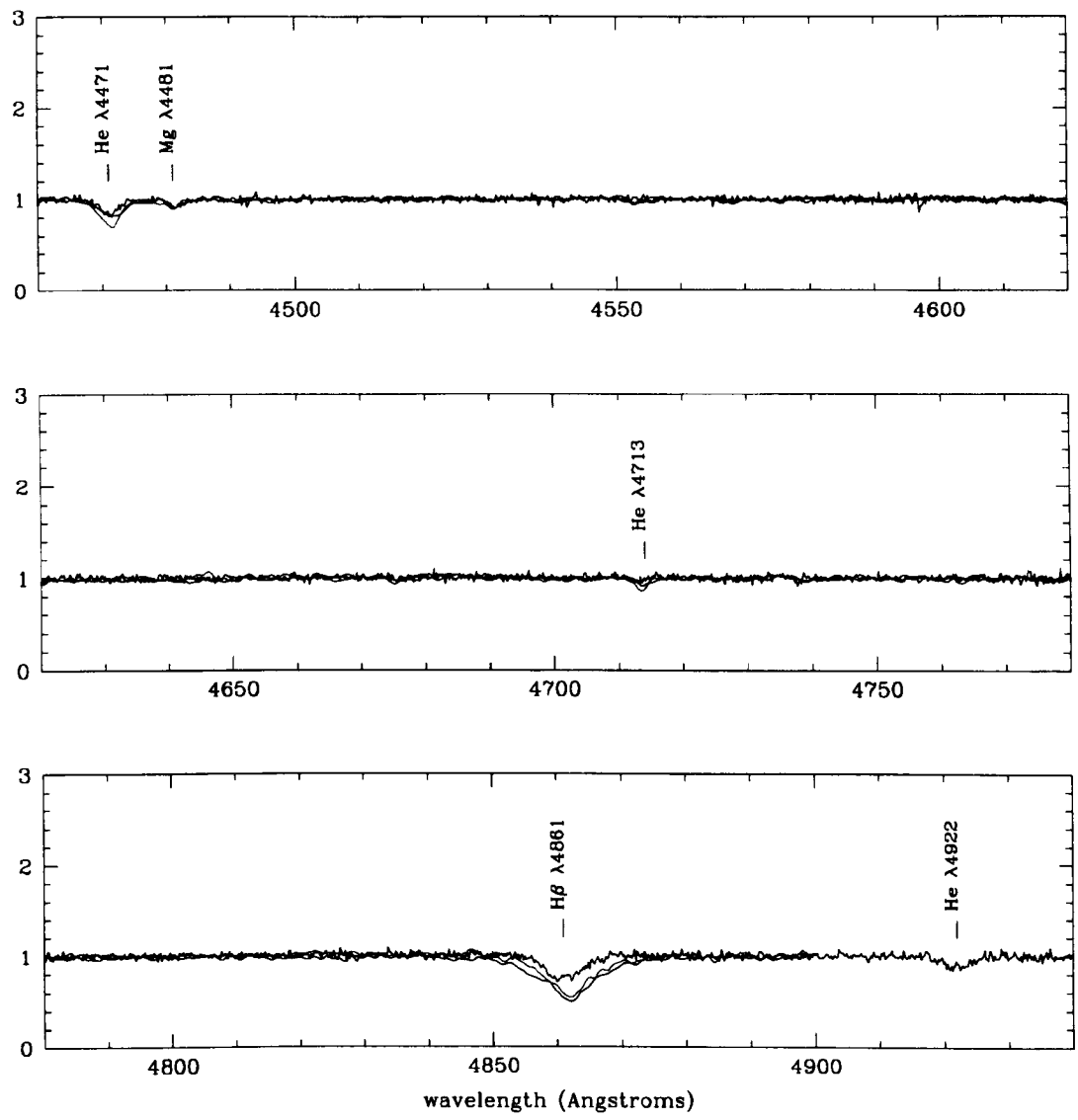
He λ4471
Mg λ4481
He λ4713
Hβ λ4861
He λ4922
wavelength (Angstroms)

Figure 4.2: The continuum normalized optical spectrum of LMC X-3 at phase 0.86, shown with B4V and B6V standard star spectra for comparison.

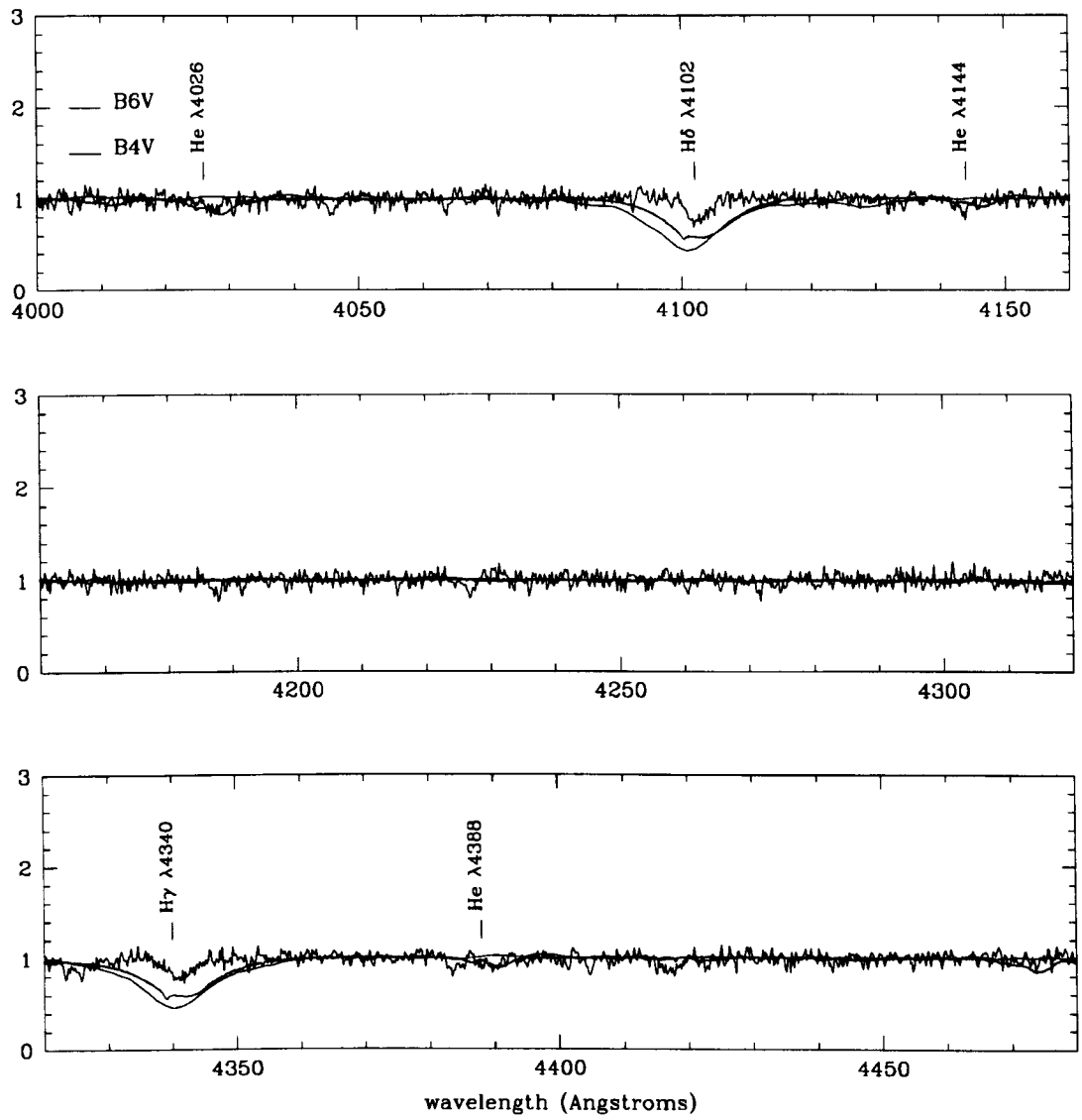

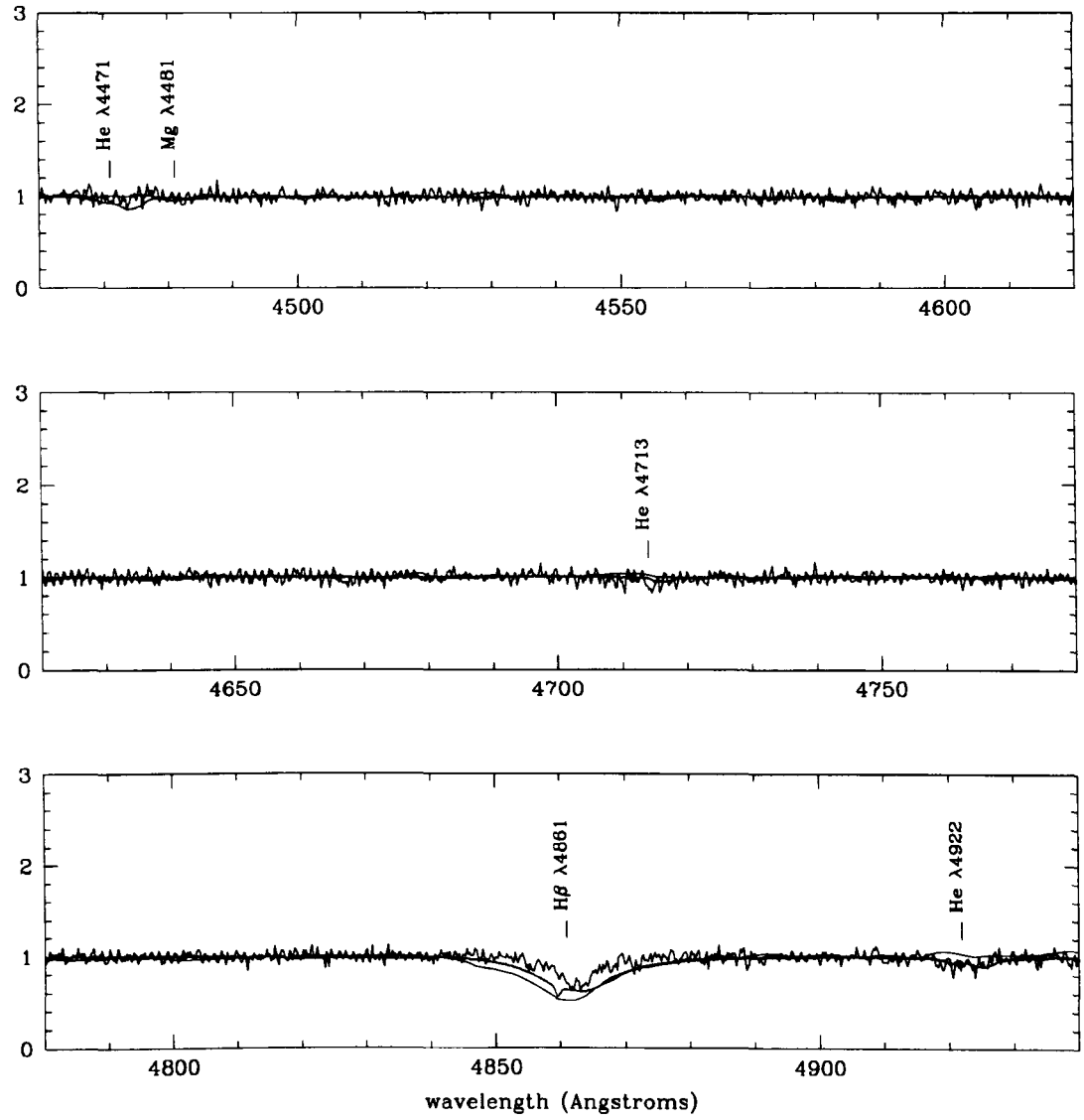
He λ4471
Mg λ4481
He λ4713
Hβ λ4861
He λ4922
wavelength (Angstroms)

Table 4.2: Cowley et al's (1983) radial velocity data for LMC X-3, with phases and heating corrections matching those adopted for our observations.

MJD	Phase	RV_{raw} (km s^{-1})	1σ uncertainty (km s^{-1})	RV_{corr} (km s^{-1})	
				$i = 50$	$i = 70$
43584.066	0.658	85	32	72	70
44291.187	0.443	365	33	372	374
45021.165	0.635	149	27	137	134
45024.102	0.358	424	78	437	439
45278.215	0.416	472	69	481	484
45278.339	0.489	376	31.5	377	378
45279.257	0.028	362	27	362	362
45279.349	0.082	387	34.5	388	388
45280.296	0.637	128	37.5	116	113
45282.167	0.735	41	21	30	30
45282.290	0.807	74	16.5	69	69
45283.120	0.294	518	16.5	530	532
45283.225	0.355	522	36	535	537
45283.310	0.405	455	9	465	468
45284.142	0.893	130	25.5	129	129
45284.222	0.940	250	22.5	249	250
45284.334	0.006	321	19.5	321	321

To determine the spectral type of the donor star more accurately we compared our LMC X-3 spectra with standard star spectra from 'The OB Spectral Classification Atlas' (Walborn & Fitzpatrick, 1990), 'The standard star catalogue' (Jacoby & Hunter, 1984) and archive data from the ESO VLT. The spectra obtained at phase 0.22, 0.34, 0.628 and 0.633, when the heated face of the donor star is in the line of sight (refer to Figures 4.3 – 4.5), show relatively strong helium and hydrogen lines with little variance between each spectrum. As the spectrum obtained at phase 0.22 has the best signal to noise we used this spectrum to determine the spectral type of the star when seeing its heated side. This was found to be most similar to a B3V, refer to Figure 4.1.

However the spectrum obtained at phase 0.86 (refer to Figure 4.2), shows much weaker helium lines (Figures 4.7 – 4.9 and Figure 4.13) and narrower and stronger hydrogen lines (Figures 4.10 - 4.12). This is to be expected, as at this phase the donor star is nearly in the line of sight and the black hole is almost out of view, so we are seeing the cooler, unheated side of the donor star (refer to Figure 4.6). This is also apparent in the fact that we see more NII, OII and Si lines at this phase, which are typical of cooler stars. To determine the spectral type at this phase, the spectrum was first compared with that of a B4V (HD 36646 from ESO VLT archive data). This shows similar strength H and HeI lines to a B3V except for He I 4144 and He I 4922 which appear significantly weaker. It also shows the lines He I 4388, He I 4438 and He I 4471, which do not appear on the phase 0.86 spectrum. However the B6V spectrum (standard star from the Jacoby & Hunter, 1984 catalogue) does not show these lines, or any of the other HeI lines (i.e. He I 4009, 4026, 4144, 4922). As the He I 4026 line is observed in the 0.86 spectrum, a possible spectral type for the star at this phase is a B5V (refer to Figure 4.2).

From Kurucz's (1993) stellar atmosphere models, we can assume that the approximate effective temperature of a B3V star is 18700 K, and of a B5V star is 15400 K. Therefore if the real spectral type of the unheated star is a B5V, we can assume that it is being heated as a result of X-ray irradiation by a further $\sim$ 3300 K. However, if we also assume the possibility that the star may be either a B4V or B6V, we find an uncertainty on the temperature change of $\sim \pm 1650$ K.

Figure 4.3: Simulated view of binary system at phase 0.22. Made using 'binsim' software of Rob Hynes, and by using the following parameters: $P = 1.70479$; $L_x = 3{\times}10^{38}\,\mathrm{erg\,s^{-1}}$; (a) $M_x = 13.2\mathrm{M}_\odot$; $q = 2.24$ and $i = 50°$; (b) $M_x = 9.5\mathrm{M}_\odot$; $q = 1.61$ and $i = 70°$.

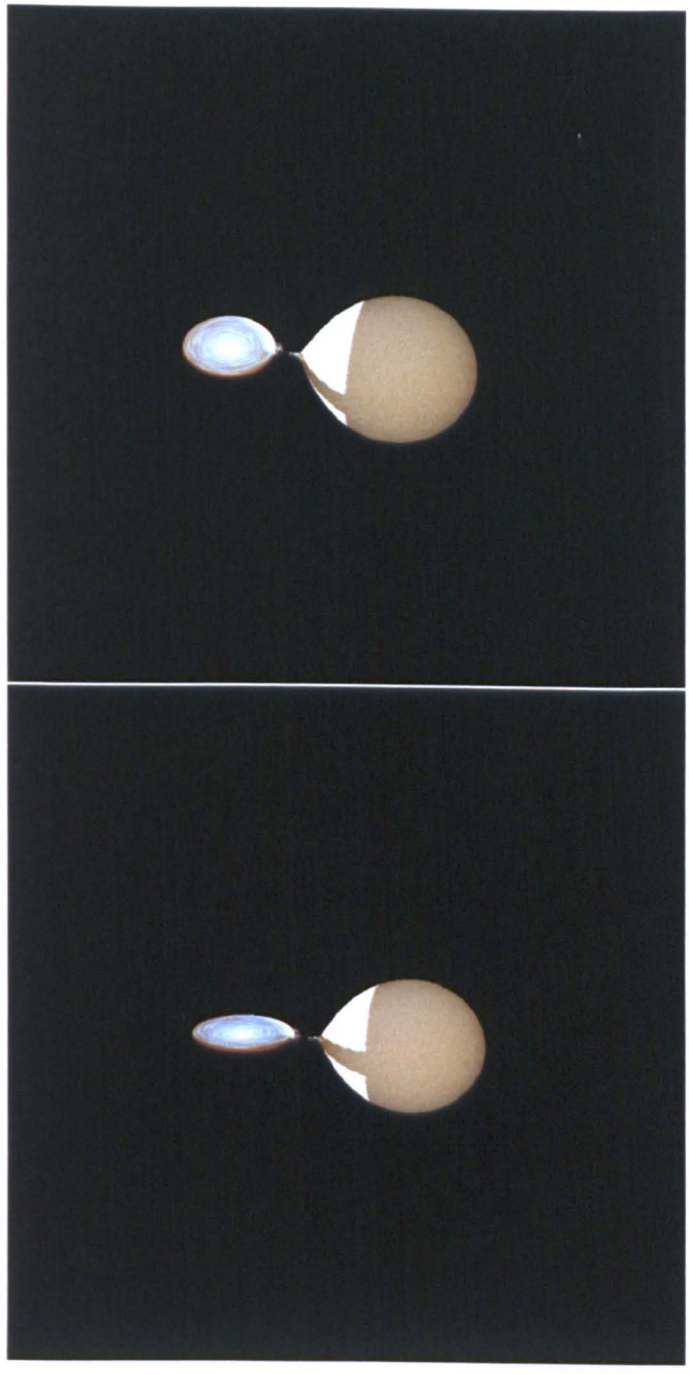

Figure 4.4: Simulated view of binary system at phase 0.34. Images obtained using the following parameters: $P = 1.70479$; $L_x = 3 \times 10^{38}$ erg s^{-1}; (a) $M_x = 13.2\mathrm{M}_\odot$; $q = 2.24$ and $i = 50°$; (b) $M_x = 9.5\mathrm{M}_\odot$; $q = 1.61$ and $i = 70°$.

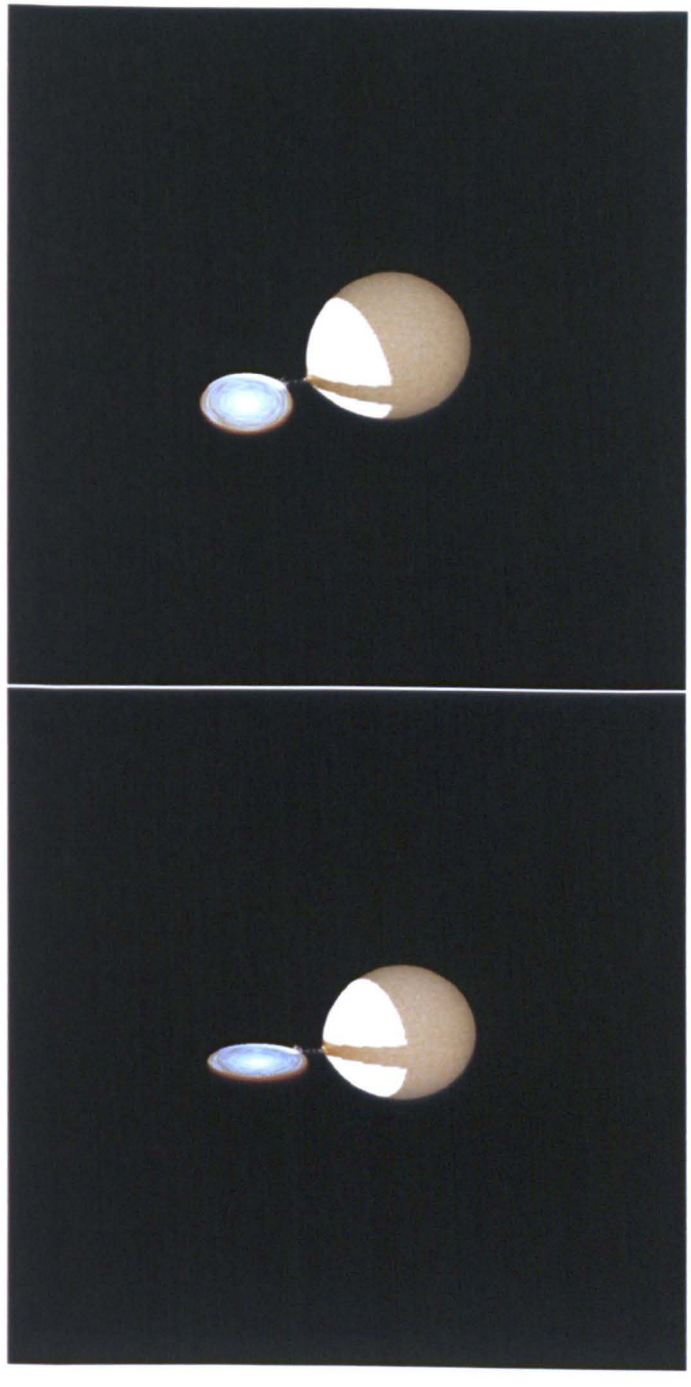

Figure 4.5: Simulated view of binary system at phase 0.63. Images obtained using the following parameters: $P = 1.70479$; $L_x = 3 \times 10^{38}$ erg s^{-1}; (a) $M_x = 13.2\mathrm{M}_\odot$; $q = 2.24$ and $i = 50°$; (b) $M_x = 9.5\mathrm{M}_\odot$; $q = 1.61$ and $i = 70°$.

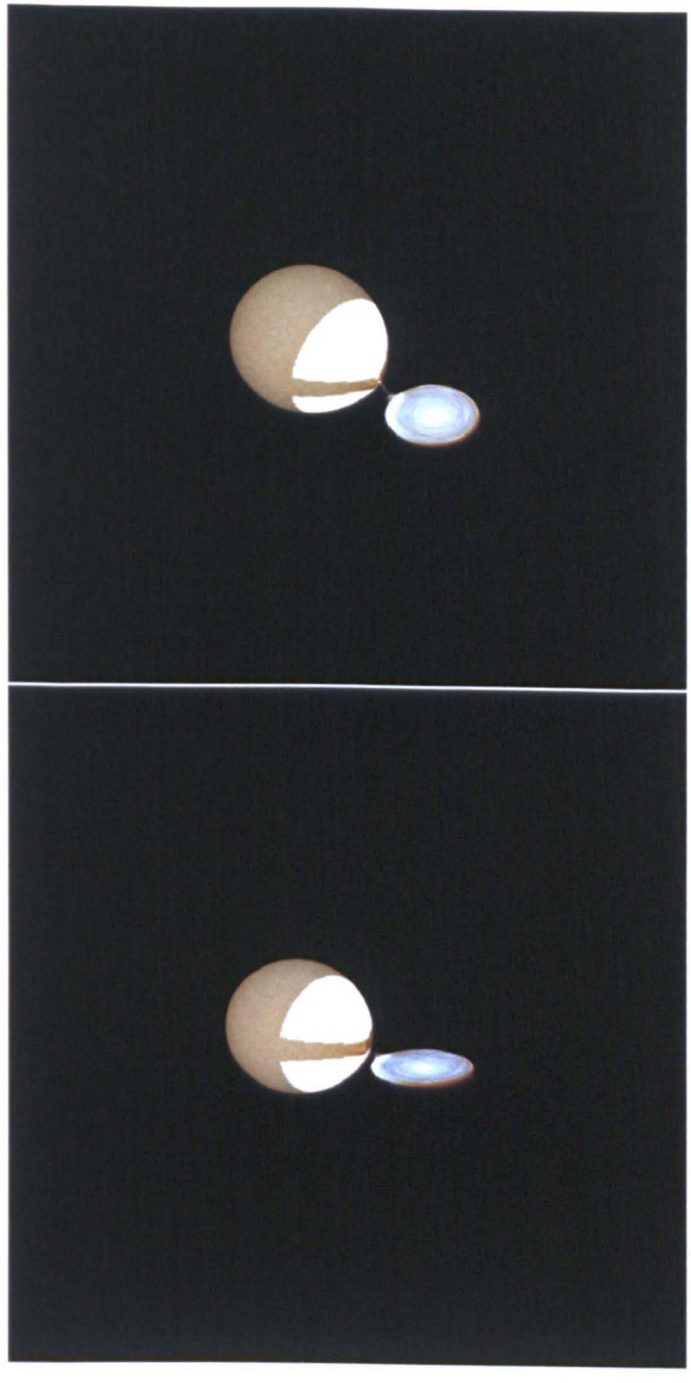

Figure 4.6: Simulated view of binary system at phase 0.86. Images obtained using the following parameters: $P = 1.70479$; $L_x = 3 \times 10^{38}$ erg s^{-1}; (a) $M_x = 13.2\mathrm{M}_\odot$; $q = 2.24$ and $i = 50°$; (b) $M_x = 9.5\mathrm{M}_\odot$; $q = 1.61$ and $i = 70°$.

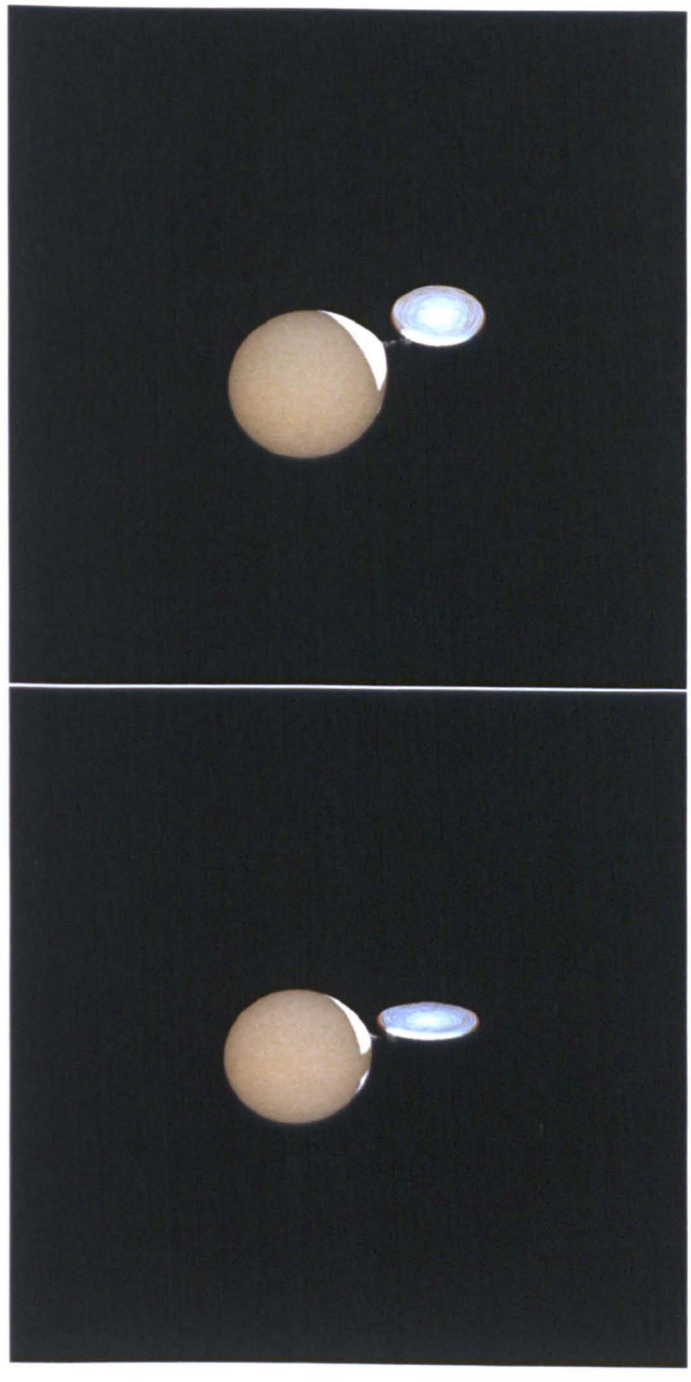

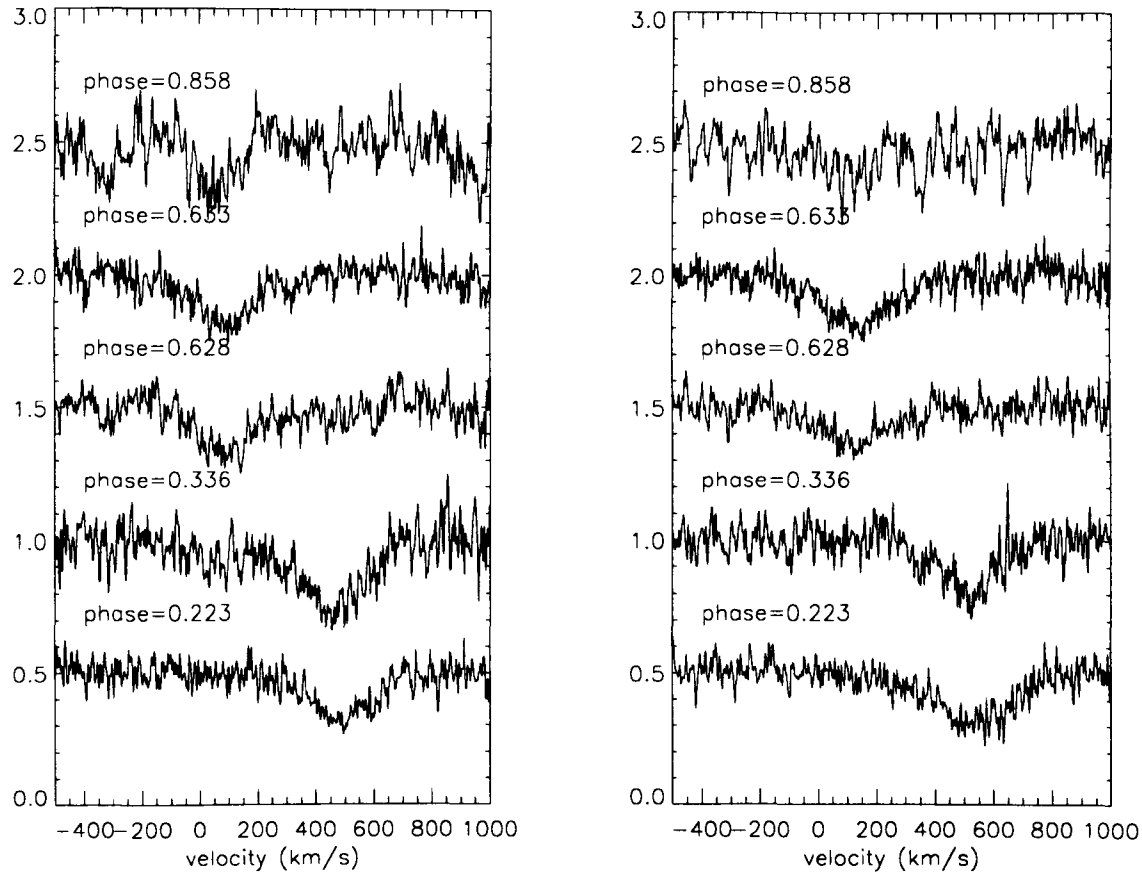

Figure 4.7: The (a) He I 3820Å and (b) He I 4026Å absorption line shown for different phases and as a function of velocity. Each spectrum is offset by 0.5 in the vertical axis, where the scale is arbitrary.

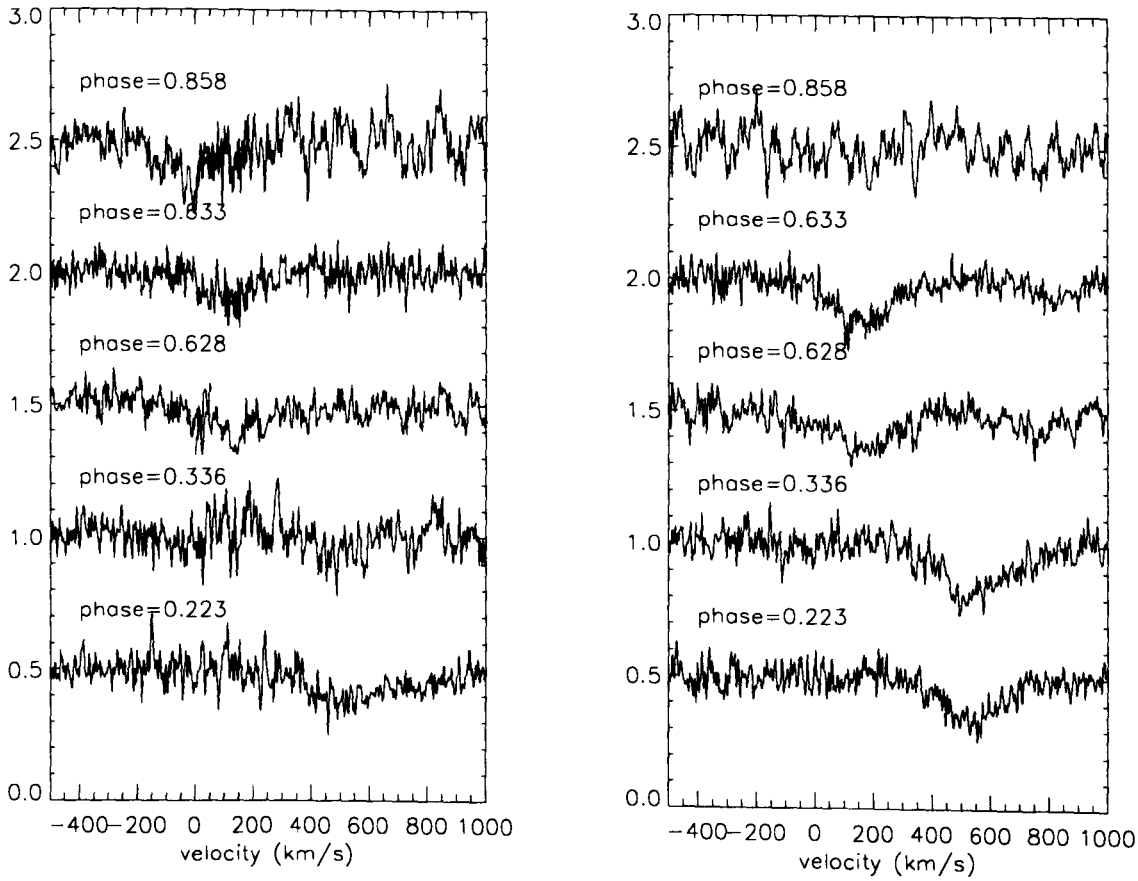

Figure 4.8: The (a) He I 4144Å and (b) He I 4471Å absorption line shown for different phases. Axis as in Figure 4.7.

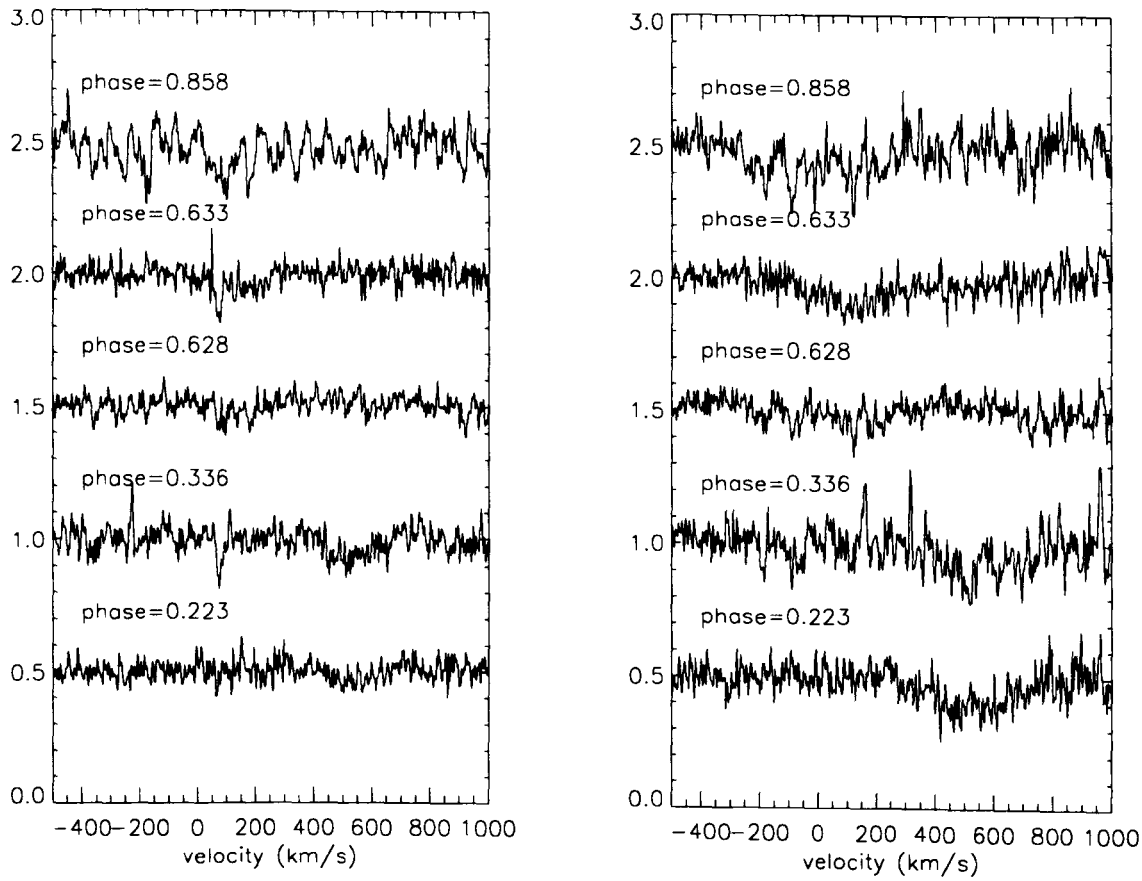

Figure 4.9: The (a) He I 4713Å and (b) He I 4922Å absorption line shown for different phases. Axis as in Figure 4.7.

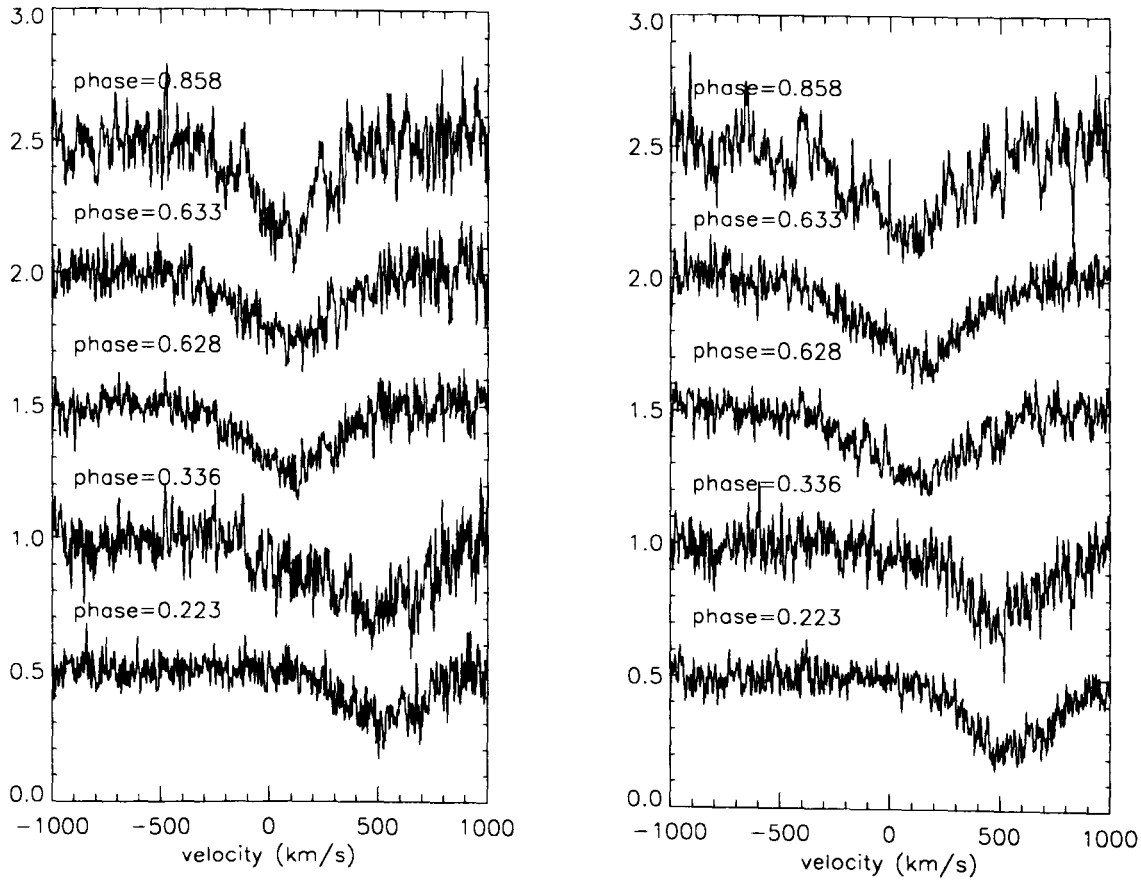

Figure 4.10: The Balmer (a) H10 and (b) H8 absorption line shown for different phases. Axis as in Figure 4.7.

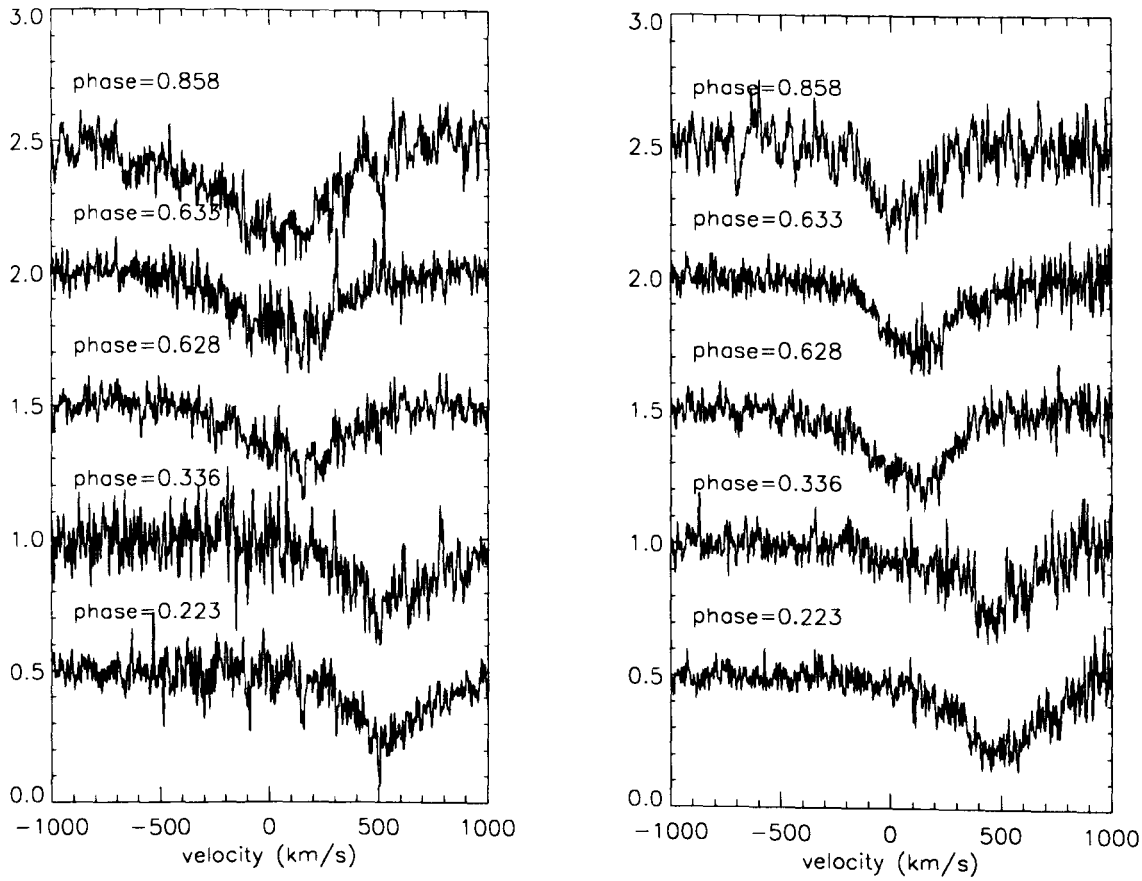

Figure 4.11: The Balmer (a) Hϵ and (b) Hδ absorption line shown at different phases. Axis as in Figure 4.7.

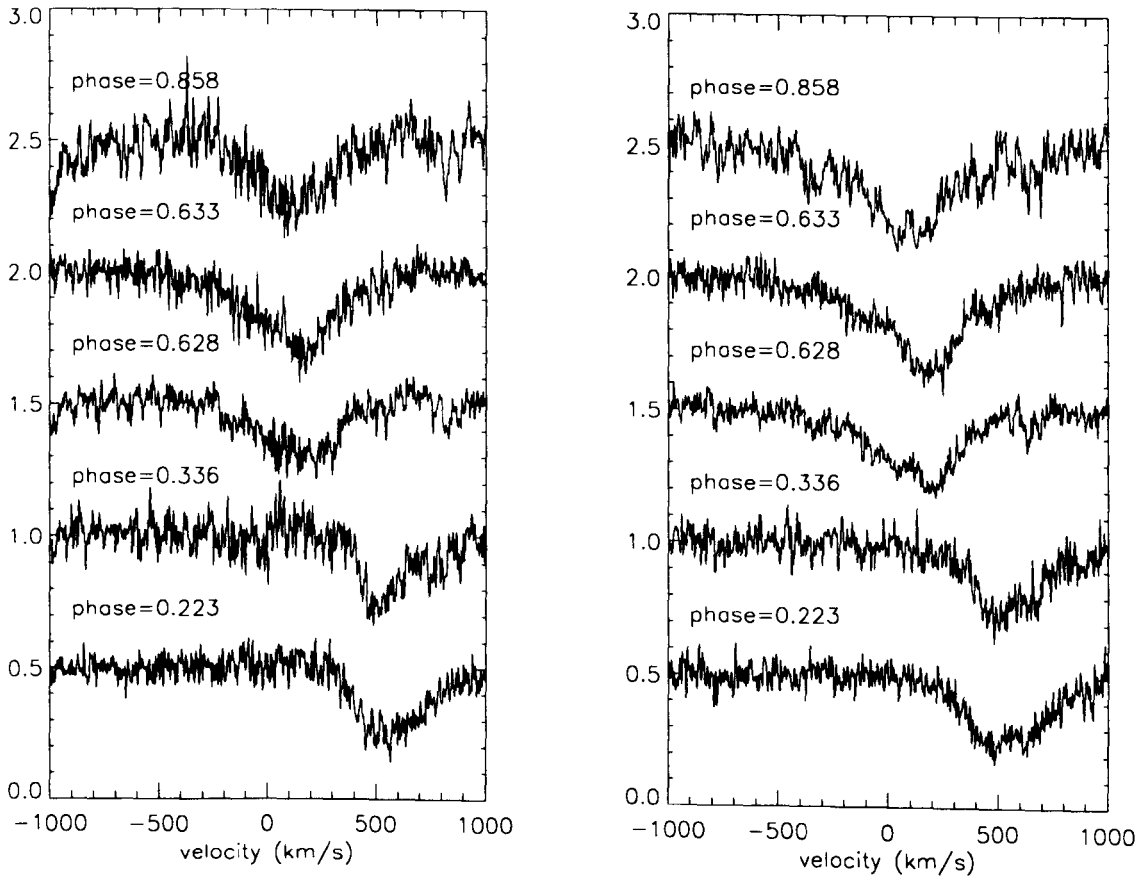

Figure 4.12: The Balmer (a) Hγ and (b) Hβ absorption line shown at different phases. Axis as in Figure 4.7.

Figure 4.13: The equivalent width (EW) of the helium lines He I 4026 (shown as black data points) and He I 4713 (shown as red data points) plotted as a function of phase.

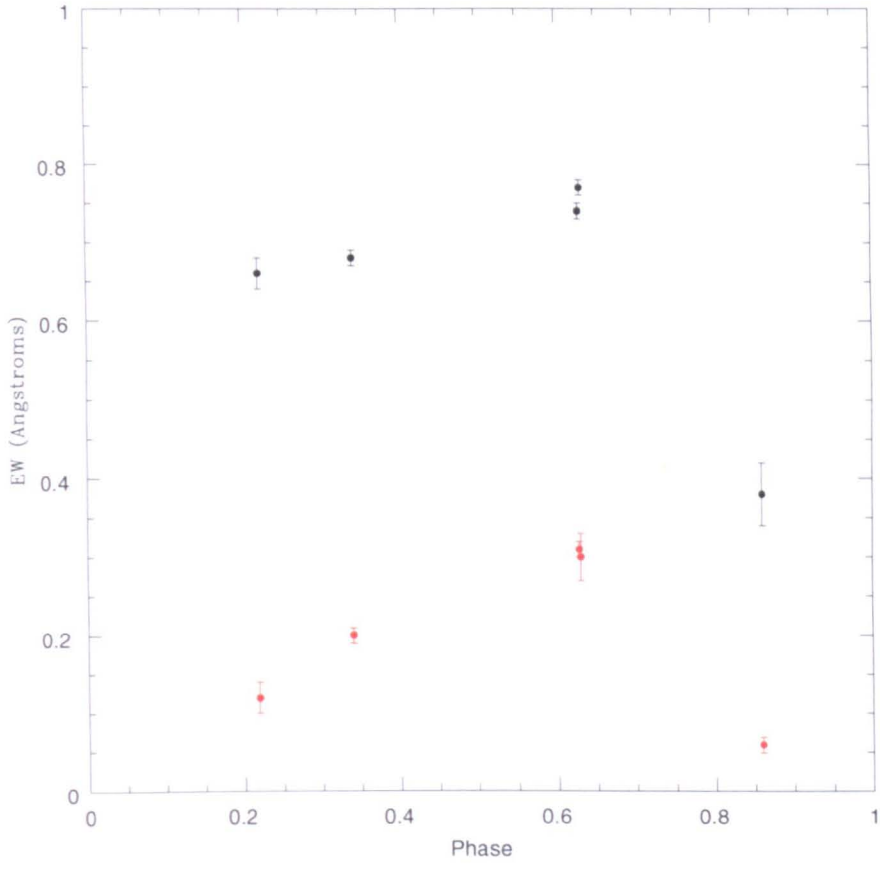

4.5 The radial velocity curve

4.5.1 Fitting the raw radial velocity curve

The heliocentric corrected veocities (Table 4.1), along with the radial velocity measurements of Cowley et al. (1983) (Table 4.2) were plotted against phase,

refer to Figure 4.14. However the phases first had to be shifted to account for the uncertainty of the van der Klis (1985) ephemeris. The uncertainty on the orbital period at the time of our observations, $\sim$ 4739 cycles after the reference time of the ephemeris, results in an uncertainty on the phase zero of up to ± 0.18956 days or ± 0.11 in phase. In order to ascertain the true phasing of our data, we fitted the combined data set (ours and Cowleys) with a variety of phase shifts applied to our five radial velocity data points. With phase shifts of: -0.10, -0.05, 0.00, +0.05 and +0.10, the reduced chi-squared values of the best-fit sinusoid to the combined data set were 50.5, 23.1, 8.5, 2.5 and 7.8 respectively (before scaling the errors on the radial velocity values to reduce the chi-squared to unity). Hence a phase shift of +0.05 applied to our data provides the best match with Cowleys data and reflects the drift in the ephemeris which has accumulated over the intervening 22 years since the definition of the ephemeris. This phase shift has been incorporated into the phase values in Tables 4.1 which therefore are the true phases relative to superior conjunction of the neutron star, adjusted for the uncertain ephemeris.

The resulting radial velocities were then fitted with a sinusoid, allowing just the mean level (γ) and semi-amplitude (K_o) as free parameters. The best fit was found by minimizing the reduced chi-squared value, which gave $\chi^2_r = 1.00$, indicating that the data are well fit by this function and that the uncertainties are of an appropriate magnitude. This resulted in the semi-amplitude of the radial velocity curve as $K_o = 242.4 \pm 4.3$ km s^{-1} and the systemic velocity as $\gamma = 301.7 \pm 3.5$ km s^{-1}. These values are listed in the upper part of Table 4.3.

4.5.2 System parameters from the raw He I radial velocity curve

The masses of the stellar components were calculated according to the method outlined in Section 1.4.2. The input parameters used for the calculation are as follows: $P = 1.70479 \pm 0.00004$ days, based on the ephemeris of van der Klis et al. (1985); $K_o = 242.4 \pm 4.3$ km s^{-1}, found from the uncorrected radial velocity curve; $M_o \sim 5.9$ M$_\odot$, assuming the donor star is of spectral type B5V. Since the system is not eclipsing we can only assume that $i < 70°$. However from the measured limit on rotational broadening we know that $i > 50°$, therefore

Figure 4.14: The uncorrected radial velocity curve for LMC X-3. Our data are shown as filled circles and those of Cowley et al. (1983) are shown as open circles. The best fit to the combined data set is indicated by the solid line. Note, the error bars indicate the scaled (by ~ 1.38) errors necessary to minimize the reduced chi-squared to unity.

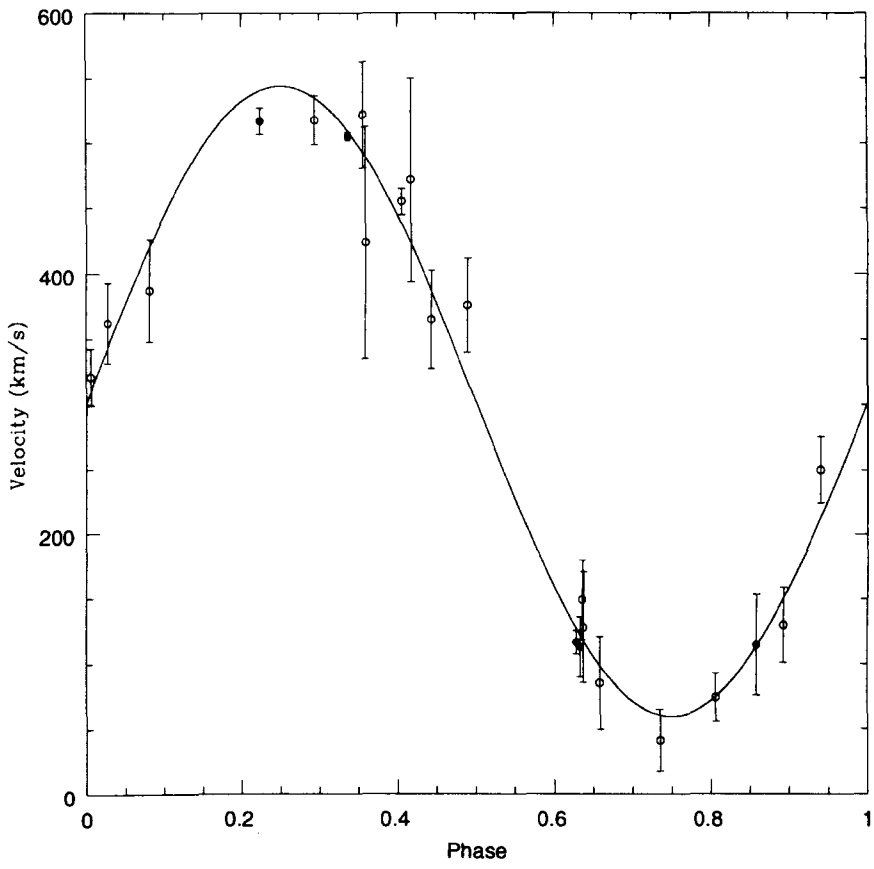

like previous authors (e.g. Soria et al. 2001; Cowley et al 1983) we set i as, $50° \leq i \leq 70°$. Given the limits on i, upper and lower limits on the mass of the black hole may be calculated. The results are shown in the upper part of Table 4.3, where solutions lying between the two extremes, corresponding to intermediate values of i, are of course also valid.

4.5.3 X-ray heating corrections

As was outlined in Section 1.4.2 and the previous Chapter (i.e. 3.4.3), X-ray heating of the donor star by the X-ray source can lead to erroneous radial velocity determinations. To correct for the heating effects we followed the example of Reynolds et al (1993), as outlined in the previous Chapter (i.e. 3.4.3) and an earlier paper (Val Baker et al. 2005), and ran models using LIGHT2 (Hill 1988), refer to Section 2.4. LMC X-3 is known to exist in both the soft and hard X-ray states, but is usually found in the soft state. Previous authors (e.g. Soria et al. 2001) have therefore assumed that the X-ray irradiation will lead to exaggerated radial velocity amplitudes (refer to Section 1.4.3). However, our spectra show that the He I absorption lines are stronger from the heated side of the donor star, which suggests that we are seeing the effects of hard X-rays rather than soft X-rays. This is also apparent in the equivalent widths of the helium lines He I 4026 and He I 4713, where Figure 4.13 shows that the equivalent width is at a maximum when we are seeing the heated side of the donor star (i.e. phase 0.22, 0.34, 0.628 and 0.633) and then drops when we are seeing the cooler side of the donor star (i.e. at phase 0.86). In fact what you would expect is for the equivalent width to decrease as the observable fraction of the heated face of the donor star becomes less. With reference to Figures 4.3 – 4.6, we can see that this fraction decreases in the following order of phase: 0.628/0.633; 0.34; 0.22; 0.86, which is what we also see in the corresponding equivalent widths. Since it is these lines that are used to generate the radial velocity curve, the true radial velocity curve must therefore have larger amplitudes than those observed.

Due to the limitations of the code and the fact that the compact companion is believed to be a black hole, we were unable to accurately represent its dimensions. Instead we set the radius and polar temperature of the object representing the black hole so as to produce a blackbody luminosity equivalent to

that needed to increase the temperature of the donor star by 3300 K. Like that of the previous Chapter, the code was required to run through three iterations before convergence. The results are shown in the lower part of Table 4.3 and the final corrected radial velocity curve is shown for $i = 50°$ and $i = 70°$ in Figures 4.15 and 4.16 respectively. The size of the corrections are $\Delta K_o = 9.4$ and 14.3 km s^{-1} for the two cases.

Figure 4.15: The heating corrected radial velocity curve for LMC X-3, when $i = 50°$. Our data are shown as filled circles and those of Cowley et al. (1983) are shown as open circles. The best fit to the combined data set is indicated by the solid line. Note, the error bars indicate the scaled (by ~ 1.23) errors necessary to minimize the reduced chi-squared to unity.

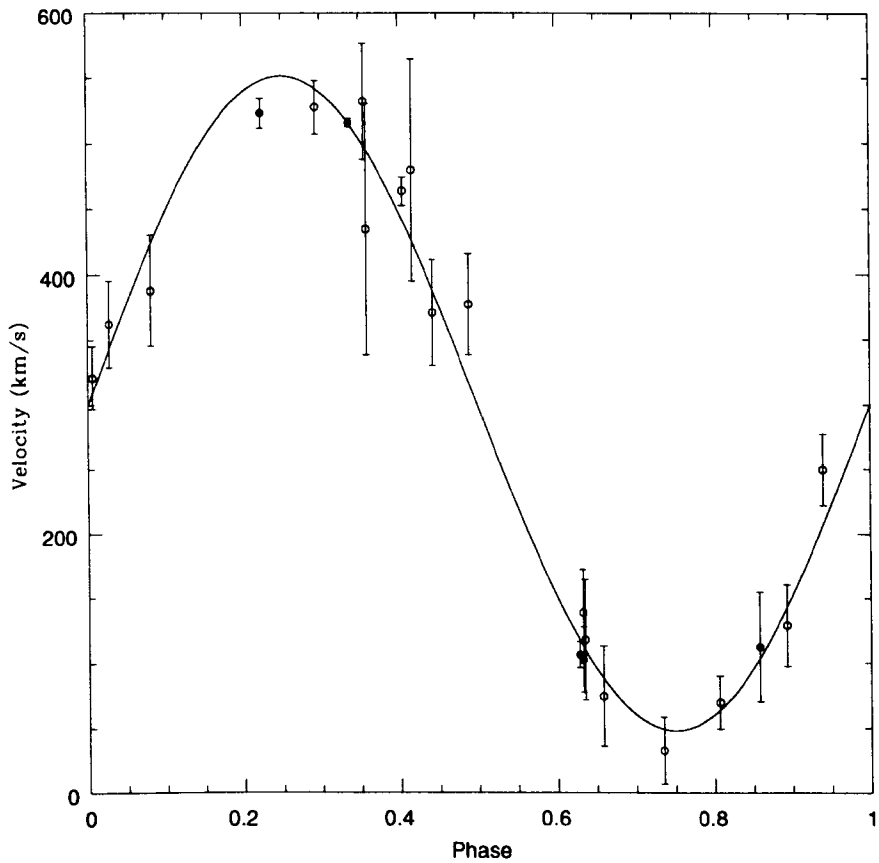

Figure 4.16: The heating corrected radial velocity curve for LMC X-3, when $i = 70°$. Our data are shown as filled circles and those of Cowley et al. (1983) are shown as open circles. The best fit to the combined data set is indicated by the solid line. Note, the error bars indicate the scaled (by ~ 1.33) errors necessary to minimize the reduced chi-squared to unity.

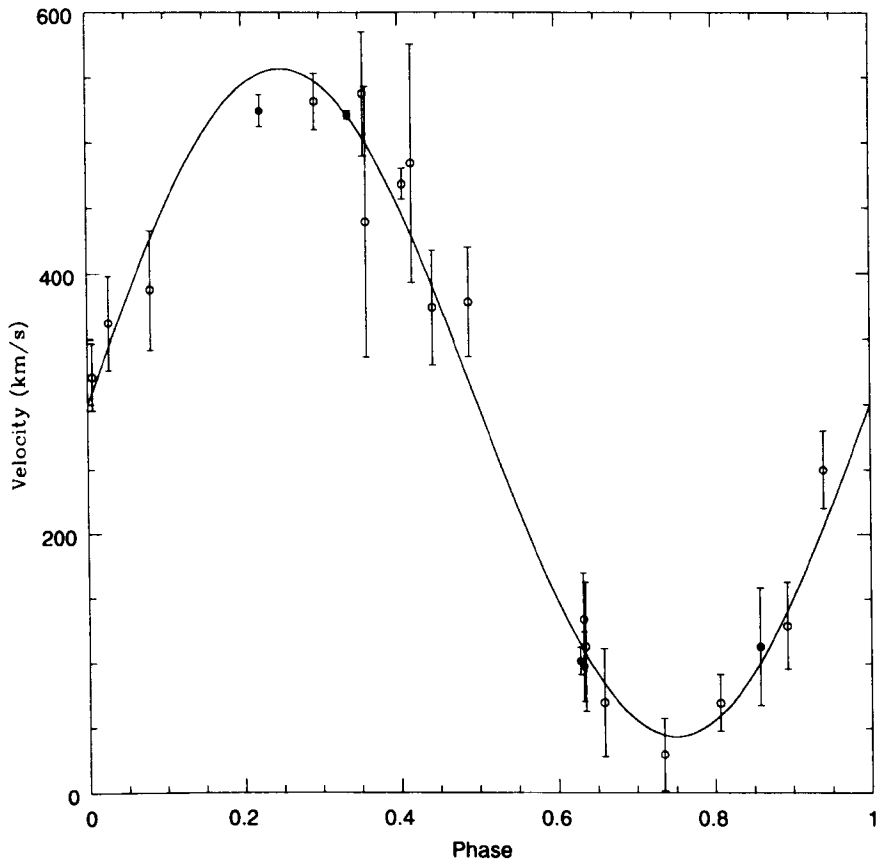

Table 4.3: System parameters for LMC X-3. The upper part of the table shows the resulting parameters from the raw radial velocity curve and the lower part shows the resulting parameters from the corrected radial velocity curve. In each case the two columns for the various inferred parameters are the limiting values assuming $i = 50°$ and $i = 70°$.

Parameter	Fit to raw radial velocity curve	
γ (km s^{-1})	301.7 ± 3.5	
K_o (km s^{-1})	242.4 ± 4.3	
	upper mass limits	lower mass limits
i (deg)	50.0	70.0
q	2.09	1.46
K_x (km s^{-1})	116.27	166.30
M_x ($M_\odot$)	12.3	8.6

Parameter	Fit to corrected radial velocity curve	
γ (km s^{-1})	300.0 ± 4.1	
	upper mass limits	lower mass limits
i (deg)	50.0	70.0
K_o (km s^{-1})	251.8 ± 4.6	256.7 ± 4.9
q	2.24	1.61
K_x (km s^{-1})	112.53	159.41
M_x ($M_\odot$)	13.2	9.5

4.6 Discussion

The raw value for the semi-amplitude of the radial velocity curve ($K_o \sim 242$ km s^{-1}) and the corresponding limits on the black hole mass ($8.9 \leq M_x \leq 12.3$ M$_\odot$) are both comparable with those found by Cowley et al. (1983). Our value for K_o being slightly larger and the mass constraints being $\sim 50\%$ tighter than that of Cowley et al.'s (1983). In determining K_o and M_x, we used Cowley et al's (1983) data set plus our five spectra, so you would expect there to be little discrepancy between our results and those of Cowley et al's (1983). However they assumed that the donor star was a B3V with a mass range of $4 \leq$ M$_o$ ≤ 8 M$_\odot$, and although the mass we assumed for the donor star is within this range we only set M_o at one value (i.e. $M_o = 5.9$ M$_\odot$), which resulted in a tighter constraint on the masses, and a higher amplitude radial velocity curve. Cowley et al. (1983) did not apply heating corections so we were not able to make a comparison with our heating corrected values for K_o and M_x.

Soria et al. (2001) also used Cowley et al's (1983) data to determine the mass of the black hole, but did not add any new data points when making the calculations. They assumed a spectral type for the donor star as a B5IV with a mass of, $M_o \sim 4.7$ M$_\odot$ and hence found a lower limit for the mass of the black hole as, $M_x > 7.3$ M$_\odot$. This value is comparable with that of Cowley et al's (1983) and as we used a higher mass for the donor star it is smaller than ours as expected, but comparable with the lower limit found from our raw radial velocity curve. Based on our spectral classification of the unheated face of the donor star as a B5V, we assumed that the donor star is being heated from the X-ray irradiation by a further 3300K. Contrary to expectation (e.g. Soria et al. 2001) we found that the X-ray irradiation causes the helium absorption lines from the heated atmosphere to be stronger rather than weaker (refer to Figures 4.7 – 4.9 and Figure 4.13), implying that we are seeing the effects of hard X-rays rather than soft X-rays. The resulting heating corrected radial velocity amplitude was therefore larger than the raw values by ~ 12 km s^{-1} and the corresponding mass limits were larger by ~ 1 M$_\odot$ (i.e. $251.8 \leq K_o \leq 256.7$ km s^{-1}; $9.5 \leq M_x \leq 13.2$ M$_\odot$). As we assumed the heating effects to be dominated by the hard X-ray as oppose to the soft X-ray, our heating corrected values for the mass of the black hole are not at all comparable with those of Soria et al's (2001) heating corrected values

(i.e. $M_x > 5.8\ M_\odot$). In addition, we note that the uncertainty in the spectral type of the heated face may give a systematic uncertainty of $\sim \pm 1650$ K in its temperature as noted earlier. This results in a corresponding uncertainty in the resulting radial velocity amplitude of $\Delta K_o \sim \pm 2.5$ km s^{-1}, and in the compact companion mass determination of $\Delta M_x \sim \pm 1\ M_\odot$. In Chapter 7, we consider how better measurements of the black hole mass may be obtained.

Chapter 5

Potential Be star / black hole candidates

This chapter presents new optical spectroscopy of eight potential black hole Be X-ray binaries. Their radial velocities are determined at a range of epochs and the likelihood of the system containing a black hole is discussed in each case. Unfortunately in most cases the service data obtained were not of good quality or too few useable spectra were obtained in order to draw firm conclusions.

5.1 Introduction

The known Be X-ray binaries are systems where the donor star is a Be star and the compact companion is a neutron star. However based on the fact that over two thirds of HMXB are Be stars, it seems unusual that none of these systems contain black holes. From population synthesis studies Podsiadlowski et al. (2003) suggest that black holes are most likely born into binary systems with circular orbits and orbital periods less than 30 days. This is contrary to Be X-ray binary systems containing neutron stars which generally have highly eccentric orbits with long orbital periods.

According to Negueruela and Okazaki (2001), Be systems with short orbital

periods and hence low eccentricity should experience efficient truncation of their circumstellar disc and would therefore not be able to produce regular periodic type I X-ray outbursts. Instead only rare type II X-ray outbursts would be possible (refer to chapter 1.3.2). Based on these results, Zhang et al. (2004) suggest that black hole Be X-ray binaries do exist, but due to their short orbital periods only show these rare type II X-ray outbursts and therefore could be 'hiding', unrecognised in HMXB catalogues as unclassified objects that may have only once been seen to emit X-rays. If this is the case, then one possible way to detect these black hole/Be star X-ray binaries would be to measure the radial velocity shift of the Be star as it orbits with its compact companion. From Equation 1.8, the expected radial velocity amplitudes in each case can be calculated, (refer to Table 5.1 and 5.2). For a typical Be star mass of 5 – 20 $M_{\odot}$ in a 30 – 100 day orbit with a $1.4M_{\odot}$ neutron star, the maximum orbital radial velocity amplitude of the Be star (i.e. if the system is seen edge on) is 10 – 30 km s^{-1}. In contrast, for the same range of Be star masses in a 10 – 30 day orbit with a 3 – $15M_{\odot}$ black hole, the maximum radial velocity amplitude of the Be star is 25 – 200 km s^{-1}. Therefore if we were to observe a large radial velocity amplitude in excess of 30 km s^{-1}, it would clearly indicate a black hole as the compact companion.

5.2 Potential targets and their characteristics

The HMXB catalogue of Liu et al. (2000) contains many Be systems that have displayed at least one observed giant X-ray outburst, but have no detected X-ray pulse period which would indicate the presence of a neutron star. Based on this criteria and the fact that no orbital period was known for any of them, the following seven systems were chosen as possible Be X-ray binary systems harbouring a black hole: HD 34921; DM+53 2262; SAO 49725; LS 4356; LS 3417; HR 4830 and HR 4899.

After selecting these targets, further observations of some of the objects were published which suggested that certain of them may contain white dwarfs or neutron stars as their compact companions. Nonetheless, we continued with

Table 5.1: The expected radial velocity amplitudes for a system seen edge on (i.e. $i = 90°$).

		K_o (km s^{-1})		
M_o ($M_\odot$)	M_x ($M_\odot$)	$P = 10$ days	$P = 20$ days	$P = 30$ days
5	1.4	40	32	28
10	1.4	27	22	19
15	1.4	21	17	15
20	1.4	18	14	13
5	3	74	59	51
5	5	107	85	74
5	10	163	129	113
5	15	201	160	140
10	3	54	43	37
10	5	81	65	56
10	10	134	107	93
10	15	173	138	120
15	3	43	34	30
15	5	67	53	47
15	10	116	92	80
15	15	154	122	107
20	3	37	29	25
20	5	58	46	40
20	10	102	81	71
20	15	139	110	96

Table 5.2: The expected radial velocity amplitudes for a system seen at an inclination, $i = 20°$).

		K_o (km s^{-1})		
M_o ($M_\odot$)	M_x ($M_\odot$)	$P = 10$ days	$P = 20$ days	$P = 30$ days
5	1.4	14	11	10
10	1.4	9	7	7
15	1.4	7	6	5
20	1.4	6	5	4
5	3	25	20	18
5	5	36	29	25
5	10	56	44	39
5	15	69	55	48
10	3	18	15	13
10	5	28	22	19
10	10	46	36	32
10	15	59	47	41
15	3	15	12	10
15	5	23	18	16
15	10	40	31	27
15	15	53	42	36
20	3	13	10	9
20	5	20	16	14
20	10	35	28	24
20	15	47	38	33

our investigations to see whether we could confirm or refute these suggestions. HR 4830, LS 3417, DM+53 2262 and HR 4899 were all found to be associated with X-ray sources discovered by the *HEAO-1* all sky survey (Wood et al. 1984; Tuohy et al. 1988). The association was based on the cross referencing of the *HEAO-1* X-ray sources with that of published literature, where any Be stars found to be located within the positional error box of the X-ray experiment were consequently associated with the corresponding X-ray source (Tuohy et al. 1988). However, Tuohy et al. (1988) warned that the relatively large error boxes could make some of these identifications uncertain. It is therefore stressed that the associated X-ray sources in these four systems (i.e. HR 4830, LS 3417, DM+53 2262 and HR 4899) are merely the proposed X-ray companions and have not been confirmed.

HR 4830 is a B0.5 IIIe[1] star (Codina et al. 1984; Chevalier & Ilovaisky, 1998) with a known radial velocity amplitude of ~ 35 km s^{-1}. It was classified as a Be star based on the presence of double peaked emission lines in the optical spectra (Wackerling, 1970) which are observed to show rapid variations and extreme line broadening (Smith & Balona, 2006). It is the proposed optical counterpart to the highly variable X-ray source 1H1249-637 (Wood et al. 1984; Torrejon & Orr, 2001; Smith & Balona, 2006), with an apparent period of ~ 14 ks which has been suggested as due to partial occultation of a hot spot on the surface of the compact companion (Torrejon & Orr, 2001). This would therefore indicate that the compact companion in this case is a white dwarf or neutron star and not a black hole. The observed X-ray luminosity, $L_x = 5.13 \times 10^{32}$ erg s^{-1} (Codina et al. 1984; Chevalier & Ilovaisky, 1998) is indicative of a persistent low luminosity source, possibly produced by a neutron star in a very wide orbit accreting matter from the stellar wind (Torrejon & Orr, 2001). The luminosity is however an order of magnitude lower than that usually observed in Be XRBs during quiescence or low states (i.e. $\sim 10^{33-34}$ erg s^{-1}, Negueruela, 1998), but it does fall within the predicted range of luminosities for wind accreting white dwarfs (i.e. $\sim 10^{29-33}$ erg s^{-1}, Waters et al. 1989). Its X-ray characteristics, namely high X-ray temperature, erratic variability on timescales of hours and optical metallic emission lines are very similar to γ Cas (Smith & Balona, 2006). HR 4830 has therefore been suggested to be a system containing a magnetized white dwarf in a wide orbit, accreting from the stellar wind (Waters et al. 1989;

[1] where 'e' denotes the presence of emission lines

Torrejon & Orr, 2001), but it could equally well contain a black hole.

LS 3417 is the proposed optical counterpart to the X-ray source 1H1555-552 (Torrejon & Orr, 2001) and has been classified as a B2IIInpe[2] and a B2nne[3] by Garrison et al. (1977) and Reed & Beatty, (1995) respectively. However from its observed photometric colours Torrejon & Orr (2001) calculated the reddening and by using the calibration of Halbedel (1993), found a spectral type of B1-1.5 (Torrejon & Orr, 2001), where its Be nature has been confirmed by both Wackerling (1970) and Coe et al. (1997). The X-ray spectrum is described by a hot diffuse plasma at $kT \sim 3.9 \pm 0.1$ keV, with a luminosity of $L_x \sim 5.8 \times 10^{31}$ erg s^{-1} for a class V and $L_x \sim 2.1 \times 10^{32}$ erg s^{-1} for a class III. In either case the luminosity is indicative of a persistent low luminosity Be XRB (Torrejon & Orr, 2001).

DM+53 2262 is an early type O9-B0 star (Torrejon & Orr, 2001) and has been observed to show large photometric variations and large Hα equivalent widths indicative of a long period Be XRB (Torrejon & Orr, 2001). The associated X-ray companion 1H1936+54, was observed by BeppoSAX but was found to be completely absent in the 2 – 10keV range and just at the limit of detection in the 0.1 – 2keV range (Torrejon & Orr, 2001). This lack of X-ray detection however does not exclude its nature as a Be XRB, as it may have just been in a quiescent or low state. The luminosity is found to be, $L_x < 9 \times 10^{27}$ erg s^{-1}, which is several orders of magnitude lower than the expected coronal emission from an early type star (Torrejon & Orr, 2001).

HR 4899 is the B5Ve proposed optical counterpart to the X-ray source 1255-567 (Nicolet, 1978; Chevalier & Ilovaisky, 1998; Slettebak, 1982) and has a known radial velocity amplitude of ~ 20 km s^{-1}. It is observed to show small optical variability and has a luminosity of $L_x = 2.57 \times 10^{31}$ erg s^{-1} (Chevalier & Ilovaisky, 1998), indicative of a persisetent low luminosity Be XRB.

The sources SAO 49725 and LS 4356 were originally discovered in a systematic cross correlation between the ROSAT all sky survey and SIMBAD (Motch et al. 1997). New observations of these systems by Lopes de Oliveira et al. (2006) confirm a hard X-ray spectrum which can be equally well fitted by a thermal plasma with $T = 10^8$K and solar abundances or by a power-law plus iron line

[2]Where 'n' denotes the presence of broad absorption lines associated with fast rotation, and 'p' denotes the presence of an unspecified peculiarity.

[3]Where 'nn' denotes the presence of very broad spectral lines associated with very fast rotation.

model with a photon index of $\sim$ 1.5 - 1.8, both with a soft thermal component with $T \sim 10^7$K. Note the iron line is clearly detected in LS 4356 and only probably detected in SAO 49725. The luminosity of $L_x \sim 10^{32-33}$ erg s^{-1} is unusual for normal early type stars as it is midway between those radiated by normal stars and classical Be XRB in quiescence. Based on these peculiarities Motch et al. (1997) suggested that they are likely new Be XRBs and due to their modest luminosity are possibly systems containing a white dwarf. Optical observations reveal a spectral type of B0.5III - Ve and confirm a large and apparently stable circumstellar disc (i.e. from intense quasi-stable Balmer emission line profiles) in both sources (Motch et al. 1997; Lopes de Oliveira et al. 2006). SAO 49725 is the proposed optical counterpart to 2030.5+475, which has been observed to exhibit X-ray variability by $\sim$ 80% on timescales as short as 1000s and LS 4356 is the proposed optical counterpart to J1744.7-2713, which has been observed to show large oscillations in the X-ray light curve with a period of P = 3200 seconds (Lopes de Oliveira et al. 2006).

HD 34921 is a B0IVpe star (Polcaro, 1990; Rossi, 1991; Buscombe, 1980) whose Be nature has been confirmed with near infra-red spectroscopy (Clark et al, 1999). The associated X-ray companion 0521+373 (Polcaro, 1990), has a hard X-ray spectrum with a luminosity (i.e. $L_x = 2.8 \times 10^{33}$ erg s^{-1}, Chevalier & Ilovaisky, 1998), similar to that of LS 4356 and SA0 49725.

5.3 Observations and data reduction

Optical spectroscopy of the seven systems were obtained from observations taken at the La Palma, Calar Alto and Sutherland observatories. The spectra were all obtained in service mode; those at SAAO were part of the commissioning runs for SALT, the Southern African Large Teescope. Consequently, as the telescope was still being tested, many of the spectra are not of good quality. During the period January 1999 and June – September 2004, two spectra were taken for DM+53 2262 and SAO 49725 and three for HD 34921, and during the period April – August 2006, fifty-one useable spectra of HR 4830, nineteen useable spectra of LS 3417, twenty two useable spectra of HR 4899 and fourteen useable spectra of LS 4356 were taken. As well as the target stars the radial velocity standard stars KY And, HR 153, HR 1810, HR 4930 and HR 6118 were also

observed. Refer to Table 5.3 for a list of dates, number of spectra obtained and the telescopes used for the observations. In each case[4] the observations covered the wavelength range 4000Å to 4800Å and used a grating spectrograph which gave a resolution of approximately 0.2Å per pixel.

All spectra were reduced using sandard IRAF routines and extracted using optimal extraction procedures. The extracted spectra were then continuum fitted and the resulting target spectra were cross correlated with those of the radial velocity standard star. An example of one continuum normalized spectrum of each star is shown in Figures 5.1 – 5.7, where in each case the prominent lines are shown. The spectra all appear to be consistent with the previously published spectral types.

In the case of the data obtained from the South African Astronomical observatory (i.e. HR 4830, LS 3417, LS 4356 and HR 4899) and the echelle data obtained for HD 34921, many of the observed hydrogen and helium lines were too noisy and/or the available spectral absorption lines did not always match up with those of the standard stars. In this case the radial velocities were determined by fitting Gaussians to the available hydrogen and helium lines, refer to Table 5.4 for a list of the resulting heliocentric velocities for the systems HR 4830, LS 3417, LS 4356, HR 4899 and HD 34921. The radial velocities were therefore only determined by cross correlation with a standard star for the systems SAO 49725 and DM+53 2262. The standard star used in both cases is the B2IV star HR 153, which has a known radial velocity of 2.0 km s^{-1}. The resulting heliocentric radial velocities are shown in Table 5.5.

[4]except for the spectra of HD 3491 observed on the 29th January 1999, as this was obtained with an echelle spectrograph with a resolution of 0.06Å/ pixel, covering a wavelength range of 4260Å – 10100Å

Table 5.3: List of dates, no. of spectra and telescopes used for the observations.

Date	Object	Telescope	Spectra
29-01-1999	HD 34921	CA220, Calar Alto	2
30-06-2004	DM+53 2262	WHT, La Palma	1
30-06-2004	SA0 49725	WHT, La Palma	1
01-09-2004	DM+53 2262	WHT, La Palma	1
01-09-2004	SA0 49725	WHT, La Palma	1
22-09-2004	HD 34921	WHT, La Palma	1
11-04-2006	HR 4830	SALT, SAAO	1
26-04-2005	HR 4899	SALT, SAAO	1
28-04-2005	HR 4830	SALT, SAAO	1
28-04-2005	LS 3417	SALT, SAAO	2
28-04-2005	LS 4356	SALT, SAAO	1
29-04-2005	HR 4899	SALT, SAAO	2
29-04-2005	HR 4830	SALT, SAAO	1
06-05-2005	LS 4356	SALT, SAAO	2
07-05-2005	HR 4830	SALT, SAAO	11
08-05-2005	HR 4899	SALT, SAAO	8
08-05-2005	HR 4830	SALT, SAAO	6
09-05-2005	HR 4899	SALT, SAAO	6
09-05-2005	HR 4830	SALT, SAAO	20
25-05-2005	LS 3417	SALT, SAAO	1
25-05-2005	HR 4830	SALT, SAAO	2
25-05-2005	HR 4899	SALT, SAAO	1
25-05-2005	LS 4356	SALT, SAAO	1
08-06-2005	HR 4830	SALT, SAAO	3
08-06-2005	LS 3417	SALT, SAAO	1

Date	Object	Telescope	Spectra
15-06-2005	HR 4830	SALT, SAAO	2
15-06-2005	LS 4356	SALT, SAAO	3
16-06-2005	HR 4830	SALT, SAAO	2
16-06-2005	LS 3417	SALT, SAAO	2
17-06-2005	HR 4830	SALT, SAAO	2
17-06-2005	LS 4356	SALT, SAAO	2
17-06-2005	LS 3417	SALT, SAAO	2
18-06-2005	HR 4899	SALT, SAAO	1
19-06-2005	HR 4830	SALT, SAAO	2
19-06-2005	LS 3417	SALT, SAAO	1
20-06-2005	LS 3417	SALT, SAAO	1
20-06-2005	HR 4830	SALT, SAAO	1
20-06-2005	LS 4356	SALT, SAAO	1
20-06-2005	HR 4899	SALT, SAAO	1
19-07-2005	LS 3417	SALT, SAAO	2
20-07-2005	LS 3417	SALT, SAAO	2
25-07-2005	LS 3417	SALT, SAAO	2
28-07-2005	HR 4899	SALT, SAAO	2
18-08-2005	LS 3417	SALT, SAAO	1
18-08-2005	LS 4356	SALT, SAAO	2
20-08-2005	LS 3417	SALT, SAAO	2
20-08-2005	LS 4356	SALT, SAAO	2

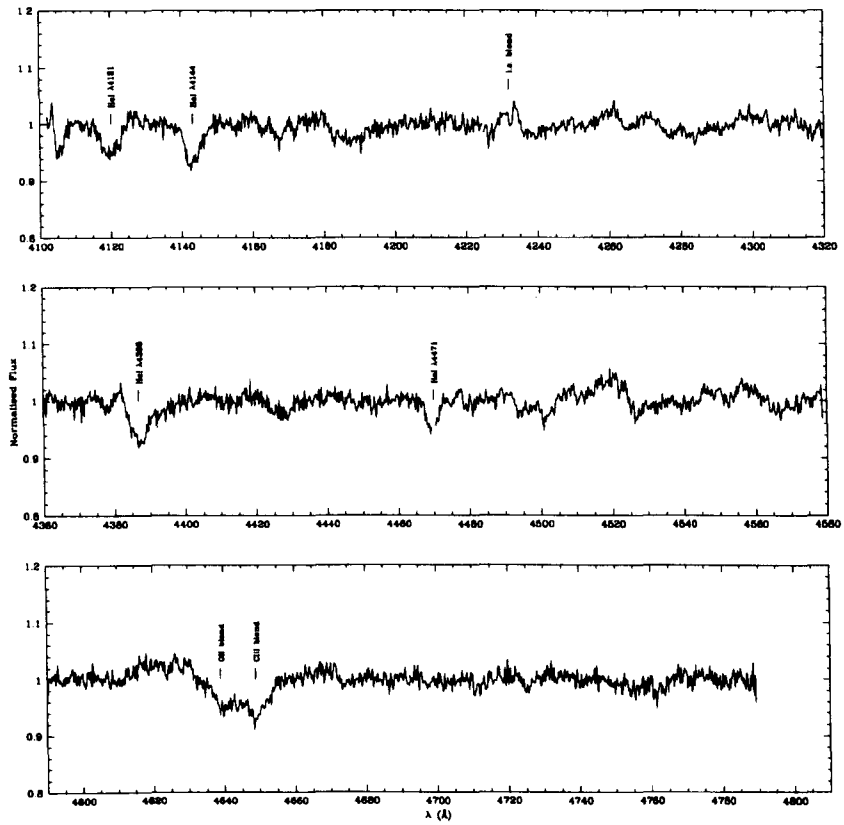

Figure 5.1: A continuum normalized spectrum of LS 3417 obtained on the 28th April 2005.

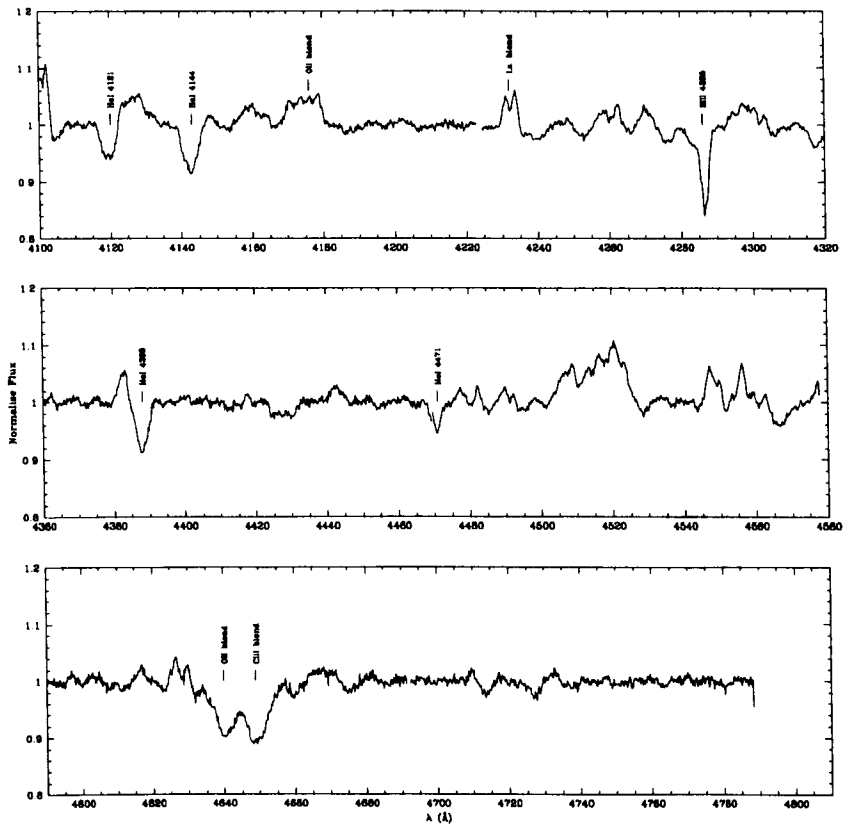

Figure 5.2: A continuum normalized spectrum of LS 4356 obtained on the 25th May 2005.

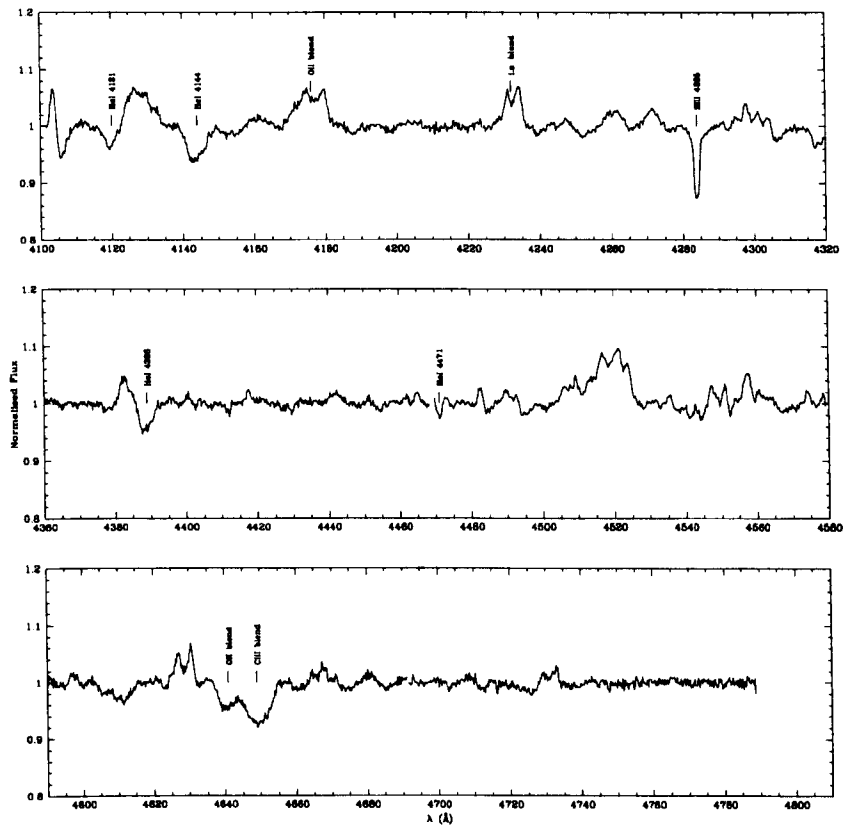

Figure 5.3: A continuum normalized spectrum of HR 4830 obtained on the 9th May 2005.

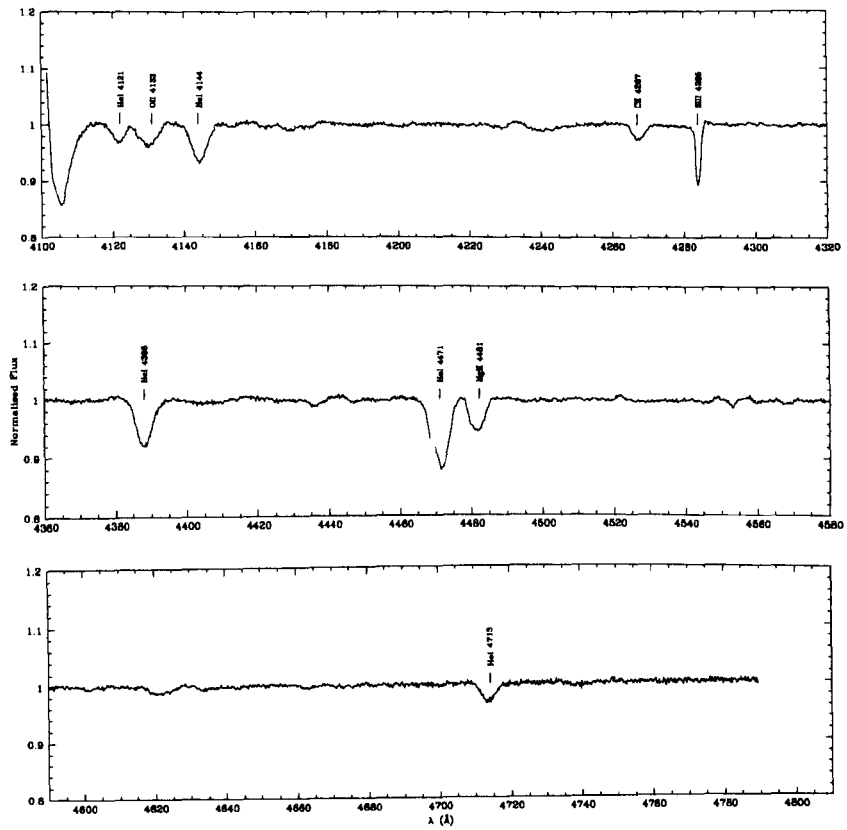

Figure 5.4: A continuum normalized spectrum of HR 4899 obtained on the 29th April 2005.

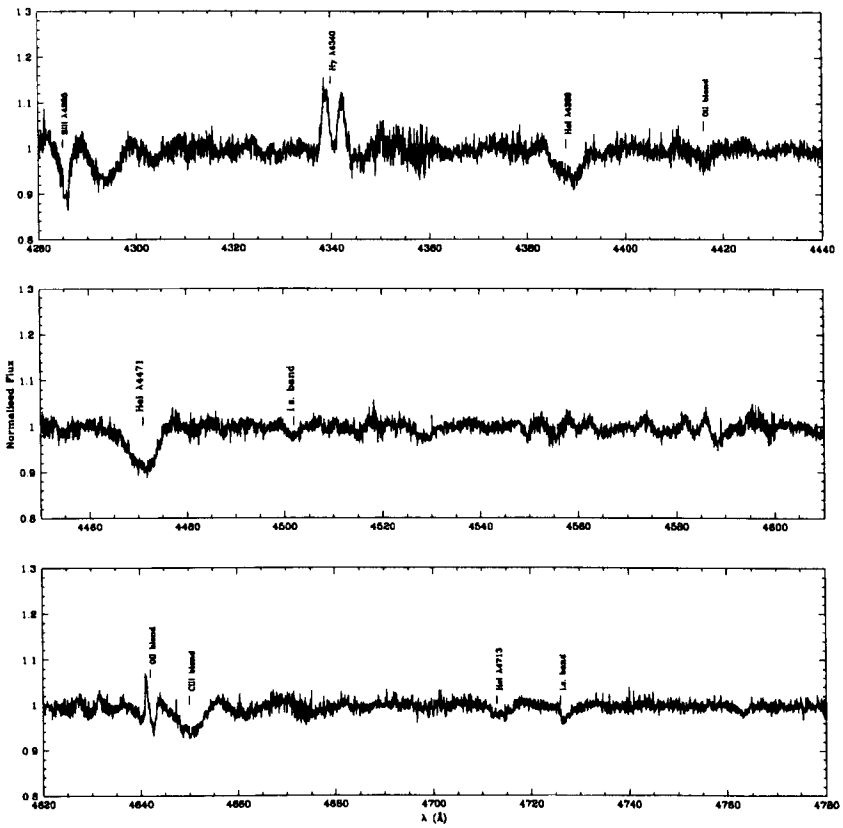

Figure 5.5: A continuum normalized spectrum of HD 34921 obtained on the 29th January 1999.

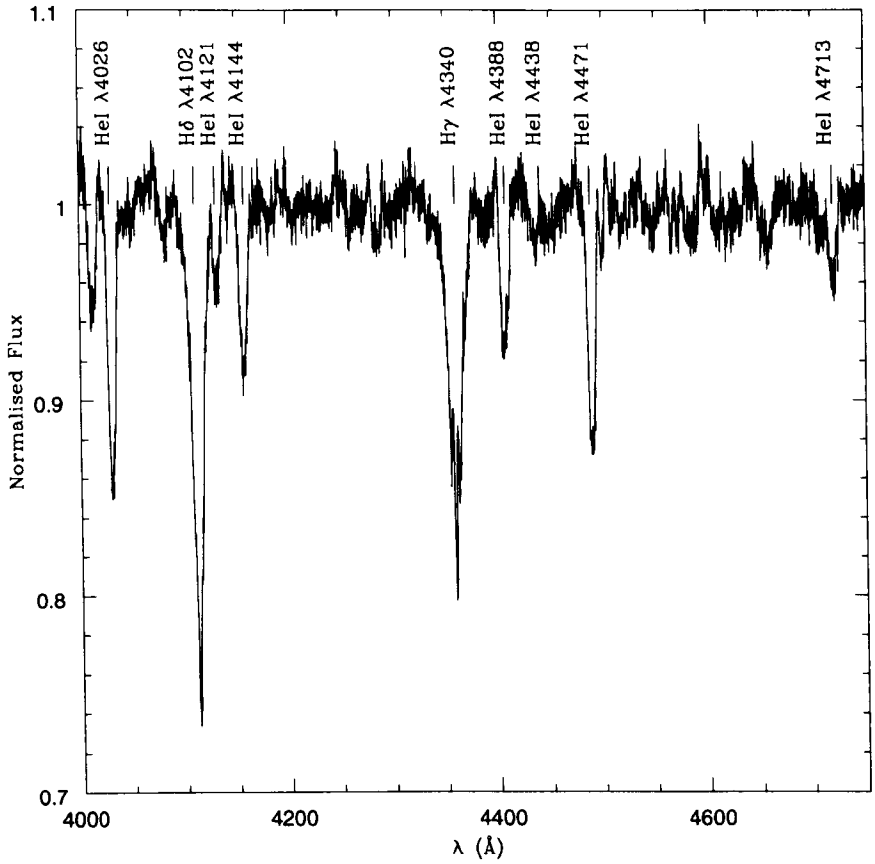

Figure 5.6: A continuum normalized spectrum of DM+53 2262 obtained on the 30th June 2004.

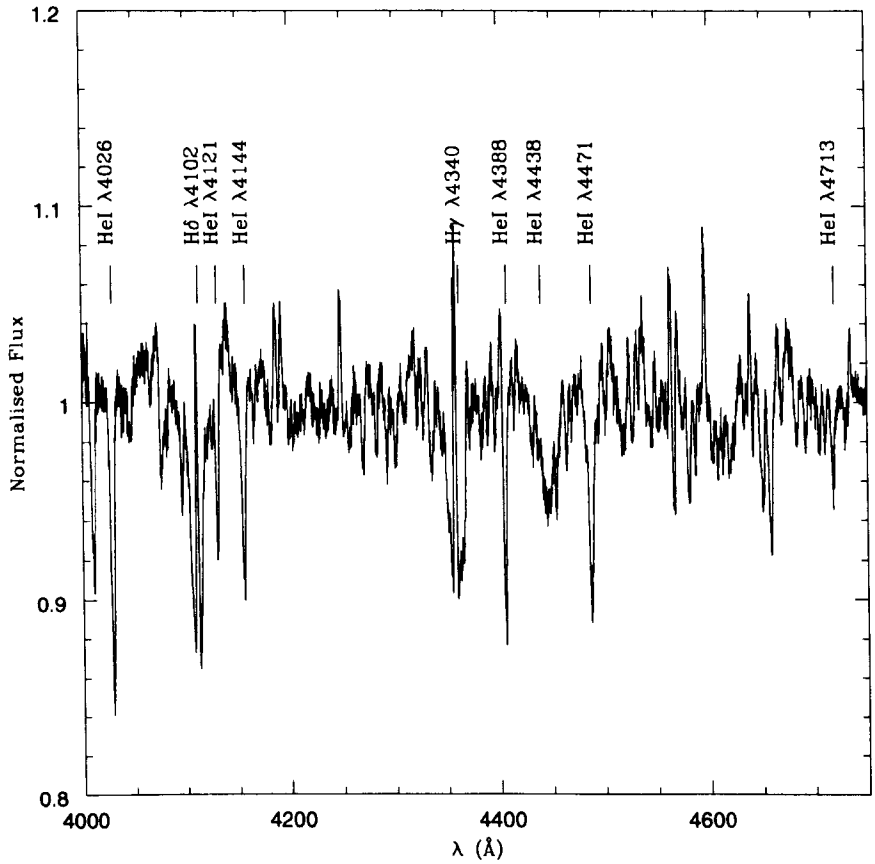

Figure 5.7: A continuum normalized spectrum of SAO 49725 obtained on the 30th June 2004.

Table 5.4: The heliocentric radial velocities found from Gaussian fits to the helium lines.

	Line	HeI4121		HeI4144		HeI4388	
Star	MJD	RV	ΔRV	RV	ΔRV	RV	ΔRV
		(km s^{-1})		(km s^{-1})		(km s^{-1})	
LS 3417	53853.87	-51.0	11.8	-37.5	3.0	-16.9	8.3
LS 3417	53880.76	-50.3	1.2	-73.8	0.7	-18.0	5.1
LS 3417	53894.77	-64.5	2.1	-64.3	0.7	2.4	4.6
LS 3417	53902.97	-87.6	5.9	-54.0	2.1	-8.8	15.8
LS 3417	53903.97			-36.7	7.0		
LS 3417	53905.99						
LS 3417	53906.76						
LS 3417	53935.9						
LS 3417	53936.9						
LS 3417	53940.89						
LS 3417	53965.82						
LS 3417	53967.8						
LS 4356	53853.97			-7.3	2.9		
LS 4356	53861.96			-30.5	6.5		
LS 4356	53881.93			-73.4	0.3		
LS 4356	53901.85			80.0	13.2		
LS 4356	53903.82			106.3	5.3		
LS 4356	53906.82						
LS 4356	53965.89						
LS 4356	53967.90						
HR 4830	53836.86			32.0	2.1		
HR 4830	53853.84			30.5	3.6		
HR 4830	53854.76			22.1	0.9		
HR 4830	53862.76			21.1	7.0		
HR 4830	53863.81			-3.5	1.3		
HR 4830	53864.82			-1.0	5.7		
HR 4830	53880.92			-14.2	0.2		

	Line	HeI4121		HeI4144		HeI4388	
Star	MJD	RV	ΔRV	RV	ΔRV	RV	ΔRV
		(km s^{-1})		(km s^{-1})		(km s^{-1})	
HR 4830	53894.72	-39.8	2.3	-36.6	0.5		
HR 4830	53901.81			-0.2	6.6		
HR 4830	53902.71			39.9	4.6		
HR 4830	53903.80			9.3	2.9		
HR 4830	53905.71						
HR 4830	53906.80						
HR 4899	53852.04	34.8	4.2	20.7	0.3	-8.1	0.6
HR 4899	53854.74	61.8	0.4	43.4	0.1	21.0	3.3
HR 4899	53863.77	50.5	1.8	36.3	1.9	-5.8	1.8
HR 4899	53864.77	52.4	5.8	37.6	5.8	-4.7	6.7
HR 4899	53880.92	23.8	1.9	16.5	0.7	51.3	1.2
HR 4899	53904.89						
HR 4899	53906.85						
HR 4899	53944.75						
HD 34921	51207.88						
HD 34921	51207.89						
HD 34921	53271.17	-106.1	0.6	65.2	26.2	41.1	1.8

	Line	HeI4471		HeI4713	
Star	MJD	RV (km s^{-1})	ΔRV	RV (km s^{-1})	ΔRV
LS 3417	53853.87			-105.3	1.0
LS 3417	53880.76			-20.7	0.6
LS 3417	53894.77			94.0	8.9
LS 3417	53902.97			-121.9	28.4
LS 3417	53903.97			-41.3	5.9
LS 3417	53905.99			29.6	11.2
LS 3417	53906.76			19.2	5.3
LS 3417	53935.9			-13.4	15.1
LS 3417	53936.9			-33.6	38.6
LS 3417	53940.89			-0.7	9.3
LS 3417	53965.82			-15.4	0.3
LS 3417	53967.8			-20.8	7.3
LS 4356	53853.97				
LS 4356	53861.96				
LS 4356	53881.93				
LS 4356	53901.85				
LS 4356	53903.82				
LS 4356	53906.82			-36.0	7.0
LS 4356	53965.89			-74.2	18.5
LS 4356	53967.90			-30.4	4.9

	Line	HeI4471		HeI4713	
Star	MJD	RV	ΔRV	RV	ΔRV
		(km s^{-1})		(km s^{-1})	
HR 4830	53836.86				
HR 4830	53853.84				
HR 4830	53854.76				
HR 4830	53862.76				
HR 4830	53863.81				
HR 4830	53864.82				
HR 4830	53880.92				
HR 4830	53894.72				
HR 4830	53901.81				
HR 4830	53902.71				
HR 4830	53903.80				
HR 4830	53905.71			6.9	3.5
HR 4830	53906.80			-43.4	4.8
HR 4899	53852.04			-47.4	1.3
HR 4899	53854.74			10.1	1.7
HR 4899	53863.77			-8.4	3.0
HR 4899	53864.77			-7.2	8.6
HR 4899	53880.92			133.7	5.4
HR 4899	53904.89			12.4	3.2
HR 4899	53906.85			68.5	0.3
HR 4899	53944.75			-6.8	2.7
HD 34921	51207.88	-28.2	2.8	19.9	0.3
HD 34921	51207.89	-42.8	2.4	11.1	3.6
HD 34921	53271.17	-28.2	0.3	-39.1	12.8

Table 5.5: The heliocentric radial velocities found from cross correlation with HR 153.

Star	MJD	RV(km s^{-1})	ΔRV
DM+53 2262	53187.22	90.9	3.4
DM+53 2262	53250.05	91.2	5.7
SA0 49725	53187.22	-16.7	4.6
SA0 49725	53250.06	-29.2	4.4

5.4 Data analysis

From Table 5.4, we can see that the resulting radial velocities found from Gaussian fits to the individual spectral lines in the same spectrum (i.e. He I 4121; 4144; 4388; 4471; 4713), are significantly different from each other, where in some cases the difference is comparable with that of the radial velocity. Such a disrepancy cannot therefore be due to the uncertainties in the Gaussian fits. It may however, be that the spectral lines are coming from different parts of the system or that they are contaminated or affected by the circumstellar disc. The X-ray irradiation of the donor star by the X-ray source may be having an effect on the observed spectral lines, especially if the X-rays are soft X-rays (refer to Section 1.4.3) as these will affect the spectral lines differently.

To look for any significant radial velocity amplitudes, radial velocity curves were therefore plotted for each line. However, the only spectral lines that were observable in a sufficient amount of the data for a curve to be plotted, were the He I 4144 and He I 4713 lines. Refer to Figures 5.8 – 5.15 for the resulting radial velocity curves for LS 3417, LS 4356, HR 4830 and HR 4899 respectively.

The He I 4144 radial velocity curves generally have more data points and are less messy, where an apparent radial velocity variation can be seen in each case. Note, there are still too few data points for a sinusoidal fit to be made, so in each case only a rough amplitude of variability can be quantified.

The star HD 34921 only has 3 data points, and therefore does not have sufficient data for a radial velocity curve to be plotted. However, from the radial velocities found from the He I 4471 and He I 4713 lines, we can see that the radial velocity changes by $\sim$ 60 km s^{-1} in $\sim$ 5 years.

The stars DM+53 2262 and SA0 49725 also have insufficient data for a radial velocity curve to be plotted. However, from Table 5.5 we can see that over the $\sim$ 63 days of data coverage the radial velocity of DM+53 2262 does not change significantly and the radial velocity of SAO 49725 only changes by ~ 12.5 km s^{-1}.

5.5 Discussion

Unfortunately the data set for each star is insufficient to draw any real conclusions. However, the data that we obtained from the SALT telescope in South Africa, are just about sufficient to plot radial velocity curves. In the case of LS 3417, the scatter shown by the He I 4144 radial velocity values has an amplitude variation of $\sim 15-25$ km s^{-1} (refer to Figure 5.8). In which case, according to Tables 5.1 and 5.2, the compact companion is most probably a neutron star or white dwarf and not a black hole. Previous observations of LS 3417 have found no evidence of high frequency pulsations, but have reported X-ray features similar to those of a white dwarf (Lopes de Oliveira et al. 2006), so it is very probable that this system has a white dwarf as the compact companion.
The scatter in the He I 4144 radial velocity values for LS 4356, appears to have an amplitude variation of $\sim 90 - 100$ km s^{-1} (refer to Figures 5.10). In which case, it is highly likely that the compact companion is a black hole, however before this can be confirmed, more observations would be needed to determine its period, inclination and stellar mass etc.
HR 4830, also appears to show an amplitude variation in the scatter of its He I 4144 radial velocity values, with an amplitude of $\sim 30 - 40$ km s^{-1} (refer to Figures 5.12). This system already has a known radial velocity amplitude of 35 km s^{-1} and a suggested spin period of 14ks (Torrejon & Orr, 2001), and is therefore most likely to be a neutron star. However, the proposed spin period is much larger than those usually found for neutron stars and implies an orbital period of $\sim 10^2$ days (Apparao, 1994), which agrees well with the peak of the orbital period distribution calculated for white dwarf/Be star systems (Raguzova, 2001).
HR 4899 also appears to show an amplitude variation in the scatter of its He I 4144 radial velocity values, with an amplitude of $\sim 10 - 20$ km s^{-1} (re-

fer to Figures 5.14). This system also has a known radial velocity amplitude of 13 km s^{-1} and is therefore most probably a neutron star and not a black hole. However in each of these four systems (LS 3417; LS 4356; HR 4830 and H4 4899), these amplitude variation values are only illustrative and much more data is needed in order to do a realistic fit. It should also be noted again that the associated X-ray sources in these four systems have not been confirmed.

The systems HD 34921, DM+53 2262 and SAO 49725 did not have sufficient data for a radial velocity curve to be plotted. However the radial velocity of DM+53 2262 does not appear to show significant variation between the two data points, whereas HD 34921 and SA0 49725 do show some variation. Obviously in order to make some accurate conclusions about these seven systems more data needs to be obtained.

In conclusion, whilst the data we have obtained are very noisy and incomplete, there is some evidence that LS 3417, HR 4830 and HR 4899 contain neutron star or white dwarf companions and that one object LS 4356 may indeed contain a black hole. It should be noted however, that the associated X-ray source in each of these systems is not confirmed. More high quality data spanning several weeks or months on each object are therefore needed in order to confirm their binary nature, the X-ray companion and the radial velocity variations. In the meanwhile, the question of the existence of black hole/Be star X-ray binaries remains unsolved.

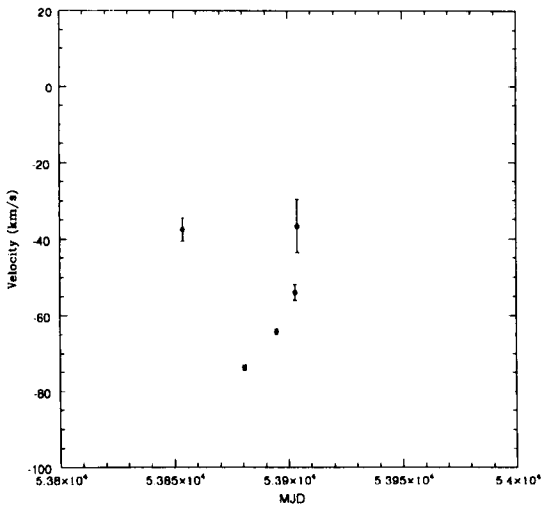

Figure 5.8: The He I 4144 radial velocity curve for LS 3417.

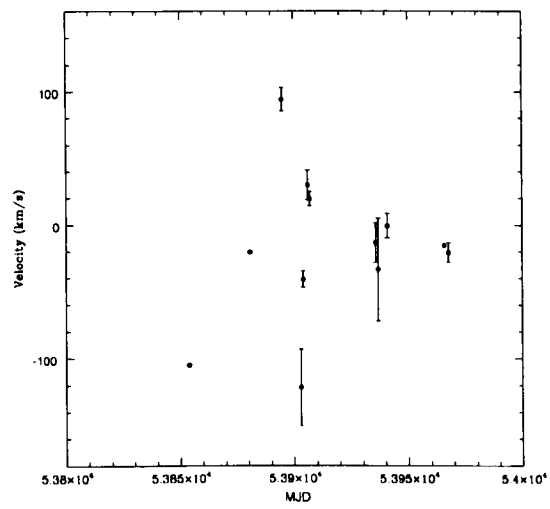

Figure 5.9: The He I 4713 radial velocity curve for LS 3417.

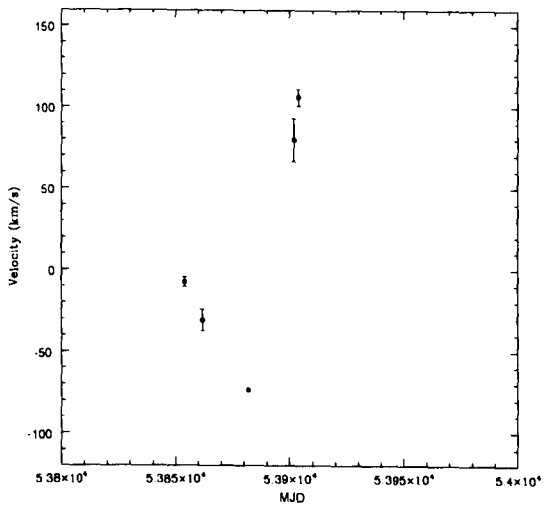

Figure 5.10: The He I 4144 radial velocity curve for LS 4356.

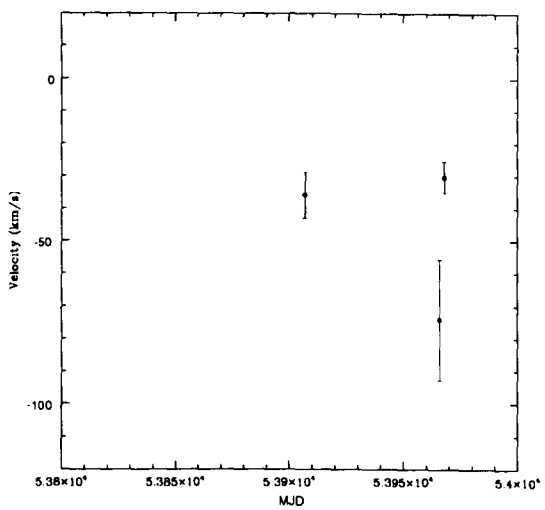

Figure 5.11: The He I 4713 radial velocity curve for LS 4356.

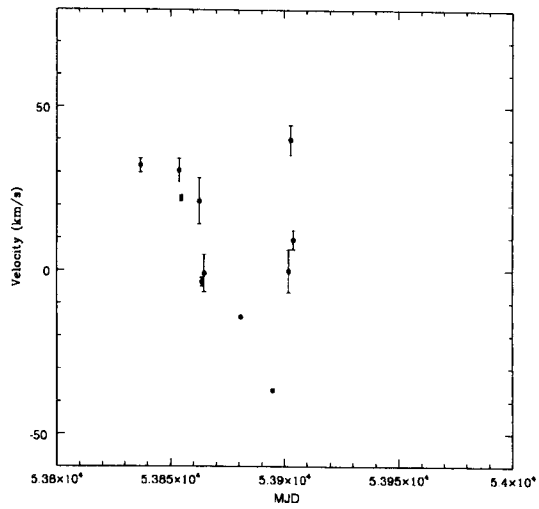

Figure 5.12: The He I 4144 radial velocity curve for HR 4830.

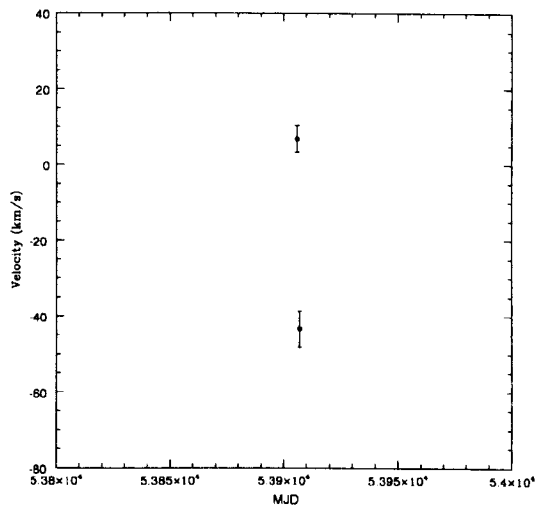

Figure 5.13: The He I 4713 radial velocity curve for HR 4830.

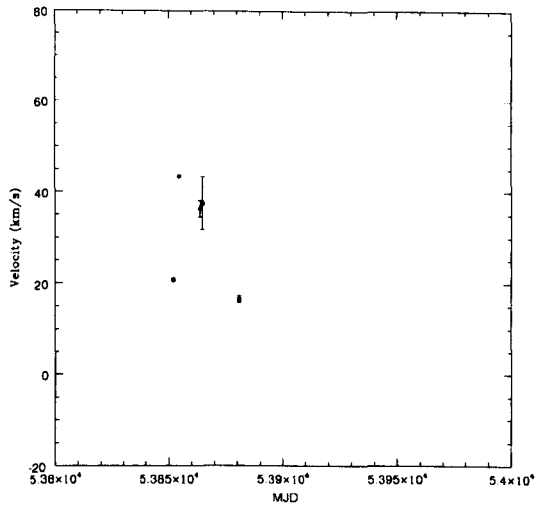

Figure 5.14: The He I 4144 radial velocity curve for HR 4899.

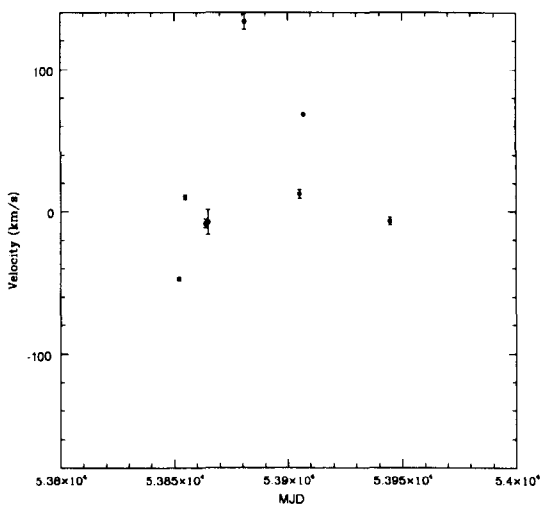

Figure 5.15: The He I 4713 radial velocity curve for HR 4899.

Chapter 6

The Be X-ray binary systems X Per and A0535+26

This chapter presents new high resolution optical spectroscopy of the high mass Be X-ray binaries A0535+26 and X per. The observed Hα emission lines are compared with previous data of Clark et al. (2001) and Grundstrom et al. (2007), and discussed in terms of their evolution with time and the changing state of the circumstellar disc. The other observed hydrogen (Hβ, Hγ) and helium (He I 5876, 6678, 7065) emission lines are then compared with the Hα line.

6.1 Emission line profiles of Be X-ray binaries

Be X-ray binaries are known to consist of a neutron star in orbit around a Be star, where the X-ray behaviour can be described in terms of the system's eccentricity and the size of its circumstellar disc, refer to Section 1.3.2 and Chapter 5. The circumstellar disc is usually detected in the form of an optical/infra-red excess and/or the Balmer emission lines, most notably being the Hα emission line.

Variations in the Hα line, measured in terms of the equivalent width (EW), are positively correlated with the V magnitude, and are believed to reflect changes in the circumstellar disc (Clark et al. 1998a, b) i.e. photometric bright states and large Hα equivalent widths correspond to times of increased disc density and faint states with weak Hα lines correspond to a low disc density (Clark et al. 1998a).

The observed emission line profiles can be divided into two classes (Hanuschik, 1986; Hummel, 1994), with class 1 showing symmetric profiles of double-peak, wine-bottle and shell type (refer to Figure 6.1), and class 2 showing asymmetric profiles where the violet (V) and red (R) peaks are observed to vary cyclically in line strength.

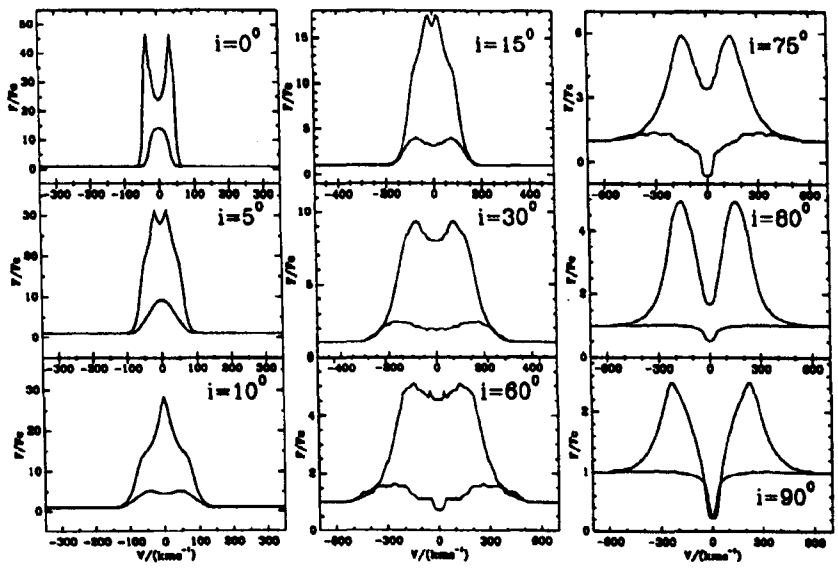

Figure 6.1: Schematic diagram of the different emission line profiles observed in class 1, taken from Hummel (1994). Wine-bottle type are shown in the left panels, double peak in the centre panels and shell type in the right panels. Note, these are calculated emission line profiles, where the upper curves are determined assuming an optically thick model (i.e. $N_o = 10^{14}$ cm^{-3}) and the lower curves are determined assuming an optically thin model (i.e. $N_o = 10^{12}$ cm^{-3}).

The symmetric profiles of class 1 can be explained in terms of being produced in a vertically extended Keplerian disc, where the double-peak structure is generated by the rotational broadening distribution of emitting particles (Smak, 1969;

1981; Huang, 1972; Horne & Marsh, 1986; Hummel, 2000). The difference in the shapes of the profiles is believed to be caused by the natural combination of kinematical broadening and broadening by non-coherent scattering (Hummel & Dachs, 1992; Hummel & Hanuschik, 1997), where shell type profiles are observed at high inclination angles and wine-bottle type profiles are observed at low inclination angles (Hanuschik et al. 1988; Hummel & Hanuschik, 1997; Hummel, 2000), (refer to Figure 6.1).

The asymmetric line profiles of class 2, can also be explained in terms of a vertically extended Keplerian disc, but with the presence of a density perturbation in the form of a global one-armed oscillation (Okazaki, 1991; Hummel & Hanuschik, 1997). Such a perturbation was first suggested by Kato (1983) and later developed by Okazaki (Okazaki, 1991, 1996, 1997) into a model based on the theoretical result that the low-frequency, one-armed oscillations are the only possible oscillations in geometrically thin discs (Kato, 1983, 1989; Okazaki & Kato 1985; Adams et al. 1989). These global one-armed oscillations have been shown to explain the cyclic long term V/R variations observed in the class 2 profiles and is now the generally adopted model (Hummel & Hanuschik, 1994; Hanuschik et al. 1995; Okazaki, 1996; Hummel, 2000). However the exact extension of perturbation in the disc is not yet fully known and the model is therefore unable to successfully predict the cycle length of the V/R variability (Firt & Harmanec, 2006).

For such predictions to be made the observable system parameters need to be known to greater accuracy and confidence. Many of the system parameters can be determined from the emission line profiles. For example, if a Keplerian velocity distribution is assumed, the radius of the circumstellar disc can be determined from the separation of the doubly peaked emission lines (Huang, 1972) i.e. $\Delta V = 2V_d \sin i$ where ΔV is the velocity determined from the peak separation and $V_d \sin i$ is the projected velocity at the outer edge of the emitting region. Therefore the velocity at the outer edge of the disc is found from, $V_d = (\Delta V)/(2 \sin i)$, and the radius at the outer edge of the emitting region is given by[1]:

[1]It should be noted that in cases where the spectrum is not of good enough quality to measure the peak separation accurately, the known correlation between ΔV and Hα equivalent width (Hanuschik, 1989; Zamanov et al. 2001), can be used to derive values for R_d.

$$R_d = \frac{GM}{V^2} = \frac{GM_\star \sin^2 i}{(0.5\Delta V)^2} \tag{6.1}$$

where $M_\star$ is the stellar radius.

It should be noted that the determined radius in this case is that of the emitting region and therefore not necessarily representative of the true circumstellar radius. To obtain a clearer picture of the actual extent of the disc geometry, observations can be made using optical long baseline interferometry (e.g. Thom et al. 1986; Stee et al. 1995; 2000; Quirrenbach et al. 1993; 1997; Chesneau et al. 2005; Tycner et al. 2005; 2006). The observations are generally focused on the angular resolution of the discs in the narrow spectral band, centred on the Hα emission line. Such studies have revealed that the matter responsible for the visible continuum and emission lines is not spherically distributed (Stee et al. 2001; Tycner et al. 2006), where Stee et al. (1998) found that the extent of the emitting regions increases as He I 6678; Hβ, Hα. An example of this is shown in the intensity plots of γ Cas (refer to Figure 6.2), where you can see that the disc is clearly emitting at radii beyond that of the Hα emitting radius. In this case therefore it is clear that the circumstellar radius R_d, determined from the Hα emission line, would not be indicative of the true circumstellar radius. At present however most of these studies are limited to nearby stars, so for more distant targets we have to rely on indirect methods in order to make estimations about the disc size and geometry.

As outlined in Section 1.3.2 and Chapter 5, the radius of the circumstellar disc is limited by the truncation radius due to the presence of resonances between the neutron star orbital period and the Keplerian orbital periods of the matter in the circumstellar disc, (Okazaki & Negueruela, 2001). These truncation radii, R_n, are given by

$$\frac{R_n}{R_\star} = \left(\frac{GM_\star}{4\pi^2}\right)^{\frac{1}{3}} \frac{1}{R_\star} \left(\frac{P_{orb}}{n}\right)^{2/3} = \frac{rM_\star^{1/3}}{n^{2/3}R_\star} \tag{6.2}$$

where n is an integer which determines the resonance involved (e.g. $n = 3$ for the 3:1 resonance); the donor star's stellar radius, $R_\star$ and mass, $M_\star$, are given in terms of solar units; and r is a constant given by

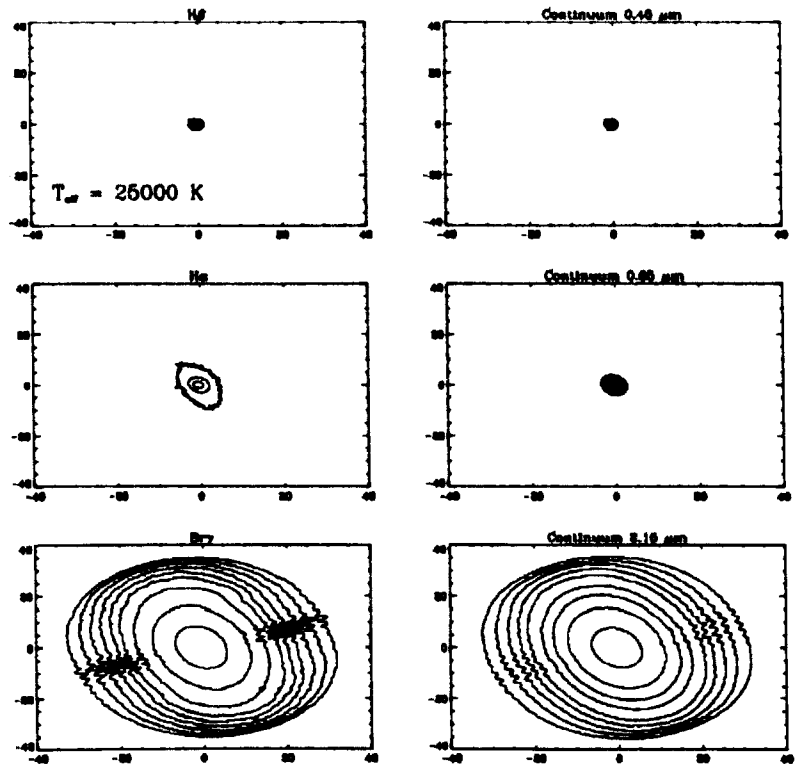

Figure 6.2: Intensity maps with parameters representative of the Be star γ Cas (Stee & Bittar, 2001). From the upper left to the lower right respectively in the Hβ line, Continuum at 0.48μm, Hα line, Continuum at 0.65μm, Brγ line, Continuum at 2.16μm, within a spectral bandwidth of 40Å. The axis are in units of the stellar radius. North is up and East is left.

$$r = \left(\frac{M_{\odot}G}{4\pi^2}\right)^{2/3} \frac{P_{orb}^{2/3}}{R_{\odot}} \tag{6.3}$$

Studying the emission line profiles of Be/X-ray binaries and their evolution with time, is therefore of great importance as it allows us to investigate the changing state of the circumstellar disc and the resulting accretion on to the neutron star.

6.2 Overview of A0535+26

A0535+26 (V725 Tau) is a hard Be X-ray transient pulsar (Coe et al. 2006; Sunyaev et al. 1989; Motch et al. 1991). It was discovered in 1975 by the *Ariel 5* survey during a type II outburst (Coe et al. 1975; Rosenberg, 1975) and became a prototype of the Be X-ray binary class. The optical counterpart was identified as the O9.7-B0IIIe star, HDE 245770 (Liller, 1975; Giovannelli & Sabau Graziati, 1992; Steele et al. 1998), however the luminosity class is not confirmed, as it is based on spectral lines that were affected by disc emission (Wang & Gies, 1998; Grundstrom et al. 2007).

A0535+26 is known to display both type I and II X-ray outbursts, which is expected in systems of intermediate eccentricity (i.e. $e = 0.47 \pm 0.02$, Motch et al. 1991; Finger et al. 1994; Negueruela, 1998). Observations of the type I X-ray outbursts, of a few hundred milli-crab are normally seen at periastron (Motch et al. 1991; Clark et al. 1998a). These outbursts reveal an approximate orbital period of around 110 days (Hayakawa, 1981; Warwick et al. 1981; Nagase et al. 1982; Priedhersky & Terrell, 1983; Hutchings, 1984; Finger et al. 1996). During times of X-ray emission, a pulse period of $P_{pulse} = 103$ seconds is also seen (Hayakawa, 1981; Motch et al. 1991; Finger et al. 1994; Clark et al. 1998a). Analysis of the Doppler shifts of this X-ray pulsation allow determination of an accurate orbital period to be $P_{orb} = 111.38 \pm 0.11$ days (Larionov et al. 2001; Coe et al. 2006).

The emission from the disc, in the form of optical and infrared continuum and Balmer emission lines, is known to display temporal variations (Clark et al. 1998b; Lyuty & Zaitseva, 2000; Haigh et al. 2004), but these are not correlated with the orbital period, and instead have dominant timescales of $\sim$ 1500 days and $\sim$ 103 days. The 103 day periodicity is the beat period of the orbital pe-

riod and the 1500 day periodicity (Larionov et al. 2001), which is believed to be caused by retrograde precession of the circumstellar disc (Haigh et al. 2004). Temporal variations in the circumstellar disc are also apparent in the form of V/R cyclic variations in the Hα emission profile, and are most likely attributed to a global one-armed density oscillation (Clark et al. 1998a). The cycle observed in A0535+26 is $\sim$ 1 year, and is the shortest cycle ever observed (i.e. typical cycles are $\sim 7 - 10$ years for other Be stars), (Clark et al. 1998a). This variability is also seen in the Hβ line, which is produced closer to the star than Hα, thus suggesting that any density perturbation in the circumstellar disc of A0535+26 extends to smaller radii than the Hα emission zone (Clark et al. 1998a).

Observations of type II X-ray outbursts have, to date, been observed 5 times, typically reaching $2 - 3$ Crab intensity (in the $2 - 20$keV range) in each burst. The first recorded outburst in April 1975 marked the discovery of A0535+26, and since then outbursts seem to recur every 5 years in groups of two with the third one missing (i.e. April 1975 (Rosenberg et al. 1975; Coe et al. 1975); October 1980 (Nagase et al. 1982); April 1989 (Sunyaev, 1989); February 1994 (Finger et al. 1996); May/June 2005 (Coe et al. 2006)). These outbursts seem to correlate with the cycles of circumstellar disc loss and reformation determined from the Hα[2] equivalent width and photometric variations. For example, in 1994 the Hα equivalent widths were at a low, exhibiting the longest minimum observed in 10 years, and suggesting a significant reduction in the base density of the disc (Clark et al. 1998a). This is also apparent in infra-red observations, which show a reduction in the Paschen series flux between December 1993 and September 1994 (Clark et al. 1998b). This reduction in disc density preceded the observed giant outburst of 1994 (Finger et al. 1996), as the matter in the outer regions of the circumstellar disc (between the 2 outer truncation radii) would have been dumped and accreted by the neutron star to form the giant burst, thus resulting in a smaller circumstellar disc.

The disc was then observed to carry on reducing in size until almost complete disc loss in 1998 (Clark et al. 1998a; Haigh et al. 1999; Lyuty & Zaitseva 2000; Haigh et al. 2004; Coe et al. 2006). This correlates with the fact that no type II X-ray outburst was observed in 2000 (i.e. $\sim$ 5 years after the last outburst in

[2]The He I 6678 emission line is observed to show similar behaviour to the Hα line, (Coe et al. 2006; Grundstrom et al. 2006).

1994), and no X-ray detections were reported in the period 1995 – 2004.

Over the next few years however, the circumstellar disc was observed to reform (Coe et al. 2006) and attained its former strength in 2005 (Grundstrom et al. 2007), which correlates with the observed outbursts of May/June 2005 (Tueller et al. 2005; Smith et al. 2005; Coe et al. 2006; Grundstrom et al. 2006). The first of these outbursts occurred on the 6th May 2005 (i.e. at phase 0.91), reaching luminosities of $L_x = 1.3 \times 10^{37}$ erg s^{-1}, and lasting $\sim$ 75 days, which is the longest ever observed outburst in this system (Coe et al. 2006; Grundstrom et al. 2007).

The X-ray spectra during the outburst can be well presented by a power-law component with $\Gamma = 1.0 \pm 0.2$ and an exponential cut off of 25 ± 5 keV, consistent with previous type II outbursts, (Coe et al. 2006). However the outburst profile displayed an exponential flux rise with rapid decay instead of the typical rapid rise and slow decay observed in most type II outbursts (Coe et al. 2006). Approximately 15 days after its decay it was then accompanied by a second smaller outburst (Coe et al. 2006; Grundstrom et al. 2007) similar to that of V635 Cas. However, instead of the circumstellar disc dispersing after the second outburst, optical data (refer to Figure 6.3) suggests that the circumstellar disc remained large and in fact continued to grow beyond periastron passage (Coe et al. 2006; Grundstrom et al. 2007). This is consistent with the X-ray light curves of Grundstrom et al. (2007) (refer to Figure 6.3) and in the emission strength of Hβ (Motch et al. 1991), which show a maximum past periastron passage (i.e. at phase 0.3).

It is therefore suggested that the mass transfer process in A0535+26 is supported by the strong tidal forces that exist near periastron (Grundstrom et al. 2007), where the arm closest to the neutron star is able to lift material outside of the disc boundary providing a source of gas accretion at phases beyond periastron (Okazaki et al. 2002). The fact that the circumstellar disc remains large and does not disperse could also explain the unusual rapid decay observed in the outburst profile, where the slower rise could be attributed to the formation of an accretion disc around the neutron star (Coe et al. 2006).

The presence of a transient accretion disc has previously been suggested by Motch et al. (1991) who found that the specific angular momentum of accreted material is much larger during type II outbursts than in those of type I. The detection of quasi-periodic oscillations during type II outbursts, also seems to

suggest the presence of an accretion disc, (Finger et al. 1996).

During the quiescent X-ray state, when no type I or II outbursts are observed, A0535+26 has been shown to display pulsations (Motch et al. 1991) and low intensity X-ray emission modulated with the orbital period (Negueruela et al. 2001; Orlandini et al. 2004). This is unusual as we would expect the circumstellar disc to be non-existent and therefore unable to provide a source of matter for accretion by the neutron star (i.e. due to the propeller effect, Stella et al. 1986). However according to Ikhsanov (2001) an accreting plasma can enter the magnetosphere through magnetic line reconnection. This seems to be the case in A0535+26, where the mass capture rate at periastron passage (i.e. $\dot{M} \sim 10^{-9} \mathrm{M}_{\odot} \mathrm{yr}^{-1}$) is sufficient to explain the observed L_x, and thus the modulation (Coe et al. 2006).

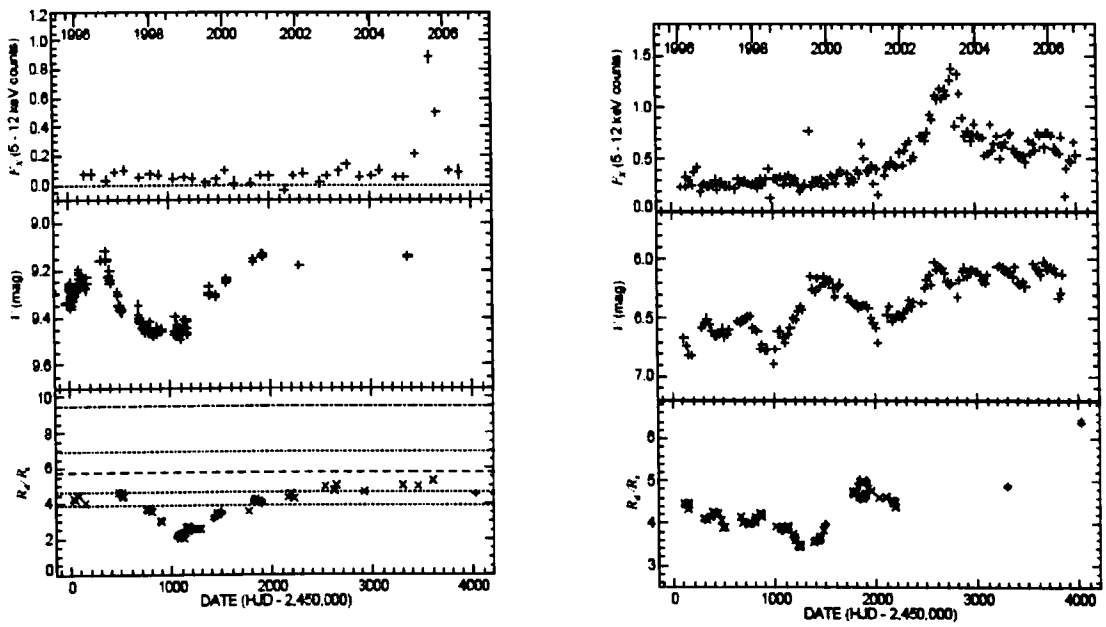

Figure 6.3: Time evolution of the X-ray flux (top panel), V magnitude (middle panel), and disc radius (bottom panel) of (a) A0535+26 and (b) X Per, from Grundstrom et al. (2007).

6.3 Overview of X Per

X Per is one of the brightest and most famous of the Be X-ray binaries. It consists of the persistent, low luminosity pulsar 4U 0352+30 (Braes & Miley, 1972; van den Bergh, 1972; Brucato & Kristian, 1972; Weisskopf et al. 1984) and the O9.5III-B0Ve star HD 24534 (Slettebak, 1982; Fabregat et al. 1992; Lyubimkov et al. 1997; Roche et al. 1997). The pulse period of $P_{pulse} \sim 837$ seconds, was found with the *Uhuru* satellite (White et al. 1976; 1977), and is one of the longest periods ever observed in an accreting pulsar (Bildsten et al. 1997; Haberl et al. 1998). Timing analysis of the pulsar carried out by Delgado-Marti et al. (2001) using *RXTE* observations, reveal an orbital period of $P_{orb} = 250.3$ days (White et al. 1976; Coburn et al. 2001) and an eccentricity of $e = 0.11$. This orbital period is in agreement with the predicted period of ~ 266 days found from the Corbet diagram[3] (Delgado-Marti et al. 2001). Previous studies had suggested an orbital period of ~ 580 days (Hutchings et al. 1974; 1975; Hutchings 1977), but this was later found to be based on erroneous data (Penrod & Vogt, 1985).

X Per is the prototype for the sub-class of persistent Be X-ray binary sources, (Reig & Roche, 1999). Such systems are known for their low X-ray luminosity, lack of significant variability and weak magnetic field (i.e. $\leq 10^{12}$ G, Li et al. 1999). X-ray monitoring of X Per shows little variability with no major outbursts observed (Roche et al. 1997; Clark et al. 2001). The luminosity is observed to vary slightly on timescales of years i.e. from as high as $\sim 3 \times 10^{35}$ erg s^{-1} [4] (Delgado-Marti et al. 2001) to as low as $\sim 4.2 \times 10^{34}$ erg s^{-1} (Coburn et al. 2001).

The weak magnetic field of X Per (i.e. $\sim 3.3 \times 10^{12}$ G at the polar cap) has been confirmed by the presence of a 29 keV cyclotron resonance scattering feature found with *RXTE* data by Coburn et al. (2001). Such features are not usually observed in low luminosity systems, making X Per the lowest luminosity source to exhibit one (Coburn et al. 2001). Taking this feature into account, Coburn et al. (2001) found that the X-ray spectrum is best-fitted by a combination of a 1.45 ± 0.02 keV blackbody and a power-law with a photon index of 1.83 ± 0.03.

[3]The Corbet diagram shows the relation between pulse period and orbital period and was developed by Corbet, 1986 (Corbet 1986; van den Heuvel & Rappaport, 1987).

[4]Note, this luminosity determination is based on a distance of 1.3kpc.

Compared to the spectra of other accreting pulsars, the spectrum of X Per is very unusual and is thought to be due to the lower mass accretion rate typical of these persistent sources (Coburn et al. 2001).

Unlike the X-ray the optical light shows significant spectroscopic and photometric variability, with the V magnitude ranging from $\sim 6.1 - 6.8$ (Mook et al. 1974; Roche et al. 1997). This variability has been recorded since 1913 by the University of Michigan (Clark et al. 2001) up until the present day (Roche et al. 1993; Norton et al. 1991; Clark et al. 2001). The recurrent optical brightening and fading appears to follow a 6 – 7 yr cycle (Dorren et al. 1979; Dorren & Guinan, 1980; Roche et al. 2000), which has been suggested to be due to the formation and dissipation of the circumstellar disc.

Long term optical observations by Roche et al. (1993) and Clark et al. (2001), during the period 1986 – 1994, show the system in transition from a Be star to a disc-less B star and back to a Be star again. For example, the period starting March 1986 exhibited a photometric bright state with corresponding bright double peaked Hα emission lines, followed by a subsequent fading of ~ 0.6 magnitude between May 1988 and June 1989. This photometric fading was accompanied by a steady decrease in the Hα equivalent width, until July 1990 when Hα was no longer seen in emission, thus indicating an episode of complete disc loss (Norton et al. 1991; Fabregat et al. 1992).

The system remained in a disc-less state until October 1991 when Hα became visible again as a weak double-peaked profile. The Hα line intensity and equivalent width increased steadily as the disc continued to grow, when in April 1993 it reached sufficient density for continuum emission to be observed. This was confirmed with the presence of a rapid photometric brightening, increasing by 0.6 magnitude between April 1993 and October 1994.

This recurrent optical fading observed every 6 – 7 years does not always result in complete disc loss (refer to Figure 6.3). For example, in October 1994 after the disc had reformed from the previous disc loss episode, the V band continuum emission started to drop to its former low (i.e. decreasing by ~ 0.5 magnitude in ~ 1 year), suggesting a decrease in disc density. However, instead of the emission lines slowly disappearing, the Hα equivalent width continued to increase, thus indicating a constant line flux, and showing that an decrease in

photometric magnitude can occur independently of the Hα emissivity[5].

The system stayed in this prolonged period of low-level continuum and line emission, displaying only small variations (i.e. $\delta V \sim 0.2$ magnitude; $\delta EW \sim 0.2$Å) until July 1996 when a dramatic brightening occured signalling the onset of disc growth and the beginning of a new cycle. The V magnitude continued increasing for the next year then decreased again followed by an abrupt brightening of 0.5 magnitude (refer to Figure 6.3). The equivalent width also started to increase reaching a peak ($\sim$ 17Å) approximately one year after the photometric peak. Such a lag between photometric magnitude and equivalent width is a common feature of Be stars and is indicative of the differences in spatial origin between the continuum and line emission, as suggested by Clark et al. (2001), (Grundstrom et al. 2007).

In early 1999 a plateau was then observed followed by a slow decline. However like the optical fading of 1994/1995, the system did not go into a disc-less state and instead the system steadily became brighter reaching peaks higher than any seen for the past few decades (Grundstrom et al. 2007). The corresponding Hα equivalent width also reached its largest values indicating significant disc growth between 2002 and 2006 (Roche et al. 1993; Picconi et al. 2000; Clark et al. 2001) . This was reflected in a slow increase in X-ray flux (refer to Figure 6.3) that was observed to reach a record high in 2003 (Grundstrom et al. 2007) and confirmed that the X-ray source is powered by mass accretion from the Be star disc (Grundstrom et al. 2007).

The X-ray light curves around this time showed X-ray maximum occurs at $\sim$ phase 0.25, suggesting that like that of A0535+26 the mass transfer process in X Per is supported by strong tidal forces and thus provides a source of gas accretion at phases beyond periastron (Okazaki et al. 2002; Grundstrom et al. 2007).

As well as the distinct long term optical variability observed in X Per, V/R cyclic variations in the Hα emission profile, like that of A0535+26 are also observed. These variations have been observed since the early 1900's (Mc Laughlin, 1937; Cowley et al. 1972; Wackerling, 1972; Galkina, 1980; Clark et al. 2001) with

[5]Clark et al. (2001) suggested that as the Hα emissivity region is more optically thick and formed over a wide range of disc radii and that the continuum emission is formed in the inner part of the disc, such independent changes imply that disc evolution cannot just be understood in terms of changes in base disc density, but must also involve variations of the radial density gradient of the disc.

periods ranging from 0.2 - 6 years (Clark et al. 2001). The profile as a whole shifts blueward when the red peak is stronger and vice-versa, where the V/R variations are presumably due to a global one-armed density oscillation (Clark et al. 2001), like that of A0535+26 and most Be stars.

The emission line profiles of He I 6678 show similar V/R variability to that of Hα, following roughly the same pattern (Clark et al. 2001). However instead of a double-peaked profile, He I 6678 has been found to show a complicated multi-component structure with strong variability. This generally 4-peaked profile seems to appear when emission at large velocities (i.e. in excess of the stellar rotation velocity) is significant (Clark et al. 2001). Clark et al. (2001) suggests that at this time the density of material in the equatorial plane had increased at very small radii and the radial density gradient is therefore not represented by a simple power-law. The outer peaks are then observed to migrate towards the line centre, which they suggest results from the change in the radial density distribution back toward a simple power-law (Clark et al. 2001).

6.4 Disc resonances in X Per and A0535+26

Resonances between the neutron star orbital period and the matter in the circumstellar disc of the Be star are known to occur (refer to Section 1.3.2, Chapter 5 and Section 6.1), where the radius of the disc will be truncated at specific resonance radii and can be found from Equation 6.2. As was discussed in Section 1.3.2, systems with low eccentricity will likely be truncated at the 3:1 resonance radius whereas systems with high eccentricity will be truncated at higher resonance radii (Negueruela et al. 2001; Okazaki & Negueruela, 2001).

A0535+26 is of intermediate eccentricity and is therefore too eccentric to be truncated at the 3:1 resonance radius and instead is expected to be truncated at a higher resonance radius. By applying the viscous decretion disc model and assuming the orbital soulutions of Finger et al. (1996), Okazaki & Negueruela (2001) determined likely resonances for truncation to occur in A0535+26. They found that when assuming a relatively high viscosity (i.e. $0.11 \leq \alpha \leq 0.4$) the disc is likely to be truncated at the 4:1 resonance radius and when assuming a lower viscosity (i.e. $0.038 \leq \alpha \leq 0.11$) it is likely to be truncated at the 5:1 resonance radius. The corresponding truncation radii were then determined from

Equation 6.2, by assuming the star to be of spectral type B0III, with $R_\star = 15R_\odot$ and $M_\star = 20M_\odot$ (Grundstrom et al. 2007)[6].

At the 4:1 resonance, the truncation radius ($R_t \sim 6.6R_\star$, Grundstrom et al. 2007) is slightly larger than the critical lobe radius at periastron. Therefore as type I outbursts are known to occur the disc must have reached this radius and be of relatively high viscosity. However, in times of quiescence we can assume that the viscosity decresed and the disc shrunk to a lower truncation radius (i.e. the 5:1 resonance radius, $R_t \sim 5.7R_\star$, Grundstrom et al. 2007) (Okazaki & Negueruela, 2001).

Coe et al. (2006) estimated the disc radii, for the period 2001 – 2005, using Equation 6.1 and assuming a stellar mass of $M_\star = 20M_\odot$, and an inclination of $i = 27°$ (found from the mass function of Finger et al. 1996). The resulting disc radii were smaller than those found by Haigh et al. (2004), but seemed to correlate with the resonance radii of Okazaki & Negueruela, (2001). For example in December 2001 to December 2003, the estimated disc radius ($R_d = 4.8 \times 10^{10}$ m), was approximately the same as the predicted 7:1 resonance radius. The disc was therefore of low viscosity and reduced size, explaining the fact that during this time no type I or II X-ray outbursts were exhibited. Then in March 2005, shortly before the May/June outburst, the estimated disc radius ($R_d = 6.8 \times 10^{10}$ m) was roughly between the 4:1 and 5:1 resonance radius suggesting that the disc was of sufficient size to allow active mass transfer and thus explaining the observed outburst. Finally in August 2005, shortly after the outburst the estimated disc radius ($R_d = 10.7 \times 10^{10}$ metres) was smaller than the 3:1 resonance radius suggesting continued growth of the disc instead of the expected dispersal.

Grundstrom et al. (2007) also estimated the disc radius of A0535+26, but instead used the Hα equivalent width and adopted values of T_{eff}, i and R_{out}, (refer to Grundstrom & Gies, 2006). They defined the disc radius (R_{HWHM}) as 'the distance along the major axis from the star where the integrated Hα emission intensity of the disc declines to half of the peak value found at a position immediately adjacent to the photosphere'. Their values were slightly larger than those of Coe et al. (2006) which was expected as Coe et al. (2006) derived

[6]Note in the case of A0535+26, the resonance is with the beat period and not the orbital period of 110 days (Larionov et al. 2001), so the beat period of 103 days is used in Equation 6.2.

a velocity weighted by the brighter parts of the Hα emitting region whereas Grundstrom et al. (2007) derived a velocity corresponding to an outer boundary between the brighter and fainter parts of the Hα emitting region. The difference is negligible except for the data obtained in August 2005, as Coe et al. (2006) determined R_d from the Hα equivalent width using a linear extrapolation instead of a standard power-law (e.g. Zamanov et al. 2001). However, as the estimated disc radii in all cases are approximately equal to the determined truncation radii, it would suggest that the entire disc emits in the Hα (Grundstrom et al. 2007).

X Per is of low eccentricity and is therefore expected to be truncated at the 3:1 resonance radius (Okazaki & Negueruela, 2001). This is supported by Clark et al. (2001) who show that the disc will be truncated at the 3:1 resonance radius if $\alpha > 7 \times 10^{-4}$. Assuming a spectral type of B0Ve, with $R_\star = 6.5 R_\odot$ and $M_\star = 15.5 M_\odot$, Grundstrom et al. (2007) used Equation 6.2 to determine the truncation radius at the 3:1 resonance. They found $R_t = 31 R_\star$, which is smaller than the separation between the Be star and the neutron star at periastron, which is assumed to be the mean Roche radius at periastron ($\sim 34 R_\star$), (Grundstrom et al. 2007). The truncation is therefore expected to be efficient, such that the neutron star is unable to accrete sufficient gas at periastron passage for type I outbursts to be observed. As a result the material ejected from the star tends to accumulate in the circumstellar disc, increasing the density distribution and hence exhibiting persistent low X-ray luminosity.

Using Equation 6.1 and assuming an inclination of $i = 30°$, Clark et al. (2001) estimated the disc radii for the period after complete disc loss when the disc had reformed. They found that the radius (or at least the Hα emitting radius) increased from $1.1 R_\star$ to $8.6 R_\star$ between October 1991 and April 1997. According to the photometric and spectroscopic data of Clark et al. (2001), the disc radius at this time had stopped growing, and with only a radius of $8.6 R_\star$ was therefore well below the truncation radius and hence the separation at periastron.

Grundstrom et al. (2007), using the same methods as in the case of A0535+26, also estimated the disc radii of X Per for the period 1996 to 2006. Contrary to Clark et al. (2001) they found a smaller disc radius of $\sim 4 R_\star$ in the period 1996 – 1998, reaching $\sim 5 R_\star$ in 2000 and peaking at $\sim 6.4 R_\star$ in 2006. The recent increase in X-ray flux observed in 2003 suggests the accretion of gas from the Be star disc to the neutron star has occurred (Grundstrom et al. 2007). However

this increase correlates with an estimated disc radius of $R_d \sim 5R_\star$ (Grundstrom et al. 2007), which is even smaller than the previous radius of $R_d = 8.6R_\star$ and therefore much smaller than R_t and the separation radius at periastron. Grundstrom et al. (2007) suggest two possible explanations. Firstly, like in the case of A0535+26, strong tidal forces that exist at periastron may aid the mass transfer. If this is the case, it is expected that the mass transfer will occur predominantly after periastron, which is exacly what is seen in the X-ray light curves (refer to Section 6.3). Secondly, the actual disc may extend beyond the radius that has been calculated[7], and may be sufficient to power the accretion driven X-ray flux.

6.5 New echelle spectroscopy of X Per and A0535+26

High resolution optical spectroscopy of both X Per and A0535+26 were obtained from observations taken at the La Palma, Calar Alto and Pic du Midi observatories. During the period March 1998 to December 2004, nine spectra of X Per were taken covering the wavelength range 3960Å to 7100Å, and during the period November 1998 to January 1999, four spectra of A0535+26 were taken covering the wavelength range 4000Å to 8700Å. In each case a grating spectrograph was used which gave a resolution of approximately 0.06 – 0.07Å per pixel. Refer to Tables 6.1 and 6.2 for a list of dates, telescopes and instruments used for the observations of X Per and A0535+26 respectively.
The first three spectra obtained for X Per cover a time of disc growth, the spectra obtained from observations 4 – 6 are from a time when the disc had stopped growing and was in a plateau state and those obtained from observations 7 – 9 were during another period of disc growth. The spectra obtained for A0535+26 however, cover a time of complete disc loss, where the spectrum obtained at observation 1 was during complete disc loss and those obtained from observation 2 – 4 were at a time when the disc was starting to reform.

[7]If the Hα peak separation remains constant, it cannot be assumed that the outer edge of the disc has ceased to expand, as the material outside this implied radius may just be too diffuse to contribute sugnificantly to line emission (Clark et al. 2001).

Table 6.1: Table of observation dates, telescopes and instruments used for X Per.

Obs.	Date	Telescope	Instrument	MJD	Phase
1	08-03-1998	INT, La Palma	IDS	50880.845	0.661
2	08-03-1998	INT, La Palma	IDS	50880.858	0.661
3	07-11-1998	WHT, La Palma	UES	51124.049	0.634
4	28-01-1999	CA220, Calar Alto	NN	51206.923	0.966
5	28-01-1999	CA220, Calar Alto	NN	51206.927	0.966
6	02-08-1999	CA220, Calar Alto	CAFOS2.2	51392.174	0.707
7	20-12-2003	CA220, Calar Alto	NN	52993.904	0.117
8 (blue)	05-12-2004	T2M Bernard Lyot, Pic du Midi	MUSICOS	53344.866	0.521
8 (red)	05-12-2004	T2M Bernard Lyot, Pic du Midi	MUSICOS	53344.889	0.521
9 (blue)	07-12-2004	T2M Bernard Lyot, Pic du Midi	MUSICOS	53346.117	0.526
9 (red)	06-12-2004	T2M Bernard Lyot, Pic du Midi	MUSICOS	53345.878	0.525

Table 6.2: Table of observation dates, telescopes and instruments used for A0535+26.

Obs.	Date	Telescope	Instrument	MJD	Phase
1	07-11-1998	WHT, La Palma	UES	51124.053	0.417
2	28-01-1999	CA220, Calar Alto	NN	51206.983	0.162
3	28-01-1999	CA220, Calar Alto	NN	51206.998	0.162
4	29-01-1999	CA220, Calar Alto	NN	51207.926	0.169

All spectra were reduced using standard IRAF routines and extracted using optimal extraction procedures. The extracted spectra were then continuum fitted using DIPSO. Orbital phases corresponding to each spectrum were calculated

using the relevant ephemeris, where a barycentric correction was applied to the MJD before the phases were calculated. The ephemeris from Delgado-Marti et al. (2001) was used for X Per, which gives the centre time of the Nth periastron passage as:

$$t_{N\pi/2}/\mathrm{MJD} = 51215.5(\pm 0.5) + 249.9(\pm 0.5)N \quad (6.4)$$

For A0535+26 the ephemeris of Larionov et al. (2001) was used, which gives the centre time of the Nth periastron passage as:

$$t_{N\pi/2}/(\mathrm{JD}) = 2446734.3(\pm 2.6) + 111.38(\pm 0.11)N \quad (6.5)$$

The resulting spectra were converted to a velocity scale and the individual spectral emission lines were plotted as a function of time, refer to Figures 6.4 – 6.6 and 6.7 – 6.9 for X Per and A0535+26 respectively. The spectral profiles were then fitted with Gaussians such that the equivalent width, peak intensities and peak separation could be determined. The Gaussian fits to the double peaked profiles were fitted such that both the violet and red peaks were fitted, like that of Zamanov et al. (2001) and Grundstrom et al. (2007). In both cases the fits were restricted to the inner part of the profile and were unable to take into account the large extended wings.

From the measured peak separation and by using Equation 6.1, like that of Clark et al. (2001) and Coe et al. (2006), the disc radius, R_d was determined. In the case of X Per we assumed $M_\star = 15.5\mathrm{M}_\odot$, $\mathrm{R}_\star = 6.5\mathrm{R}_\odot$ and $i = 30°$, and for A0535+26 we assumed $\mathrm{M}_\star = 20\mathrm{M}_\odot$, $\mathrm{R}_\star = 15\mathrm{R}_\odot$ and $i = 27°$. Refer to Tables 6.3 and 6.4 for the resulting spectral line measurements and Figures 6.10 – 6.15 and 6.16 – 6.19 for the corresponding time variability plots of X Per and A0535+26 respectively.

Table 6.3: Spectral line measurements of X Per, i.e. the equivalent width (EW); the radial velocity (RV) for both the violet (V) and red (R) peaks; the peak separation δV; and the calculated circumstellar disc radii (R_d is given in units of $R_\star$, where $R_\star = 6.5\ R_\odot$).

MJD	EW Å	V/R	RV(V) (km s^{-1})	RV(R) (km s^{-1})	δV (km s^{-1})	R_d ($R_\star$)	Error ($R_\star$)
Hγ							
51206.92	-0.13	1.05	-68	162	230	8.57	0.09
51206.93	-0.13	1.04	-69	155	224	9.03	0.07
51392.17	-0.15	0.92	-156	76	232	8.48	0.08
52993.90	-0.44	1.01	-64	120	183	13.52	0.40
53344.87	-0.52	1.01	-69	113	182	13.69	0.05
53346.12	-0.48	0.99	-61	119	180	14.08	0.24
Hβ							
50880.85	-1.75	1.15	-71	86	157	18.56	0.070
50880.86	-1.52	1.16	-71	77	148	20.84	0.36
51124.05	-1.12	0.80	-125	89	214	9.97	0.17
51206.92	-1.09	1.09	-67	121	188	12.92	0.12
51206.93	-1.06	1.08	-65	118	183	13.63	0.05
51392.17	-1.02	0.88	-121	60	182	13.78	0.12
52993.90	-1.52	1.01	-69	103	172	15.34	0.24
53344.87	-1.79	0.99	-75	95	170	15.75	0.20
53346.12	-1.80	0.99	-74	97	171	15.60	0.05
Hα							
50880.85	-13.42	1.21	-101	16	117	33.21	0.37
50880.86	-13.56	1.17	-101	18	119	32.20	0.54
51124.05	-9.36	0.77	-63	55	117	32.95	0.21
51206.92	-4.89	1.04	-95	92	187	13.01	0.05
51206.93	-6.57	1.09	-87	83	171	15.64	0.12
51392.17	-6.31	0.83	-152	22	174	14.97	0.13
52993.90	-14.96	1.03	-81	64	145	21.57	0.06
53344.89	-16.36	0.98	-92	51	143	22.26	0.07
53345.88	-16.24	0.98	-91	50	141	22.94	0.12

MJD	EW Å	V/R	RV(V) (km s^{-1})	RV(R) (km s^{-1})	δV (km s^{-1})	R_d ($R_\star$)	Error ($R_\star$)
HeI5876							
50880.85	-1.71	1.12	-111	100	210	10.28	0.42
50880.86	-1.95	1.20	-111	17	128	27.77	1.65
51124.05	-1.19	0.92	-226	78	305	4.90	0.03
51206.92	-0.71	1.11	-108	123	231	8.50	0.05
51206.93	-0.61	1.10	-110	130	240	7.91	0.04
51392.17	-0.53	0.94	-192	36	228	8.77	0.06
52993.90	-0.50	1.00	-117	92	210	10.33	0.04
53344.89	-0.41	1.00	-128	81	209	10.40	0.05
53345.88	-0.46	1.01	-124	83	207	10.57	0.02
HeI6678							
50880.85	-0.94	1.09	-88	271	359	3.52	0.01
50880.86	-1.05	1.07	-89	278	367	3.38	0.01
51124.05	-0.53	0.97	-219	156	375	3.23	0.01
51206.92	-0.21	1.07	-94	196	289	5.43	0.07
51206.93	-0.20	1.05	-94	204	299	5.10	0.23
51392.17	-0.24	0.97	-174	49	223	9.16	1.42
52993.90	-0.25	0.99	-84	113	197	11.69	0.12
53344.89	-0.11	1.02	-112	98	210	10.32	0.02
53345.88	-0.11	1.00	-116	102	218	9.57	0.05
HeI7065							
50880.85	-0.71	1.24	-91	94	185	13.27	0.34
50880.86	-1.88	1.20	-95	62	157	18.52	0.83
51124.05	-1.51	0.98	-211	107	317	4.52	0.03
51206.92	-0.86	1.13	-102	146	248	7.37	0.93
51206.93	-0.82	1.11	-90	157	247	7.45	0.07
51392.17	-0.52	0.93	-146	72	217	9.62	0.06
52993.90	-0.45	1.01	-103	121	224	9.07	0.11
53344.89	-0.43	1.00	-107	108	216	9.79	0.04
53345.88	-0.42	1.03	-103	108	211	10.22	0.22

Table 6.4: Spectral line measurements of A0535+26, i.e. the same parameters as in Table 6.3, except R_d is given in units of $R_\star$, where $R_\star = 15\ R_\odot$.

MJD	EW Å	V/R	RV(V) (km s^{-1})	RV(R) (km s^{-1})	δV (km s^{-1})	R_d ($R_\star$)	Error ($R_\star$)
Hγ							
51124.05	0.00						
51206.98	0.49		35				
51207.00	0.65		60				
51207.93	0.22		114				
Hβ							
51124.05	1.53		-9				
51206.98	0.67		41				
51207.00	0.83		47				
51207.93	0.88		44				
Hα							
51124.05	1.13		-57				
51206.98	-1.27	1.01	-207	243	450	1.03	0.001
51207.00	-0.96	1.02	-208	243	451	1.03	0.003
51207.93	-1.43	1.01	-202	236	438	1.09	0.001
HeI5876							
51124.05	0.92		-51				
51206.98	-0.71	0.96	-254	327	581	0.62	0.012
51207.00	-0.65	0.98	-277	313	589	0.6	0.008
51207.93	-0.44	1.01	-267	300	567	0.65	0.010
HeI6678							
51124.05	0.85		-32				
51206.98	-0.47	0.99	-264	317	580	0.62	0.015
51207.00	-0.54	0.97	-270	309	579	0.63	0.002
51207.93							
HeI7065							
51124.05	0.61		-55				
51206.98	-0.29	1.03	-242	335	577	0.63	0.005
51207.00	-0.33	1.01	-238	333	571	0.64	0.003
51207.93							

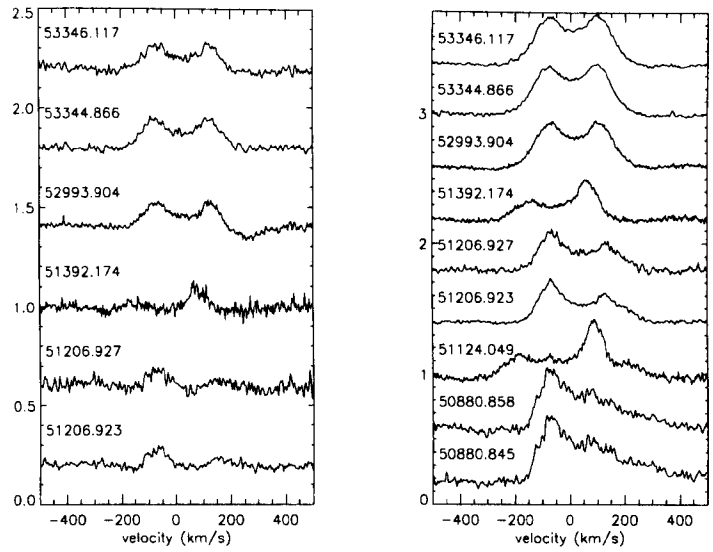

Figure 6.4: The (a) Hγ and (b) Hβ emission line of X Per, shown for different times and as a function of velocity. Each spectrum is offset by 0.4 in the vertical axis, where the scale is arbitrary.

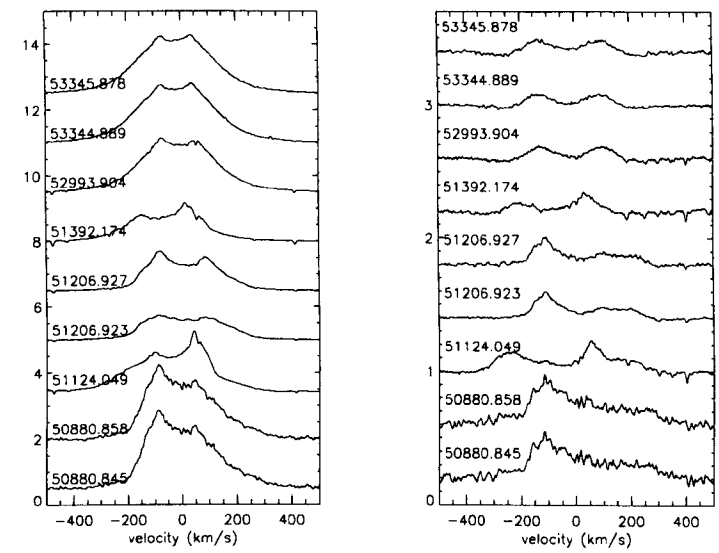

Figure 6.5: The (a) Hα and (b) He I 5876 Å emission line of X Per, shown for different times and as a function of velocity. Axis as in Figure 6.4.

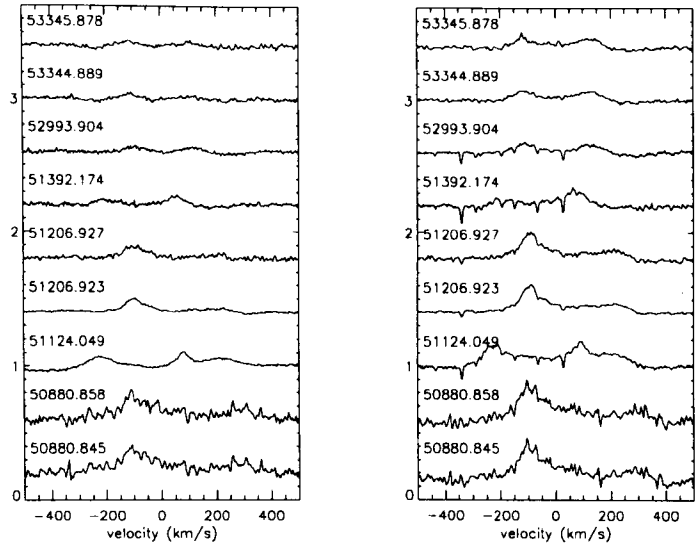

Figure 6.6: The (a) He I 6678 Å and (b) He I 7065 Å emission line of X Per, shown for different times and as a function of velocity. Axis as in Figure 6.4.

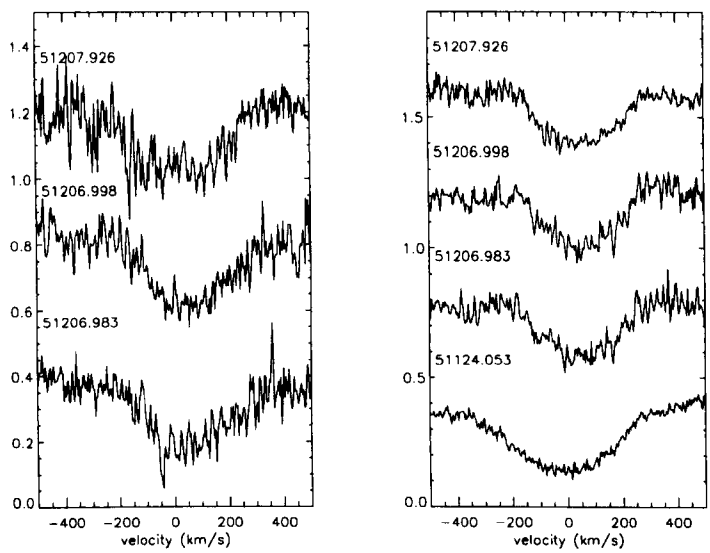

Figure 6.7: The (a) Hγ and (b) Hβ emission line of A0535+26, shown for different times and as a function of velocity. Each spectrum is offset by 0.4 in the vertical axis, where the scale is arbitrary.

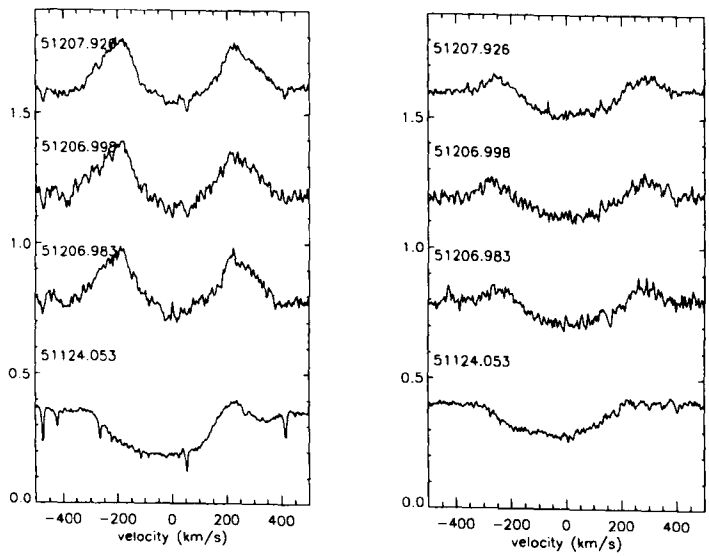

Figure 6.8: The (a) Hα and (b) He I 5876 Å emission line of A0535+26, shown for different times and as a function of velocity. Axis as in Figure 6.4.

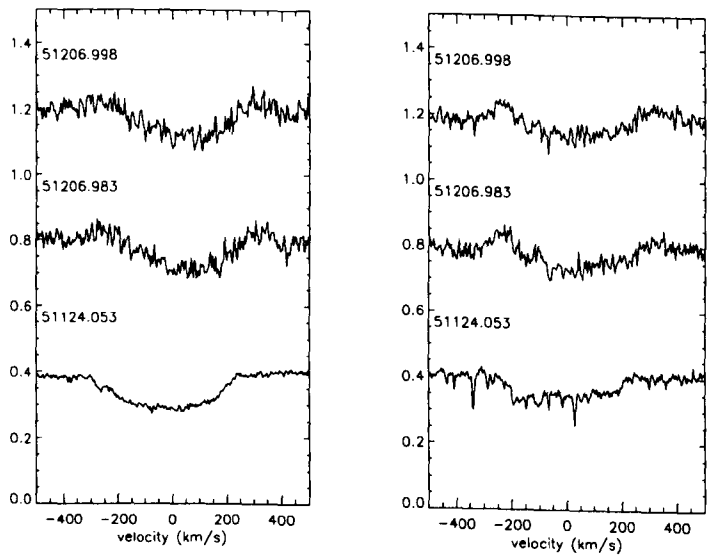

Figure 6.9: The (a) He I 6678 Å and (b) He I 7065 Å emission line of A0535+26, shown for different times and as a function of velocity. Axis as in Figure 6.4.

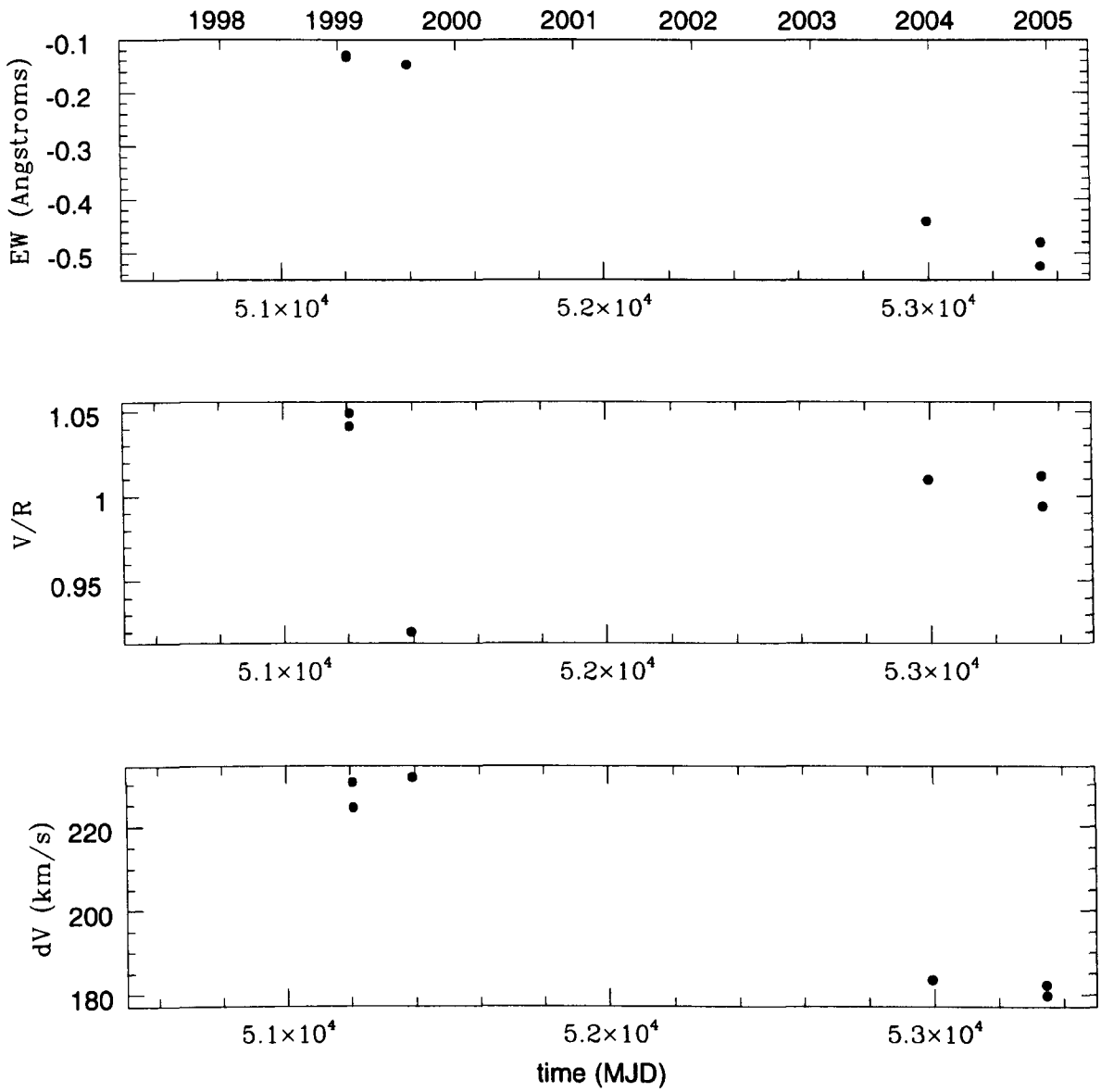

Figure 6.10: Time variability of the main parameters of the Hγ line in X Per. The top panel displays equivalent width in Å, the middle panel diplays the V/R intensity variability, and the bottom panel displays the peak separation in km/s. Note the errors for EW are of the order ~ 0.02 and those of the peak separation are shown in Table 6.3.

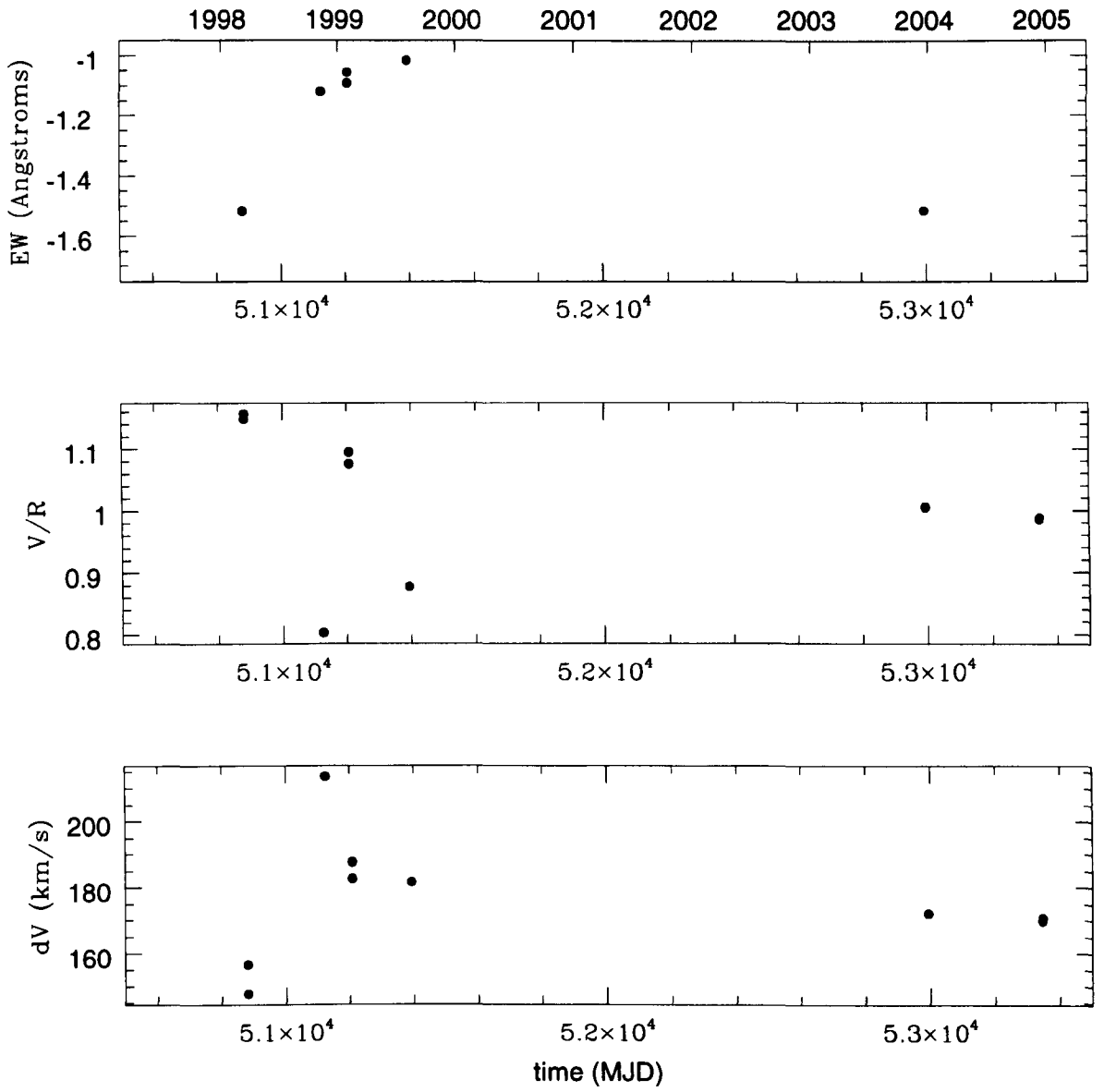

Figure 6.11: Time variability of the main parameters of the Hβ line in X Per. Panels are the same as those in Figure 6.10.

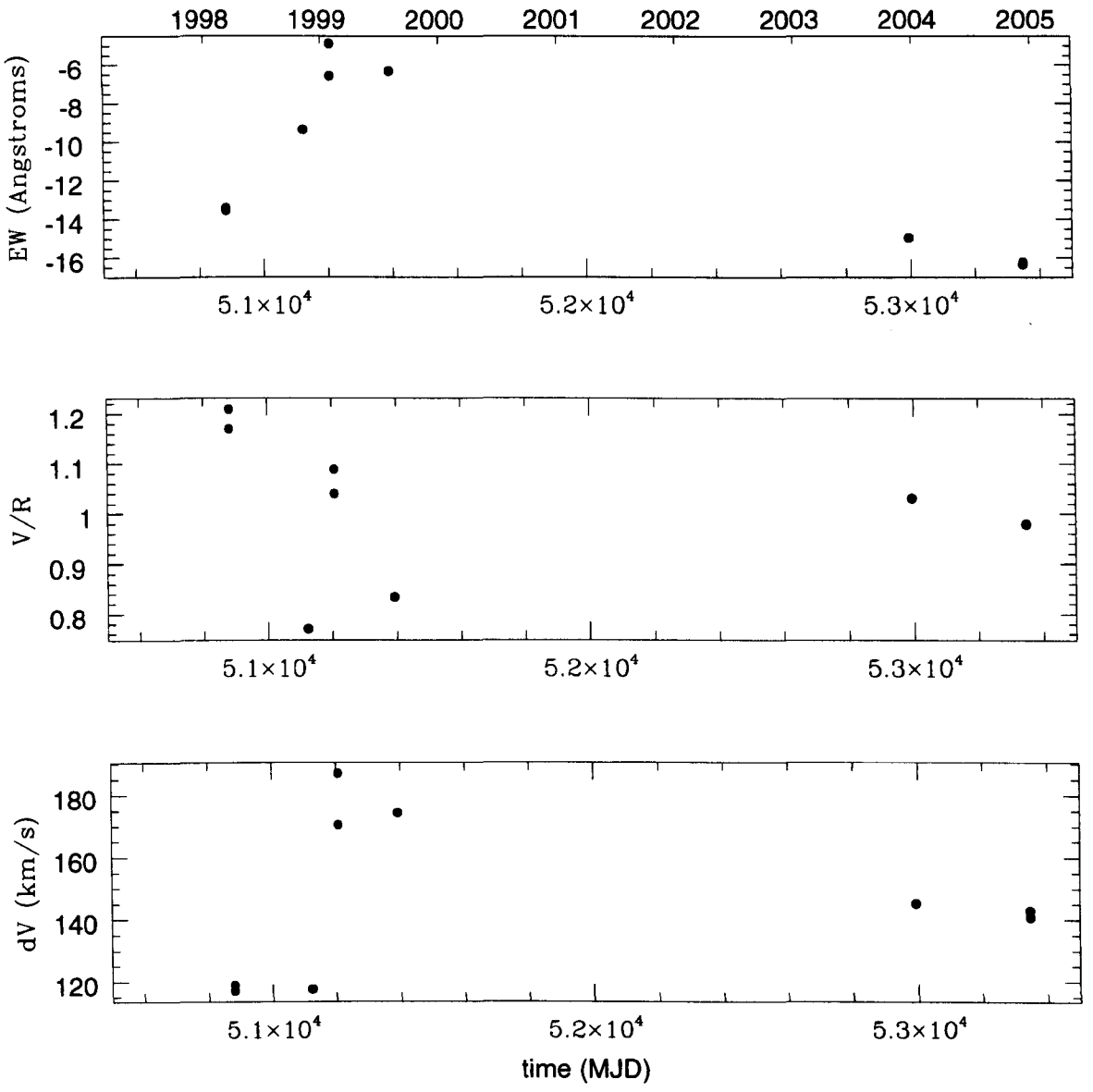

Figure 6.12: Time variability of the main parameters of the Hα line in X Per. Panels are the same as those in Figure 6.10.

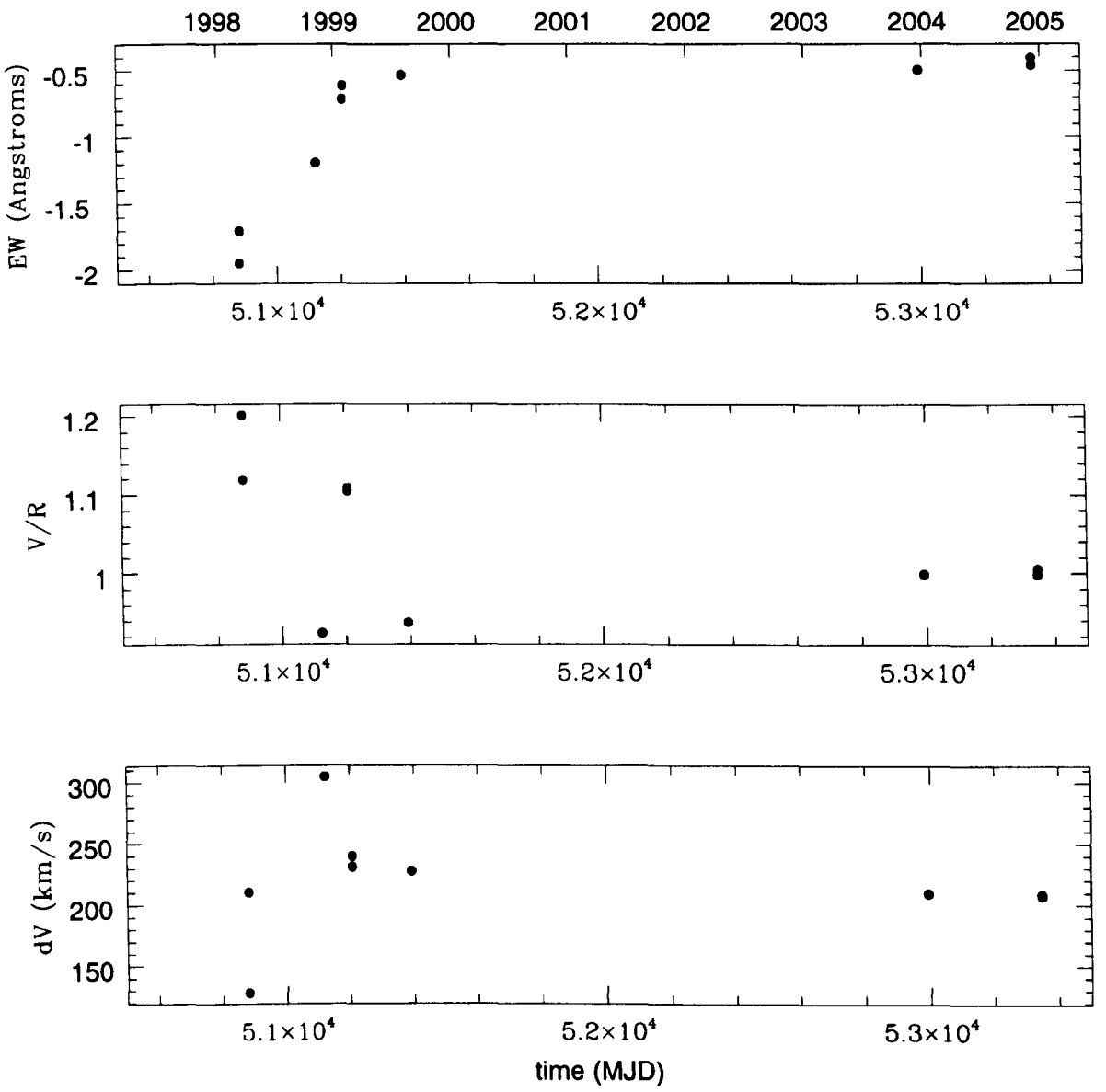

Figure 6.13: Time variability of the main parameters of the He I 5876 line in X Per. Panels are the same as those in Figure 6.10.

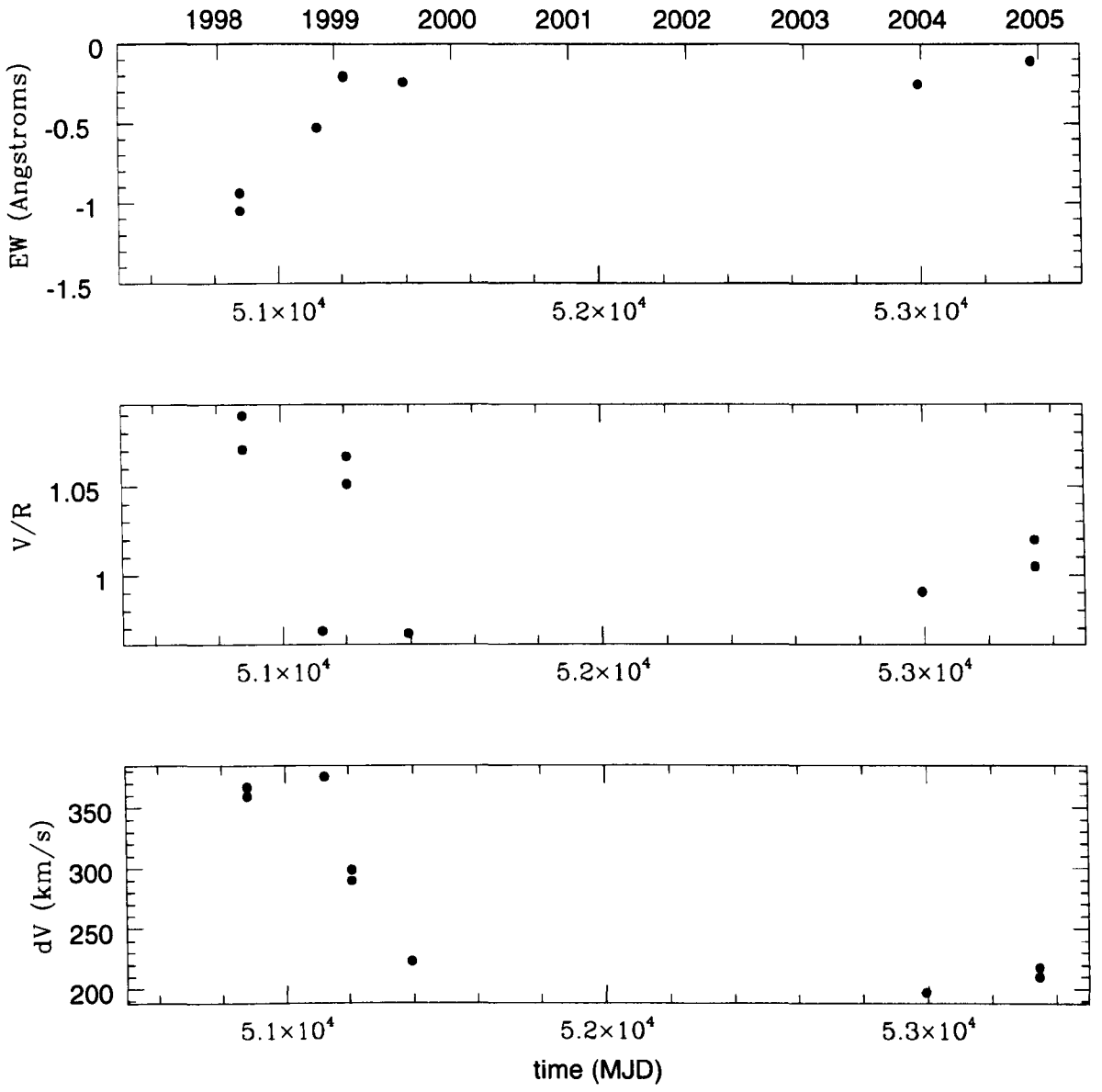

Figure 6.14: Time variability of the main parameters of the He I 6678 line in X Per. Panels are the same as those in Figure 6.10.

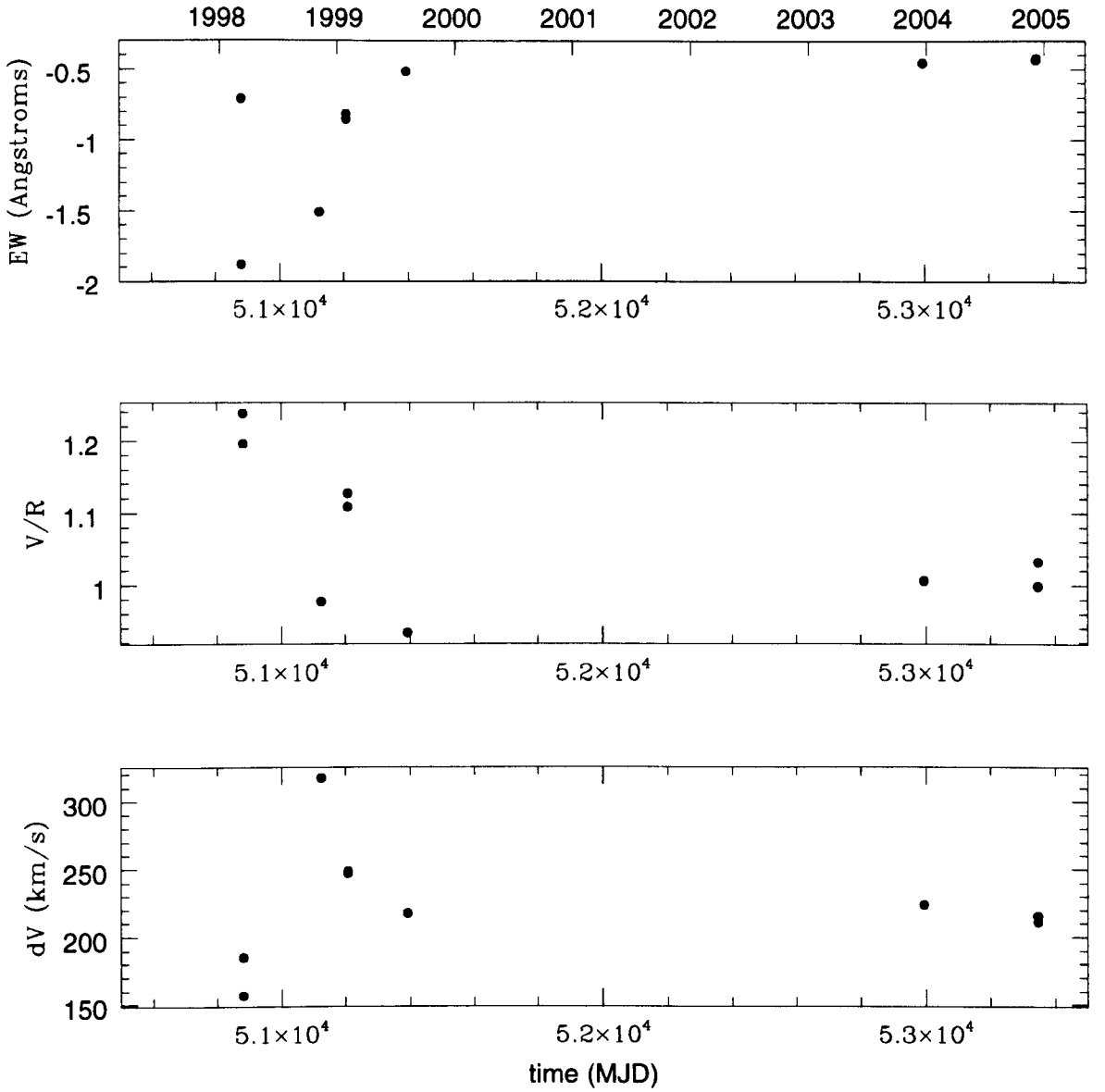

Figure 6.15: Time variability of the main parameters of the He I 7065 line in X Per. Panels are the same as those in Figure 6.10.

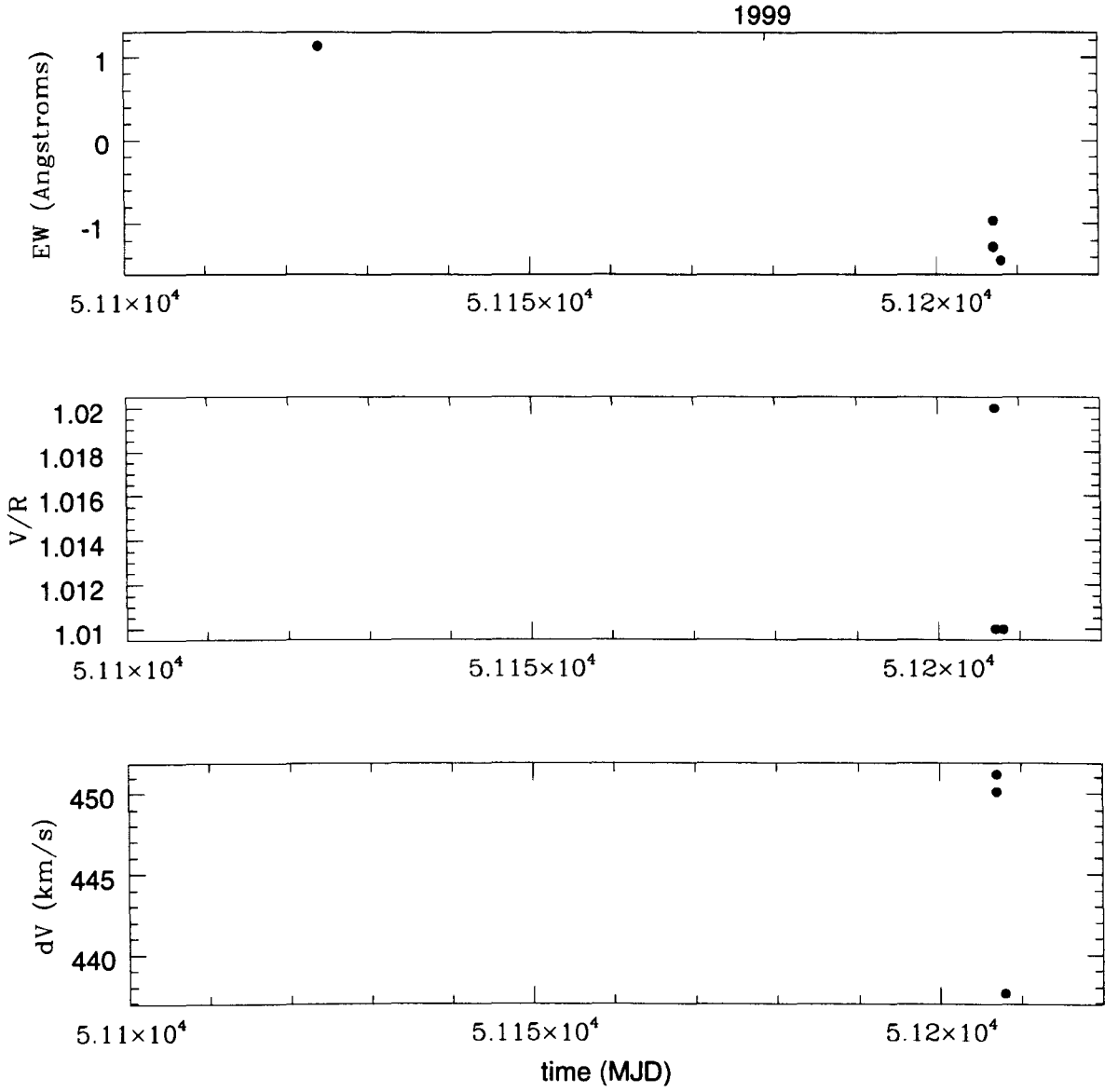

Figure 6.16: Time variability of the main parameters of the Hα line in A0535+26. Panels are the same as those in Figure 6.10. Note the errors for EW are of the order ~ 0.02 and those of the peak separation are shown in Table 6.4.

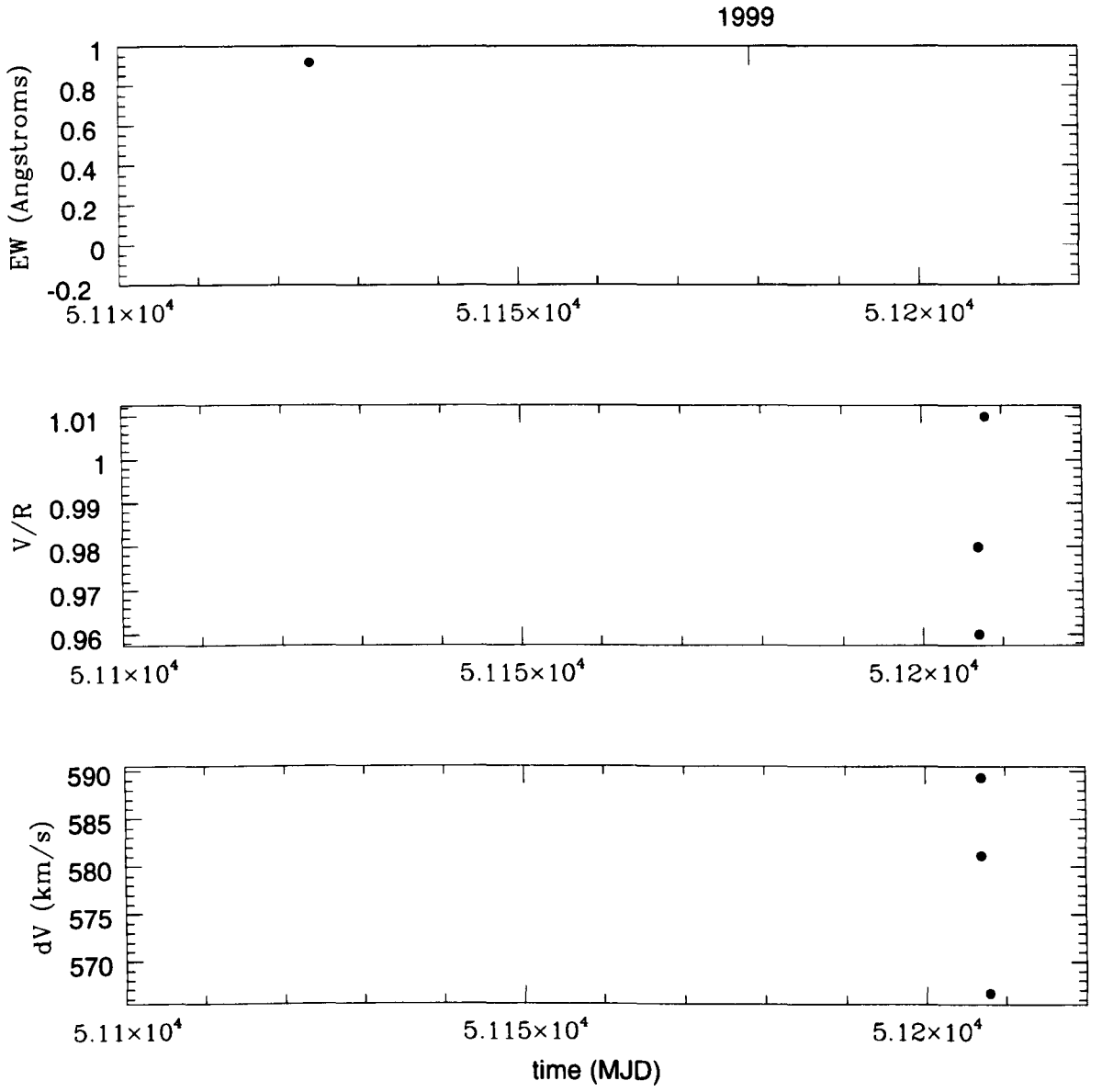

Figure 6.17: Time variability of the main parameters of the He I 5876 line in A0535+26. Panels are the same as those in Figure 6.16.

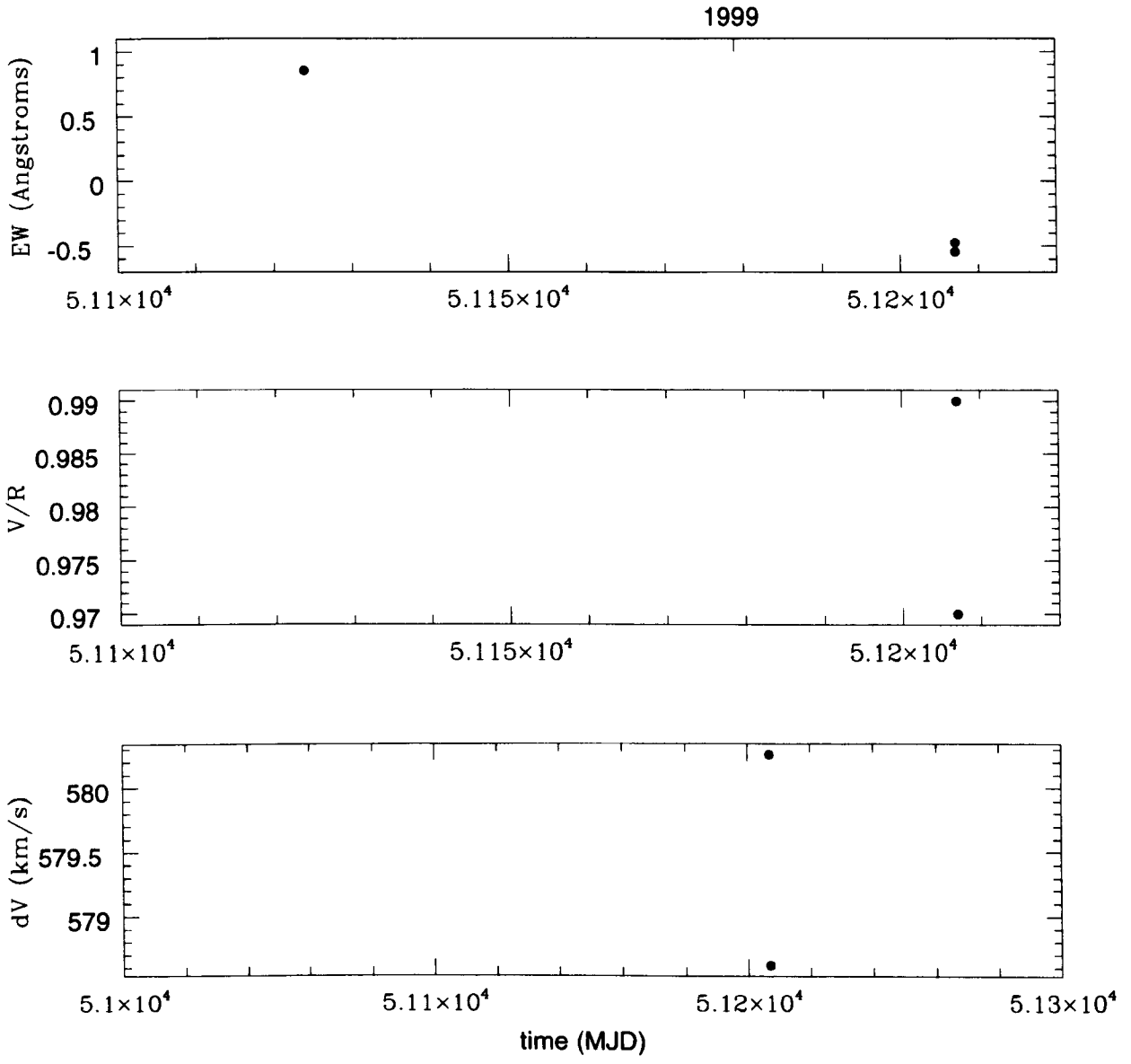

Figure 6.18: Time variability of the main parameters of the He I 6678 line in A0535+26. Panels are the same as those in Figure 6.10.

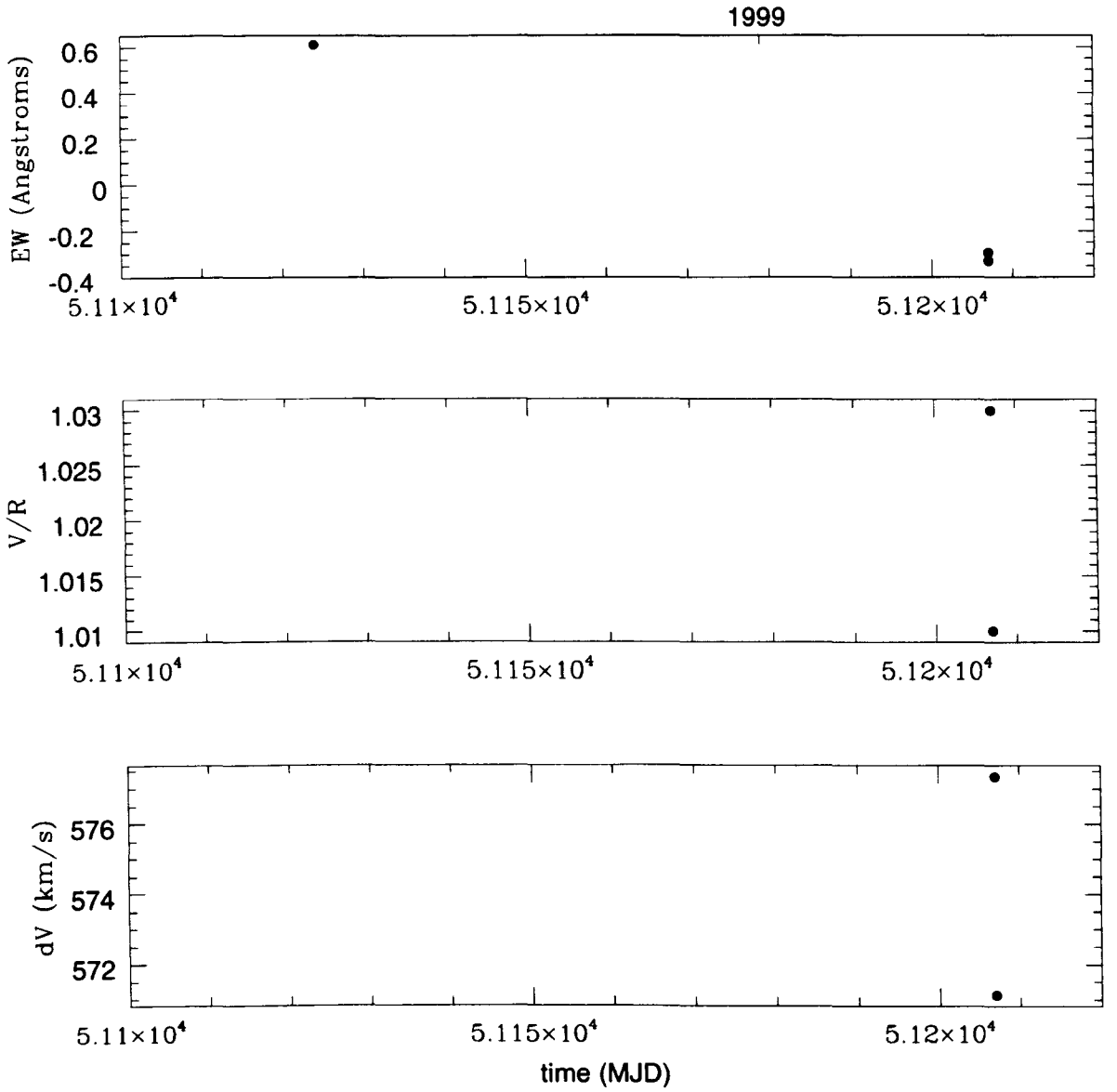

Figure 6.19: Time variability of the main parameters of the He I 7065 line in A0535+26. Panels are the same as those in Figure 6.10.

6.6 Extending the long term variability study

Both X Per and A05353+26 have been studied extensively throughout the last century. The combination of all these data sets provides us with a large data set from which more accurate conclusions about the different variability cycles can be drawn.

6.6.1 The disc phase variability

As noted earlier the circumstellar discs of Be X-ray binaries are known to vary between phases of disc growth and disc dispersal, corresponding to observed phases of optical brightening and fading respectively. This brightening and fading of the disc is also apparent in the equivalent widths of the spectral lines, where the equivalent width increases with decreasing peak separation and indicates phases of disc growth, and the equivalent width decreases with increasing peak separation and indicates phases of disc dispersal and in some cases complete disc loss.

Our resulting spectral line measurements for X Per and A0535+26 (Figures 6.10 – 6.19) show that like that of previous studies, the peak separation decreases as the equivalent width increases, and vice-versa, where the different values observed between the spectral lines is indicative of their emissivity region. For example, we see that Hα generally has the smallest peak separation and therefore emits in the outer regions of the disc, whereas He I 6678 generally has the largest peak separation and therefore only emits in the inner regions of the disc. This is also apparent in the inferred disc radii (refer to Table 6.3 and 6.4), where Hα has the largest inferred radii and therefore emits over the largest range, whereas He I 6678 has the smallest inferred radii and therefore emits over a smaller range within the inner radii of the disc.

From previous studies (e.g. Dorren et al. 1979; Dorren & Guinan, 1980; Roche et al. 1999) it is known that the circumstellar disc of X Per follows an approximately 6 – 7 year disc growth and dispersal cycle. By comparing our Hα and He I 6678 data with those of Grundstrom et al. (2007) and Clark et al. (2001) (refer to Figures 6.20 and 6.21), we can see that our data are from a period of overall long term disc growth. Our data however, only cover the period from

March 1998 to December 2004, encompassing the end of one disc phase and the beginning of the next i.e the disc phase of 1996 – 2002 and 2002 – present. From Figures 6.20 and 6.21 it is clear that our data agree with that of Grundstrom et al (2007) and Clark et al. (2001), where the overall trend shows that as well as the variability associated with the disc growth and dispersal cycle (i.e. $\sim 6-7$ years), the equivalent width appears to be steadily increasing with time (i.e. becoming more negative). This steady increase and corresponding decrease in peak separation implies that with each disc phase of growth and dispersal the disc is becoming bigger, and correlates with the fact that the V magnitude has recently reached a value of 6.0 (Grundstrom et al. 2007), which hasn't been observed since 1972 (Roche et al. 1993).

The calculated disc radii, however do not agree with those found by Grundstrom et al. (2007), where during the period 1996 – 1998 they find $R_d = 4\mathrm{R}_\star$ as opposed to our $\sim 33\mathrm{R}_\star$ and in 2000 they find $R_d = 5\mathrm{R}_\star$ as opposed to our $\sim 15\mathrm{R}_\star$ in January 1999 and $R_d = 22\mathrm{R}_\star$ in December 2003 and 2004. Refer to Figure 6.23 for a schematic scaled diagram of X Per where the truncation radii, R_t and our minimum and maximum calculated disc radii, R_d, are shown.

If we look at Figures 6.10 – 6.15 we can see that the equivalent width and peak separation of Hβ and Hγ follow the same trend as Hα, whereas those of He I 5876, 6678 and 7065 do not follow the same trend as Hα. For example, during the period March 1998 to August 1999 the equivalent width of the observed hydrogen lines appear to be decreasing, they then start to increase again, where by December 2004 they are back up to peak values (i.e. Hα EW ~ -16Å). However, the helium lines only follow the same pattern as Hα until 1999, when instead of increasing during the period 2003 – 2004, they stay at a constant value. This difference in trend suggests that during that time of disc growth only the outer regions were expanding and not the inner regions where there is sufficient density for helium emission.

Again, as noted earlier, the circumstellar disc of A0535+26 is known to follow a cycle of ~ 5 years, where type II X-ray outbursts normally occur at the end of each growth cycle (i.e. they recur in groups of 2 with the third one missing). Again, by comparing our Hα data with those of Grundstrom et al. (2007) (refer to Figure 6.22) it is clear that, although we only have a few data points for A0535+26 they are in good agreement. The overall trend of the data, which

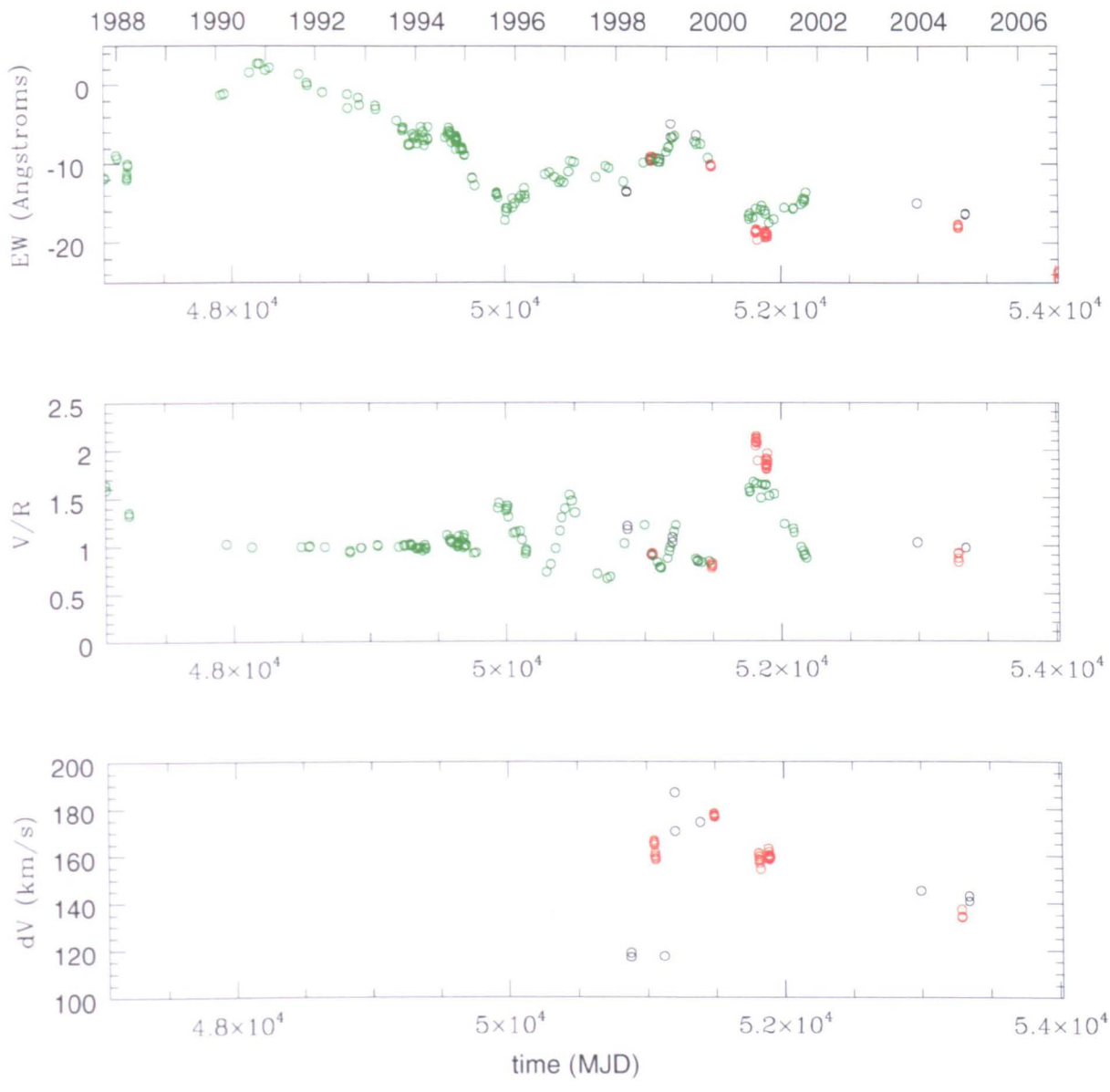

Figure 6.20: Time variability of the main parameters of the Hα line in X Per, showing our data as black dots, Grundstrom et al's (2007) data as red dots and Clark et al's (2001) data as green dots. Panels are the same as those in Figure 6.10.

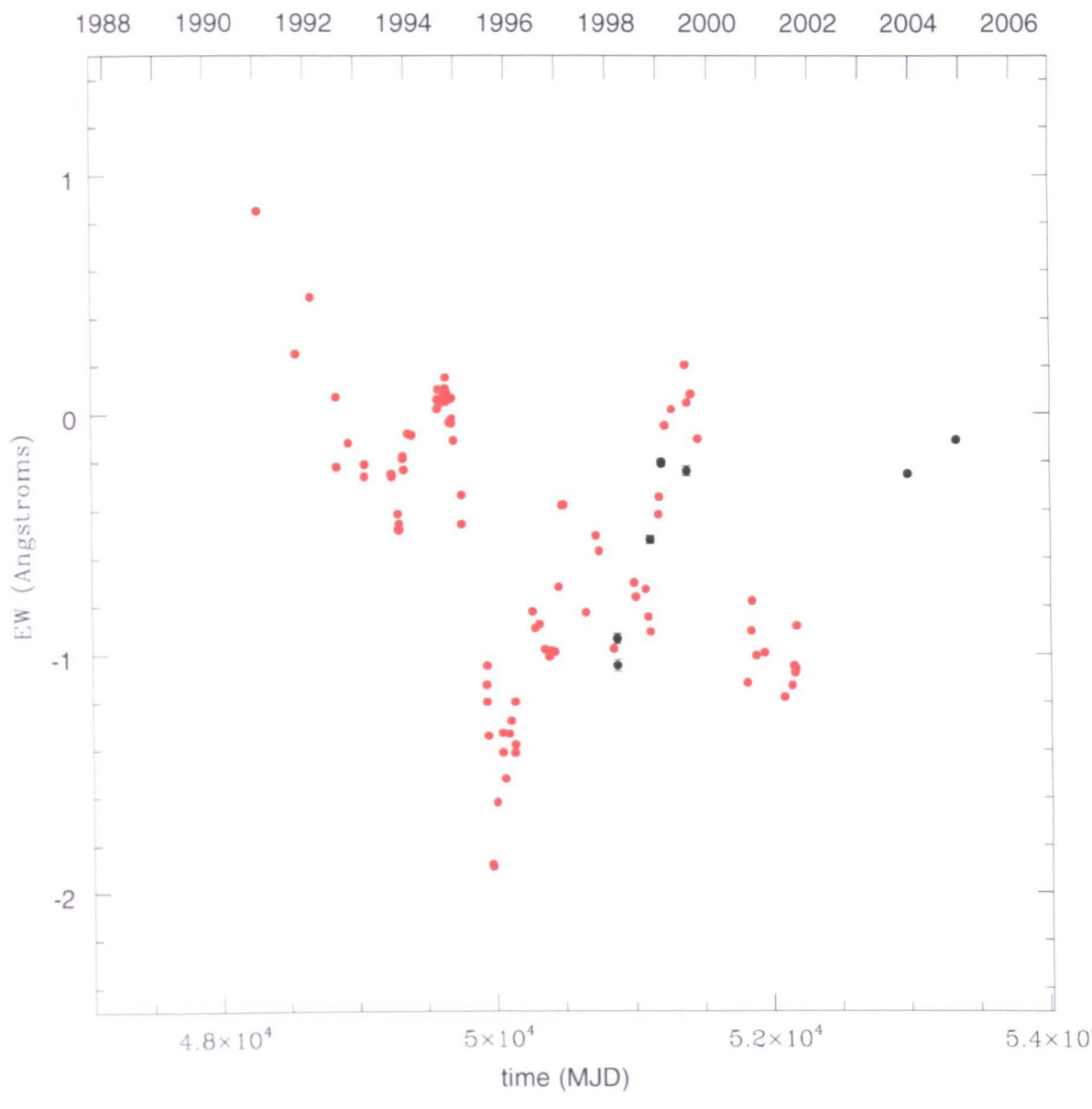

Figure 6.21: Time variability of the EW of the He I 6678 line in X Per, showing our data as black dots and Clark et al's (2001) data as red dots.

covers the period 1998 – 2006, shows a steady increase in equivalent width and corresponding decrease in peak separation implying long term gradual disc growth[8], which correlates with the fact that the disc had just experienced almost complete disc loss and was undergoing disc reformation. The calculated disc radii were also comparable to Grundstrom et al. (2007) and to Coe et al. (2006), who found R_d grew from $\sim 4.8 - 10.7 \times 10^{10}$ metres (i.e. $4.5 - 10.2$ $R_\star$) in the period December 2001 to August 2001. Our data does not cover this period but during the period of observation in 1998/1999 we find $R_d \sim 1$ $R_\star$ (i.e. $\sim 10^{10}$ metres), which is of the same order but lower as would be expected. Refer to Figure 6.24 for a schematic scaled diagram of A0535+26 where the truncation radii, R_t and our minimum and maximum calculated disc radii, R_d, are shown.

If we look at Figures 6.16 – 6.19 we can see that contrary to X Per, the equivalent width and peak separation of the helium lines (He I 5876, 6678, 7065) follow the same trend as Hα, suggesting that during this time of disc growth both the outer regions and inner regions were expanding.

6.6.2 The cyclic V/R variability

As noted earlier, cyclic V/R variability due to global one-armed oscillations are observed in most Be X-ray binary systems, including X Per and A0535+26. From Figures 6.4 – 6.9 we can see evidence of this variability (especially in the case of X Per), but due to the limited data set in both X Per and A0535+26 the cycle length is not apparent. However by comparing our V/R ratios with those of Grundstrom et al. (2007) and Clark et el. (2001), this cyclic variability becomes clearer.

In the case of X Per we see that during the period April 1990 – October 1995 (i.e. MJD 48000 – 50000) there is negligible variability (refer to the middle panel of Figure 6.20), which correlates with the fact that the disc was reforming at this time and was therefore presumably not stable enough for a global one-armed density wave to exist. Only in 1995, when the disc had reached a stable density do we begin to see such variability, which appears to follow cycle lengths of

[8]There is no data covering the period 2001 – 2006, so we can only assume that during that period the same trend is observed.

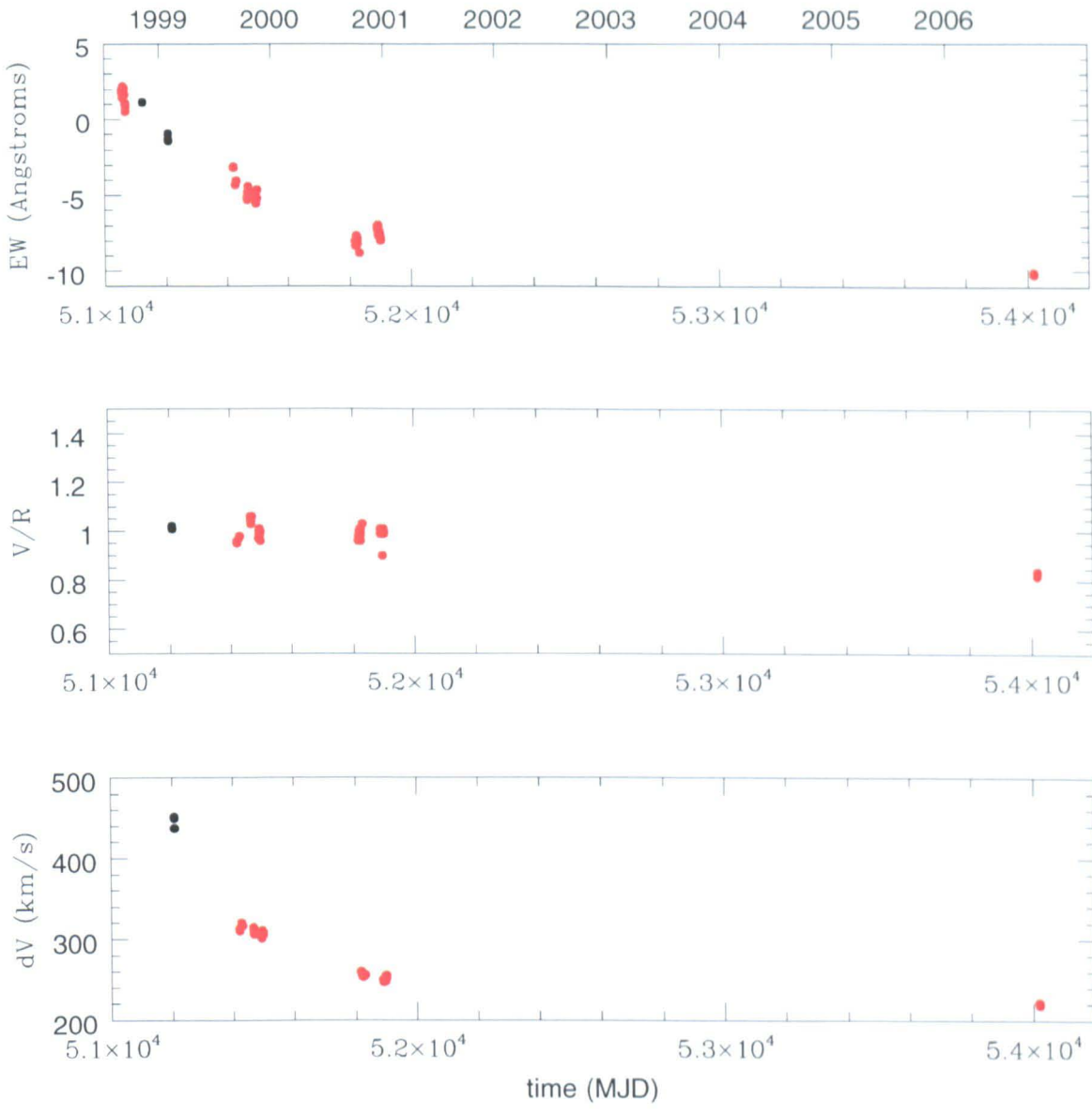

Figure 6.22: Time variability of the main parameters of the Hα line in A0535+26, showing our data as black dots and Grundstrom et al's (2007) data as red dots. Panels are the same as those in Figure 6.10.

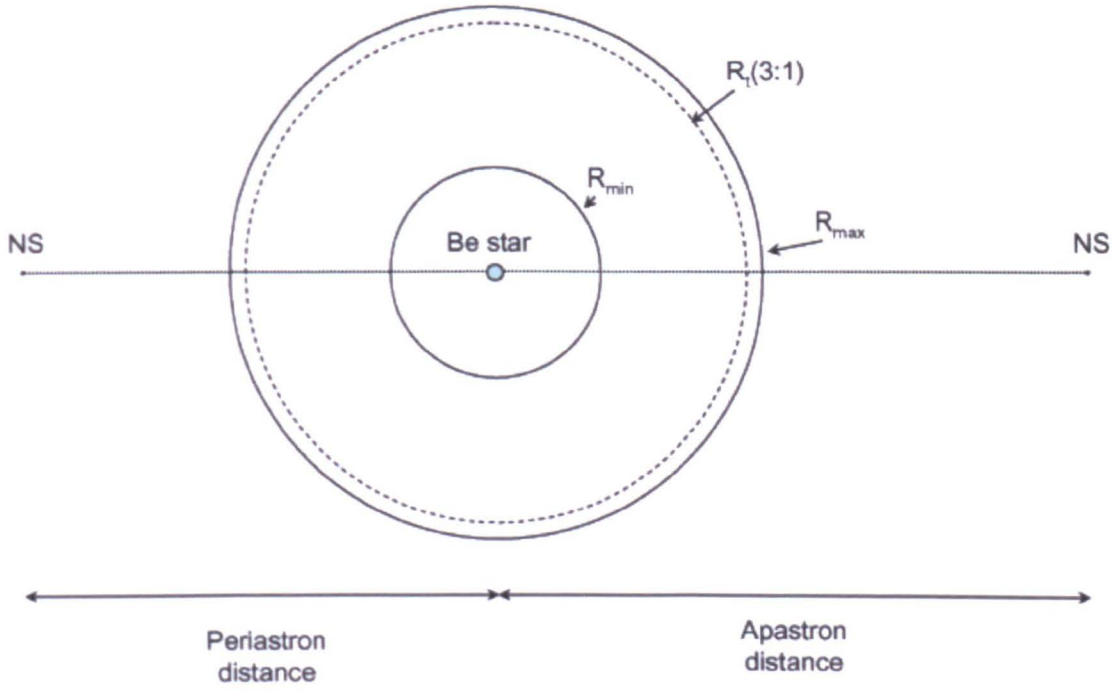

Figure 6.23: Schematic diagram of X Per shown to scale with respect to $R_\star$ where $R_\star = 6.5\mathrm{R}_\odot$. The truncation radii, $R_{t(3:1)}$ ($\sim 31\mathrm{R}_\star$), and our minimum and maximum calculated disc radii, R_{min} ($\sim 13\mathrm{R}_\star$) and R_{max} ($\sim 33\mathrm{R}_\star$) are shown along with the periastron ($\sim 59\mathrm{R}_\star$) and apastron distances ($\sim 73\mathrm{R}_\star$).

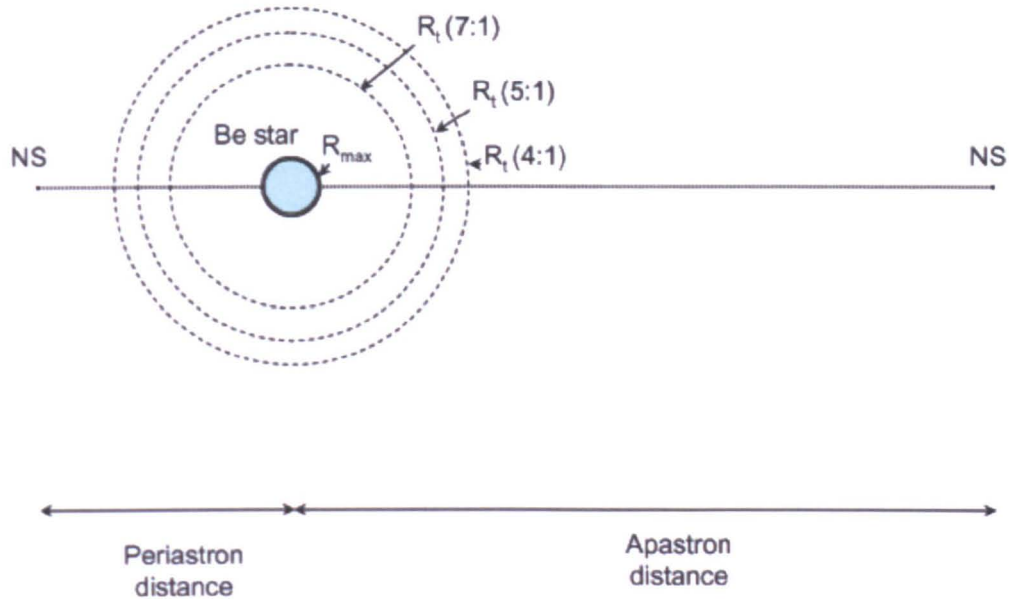

Figure 6.24: Schematic diagram of A0535+26 shown to scale with respect to $R_\star$ where $R_\star = 15\mathrm{R}_\odot$. The truncation radii, $R_{t(4:1;5:1;7:1)}$ ($\sim 7; 6; 5\mathrm{R}_\star$), and our maximum calculated disc radii, R_{max} ($\sim 1.1\mathrm{R}_\star$) are shown along with the periastron ($\sim 9\mathrm{R}_\star$) and apastron distances ($\sim 26\mathrm{R}_\star$).

$\sim 1 - 1.5$ years. In early 1998, corresponding to a time of decreased equivalent width, the V/R amplitude begins to get smaller, until September 2000 when the amplitude increases dramatically and corresponds to a time of incresed equivalent width. After September 2000, there are few data so a cycle period cannot be established, but a period of $1 - 1.5$ years seems to fit.

In the case of A0535+26 we see that for the entire period of the combined data set (i.e. July 1998 – Sept 2006) the V/R variability is negligible (refer to middle panel of Figure 6.22). This is to be expected as the start of the period corresponds to an episode of complete disc loss, which is apparent in the observed spectral lines (refer to to Figures 6.7 – 6.9). From the Hα spectral line (Figure 6.8a) we can see that it only appears as emission in January 1999. As the disc grows and becomes stable we would expect to see significant V/R variability, however we have no data between September 2000 and 2006 to confirm this, except for the one data point of Grundstrom et al. (2007) in September 2006.

In the case of both X Per and A0535+26, we can see from Figures 6.25 – 6.27 for X Per and Figures 6.28 – 6.29 for A0535+26, that the observed hydrogen and helium spectral lines seem to follow the same variability as the Hα line. However in the case of A0535+26 the Hα line appears as emission at MJD 51206.983, where as the others do not, presumably because the circumstellar disc hasn't reached sufficient temperature and density for them to be produced. The Hα line, in the case of X Per, also shows more pronounced V/R variability than the other lines.

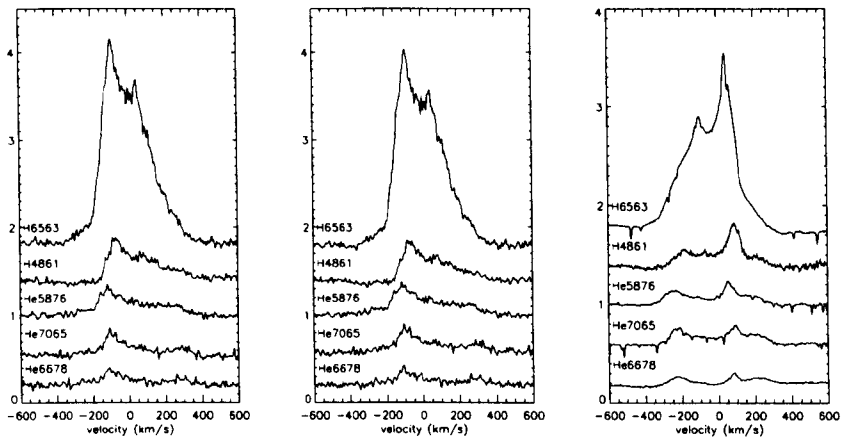

Figure 6.25: The emission lines of X Per shown as a function of velocity, at (a) MJD=50880.85 (b) MJD=50880.86 and (c) MJD=51124.1. Each spectrum is offset by 0.4 in the vertical axis, where the scale is arbitrary.

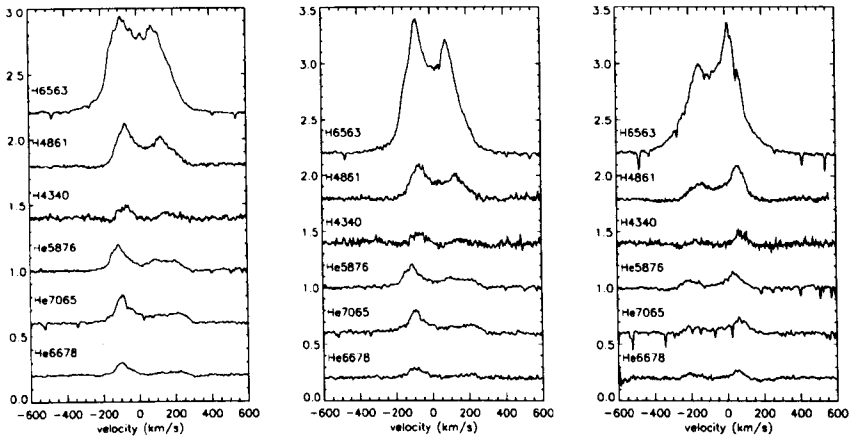

Figure 6.26: The emission lines of X Per shown as a function of velocity, at (a) MJD=51206.92 (b) MJD=51206.93 and (c) MJD=51392.2. Axis as in Figure 6.25.

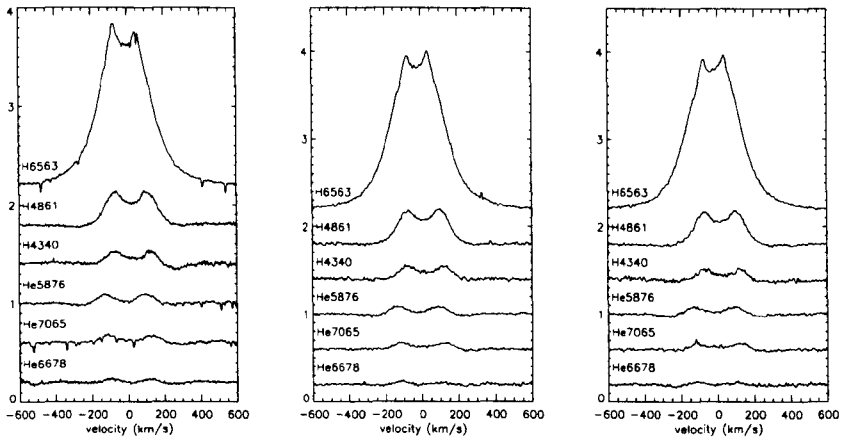

Figure 6.27: The emission lines of X Per shown as a function of velocity, at (a) MJD=52993.9 (b) MJD=53344.9 and (c) MJD=53346.0. Axis as in Figure 6.25.

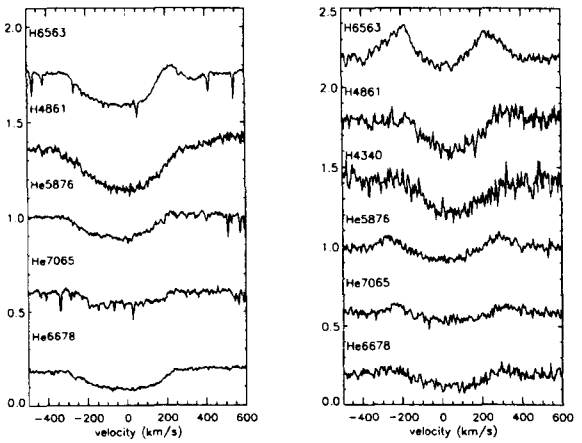

Figure 6.28: The emission lines of A0535+26 shown as a function of velocity, at (a) MJD=51124.05 and (b) MJD=51206.98. Axis as in Figure 6.25.

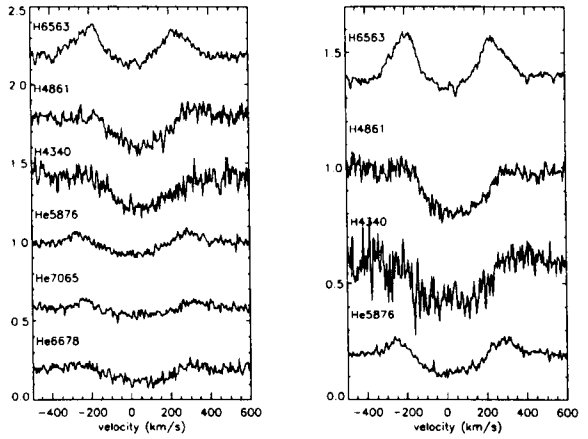

Figure 6.29: The emission lines of A0535+26 shown as a function of velocity, at (a) MJD=551206.99 and (b) MJD=51207.93. Axis as in Figure 6.25.

6.7 Discussion

We have shown that our results are consistent with those of Grundstrom et al. (2007) and Clark et al. (2001), except in the case of X Per where we found R_d to be larger than that determined by Grundstrom et al. (2007) (i.e. in the period 1996 - 1998, Grundstrom et al. (2007) found $R_d = 4R_\star$ as oppose to our $33 \pm 0.4R_\star$, and in 2000 they found $5R_\star$ as oppose to our $15 \pm 0.1R_\star$ in January 1999 and $22 \pm 0.1R_\star$ in December 2003 and 2004). The uncertainties on our determined values of R_d do not seem to account for the discrepancy between our values and those of Grundstrom et al. (2007). However Clark et al. (2001) also found the disc radius R_d, of X Per to be larger than that determined by Grundstrom et al. (2007) (i.e. in the period 1991 - 1997 Clark et al. (2001) found R_d to increase from 1.1 - $8.6R_\star$, whereas during the period 1996 - 1998 Grundstrom et al. (2007) found $R_d \sim 4R_\star$). A possible reason for such a discrepancy between our values and Clark et al.'s (2001) with those of Grundstrom et al. (2007), could therefore be due to the fact that Grundstrom et al. (2007) determined R_d from velocities corresponding to an outer boundary between the brighter and fainter parts of the Hα emitting region, whereas we calculated R_d from velocities corresponding to the brighter parts of the Hα emitting region. The Hα emission must have therefore been relatively constant in the radial di-

rection of the disc, such that the R_d derived from the Hα peak separation was indicative of the true Hα emitting radius. If this was the case then Grundstrom et al. (2007) would have assumed an outer boundary smaller than the true outer boundary.

However without optical interferomtric observations of X Per, we are unable to determine which method is the most reliable. Both our results and Clark et al.'s (2001) are larger than Grundstrom et al.'s (2007) which at least suggests that it is not a discrepancy in the data but rather due to the different methods used. The method used by Grundstrom et al. (2007) has been shown to be consistent with the Hα disc radii observed directly through long baseline interferometry (Grundstrom and Gies, 2006)[9]. But we can't ignore the fact that we are seeing Hα emission at these larger radii, which highlights the complexity of these circumstellar discs and how much we still do not understand about them.

If our values for R_d our correct, then although larger they are still below the 3:1 truncation radius (i.e. $R_t = 31\mathrm{R}_\star$), with only the radius found during the period 1996 – 1998 being approximately the same as the truncation radius. During the time of increased X-ray flux in 2003, our R_d was $\sim 15 - 22\mathrm{R}_\star$ and therefore still smaller than the truncation radius and the separation at periastron passage, suggesting that the mass transfer at this time was aided by the strong tidal forces that exist near periastron.

The combined data range for both X Per and A0535+26 start at a period immediately after complete disc loss when the disc is starting to reform. This is why the long term trend shows a steady increase in disc growth as well as the disc growth and dispersal cycles of 6 – 7 years and 5 years respectively. In both cases the disc dispersal cycles do not always result in complete disc loss and/or an X-ray outburst or period of increased X-ray flux, and it is still not clear why this is. In the case of X Per we see that the latest period of disc dispersal in 2001/2002 resulted in a period of increased X-ray flux but not in disc loss. The time before that in 1995/1996 there was no increased X-ray flux and no disc loss. In the case of A0535+26 we see that the latest outburst did not result in disc loss and instead it continued to grow. The previous outburst in 1994 did result in complete disc loss, which was observed in 1998.

However in systems that experience efficient truncation, like that of X Per and A0535+26, once the disc has reached the radius at which it is truncated the

[9]Note, this is only in the case of nearby stars.

density of the disc is expected to grow until as suggested by Okazaki (2002), the disc becomes sufficiently optically thick to continuum radiation for radiation driven warping to become possible. Depending on the extent of the distortion in the disc it will then presumably either lead to disc dispersal with no accompaning outburst or an outburst followed by disc dispersal and in some cases complete disc loss.

In the case of the V/R variability this only seems to occur when the disc is of a certain critical density. It has been suggested by Hanuschik (1995) that the onset of a density wave may be triggered at some critical density, where the disc becomes unstable to density perturbations and a density wave is formed. This is apparent in both X Per and A05353+26, where V/R variability is not observed until the equivalent width has reached a high enough value. The onset of the V/R cycle corresponds to low amplitude variations which increase with the growth of the mode. The amplitude of the variability is also observed to change depending on the equivalent width, where the amplitude increases with increasing equivalent width and decreases with decreasing equivalent width. It therefore seems that the circumstellar disc must reach a sufficient density before a density wave can exist. Then as the disc grows the density wave and the amplitude of the observed variability grows.

As mentioned in Section 6.1 the mechanism of confinement for such a wave is not entirely understood. However Clark et al. (2001) assume that it is due to the optically thin line force of Chen & Marlborough (1994). Based on this and the equations used by Okazaki (2002), they constructed an unperturbed model, and considered the effects of a linear perturbation by using the equations in Negueruela et al. (2001). They found that the one-armed (m=1) density wave is confined to $r \leq 10R_{\star}$ and precesses in a prograde manner. The predicted precession period is 2.5 years with a mode growth time of $\sim$ 5.7 years. This agrees with the observations of Clark et al. (2001) except for the period of 1995 – 1998, when the disc had reformed after complete disc loss, where the variability cycle is observed to decrease from 2 years to 0.6 years over 3 cycles. The Hα equivalent width was decreasing during this time and the photometric magnitude was fluctuating at a low level, therefore supporting the suggestion that the disc structure was changing during this period (Clark et al. 2001). From the combined data of our observations with those of Grundstrom et al. (2007) and Clark et al. (2001), during this period, we find cycle lengths of 1 –

1.5 years. Either way, it is clear that the model does not always agree with the observations, and as suggested by Clark et al. (2001) needs to include non-linear effects before any real predictions can be made.

6.8 Summary

In combining our spectral data with those of Grundstrom et al. (2007) and Clark et al. (2001), we have added to the long term data set of X Per and A0535+26. In each case the disc growth cycles and the V/R variability cycles have been revealed through Hα spectral line measurements, where our line measurements were found to be in good agreement with those of Grundstrom et al. (2007) and Clark et al. (2001). The long term data set of X Per and A0535+26 (refer to Figure 6.20 and 6.22) both start at a time when the system had just experienced complete disc loss and was beginning to reform. However, although the data range encompasses $\sim 2-3$ disc phases in each case, none of the disc dispersal episodes are observed to result in complete disc loss. Instead, what is observed is an overall steady increase in the equivalent width and corresponding decrease in in peak separation, suggesting that the disc needs to be of sufficient density before the disc dispersal/truncation mechanism is efficient enough to result in complete disc loss.

In presenting high resolution spectra we have been able to study and compare the behaviour of the different spectral lines, namely Hα, Hβ, Hγ, He I 5876, He I 6678 and He I 7065. In the case of X Per, we find that the equivalent width and peak separation of Hβ and Hγ follow the same trend as Hα, where as those of He I 5876, 6678 and 7065 remain constant during a period of disc growth (i.e. in 2003 – 2004), suggesting that during this period only the outer regions were expanding and not the inner regions. In the case of A0535+26 however, both the hydrogen and helium line measurements follow the same trend as Hα, suggesting that all the regions of the disc were growing at the same rate. This is to be expected, as these line measurements were taken at a time during disc reformation. The observed V/R variability in both X Per and A0535+26, appears to follow the same cycle in all of the spectral lines, suggesting that the density wave is present throughout the disc.

Chapter 7

Conclusions and Future Work

This chapter summarizes the results and conclusions found in the previous chapters and discusses the potential for future work in each case.

7.1 Masses of compact companions

As discussed in Chapter 1, determining the masses of the compact companions in binary systems is very important to the study of dense matter as well as the study of binary stars in general.

7.1.1 SMC X-1

SMC X-1 is one of 10 known eclipsing XRB pulsars, and one of only 6 that have had their stellar masses determined (including Vela X-1; Her X-1; LMC X-4; Cen X-3; and QV Nor). Based on our heating corrections and the model calculations for type II and Ib supernovae of Timmes et al. (1996), we concluded that the mass of the neutron star in SMC X-1 lies in the upper end of the heating corrected mass determinations and is therefore, $M_x = 1.21 \pm 0.10$ $M_\odot$.

We also suggested a possible site for the observed He II 4686 emission, as a hot-spot where a stream of material accreting via Roche-lobe overflow impacts the outer edge of the neutron star's accretion disc. If this is the case, then it supports the assumption that at least some of the accretion occurs via Roche-lobe overflow, and allows us to test the supposed precession period of ~ 55 days (e.g. Wojdowski et al. 1998).

In obtaining high quality data covering the super-orbital cycle, we could track the variation of the He II 4686 emission line radial velocity and equivalent width. The observed variation should follow the precession cycle, thereby confirming the origin of the He II 4686 emission line and allowing us to determine the precession period accurately. If we were able to obtain sufficient data, we could perform a Doppler analysis of the He II 4686 emission line, which would provide us with more accurate results.

7.1.2 OAO 1657-415 and EXO 1722-363

Of the four eclipsing XRB pulsars that have not had their masses determined, only three (i.e. OAO 1657-415 and EXO 1722-363 and XTE J1855-026) have known counterparts, whereas the counterpart to IGR J18027-2016 has not yet been identified (Hill et al. 2005). The counterparts to OAO 1657-415 and EXO 1722-363, were only recently identified (Chakrabarty et al. 2002; Zurita Heras et al. 2006) and as yet no spectroscopy or radial velocity measurements have been published. It would therefore be of great importance to the study of neurton star masses if the stellar masses could be determined in each case.

OAO 1657-415 was discovered by the *Copernicus* satellite in 1978 (Polidan et al. 1978). It was initially associated with the massive binary V861 Scorpii, until a more precise source position was revealed from *HEAO-1* and *Eintein* observations (White & Pravdo, 1979; Parmar et al. 1980). It was later identified photometrically by Chakrabarty et al. (2002), as a highly reddened supergiant (B0-6I) at a distance of about 6.5kpc with an extinction of $A_V \sim 20.4$. The mass transfer is believed to be via wind accretion (Mereghetti et al. 1991), however its postition in the Corbet diagram lies between the regions populated by wind-fed systems and those fed by Roche-lobe overflow, refer to Figure 7.1.

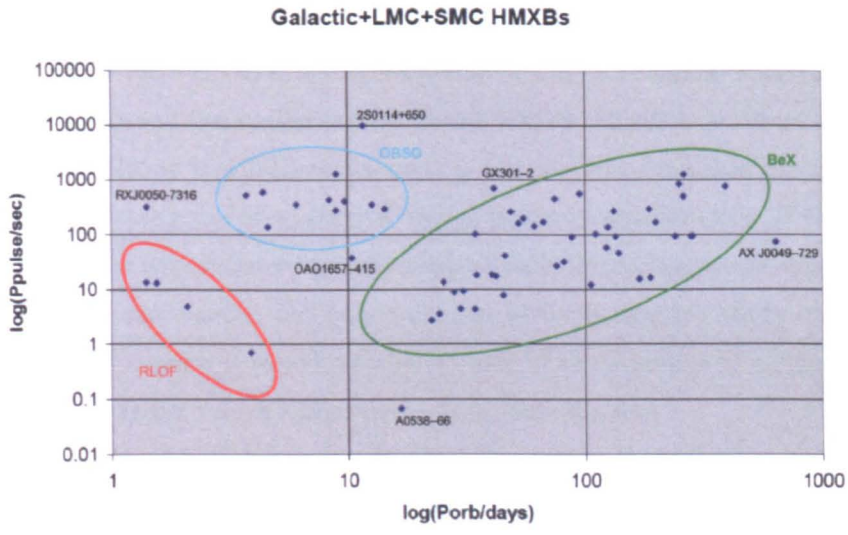

Figure 7.1: The Corbet diagram showing the relation between pulse period and orbital period, where the subset RLOF refers to Roche-lobe overflowing systems, OBSG refers to type O-B supergiant systems, and BeX refers to the Be XRBs. The position of OAO 1657-415 is clearly shown on the diagram in between the OBSG and BeX systems.

The reason for this may be that OAO 1657-415 has been through a previous phase of Roche-lobe overflow, or that its donor is of sufficiently late spectral type for its wind to be slower and more dense. The pulsar has a pulse period of $P_{pulse} = 38.22$ seconds (White & Pravdo, 1979; Parmar et al. 1980), observations of which revealed a 10.4 day eccentric orbit ($e \sim 0.1$) with a 1.7 day eclipse (Chakrabarty et al. 1993). Among the eclipsing XRB pulsars the significant eccentricity of OAO 1657-415 is comparable only to that of Vela X-1, which consists of one of the most massive known neutron stars. It would therefore be interesting to see if OAO 1657-415 also has an over massive neutron star like that of Vela X-1.

EXO 1722-363 was discovered by the Galactic plane scan observations of Warwick et al. (1988) and subsequently confirmed as a 413.9 second X-ray pulsar by *Ginga* (Tawara et al. 1989). Later *RXTE* observations discovered the 9.7 day orbital period and showed the system to have a 1.26 day eclipse (Corbet et al. 2005). However it was not until recently that combined *INTEGRAL* and *XMM-Newton* observations allowed for the identification of the infra-red coun-

terpart to the system. The observed infra-red magnitudes are very similar to that of OAO 1657-415 so it is suspected that it will be of similar spectral type. Based on this and the similar orbital period EXO 1722-363 is a virtual twin of OAO 1657-415, so it will therefore be very interesting to measure the mass of the neutron star and see whether it shares further characteristics. If we were able to obtain near infra-red spectroscopy of both these sources and determine the neutron star masses, not only would it be furthering the study of direct neutron star masses, it would also be the first determinations of neutron star masses from radial velocity measurements in the infra-red.

From Equation 1.9 we know that if the stellar radius is not known, there is a degeneracy in determining the Roche-lobe filling factor β, and the system inclination i, from the eclipse duration. This was the case with SMC X-1, therefore the system masses could only be determined from the radial velocity curve in the two limits $\beta = 1$ and $i = 90°$. Therefore in the case of OAO 1657-415 and EX0 1722-363, a first objective would be to obtain combined H & K band spectra of the sources in order to perform non-LTE model atmosphere analyses, which may reveal chemical abundances that will suggest the degree of pre-supernova mass transfer. By accounting for this extra abundance a more accurate spectral type and hence stellar radius can be determined.

To construct the first radial velocity curve of these systems, at least twenty K-band spectra of the infra-red counterparts would be required. The infra-red spectra of B type supergiants typically show absorption lines due to the hydrogen Bracket series and neutral helium (Hanson et al 1996; 1998; Meyer et al 1998), where in the K band we would expect to see He I 2.058 μm, He I 2.113 μm and Brγ (i.e. 2.166 μm). With a medium resolution of $\sim$ 3000 a velocity resolution of 100 km s^{-1} could be obtained resulting in an accuracy of $\sim \pm 10$ km s^{-1}. Possible template stars to be used for cross-correlation are the nearby radial velocity standard supergiants HD 154313 and HD 168728. The former is a B0Iab and the latter is a B6Iab and therefore spans the range of spectral types predicted for OAO 1657-415 and EXO 1722-363.

The estimated stellar masses in OAO 1657-415 and EXO 1722-363 are $\sim$ 15 M$_\odot$ for the donor star and $\sim$ 1.4 M$_\odot$ for the neutron star. Based on these masses we can predict the expected radial velocity amplitude of the donor star in OAO 1657-415 (i.e. the better constrained of the two systems), but emphasize that those of EXO 1722-363 will be very similar. Given a 10.4 day orbital

period with $e \sim 0.1$, and the fact that the orbit is close to edge-on, we find the radial velocity amplitude will be ~ 21 km s^{-1}. In order to assess how accurately the radial velocity amplitude, and hence neutron star mass, may be determined from the proposed observations, simulated sets of observational radial velocities have been constructed. For each of the 1000 trial sets of simulated data, 20 observation times, randomly distributed in orbital phase have been chosen. For each of these observation times a predicted radial velocity based on the parameters above and assuming a 1σ uncertainty of 10 km s^{-1}, have been calculated. The points and error bars in Figure 7.2 show the results of one typical data set drawn from the 1000 trials.

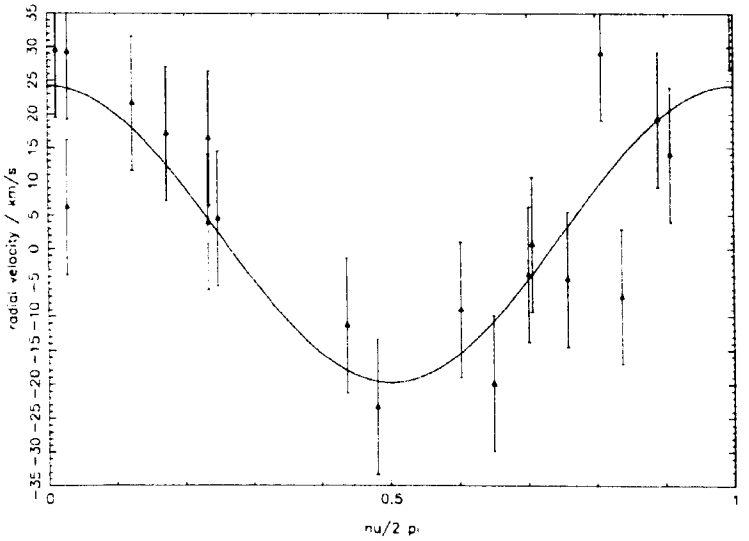

Figure 7.2: The simulated radial velocity curve of the donor star in OAO 1657-415, comprising twenty radial velocities at random orbital phase, each with an uncertainty of 10 km s^{-1}. The radial velocity is given by $v = K_o(e + \cos\nu)$ where K_o is the semi-amplitude of the radial velocity curve and is given by $K_o = 2\pi a_1 \sin i/P(1 - e^2)^{0.5}$, and ν is the true anomaly given by $\tan(\nu/2) = (1 + e/1 - e)^{0.5}\tan(E/2)$. E is the eccentric anomaly of the orbit which is related to the mean anomaly by $E - e\sin E = M$ where the mean anomaly $M = (t - T_0)2\pi/P$ where T_0 is the time of periastron passage. The solid line shows the best-fit to these simulated data and corresponds to a semi-amplitude of $K_o = 22.0 \pm 3.1$ km s^{-1}.

For each such trial set of simulated data a best-fit sinusoid has been fitted and its amplitude and associated uncertainty have been determined. The smooth curve in Figure 7.2 shows the best-fit to this one particular simulated data set. The average radial velocity amplitude from the 1000 trials is 21.0 km s^{-1} (as expected) with a standard deviation of 1.2 km s^{-1}. The average uncertainty in the amplitude from any single trial is $\pm$2.5 km s^{-1}. This value therefore represents the typical uncertainty in the radial velocity amplitude that we may expect to measure. Combining an uncertainty of 2.5 km s^{-1} in the semi-amplitude of the donor star's radial velocity curve with the uncertainties in the other orbital parameters (Chakrabarty et al 1993) of the system results in a neutron star mass that has an uncertainty of about $\pm$0.13 $M_\odot$. This accuracy is sufficient to distinguish between the peaks in the predicted bimodal neutron star mass distribution of Timmes et al (1996). The usability of radial velocity spectra with comparable accuracy to those predicted here is illustrated by the determination of the neutron star mass in SMC X-1 (refer to Chapter 3).

7.1.3 LMC X-3

LMC X-3 is one of 18 confirmed black hole XRBs and of these it is one of only 4 black hole HMXBs. Of these, Cyg X-1 and LMC X-1 contain O stars, with masses similar to those seen in systems containing neutron stars. The other two, LMC X-3 and J1819.3-2525 contain rather less massive B stars (i.e. $M_\star \leq 8\ M_\odot$), where no equivalent neutron star binaries are known. However, none of these black hole candidates have tightly constrained masses. Accurate mass determination is therefore important to further the study of these dense objects as well as black hole XRBs in general.

The spectral type of LMC X-3 is known to vary with phase due to the intense heating of the donor star by the X-ray source. By assuming a spectral type of B5V, which is heated by a further $\sim$ 3300 K to appear as a B3V, we took heating corrections into account and concluded that the mass of the black hole in LMC X-3 lies in the range, $9.5 \leq M_x \leq 13.2\ M_\odot$.

Unfortunately we did not have enough data (i.e. only 5 spectra), so we were not able to make a detailed analysis of how the spectral type changed with phase. This uncertainty in the spectral type resulted in a mass uncertainty of

$\sim \pm 1$ $M_{\odot}$ at each of the extremes of the mass range. To improve the accuracy of the mass determinations sufficient data with good orbital phase coverage would be required. Detailed stellar atmosphere fitting to the individual spectra could then be performed at each phase, so that the underlying spectral type (i.e. before the star is affected by X-ray irradiation) and the heating effects could be determined to greater accuracy. However as the system is not eclipsing the resulting mass would still be limited by the assumed range on the inclination (i.e. $50° \leq i \leq 70°$).

Our results did not agree with those of Soria et al. (2003), as based on our spectral observations, we assumed the heating effects to be the result of hard X-rays as opposed to soft X-rays. In future studies it would therefore be interesting to obtain simultaneous X-ray and optical observations to enable a corresponding analysis of the X-ray spectra.

7.2 Be X-ray binaries

The phenomena of Be stars is yet to be completely understood. However from multi-wavelength studies of these interesting objects, a clearer picture has begun to emerge. One of the most interesting aspects of the phenomena is the disc growth and dispersal cycles. What is the machanism driving these cycles and why do times of disc dispersal not always result in complete disc loss? As noted earlier, the long term data set of X Per and A0535+26 reveals $\sim 2-3$ disc phases where none of these result in complete disc loss. The measured equivalent width is observed to increase (i.e. become more negative) progressively with each disc phase suggesting that the disc needs to be of sufficient density before the disc dispersal/truncation mechanism is efficient enough to result in complete disc loss.

The onset of a density wave, as suggested by Hanuschik (1995) also needs the disc to be of some critical density, where as the disc grows the amplitude of variability increases. The V/R variability observed in the hydrogen and helium emission lines of X Per and A0535+26 all follow the same cycle, implying that the density wave is present throughout the disc. Does this density wave affect the disc growth cycle? What determines the cycle length of the V/R variability and why is it observed to change (e.g. in the case of X Per)? For such questions

to be answered and for these systems to be understood in greater detail, long-term multi-wavelength studies of a range of these objects needs to be carried out. The disc phases and V/R variability can then be tracked closely, so that they are known accurately. The behaviour of the disc as represented by the spectral emission lines, should then be looked at with reference to the corresponding optical and X-ray photometry to obtain an overall picture of what is happening. As the efficiency and effects of truncation varies between the different types of Be XRB systems (i.e. depending on the eccentricity), the resulting behaviour should then be reviewed in terms of the type of Be XRB system. Then with the help of non-linear purturbation models, we can gain greater understanding of these systems.

7.3 Potential Be star / black hole candidates

As discussed in Chapter 5, Be XRB systems usually contain a neutron star as the compact companion. But as suggested by Zhang et al. (2004) it is thought that close orbit low eccentricity Be XRB systems, that are not known to exhibit type I X-ray outbursts, could contain a black hole as the compact companion. Our study aimed to observe potential systems and conclude whether this was the case in these particular systems.

7.3.1 Observed sources

Unfortunately we did not have enough data for each source, and in most cases the data we did have were of poor quality. However, in the case of the objects obtained with SALT (i.e. LS 3417; LS 4356; HR 4830 and HR 4899) we were able to obtain a rough amplitude of variability. The variability observed in the systems HR 4830 and HR 4899, both confirmed previously published values, where the radial velocity amplitudes imply that the X-ray source in both systems are most likely neutron stars. However the observed luminosity of HR 4830 has led to the suggestion that this sytem contains a magnetized white dwarf (Waters et al. 1989; Torrejon & Orr, 2001). It would be interesting to see if this is the case, as there are no known white dwarf/Be star XRB systems.

The system LS 3417 was found to have a radial velocity amplitude of ~ 20 km s^{-1}, which depending on the system inclination and donor star mass, could be indicative of either a white dwarf or a neutron star. There has been no evidence of pulsations from this system and the reported X-ray features of LS 3417 are said to be similar to that of a white dwarf. Therefore, and for the reasons stated above, it would be of great interest to see if this system is a white dwarf/Be star XRB.

The system that turned out to be of most interest is LS 4356, as it appeared to have a radial velocity amplitude of ~ 95 km s^{-1} and is therefore very likely to be a black hole/Be star XRB. Obviously there was not enough data to make any firm conclusions, so obtaining sufficient optical spectroscopy in the future would be of great interest. If the X-ray source in this system is then found to be a black hole, it would make LS 4356 the first known black hole/Be star XRB.

In the case of the systems HD 34921; DM+53 2262 and SAO 49725, there were too few data points to draw any conclusions at all. It would therefore be interesting to observe these systems again as potential black hole/Be star XRBs.

7.3.2 Possible sources to be observed

Based on the same criteria as outlined in Section 5.2, a list of further potential black hole/Be star XRBs were chosen from the HMXB catalogue of Liu et al. (2000), refer to Table 7.1. In obtaining sufficient optical spectroscopy of each of these objects we would be able to see if any of these objects appeared to display radial velocity amplitude variations in excess of 30 km s^{-1}. Any that did, could then be observed in more detail in order achieve conclusive results.

7.4 Conclusions

The observations and analysis presented in this thesis have demonstrated the importance of taking into account the heating of the donor star by the compact companion in an XRB, when using the motion of that donor star to measure the mass of the compact companion. By neglecting this heating effect, or assuming that the X-rays have a different effect to that which they actually have, the mass

Table 7.1: List of Be XRB sources to be observed as potential black hole systems.

Source	Be star	Spectral type	P_{orb} days	Reference
J0032.9-7348				Kahabka et al. 1996; Stevens et al. (1999)
0051.9-7311	SMC 25			Schmidtke et al. (1999)
0052.9-7158	SMC 32			Schmidtke et al. (1999)
RXJ0058.3-7229				Schmidtke et al. (1999)
RXJ0101.0-7206		B3.5Ve		Stevens et al. (1999)
0103-762				Tuohy et al. (1988)
RXJ0516.0-6916				Cowley et al. (1997)
RXJ052.5-6932		O8e	24.4	Schmidtke et al. (1999); Edge et al. (2004)
RXJ0532.4-6535	RGC 36			Reid et al. (1988)
RXJO535.0-6700	RGC 28	B0Ve		Reid et al. (1988)
2202+501	V2175 Cyg			Wood et al. (1984); Tuohy et al. (1988)
2214+589	GG3 71			Tuohy et al. (1988); Howarth (1983)

determined from the radial velocity curve will not reflect accurately the mass of the neutron star or black hole in question. Nevertheless this is a powerful technique and there are still further objects for which such measurements can be performed in the future.

The observations and analysis have also demonstrated that much remains to be discovered concerning Be XRBs. The long term evolution of the Be star disc, its formation and dispersal, and how it interacts with the compact companion are all still uncertain. Finally, there are the first intriguing hints that XRBs containing a Be star and a black hole may indeed exist. If such systems can be discovered and monitored closely, they may give further clues about the behaviour of Be stars in such systems, and lead to a clearer understanding of their evolution in the future.

Bibliography

[1] Ables, J. G., 1969, Proc. Astron. Soc. Australia, 1, 237

[2] Adams, F. C., Ruden, S. P., & Shu, F. H., 1989, Astrophysical Journal, 347, 959

[3] Agrawal, V. K. & Bhattacharya, S., 2003, Astronomy & Astrophysics, 398, 223

[4] Alpar, M. A., Cheng, A. F., Ruderman, M .A. & Shaham, J., 1982, Nature, 300, 728

[5] Apparao, K. M. V., 1994, Astronomy & Astrophysics, 291, 775

[6] Augello, G., Iaria, R., Robba, N. R., Di Salvo, T., Burderi, L., Lavagetto, G. & Stella, L., 2003, Astrophysical Journal, 596, L63

[7] Avni, Y., 1976, Astrophysical Journal, 209, 574

[8] Backer, D. C., Kulkarni, S. R., Heiles, C. E., Davis, M .M. & Goss, W. M., 1982, Nature, 300, 615

[9] Barret, D., Olive, J. F., Boirin, L., Done, C., Skinner, G. K. & Grindlay, J. E., 2000, Astrophysical Journal, 533, 329

[10] Bednarek, W., 2000, Astronomy & Astrophysics, 362, 646

[11] Bednarek, W. & Giovannelli, F., 2007, Astronomy & Astrophysics, 464, 437

[12] Bignami, C. F., Maraschi, L. & Treves, A., 1977, Astronomy & Astrophysics, 55, 155

[13] Bildsten et al., 1997, Astrophysical Journal, 113, 367

[14] Bonnet-Bidaud, J.M., & van der Klis, M. 1981, Astronomy & Astrophysics, 97,134

[15] Bowyer, S., Bryam, E. T., Chubb, T. A. & Friedman, M., 1965, Sci, 147, 394

[16] Boyd, P. T., Smale, A. P., Homan, J., Jonker, P. G., van der Klis, M. & Kuulkers, E., 2000, Astrophysical Journal, 542, L127

[17] Bracewell, R.N., 1965, *The Fourier Transform and its Aplications*, McGraw-hill, New York

[18] Braes, L. E. E. & Miley, G. K., 1972, Nature, 235, 273

[19] Brault J. W. & White, O. R., 1971, Astronomy & Astrophysics, 13, 169

[20] Brucato, R. J. & Kristian, J., 1972, Astrophysical Journal, 173, L105

[21] Buscombe, W., 1980, *MK Classification, 4^{th} General Catalogue*, Evanson

[22] Buser, R. & Kurucz, R. L., 1978, Astronomy & Astrophysics, 70, 555

[23] Carbon, D. F. & Gingerich, O. J., 1969, *Theory & Observation of Normal Stellar Atmospheres*, Edt. O. J. Gingerich, M.I.T. Press: Cambridge, p.377

[24] Chakrabarty, D., et al., 1993, Astrophysical Journal, 403, L33

[25] Chakrabarty, D., Wang, Z., Juett, A. M., Lee, J. C. & Roche, P., 2002, Astrophysical Journal, 573, 789

[26] Chakrabarty, D., Morgan, E. H., Muno, M. P., Galloway, D. K., Wijnands, R., van der Klis, M. & Markwardt, C. B., 2003, Nature, 424, 42

[27] Chakrabarty, D., 2004, ASP Conference Series

[28] Charles, P. & Coe, M. J., 2003, arXiv:astro-ph/0308020v2

[29] Chevalier, C. & Ilovaisky,S. A., 1998, Astronomy & Astrophysics, 330, 201

[30] Chen, H. & Marlborough, J. M., 1994, Astrophysical Journal, 427, 1005

[31] Chen, W. et al., 1997, Astrophysical Journal, 491, 312

[32] Chesneau, O., et al., 2005, Astronomy & Astrophysics, 435, 275

[33] Clark J. S., Tarasov, A. E., Steele, I. A., Coe, M. J., Roche, P., Shrader, C., Buckley, D. A. H., Larionov, V., Larionova, L., Lyuty, V. M., Zaitseva, G. V., Grunsfeld, J., Fabregat, J. & Parise, R., 1998b, Monthly Notices of the Royal Astronomical Society, 294, 165

[34] Clark, J. S., Steele, I. A., Coe, M. J. & Roche, P., 1998, Monthly Notices of the Royal Astronomical Society, 297, 657

[35] Clark, J. S., Steele, I. A., Fender, R. P. & Coe, M. J., 1999, Astronomy & Astrophysics, 348, 888

[36] Clark, J. S., Tarasov, A. E., Okazaki, A. T., Roche, P. & Lyuty, V. M., 2001, Astronomy & Astrophysics, 380, 615

[37] Coburn, W., Heindl, W. A., Gruber, D. E., Rothschild, R. E., Staubert, R., Wilms, J. & Kreykenbohm, I., 2001, Astrophysical Journal, 552, 738

[38] Coburn, W., Heindl, W. A., Rothschild, R. E., Gruber, D. E., Kreykenbohm, I., Wilms, J., Kretschmar, P. & Staubert, R., 2002, Astrophysical Journal, 580, 394

[39] Coe, M. J., Carpenter, G. F., Engel, A. R. & Quenby, J. J., 1975, Nature, 256, 630

[40] Coe, M. J., Buckley, D. A. H., Fabregat, J., Steele, L. A., Still, M. D. & Torrejon, J. M., 1997, Astronomy & Astrophysics, 126, 237

[41] Coe, M. J., Reig, P., McBride, V. A., Galache, J. L. & Fabregat, J., 2006, Monthly Notices of the Royal Astronomical Society, 368, 447

[42] Codina, S. J., de Freitas Pacheco, J. A., Lopes, D. F. & Gilra, D., 1984, Astronomy & Astrophysics, 57, 239

[43] Cominsky, L., Clark, G. W., Li, F. Mayer, W. & Rappaport, S., 1978, Nature, 273, 367

[44] Cominsky, L. R. & Moraes, F., 1991, Astrophysical Journal, 370, 670

[45] Corbet, R. H. D., 1986, Monthly Notices of the Royal Astronomical Society, 220, 1047

[46] Corbet, R. H. D. & Mukai, K., 2002, Astrophysical Journal, 577, 923

[47] Corbet, R. H. D. Markwardt, C. B. & Swank, J. H., 2005, Astrophysical Journal, 633, 377

[48] Cowley, A. P., McLaughlin, D. B., Toney, J. & MacConnell, D. J., 1972, Publications of the Astronomical Society of the Pacific, 84, 834

[49] Cowley, A. P., Crampton, D., Hutchings, J. B., Remillard, R. & Penfold, J. E.,1983, Astrophysical Journal, 272, 118

[50] Cowley, A. P., Schmidtke, P. C., Ebisawa, K., Makino, F., Remillard, R. A., Crampton, D., Hutchings, J. B., Kitamoto, S. & Treves, A., 1991, Astrophysical Journal, 381, 526

[51] Cowley, A. P., Schmidtke, P. C., Hutchings, J. B. & Crampton, D., 1994, Astrophysical Journal, 429, 826

[52] Cowley, A. P. et al., 1997, PASP, 109, 21

[53] Cramer, N., 1984, Astronomy & Astrophysics, 132, 283

[54] Cumming, A., Zweibel, E. & Bildsten, L., 2001, Astrophysical Journal, 557, 958

[55] Deeter, J. E., Boynton, P. E. & Pravdo, S. H., 1981, Astrophysical Journal, 247, 1003

[56] Deeter, J. E., Boynton, P. E., Lamb, F. K. & Zylstra, G., 1989, Astrophysical Journal, 336, 376

[57] Delgado-Marti, H., Levine, A. M., Pfahl, E. & Rappaport, S. A., 2001, Astrophysical Journal, 546, 455

[58] Delvaille, J. P., Li, F. K., Liller, W. & Shao, C. Y., 1976, IAUC, 2936

[59] Dorren, J. D., Guinan, E. F. & McCook, G. P., 1979, IAU Circ. 3352

[60] Dorren, J. D. &Guinan, E. F., 1980, in Close Binary Stars: Observation and Interpretation, ed. M. Popper & R. Ulrich (Dordrecht: Reidel), 361 (DG80)

[61] Edge, W. R. T., Coe, M. J., Galache, J. L., Hill, A. B., 2004, Monthly Notices of the Royal Astronomical Society, 349, 1361

[62] Esin, A. A., McClintock, J. E. & Narayan, R., 1997, Astrophysical Journal, 489, 865

[63] Fabregat, J., Reglero, V., Coe, M. J. et al., 1992, Astronomy & Astrophysics, 259, 522

[64] Faulkner, J., Lin, D. N. C. & Papaloizou, J., 1983, Monthly Notices of the Royal Astronomical Society, 205, 359

[65] Feast, M. W., Thackeray, A. D. & Wesselink, A. J., 1961, Monthly Notices of the Royal Astronomical Society, 122, 433

[66] Fender, R. P., Hjellming, R. M. Tilanus, R. P. J., Pooley, G. G. & Deane. J. R. et al., 2001, Monthly Notices of the Royal Astronomical Society, 322, L23

[67] Fender, R. P. et al. 2004, Nature, 427, 222

[68] Finger, M. N., Cominsky, L. R., Wilson, R. B., Harmon, B. A. & Fishman, G. J., 1994, in The Evolution of X-ray Binaries, ed. S. S. Holt & C. S. Day (New York: AIP), 459

[69] Finger, M. N., Wilson, R. B. & Harmon, B. A., 1996, Astrophysical Journal, 459, 288

[70] Firt, R. & Harmanec, P., 2006, Astronomy & Astrophysics, 447, 277

[71] Foster, R. S., Waltman, E. B., Tavani, M., Harmon, B. A., Zhang, S. N., Paciesas, W. S. & Ghigo, F. D., 1996, Astrophysical Journal, 497, L81

[72] Frank, J., King, A. & Raine, D., 2002, *Accretion Power in Astrophysics: Third Edition.*, Press: Cambridge

[73] Friend, D. B. & Castor, J. I., 1982, Astrophysical Journal, 261, 193

[74] Fryxell, B. A. & Woosley, S. E., 1982, Astrophysical Journal, 258, 733

[75] Fujimoto, M. Y., Hanawa, T. & Miyaji, S., 1981, Astrophysical Journal, 247, 267

[76] Galkina, T. S., 1980, in IAU Symp. 88, Close Binary Stars: Observation and Interpretation, ed. M. J. Plavec, D. M. Popper & R. K. Ulrich (Dordrecht: Reidel), 367

[77] Galloway, D. K., 2006, astro-ph/0604345

[78] Garrison, R. F., Hiltner, W. A. & Schild, R. E., 1977, Astrophysical Journal Supplement, 35, 111

[79] Ghosh, P. & Lamb, F. K., 1979, Astrophysical Journal, 234, 296

[80] Giacconi, R., 1962, Phys. Rev. Lett., 9, 439

[81] Giacconi, R., Murray, S., Gursky, H. et al., 1972, Astrophysical Journal, 178, 281

[82] Giles, D. R. & Bolton, C. T., 1986, Astrophysical Journal, 304, 371

[83] Giles, D. R. & Bolton, C. T., 1986, Astrophysical Journal, 304, 389

[84] Giovannelli, F. & Sabau Graziati, L., 1992, Space Sci. Rev., 59, 1

[85] Gleissner, T., et al., 2004, Astronomy & Astrophysics, 414, 1091

[86] Gottlieb, E. W., Wright, E. L. & Liller, W., 1975, Astrophysical Journal, 195, L33

[87] Green, J., Bailyn, C. D. & Orosz, J. A., 2001, Astrophysical Journal, 554, 2, 1290

[88] Griffith, R. E. & Seward, F. D., 1977, Monthly Notices of the Royal Astronomical Society, 180, 75P

[89] Grundstrom E. D. & Gies, D. R., 2006, Astrophysical Journal, 651, L53

[90] Grundstrom, E. D., Boyajian, T. S., Finch, C., Gies, D. R., Huang, W., McSwain, M. V., O'Brien, D. P., Riddle, R. L., Trippe, M. L., Williams, S. J., Wingert, D. W. & Zaballa, R. A., 2007, Astrophysical Journal, 660, 1398

[91] Gunn, A. G., Hall, J. C., Lockwood, G. W., & Doyle, J. G., 1995, Astronomy & Astrophysics, 305, 146

[92] Halbedel, E. M., 1993, PASP, 105, 465

[93] Haberl, F., Angelini, L., Motch, C. & White, N. E., 1998, Astronomy & Astrophysics, 330, 189

[94] Haigh, N .J., Coe, M. J., Steele, I. A. & Fabregat, J., 1999, Monthly Notices of the Royal Astronomical Society, 310, L21

[95] Haigh, N. J., Coe, M. J. & Fabregat, J., 2004, Monthly Notices of the Royal Astronomical Society, 350, 1457

[96] Hammerschlag-Hensberg, G., Kallman, R.T., & Howarth, I.D. 1984, Astrophysical Journal, 283, 249

[97] Hanawa, T. & Fujimoto, M. Y., 1984, Publications of the Astronomical Society of Japan, 36, 199

[98] Handler, G., Balona, L. A., Shobbrook, R. R., et al., 2002, Monthly Notices of the Royal Astronomical Society, 333, 262

[99] Hanson, M. M., Conti, P. S. & Rieke, M. J., 1996, Astrophysical Journal Supplement, 107, 281

[100] Hanson, M. M., Rieke, G. H. & Luhman, K. L., 1998, Astr.J, 116, 1915

[101] Hanuschik, R. W., 1986, Astronomy & Astrophysics, 166, 185

[102] Hanuschik, R. W., Kozok, J. R. & Kaiser, D., 1988, Astronomy & Astrophysics, 189, 147

[103] Hanuschik, R. W., 1989, Astrophysics & Space Science, 161, 61

[104] Hanuschik, R. W., Hummel, W., Dietle, O. & Sutorios, E., 1995, Astronomy & Astrophysics, 300, 163

[105] Harding, A. K. & Gaisser, T. K., 1990, Astrophysical Journal, 358, 561

[106] Harmon, B. A. et al., 1995, Nature, 374, 703

[107] Harmon, B. A. et al., 1997, Astrophysical Journal, 477, L85

[108] Hasinger, G. & van der Klis, M., 1989, Astronomy & Astrophysics, 225, 79

[109] Hasinger, G., Priedhorsky, W. C. & Middleditch, J., 1989, Astrophysical Journal, 337, 843

[110] Hasinger, G., van der Klis, M., Ebisawa, K., Dotani, T. & Mitsuda, K.,1990, Astronomy & Astrophysics, 235, 131

[111] Hayakawa, S., 1981, Space Sci. Rev., 29, 221

[112] Hilditch, R.W., Howarth, I.D., & Harries, T.J. 2005, Monthly Notices of the Royal Astronomical Society, 357, 304

[113] Hill, G. & Hutchings, J. B., 1970, Astrophysical Journal, 162, 265

[114] Hill, G. & Hutchings, J. B., 1973, Astrophys. Space Sci., 20, 123

[115] Hill, G., 1979, Description of an eclipsing binary light curve computer code with application to YSEX & the WUMa code of Rucinski, Publ. Dom. Astrophys. Obs.

[116] Hill, G., 1988, Light2 User Manual, Publ. Dom. Astrophys. Obs.

[117] Hill,A.B., Walter,R., Knigge,C., Bazzano,A., Blanger,G., Bird,A.J., Dean,A.J., Galache,J.L., Malizia,A., Renaud,M., Stephen,J. & Ubertini,P., 2005, Astronomy & Astrophysics, 439, 255

[118] Hjellming, R. M. & Wade, C. M. 1971a, Astrophysical Journal, 164, L1

[119] Hjellming, R. M., 1988, in: Galactic and Extra-Galactic Radio Astronomy, eds. G. L. Verschuur and K. I. Kellermann, (Springer-Verlag, New York) p. 381

[120] Hoffman, J. A., Marshall, H. L. & Lewin, W. H. G., 1978, Nature, 271, 630

[121] Homan, J., van der Klis, M., Jonker, P. G., Wijnands, R., Kuulkers, E., Mndez, M. & Lewin, W. H. G., 2002,Astrophysical Journal, 568, 878

[122] Homer. L, Deutsch, E. W. & Anderson, S. F., 2001, Astrophysical Journal, 122, 2627

[123] Horne, K., 1986, PASP, 98, 609

[124] Horne, K. & Marsh, T. R., 1986, Monthly Notices of the Royal Astronomical Society, 218, 761

[125] Howarth, I. D., 1983, Monthly Notices of the Royal Astronomical Society, 203, 801

[126] Huang, S, 1972, Astrophysical Journal, 171, 549

[127] Hubert, A. M. & Floquet, M., 1998, Astronomy & Astrophysics, 335, 565

[128] Hummel, W. & Dachs, J., 1992, Astronomy & Astrophysics, 262, L17

[129] Hummel, W. & Hanuschik, R. W., 1994, In: Balona, L. A., Henrichs, H. F., Le Contel, J. M. (eds.) Proc. IAU Symp. 162, Pulsation, Rotation and Mass Loss of Early-Type Stars, Kluwer Academic Publisher, Dordrecht, p. 382

[130] Hummel, W., 1994, Astronomy & Astrophysics, 289, 458

[131] Hummel, W. & Hanuschik, R. W., 1997, Astronomy & Astrophysics, 320, 852

[132] Hummel, W., 2000, In: Smith, M. A., Henrichs, H. F., Fabregat, J.(eds.) Proc. IAU Colq. 175, The Be Phenomenon in Early-Type Stars. Vol. 214

[133] Hutchings, J. B., 1968, Monthly Notices of the Royal Astronomical Society, 141, 329

[134] Hutchings, J. B., Cowley, A. P., Crampton, D. & Redman, R. O., 1974, Astrophysical Journal, 191, L101

[135] Hutchings, J. B., Crampton, A. P. & Redman, R. O., 1975, Monthly Notices of the Royal Astronomical Society, 170, 313

[136] Hutchings, J. B., 1977, Monthly Notices of the Royal Astronomical Society, 181, 619

[137] Hutchings, J.B., Cowley, A. P., Osmer, P. S., & Crampton, D. 1977, Astrophysical Journal, 217, 186

[138] Hutchings, J. B. & Crampton, D., 1981, Astrophysical Journal, 247, 222

[139] Hutchings, J. B., 1984, Publications of the Astronomical Society of the Pacific, 96, 312

[140] Ikhsanov, N. R., 2001, Astronomy & Astrophysics, 367, 549

[141] In't Zand, J. J. M., Heise, J., Muller, J. M., Bazzano, A., Cocchi, M., Natalucci, L. & Ubertini, P., 1998, Astronomy & Astrophysics, 331, L25

[142] Jacoby, G.H., Hunter, D.A., & Christian, C.A.. 1984, ApJSS, 56, 257

[143] Johns, M., Koski, A., Canizares, C. et al., 1978, IAUC, 3171

[144] Johnston, M. D., Branston, H. V., Doxsey, R. E., Gursky, H., Schwartz, D. A., Schwartz, J. & van Paradijs, J., 1978, Astrophysical Journal, 255, L59

[145] Johnston, M. D., Branston, H. V. & Doxsey, R. E., 1979, Astrophysical Journal, 233, 514

[146] Kahabka, P. & Pietsch, W., 1996, Astronomy & Astrophysics, 312, 919

[147] Kato, S., 1983, Publications of the Astronomical Society of Japan, 35, 249

[148] Kato, S., 1989, In: :meyer, F., Duschl, W. J., Frank, J., Meyer-Holfmeister, E. (eds.) Theory of Accretion Disks, Kluwer Academic Publishers, Dordrecht, p.173

[149] Kelley, R. L., Jernigan, J. G., Levine, A., Petro, L. D. & Rappaport, S., 1983, Astrophysical Journal, 264, 568

[150] Kelley,R. L., Rappaport, S., Clark, G. W. & Petro, L. D., 1983, Astrophysical Journal, 268, 790

[151] Khruzina, T.S., & Cherepashchuk, A.M. 1983, Soviet Astronomy, 27, 35

[152] Khruzina T. S. & Cherepashchuk, A. M., 1984, Soviet Astr., 28, 173

[153] King, A. R. & Ritter, H., 1998, Monthly Notices of the Royal Astronomical Society, 293, L42

[154] Kirk, J. G., Ball, L., Skjaeraasen, O., 1999, Astropart. Phys., 10, 31

[155] Kopal, Z., 1959, in: Close Binary Systems, (John Wiley & Sons, New York) p. 217

[156] Kuiper, L., van Paradijs, J. & van der Klis, M., 1988, Astronomy & Astrophysics, 203, 79

[157] Kurucz, R. L., Peytremann, E. & Arett, E. H., 1974, Blanketed Model Atmospheres for Early-Type Stars, Smithsonian Inst. Press: Washington

[158] Kurucz, R. L., 1993, VizieR Online Data Catalog.

[159] Kuulkers, E., van der Klis, M., Oosterbroek, T., Asai, K., Dotani, T., van Paradijs, J. & Lewin, W. H. G., 1994a, Astronomy & Astrophysics, 289, 795

[160] Kuulkers, E. & van der Klis, M., 1995, Astronomy & Astrophysics, 303, 801

[161] Kuulkers, E., van der Klis, M. & Vaughan, B. A.,1996, Astronomy & Astrophysics, 311, 197

[162] Kuulkers, E. & van der Klis, M., 1996, Astronomy & Astrophysics, 314, 567

[163] Kuulkers, E., van der Klis, M., Oosterbroek, T., van Paradijs, J. & Lewin, W. H. G., 1997, Monthly Notices of the Royal Astronomical Society, 287, 495

[164] Larionov, V., Lyuty, V. M. & Zaitseva, G. V., 2001, Astronomy & Astrophysics, 378, 837

[165] Lattimer, J. M. & Prakash, M., 2000, Physics Reports, 333, 121

[166] Lee, U., Osaki, Y. & Saio, H., 1991, Monthly Notices of the Royal Astronomical Society, 250, 432

[167] Lejeune, T., Cuisinier, F. & Buser, R., 1998, American Astronomical Society Meeting, 130, 65

[168] Leong, C., Kellog, E., Gursky, H., Tanabaum, H. & Giaccon, R., 1971, Astrophysical Journal, 170, L67

[169] Levine, A., Rappaport, S., Deeter, J.E., Boynton, P.E., & Nagase, F. 1993, ApJ, 410, 328

[170] Lewin, W. H. G. et al., 1976, Astrophysical Journal(Letters), 207, L95

[171] Lewin, W. H. G., 1977, Amer. Sci, 65, No. 5, p. 65

[172] Lewin, W. H. G., 1983, in *Accretion-Driven Stellar X-ray Sources* P. 41, 1983

[173] Li, X.-D., Wang, Z.-R. & Qu, Q.-Y., 1999, Astronomy & Astrophysics, in press

[174] Liller, W. 1972, I.A.U. Circular, No. 2469

[175] Liller, W., 1975, IAU Circ., 2780

[176] Liu, Q. Z., van Paradijs, J. & van den Heuvel, E. P.J., 2000, Astronomy & Astrophysics, 147, 25

[177] Liu, Q. Z., van Paradijs, J. & van den Heuvel, E. P. J., 2001, Astronomy & Astrophysics, 368, 1021-1054

[178] Long, K. S., Helfand, D. J. & Grabelsky, D. A., 1981, Astrophysical Journal, 248, 925

[179] LopesdeOliveira,R., Motch,C., Haberl,F., Negueruela,I. & Janot-Pacheco,E., 2006, Astronomy & Astrophysics, 454, 265

[180] Lucke, R., Yentis, D., Friedman, H., Fritz, G., & Shulman, S. 1976, Astrophysical Journal, 206, L25

[181] Lyubimkov, L. S., Rostopchin, S. I., Roche, P. & Tarasov, A. E., 1997, Monthly Notices of the Royal Astronomical Society, 286, 549

[182] Lyuty, V. M. & Zaitseva, G. V., 2000, Astr. Lett., 26, 9

[183] Maloney, P. R. & Begelman, M. C., 1997, Astrophysical Journal, 491, L43

[184] Maraschi, L., Treves, A. & van den Heuvel, E. P. J., 1976, Nature, 259, 292

[185] Marshall, H. L., Ulmer, M. P., Hoffman, J. A., Doty, A. & Lewin, W. H. G., 1979, Astrophysical Journal, 227, 555

[186] Marshall, F. E., Becker, R.H., & White, N.E. 1983, ApJ, 266, 814

[187] Martin, E. L. et al., 1994, Astronomy & Astrophysics, 291, L43

[188] McClintock, J. E. & Remmillard, R. A., 2004, in: X-ray Binaries, eds. Lewin, W. H. G., van Paradijs, J. & van den Heuvel, E. P. J.

[189] Mc Laughlin, D. B., 1937, Astrophysical Journal, 85, 181

[190] Mereghetti, S., et al., 1991, Astrophysical Journal, 366, L23

[191] Meszaros, P., 1992, High-Energy Radiation from Magnetized Neutron Stars, (Chicago: Univ. Chicago Press)

[192] Meyer, F. & Meyer-Hoffmeister, E., 1981, Astronomy & Astrophysics, 104, L10

[193] Meyer, M, R., Edwards, S, Hinkle, K, H., Strom, S, E, 1998, Astrophysical Journal, 508, 397

[194] Milgrom, M., 1978, Astr. Ap., 208, 191

[195] Mirabel, I. F. & Rodriguez, L. F., 1994, Nature, 371, 46

[196] Mook, D. E., Boley, F. I., Foltz, C. B. & Westphfal, D., 1974, Publications of the Astronomical Society of the Pacific, 86, 894

[197] Motch, C., Stella, L., Janot-pacheco, E. & Mouchet, M., 1991, Astrophysical Journal, 369, 490

[198] Motch, C., Haberl, F., Dennerl, K., Pakull, M. & Janot-Pacheco, E., 1997, Astronomy & Astrophysics, 323, 853

[199] Nagase, F., Hayakawa, S., Kunieda, H., et al. 1982, Astrophysical Journal, 263, 814

[200] Nagase, F., 1989, in *ESA, The 23rd ESLAB Symposium on Two Topics in X Ray Astronomy.*, 1, 45

[201] Nagase, F., Corbet, R. H. D., Day, C. S. R., Inoue, H., Takeshima, T., Yoshida, K. & Mihara, T., 1992, Astrophysical Journal, 396, 147

[202] Nagase, F., 2002, Astrophysical Journal, 23, 59

[203] Negueruela, I., Reig, P., Coe, M. J. & Fabregat, J., 1998, Astronomy & Astrophysics. 336, 251

[204] Negueruela, I., 1998, Astronomy & Astrophysics, 338, 505

[205] Negueruela, I., Okazaki, A. T., Fabregat, J., et al., 2000, Astronomy & Astrophysics, submitted

[206] Negueruela, I. & Okazaki, A. T., 2001, Astronomy & Astrophysics, 369, 108

[207] Negueruela, I., Okazaki, A. T., Fabregat, J., Coe, M. J., Munari, U. & Tomov, T., 2001, Astronomy & Astrophysics, 369, 117

[208] Nice, D. J., Splaver, E. M., Stairs, I. H., Lhmer, O., Jessner, A., Kramer, M. & Cordes, J. M., 2005, Astrophysical Journal, 634, 1242

[209] Nicolet, B., 1978, Astronomy & Astrophysics, 34, 1

[210] Norton, A.J., Coe, M. J., Estela, A. et al., 1991, Monthly Notices of the Royal Astronomical Society, 253, 579

[211] Okazaki, A. T. & Kato, S., 1985, Publications of the Astronomical Society of Japan, 37, 683

[212] Okazaki, A. T., 1991, Publications of the Astronomical Society of Japan, 43, 75

[213] Okazaki, A. T., 1996, Publications of the Astronomical Society of Japan, 48, 305

[214] Okazaki, A. T., 1997, Astronomy & Astrophysics, 318, 548

[215] Okazaki, A. T. & Negueruela, I., 2001, Astronomy & Astrophysics, 377, 161

[216] Okazaki, A. T., Bate, M. R., Ogilvie, G. I. & Pringle, J. E., 2002, astro-ph/0208288

[217] Orlandini, M., et al., 2004, Nuclear Phys B 132, 476

[218] Orosz, J. A, & Bailyn, C. D, 1997, Astrophysical Journal, 482, 1086

[219] Osaki, Y., 1996, Publications of the Astronomical Society of the Pacific, 108, 39

[220] Page, M. J., Soria, R., Wu, K., Mason, K. O., Cordova, F. A., & Priedhorsky, W. C., 2003, Monthly Notices of the Royal Astronomical Society, 345, 639

[221] Parmar,A.N., Branduardi-Raymont,G., Pollard,G.S.G., Sanford,P.W., Fabian,A.C., Stewart,G.C., Schreier,E.J., Polidan,R.S., Oegerle,W.R. & Locke,M., 1980, Monthly Notices of the Royal Astronomical Society, 193, 49

[222] Paul, B., Nagase, F., Endo, T., Dotani, T., Yokogawa, J., & Nishiuchi, M. 2002, Astrophysical Journal, 579, 411

[223] Penrod, G. D. & Vogt, S. S., 1985, Astrophysical Journal, 299, 653

[224] Petterson, J. A., 1977, Astrophysical Journal, 218, 783

[225] Picconi, A., Bartolini, C., Bernabei, S., Galleti, S., Guarnieri, A. & Valentini, G., 2000b, in the Be Phenomenon in Early-Type Stars, IAU Colloquium 175 (ASP Conf. Proc. 214), ed. M. A. Smith, H. F. Henrichs & J. Fabregat (San Francisco: ASP), 585

[226] Plavec, M., 1968, Adv. Ast. and Ap., 6, 201

[227] Podsiadlowski, P., Rappaport, S. & Han, Z., 2003, Monthly Notices of the Royal Astronomical Society, 341, 385

[228] Polcaro, V. F. et al., 1990, Astronomy & Astrophysics, 231, 354

[229] Polidan, R. S., Pollard, G. S. G., Sanford, P. W. & Locke, M. C., 1978, Nature, 275, 296

[230] Popper, D. M., 1980, Ann. Rev. Astr, Ap., 18, 115

[231] Price, R.E., Groves, D.J., Rodrigues, R.M., Steward, F.D., Swift, C.D., & Toor, A. 1971, Astrophysical Journal Letters, 168, L7

[232] Priedhersky & Terrell, 1983

[233] Primini,F., Rappaport, S., Joss, P.C., Clark, G.W., Lewin, W., Li, F., Mayer, W., & McClintock, J. 1976, Astrophysical Journal Letters, 210, L71

[234] Primini,F., Rappaport, S., & Joss, P.C. 1977, Astrophysical Journal, 217, 543

[235] Pringle, J. E. 1996, Monthly Notices of the Royal Astronomical Society, 281, 357

[236] Psaltis, D., Lamb, F. K. & Miller, G. S., 1995, Astrophysical Journal, 454, L137

[237] Quaintrell, H., Norton, A. J., Ash, T. D. C., Roche, P., Willems, B., Bedding, T. R., Baldry, I. K., & Fender, R. P., 2003, Astronomy & Astrophysics, 401, 313

[238] Raguzova, N. V., 2001, Astronomy & Astrophysics, 367, 848

[239] Rappaport, S., Clark, G. W., Cominsky, L., Joss, P. C. & Li, F., 1978, Astrophysical Journal, 224, L1

[240] Quirrenbach, A., Hummel, C. A., Buscher, D. F., et al., 1993, Astrophysical Journal, 416, L25

[241] Quirrenbach, A., et al., 1997, Astrophysical Journal, 479, 477

[242] Rappaport, S. A. & Van den Heuvel, E. P. J., 1982, in: Be stars (IAU Symp. Nr. 98., (eds. Jaschek, M., & Groth, H. G.), Reidel, Dordrecht), p.327

[243] Rappaport, S. A & Joss, P. C., 1983, Accretion-Driven Stellar X-ray Sources, eds. Lewin, W. H. G. & van den Heuvel, E. P. J.

[244] Reed, B. C. & Beatty, A. E., 1995, Astrophysical Journal Supplement, 97, 189

[245] Reid, N., et al., 1988, Monthly Notices of the Royal Astronomical Society, 232, 53

[246] Reig, P. & Roche, P., 1999, Monthly Notices of the Royal Astronomical Society, 306, 100

[247] Reig, P., Larionov, V., Negueruela, I., Arkharov, A. A. & Kudryavtseva, N. A., 2007, Astronomy & Astrophysics, 462, 1081

[248] Reynolds, A.P., Hilditch, R.W., Bell, S.A., & Hill, G. 1993, Monthly Notices of the Royal Astronomical Society, 261, 337

[249] Reynolds, A.P, Quaintrell H., Still, M.D., Roche, P., Chakrabarty, D., & Levine, S.E. 1997, Monthly Notices of the Royal Astronomical Society, 288, 43

[250] Roche, P., Coe, M. J., Fabregat, J. et al., 1993, Astronomy & Astrophysics, 270, 122

[251] Roche, P., et al., 1997, Astronomy & Astrophysics, 322, 139

[252] Roche, P., et al., 1999, Astronomy & Astrophysics, submitted

[253] Rodriguez, J., Pooley, G., Hannikainen, D.C. & Lehto, H. J., 2006, astro-ph/0611218

[254] Rosenberg, F. D., Eyles, C. J., Skinner, C. G. & Willmore, A. P., 1975, Nature, 256, 631

[255] Rossi, C. et al., 1991, Astronomy & Astrophysics, 249, L19

[256] Rucinski, S. M., 1969, Acta Astronomica, 19, 125

[257] Scargle, J. D., 1989, Astrophysical Journal, 343, 874

[258] Schandl, S. & Meyer, F., 1994, Astronomy & Astrophysics, 289, 149

[259] Schmidtke, P. C., et al., 1999, Astronomical Journal, 117, 927

[260] Schreier, E., Giacconi, R., Gursky, H., Kellogg, E., & Tananbaum, H. 1972, Astrophysical Journal Letters, 178, L71

[261] Seon, K., Min, K., Yoshida, K., Makino, F., Lewin, W. H. G., van der Klis, M. & van Paradijs, J., 1997, Astrophysical Journal, 479,398

[262] Shahbaz, T., Charles, P. A., King, A. R., 1998, Monthly Notices of the Royal Astronomical Society, 301, 382

[263] Shahbaz , T. et al., 2003, Astrophysical Journal, 585, 443

[264] Shakura, N. I., Prokhorov, M. E., Postnov, K. A. & Ketsaris, N. A., 1999, Astrophysical Journal, 348, 917

[265] Shields, G. A., McKee, C. F., Lin, D. N. C. & Begelman, M. C., 1986, Astrophysical Journal, 306, 90

[266] Slettebak, A., 1982, Astrophysical Journal Supplement, 38, 205

[267] Slettebak, A., 1982, Astrophys. J. Suppl. Ser., 50, 55

[268] Smak, J. ,1969, Acta Astronomica, 19, 155

[269] Smak, J., 1981, Acta Astronomica, 31, 395

[270] Smith, D. M., Hazelton, B., Coburn, W., Boggs, S. E., Fivian, M., Hurford, G. J., Hudson, H. S., Grefenstette, B. & Gilmour, R., 2005, ATEL 557

[271] Smith, M. A. & Balona, L., 2006, Astrophysical Journal, 640, 491

[272] Sobieski, S., 1965, Astrophysical Journal Supplement, 12, 263

[273] Soria, R., Wu, K., Page, M.J., & Sakelliou, I. 2001, A&A, 365, L273

[274] Stee, Ph., de Araujo. F. X., Vakili, F., Mourard, D., Arnold, L., Bonneau, D., Morand, F. & Tallon-Bosc, I., 1995, Astronomy & Astrophysics, 300, 219

[275] Stee, Ph., 1998, Astronomy & Astrophysics, 336, 980

[276] Stee, Ph., 2000, *The Be phenomenon in Early-Type stars*, ed. M. A. Smith, H. F., Henrichs, & J. Fabregat, Publications of the Astronomical Society of the Pacific, 214, 129

[277] Stee, Ph. & Bittar, J., 2001, Astronomy & Astrophysics, 367, 532

[278] Steele, I. A., Negueruela, I., Coe, M. J. & Roche, P., 1998, Monthly Notices of the Royal Astronomical Society, 297, L5

[279] Stella, L., White, N. E. & Rosner, R., 1986, Astrophysical Journal, 308, 669

[280] Stevens, J. B., et al., 1999, Monthly Notices of the Royal Astronomical Society, 309, 421

[281] Strohmayer, T. E., Zhang, W., Swank, J. H., Smale, A., Titarchuk, L., Day, Charles & Lee, U., 1996, Astrophysical Journal, 469, L9

[282] Strohmayer, T. E., Markwardt, C. B., Swank, J. H. & In't Zand, J. J., 2003, Astrophysical Journal, 596, 167

[283] Struve, O., 1931, Astrophysical Journal, 73, 94

[284] Sunyaev, R. et al., 1989, IAUCirc, 4769

[285] Swank, J. H. & Serlemitsos, P. J., 1985, gecx.conf., 175

[286] Tamm, R. E., 1980, Astrophysical Journal, 241, 358

[287] Tamm, R. E., 1984, American Institute of physics conference series, 115, 263

[288] Tamm, R. E., 1987, Comments on Astrophysics, 11, 263

[289] Tanaka, Y. & Lewin, W. H. G., 1997, in: X-ray Binaries, eds. Lewin, W. H. G., van Paradijs, J. & van den Heuvel, E. P. J.

[290] Tawara, Y., Yamauchi, S., Awaki, H., Kii, T., Koyama, K. & Nagase, F., 1989, PASJ, 41, 473

[291] Thom, C., Granes, P., & Vakili, F., 1986, Astronomy & Astrophysics, 165, L13

[292] Thompson, T. W. J., Tomsick, J. A., Zand, J. J. M., Rothschild, R. E. & Walter, R., 2007, Astrophysical Journal, 661, 447

[293] Thorsett, S. E. & Chakrabarty, D., 1999, Astrophysical Journal, 512, 288

[294] Titarchuk, L. G., Bradshaw, C. F., Geldzahler, B. J. & Fomalont, E. B., 2001, Astrophysical Journal, 555, 45

[295] Timmes, F.X., Woosley, S.E., & Weaver, T.A. 1996, Astrophysical Journal, 457, 834

[296] Torrejon, J. M. & Orr, A., 2001, Astronomy & Astrophysics, 377, 148

[297] Treves, A., Belloni, T., Bouchet, P., Chiappetti, L., Falomo, R., Maraschi, L. & Tanzi, E. G., 1988, Astrophysical Journal, 335, 142

[298] Treves, A., et al., 1990, Astrophysical Journal, 364, 266

[299] Trumper, J. et al., 1978, Astrophysical Journal, 219, L105

[300] Tuchman, Y., Mineshige, S. & Wheeler, J. C., 1990, Astrophysical Journal, 359, 164

[301] Tueller, J., Ajello, M., Barthelmy, S., Krimm, H., Markwardt, C. & Skinner, G., 2005, ATEL 504

[302] Tuohy, I. R., Buckley, D. A. H., Remillard, R. A., Bradt, H. V., Schwartz, D. A., 1988, Proceedings of the International Symposium on the Physics of Neutron Stars and Black Holes, Edited by Y. Tanaka. Tokyo: Universal Academy Press, 1988, 93

[303] Tycner, C., et al., 2005, Astrophysical Journal, 624, 359

[304] Tycner, C., et al., 2006, Astronomical Journal, 131, 2710

[305] Underhill, A. & Doazan, V., 1982, British Astronomical Assoc. 92, 290

[306] Val Baker, A.K.F., Norton, A.J., & Quaintrell, H. 2005, Astronomy & Astrophysics, 441, 685

[307] Val Baker, A.K.F., Norton, A.J., & Negueruela, I., 2007, AIP Conf. Proc., 924, 530

[308] Van Bever, J. & Vanbeveren, D., 1997, Astronomy & Astrophysics, 322, 116

[309] van den Bergh, S., 1972, Nature, 235, 273

[310] van den Heuvel, E. P. J., 1983, in: Accretion driven stellar X-ray sources, eds. Lewin & van den Heuvel, Press: Cambrideg Univ.

[311] van den Heuvel, E. P. J. & Rappaport, S., 1987, in IAU Colloq. 92, Physics of Be stars, ed. A. Slettebak & T. D. Snow (Cambridge: Cambridge Univ. Press), 291

[312] van der Klis, M., Tjemkes, S. & van Paradijs, J., 1983, Astronomy & Astrophysics, 126, 265

[313] van der Klis, M. & Bonnet-Bidaud, J. M., 1984, Astronomy & Astrophysics, 135, 155

[314] van der Klis, M., et al 1985, A&A, 151, 322

[315] van der Klis, M., 1997, in: X-ray Binaries, ed. W. H. G. Lewin, J. van Paradijs & E. P. J. van den Heuvel, Chapter 6

[316] van der Klis, M., 2004, in: Compact Stellar X-ray sources, eds. Lewin, W. H. G. & van der Klis, M., Press: Cambrideg Univ.

[317] van der Meer, A., Kaper, L., van Kerkwijk, M.H., & van den Heuvel, E.P.J. 2005, ASP Conference Series, 797, 623

[318] van der Meer, A.; Kaper, L.; van Kerkwijk, M. H.; Heemskerk, M. H. M.; van den Heuvel, E. P. J., 2007, Astronomy & Astrophysics, 473, 513

[319] van Kerkwijk, M.H., van Paradijs, J., & Zuiderwijk, E.J. 1995, Astronomy & Astrophysics, 303, 497

[320] van Paradijs, J. & Zuiderwijk, E., 1977, Astronomy & Astrophysics, 61, L91

[321] van Paradijs, J, 1983, in: Accretion Driven Stellar X-ray sources, eds. Lewin, W. H. G. & van den Heuvel, E. P. J.

[322] van Paradijs, J. & Kuiper, L., 1984, Astronomy & Astrophysics, 138, 71

[323] van Paradijs, J. & Verbunt, F., 1984, AIPC, 115, 49

[324] van Paradijs, J., van der Klis, M., Augusteijn, T., et al., 1987, Astronomy & Astrophysics, 184, 201

[325] van Paradijs, J. & McClintock, J. E., 1995, in X-ray Binaries, eds. Lewin, van Paradijs & van den Heuvel, 58 (CUP)

[326] van Paradijs, J., 1998, in: Proc. NATO ASI Series, vol 515, The Many Faces of Neutron Stars., eds. Buccheri, R., van Paradijs, J., Alpar, M. A

[327] Verbunt, F. & van den Heuvel, E. P. J., 1995, in: X-ray Binaries, eds. Lewin, van Paridijs & van den Heuvel (CUP)

[328] Vrtilek, S. D., Raymond, J. C., Boroson, B., et al., 2001, Astrophysical Journal, 563, L139

[329] Wackerling, L. R., 1970, MmRAS, 73, 153

[330] Wackerling, L. R., 1972, Publications of the Astronomical Society of the Pacific, 84, 827

[331] Walborn, N.R., & Fitzpatrick, E.L. 1990, PASP, 102, 650

[332] Wang, Z. X. & Gies, D. R., 1998, Publications of the Astronomical Society of the Pacific, 110, 1310

[333] Warren, P.R., & Penfold, J.E. 1975, MNRAS, 172, 41

[334] Warwick, R. S., Watson, M. G. & Sims, M. R., 1981, Space Sci. Rev., 29, 373

[335] Warwick, R. S., Norton, A. J., Turner, M. J. L., Watson, M. G. & Willingale, R., 1988, Monthly Notices of the Royal Astronomical Society, 232, 551

[336] Waters, L. B. F. M., Pols, O. R., Hogeveen, J. et al., 1989, Astronomy & Astrophysics, 220, L1

[337] Webster, B.L., Martin, W.L., Feast, M.W., & Andrews, P.J. 1972, Nature Phys. Sci., 240, 183

[338] Weisskopf, M. C., et al., 1984, Astrophysical Journal, 278, 711

[339] White, N. E., Mason, K. O., Sanford, P. W. & Murdin, P., 1976, Monthly Notices of the Royal Astronomical Society,176, 201

[340] White, N. E., Mason, K. O. & Sanford, P. W., 1977, Nature, 267, 229

[341] White, N. E., Mason, K. O., Carpenter, G. F. & Skinner, G. K., 1978, Monthly Notices of the Royal Astronomical Society, 184, 1

[342] White, N. E. & Pravdo, S. H., 1979, Astrophysical Journal, 233, L121

[343] White, N. E. & Marshall, F.E., 1984, Astrophysical Journal, 281, 354

[344] White, N. E, Stella, L. & Parmer, A. N., 1988, Astrophysical Journal, 324, 363

[345] White, N. E., Nagase, F. & Parmar, A. N., 1995, The properties of X-ray binaries, in: X-ray Binaries, eds., W. H. G. Lewin, J. van Paradijs & E. P. J. van den Heuvel., Cambridge: Cambridge Univ. Press. p58

[346] Whitehurst, R. & King, A., 1991, Monthly Notices of the Royal Astronomical Society, 249, 25

[347] Wijnands, R. & van der Klis, M., 1997, AIPC, 431, 381

[348] Wijnands, R. A. D., van der Klis, M., Mendez, M., van Paradijs, J., Lewin, W. H. G., Lamb, F. K., Vaughan, B. & Kuulkers, E., 1998, Astrophysical Journal, 495, L39

[349] Wijnands, R. & van der Klis, M., 1998, Nature, 394, 344

[350] Wijnands, R. & van der Klis, M., 2001, Monthly Notices of the Royal Astronomical Society, 321, 537

[351] Willems, B. & Aerts, C., 2002, Astronomy & Astrophysics, 384, 441

[352] Wilms, J., Nowak, M. A., Pottschmidt, K., Heindl, W. A., Dove, J. B. & Begelman, M. C., 2001, Monthly Notices of the Royal Astronomical Society, 320, 327

[353] Wojdowski, P., Clark, G.W., & Levine, A.M. 1998, Astrophysical Journal, 502, 253

[354] Woo, J.W., Clark, G.W., Blondin, J.M., Kallman, T.R., & Nagase, F. 1995, Astrophysical Journal, 445, 896

[355] Wood, K. S. Meekins, J. F., Yentis, D. J. et al., 1984, Astrophys. J. Suppl. Ser., 56, 507

[356] Wu, K., Soria, R., Page, M. J., Sakelliou, I., Kahn, S. M. & de V ries, C. P., 2001, Astronomy & Astrophysics, 365, L267

[357] Zamanov, R. K., Reig, P., Marti, J., Coe, M. J., Fabregat, J., Tomov, N. A. & Valchev, T., 2001, Astronomy & Astrophysics, 367, 884

[358] Zang, W., Strohmayer, T. E. & Swank, J. H., 1998, Astrophysical Journal, 500, L167

[359] Zdziarski, A. A., Poutanen, J., Paciesas, W. S. & Wen, L., 2002, Astrophysical Journal, 578, 357

[360] Zhang, S. N., Harmon, B. A., Paciesas, W. S., Wilson, C. A. & Fishman, G. J., 1994, IAUC 6106

[361] Zhang, F., Li, X. D. & Wang, Z. R., 2004, Astrophysical Journal, 603, 663

[362] Zurita Heras, J. A., de Cesare, G., Walter, R., Bodaghee, A., Blanger, G., Courvoisier, T. J. L., Shaw, S. E. & Stephen, J. B, 2006, Astronomy & Astrophysics, 448, 261

Acknowledgements

Firstly I would like to thank my supervisor Andy Norton as well as Simon Clark and Ignacio Negueruela for their invaluable help through out my research. I would like to thank the staff at the South African Astronomical Observatory for scheduling the observations on which some of this thesis is based and Hannah Quaintrell for carrying out the observations of SMC X-1. I would also like to thank Graham Hill for the use of his LIGHT2 code and Alaistair Reynolds for the radial velocities from his paper. I am indebted to Tim Harries for providing me with a linux installation of LIGHT2 and Ron Hilditch for his invaluable, patient advice on the workings of LIGHT2. I also thank Sean Ryan for his assistance with the intricacies of cross-correlations in iraf.

Finally I would like to thank my darling husband Ariffin Yeop, for supporting me and cooking for me while I was writing up.